Distribution Agreement

In presenting this thesis or dissertation as a partial fulfillment of the requirements for an advanced degree from Emory University, I hereby grant to Emory University and its agents the non-exclusive license to archive, make accessible, and display my thesis or dissertation in whole or in part in all forms of media, now or hereafter known, including display on the world wide web. I understand that I may select some access restrictions as part of the online submission of this thesis or dissertation. I retain all ownership rights to the copyright of the thesis or dissertation. I also retain the right to use in future works (such as articles or books) all or part of this thesis or dissertation.

Signature:

Noah Alberts-Grill	10/16/2012
[Student's name typed]	Date

DYNAMIC IMMUNE CELL ACCUMULATION CORRESPONDS WITH VASCULAR INFLAMMATION DURING DISTURBED FLOW-INDUCED ATHEROGENESIS IN MOUSE CAROTID ARTERY

By

Noah Alberts-Grill

Doctor of Philosophy

Graduate Division of Biological and Biomedical Science
Immunology and Molecular Pathogenesis

_____ [Advisor's signature]
Hanjoong Jo
Advisor

_____ [Member's signature]
John D. Altman
Committee Member

_____ [Member's signature]
Timothy Denning
Committee Member

_____ [Member's signature]
Brian D. Evavold
Committee Member

_____ [Member's signature]
Andrew T. Gewirtz
Committee Member

Accepted:

_____
Lisa A. Tedesco, Ph.D. Dean of the James T. Laney School of Graduate Studies
_____ Date

DYNAMIC IMMUNE CELL ACCUMULATION CORRESPONDS WITH VASCULAR INFLAMMATION DURING DISTURBED FLOW-INDUCED ATHEROGENESIS IN MOUSE CAROTID ARTERY

By

Noah Alberts-Grill
B.A., Vassar College, 2003

Advisor:
Hanjoong Jo, PhD

An abstract of
A dissertation submitted to the Faculty of the
James T. Laney School of Graduate Studies of Emory University
in partial fulfillment of the requirements for the degree of
Doctor of Philosophy
in Immunology and Molecular Pathogenesis
Graduate Division of Biological and Biomedical Sciences
2012

Abstract

DYNAMIC IMMUNE CELL ACCUMULATION CORRESPONDS WITH VASCULAR INFLAMMATION DURING DISTURBED FLOW-INDUCED ATHEROGENESIS IN MOUSE CAROTID ARTERY

By Noah Alberts-Grill

Cardiovascular disease (CVD) is the leading cause of morbidity and mortality in the United States. The leading cause of CVD is the progressive growth of lipid-laden plaques within the large arteries of the body, a process known as atherosclerosis. This inflammatory disease is characterized by the infiltration of immune cells into the artery wall at sites that are chronically exposed to disturbed patterns of blood flow (d-flow). Immune cells accumulate within the artery wall where they establish the sustained, local inflammation required to drive plaque development. While the immunogenesis of atherosclerosis has been extensively studied over the past decade or so, the relationship between d-flow and immune cell function in the vasculature remains poorly understood. In order to overcome this knowledge gap, we used a partial carotid ligation model to generate d-flow in the left common carotid artery (LCA), which induces the rapid development of atherosclerosis within 2 weeks along the entire length of LCA in apolipoprotein E-deficient ($ApoE^{-/-}$) mice fed a high-fat diet (HFD). We developed a 10-fluorochrome, 13-parameter, flow cytometry-based immunophenotyping method to quantify the infiltration of 7 major classes of immune cells into flow-disturbed LCA during rapid atherogenesis. Using this method we provide the first quantitative description of vascular leukocyte number and composition over the entire lifespan of murine atherosclerosis, and showed that d-flow induces rapid and dynamic accumulation of monocyte/macrophages, dendritic cells, granulocytes, NK cells, and T-cells within 4 days. Leukocyte numbers peaked by 7 days, preceding atheroma development in LCA by day 14 days post-ligation. qPCR and ELISA arrays showed that leukocyte infiltration corresponds with the onset of progressive pro-inflammatory cytokine and chemokine expression in the artery wall, demonstrating the close link between d-flow, vascular leukocyte recruitment, and atherosclerosis. Flow cytometry analysis of peripheral blood leukocytes (PBLs) in our model showed that d-flow powerfully inhibits hyperlipidemia-induced leukocytosis in ligated versus sham-operated controls, suggesting that localized d-flow can influence immune function on a systemic level, independent of classical atherosclerosis risk factors such as hyperlipidemia. Together, our studies establish partial carotid ligation as an important experimental model to study the interface between vascular physiology, immunopathology, and atherosclerosis.

DYNAMIC IMMUNE CELL ACCUMULATION CORRESPONDS WITH VASCULAR INFLAMMATION DURING DISTURBED FLOW-INDUCED ATHEROGENESIS IN MOUSE CAROTID ARTERY

By

Noah Alberts-Grill
B.A., Vassar College, 2003

Advisor:
Hanjoong Jo, PhD

A dissertation submitted to the Faculty of the
James T. Laney School of Graduate Studies of Emory University
in partial fulfillment of the requirements for the degree of
Doctor of Philosophy
in Immunology and Molecular Pathogenesis
Graduate Division of Biological and Biomedical Sciences
2012

TABLE OF CONTENTS

INDEX OF FIGURES

INDEX OF TABLES

LIST OF SYMBOLS AND ABBREVIATIONS

αSMA	alpha-smooth muscle actin
ADCC	antibody-dependent cellular cytotoxicity
APC	antigen-presenting cell
ApoE	apolipoprotein-E
BDCA-2	blood DC antigen 2
BDCA-4	blood DC antigen 4
BSA	bovine serum albumin
CFSE	carboxyfluorescein succinimidyl ester
CVD	cardiovascular disease
CatK	cathepsin K
CatL	cathepsin L
CatS	cathepsin S
CMTMR	5- (and 6)-([(4-chloromethyl) benzoyl]amino) tetramethylrhodamine
CAD	coronary artery disease
CCL7	CC-chemokine ligand 7
CCL9	CC-chemokine ligand 9
CCL17	CC-chemokine ligand 17
CDP	common dendritic precursor cell
CXCL12	CX-chemokine ligand 12
CXCL16	CX-chemokine ligand 16
CX_3CL1	CX_3-chemokine ligand 1
CX_3CR1	CX_3-chemokine receptor 1

DC	dendritic cell
DTR	diphtheria toxoid receptor
d-flow	disturbed flow
EC	endothelial cell
eNOS	endothelial nitric oxide synthase
ELISA	enzyme-linked immunosorbent assay
FMO	fluorescence minus one
Flt3	fms-like thyrosine kinase 3
Flt3L	fms-like thyrosine kinase 3 ligand
GC	greater curvature
GALT	gut-associated lymphoid tissues
HSP-60	heat-shock protein 60
HSP-65	heat-shock protein 65
HDL	high-density lipoprotein
IgA	immunoglobulin type A
IgG2a	immunoglobulin type IgG2a
IgM	immunoglobulin type M
IDO	indoleamine 2,3-dioxygenase
iNOS	inducible nitric oxide synthase
ICAM-1	intercellular adhesion molecule-1
IFNα	interferon-alpha
IFNγ	interferon-gamma
IL-1	interleukin-1

IL-2	interleukin-2
IL-4	interleukin-4
IL-5	interleukin-5
IL-6	interleukin-6
IL-10	interleukin-10
IL-12	interleukin-12
IL-13	interleukin-13
IL-15	interleukin-15
IL-17	interleukin-17
IL-18	interleukin-18
IL-23	interleukin-23
CD62L	L-selectin
LOX1	lectin-type oxidized low-density lipoprotein receptor 1
LCA	left common carotid artery
LC	lesser curvature
LPS	lipopolysaccharide
LDL	low-density lipoprotein
LDLR	low-density lipoprotein receptor
M-CSF	macrophage-colony stimulating factor
MIF	macrophage migration inhibitory factor
MHC-II	major histocompatability complex class II molecule
Mo-DC	monocyte-derived DC
MCP-1	monocyte chemoattractant peptide-1

MPO	myeloperoxidase
NK cell	natural killer cell
NO	nitric oxide
OCT	optimal cutting temperature compound
oxLDL	oxidized LDL
HFD	Paigen's high-fat diet
PLSR	partial least squares regression
PBL	peripheral blood leukocytes
PBS	phosphate buffered saline
pDC	plasmacytoid DC
qPCR	quantitative real-time polymerase chain reaction
Treg	regulatory T-cell
RA	retinoic acid
RCA	right common carotid artery
SR-A	scavenger receptor A
SR-B1	scavenger receptor B1
Siglec-H	sialic acid-binding immunoglobulin-like lectin H
SMC	smooth muscle cell
TUNEL	terminal deoxynucleotidyl transferase dUTP nick end labeling
TPA	12-O-tetradecanoylphorbol-13-acetate
TMR	tetramethylrhodamine-dUTP
TF	tissue factor
TRAIL	TNF-related apoptosis inducing ligand

TLR2	toll-like receptor 2
TLR4	toll-like receptor 4
TLR7	toll-like receptor 7
TLR8	toll-like receptor 8
TLR9	toll-like receptor 9
TGF-β	transforming growth factor-beta
TNFα	tumor necrosis factor-alpha
VCAM-1	vascular cell adhesion molecule-1
vDC	vascular DC
VEGF	vascular endothelial cell growth factor
vWF	von Willebrand factor

CHAPTER 1:

GENERAL INTRODUCTION

1.1 Atherosclerosis, Disturbed Flow, and Inflammation

Although preventive therapies have improved clinical outcome and survival in acute coronary syndrome patients, cardiovascular disease (CVD) remains the leading cause of morbidity and mortality in the United States. The American Heart Association estimates that in 2007, CVD was responsible for 813,804 deaths, or 33.6 percent of all deaths. Furthermore, an estimated 81,100,000 living Americans suffer from heart disease, making it the largest health burden today (Roger et al., 2010). The leading cause of CVD is the progressive growth of lipid-laden vascular plaques, a process known as atherosclerosis. Atherosclerosis is an inflammatory disease of large arteries that is characterized by the infiltration of immune cells into the artery wall, followed by the establishment of sustained vascular inflammation and the development of lipid laden plaques which can cause myocardial infarction or stroke by occluding blood flow at the site of the lesion, or through thromboembolic means (Ku et al., 1985;Ross, 1999;Libby, 2002;VanderLaan et al., 2004;Hansson, 2005;Galkina and Ley, 2009). The inflammatory pathogenesis of atherosclerosis occurs on a systemic level, resulting in increased levels of pro-inflammatory mediators in the circulation and adipose tissues, as well as immune cell activation (Libby, 2002). However, atherosclerotic plaques only tend to occur in specific regions of the arterial tree that are exposed to disturbed patterns of blood flow (d-flow) such as the aortic sinus, the lesser curvature of the aortic arch, the root of the innominate artery, the carotid bifurcations, and numerous regions of the coronary arteries (Lutz et al., 1977;Ku et al., 1985;Asakura and Karino, 1990;Lei et al., 1995;Kleinstreuer et al., 2001;Cheng et al., 2002;Farmakis et al., 2004;VanderLaan et al., 2004;Del Gaudio et al., 2006;Suo et al., 2007). The focal pattern of disease is remarkable given that most

atherogenic risk factors including hypercholesterolemia, hypertension, diabetes, and smoking are systemic, and affect the entire circulatory tree regardless of blood flow patterns. This suggests that d-flow, with its characteristic low and oscillatory wall shear stress, is a localizing and priming factor, which interacts with systemic factors of inflammation to induce atherosclerosis. How the initial inflammation induced by d-flow interacts with systemic risk factors and immune cell function to drive atherosclerotic plaque development is not clear. The overall objective of this dissertation is to define the relationship between d-flow and immune cell function, both within and outside the artery wall, in order to further our understanding of how vascular homeostasis is disrupted, giving way to run-away inflammation and atherosclerosis.

It has been established that even in healthy, non-atherosclerotic vessels, vascular endothelium in naturally flow-disturbed areas exhibits a chronic low-grade inflammation (Jongstra-Bilen et al., 2006). The endothelial cells (ECs) that line the vascular wall in these regions express adhesion molecules like intercellular adhesion molecule-1 (ICAM-1) and vascular cell adhesion molecule-1 (VCAM-1) (Walpola et al., 1995;Endres et al., 1997;Nakashima et al., 1998;Iiyama et al., 1999;Suo et al., 2007;Nam et al., 2009), as well as expression of monocyte chemoattractant peptide-1 (MCP-1) and other chemokines (Nerem et al., 1998;Cybulsky et al., 2001;Chiu and Chien, 2011). D-flow also induces other numerous pro-inflammatory changes in EC physiology and function that are all increased during atherosclerosis such as increased cell turnover, increased reactive oxygen species production, increased permeability to macromolecules such as lipoproteins, and increased platelet adhesion (Chiu and Chien, 2011). Together, these

inflammatory chemokines and adhesion molecules mediate a vascular, steady-state biology by which resident immune cell populations traffic into and out of the atheroprone artery wall. This process has been shown to occur in the aorta of athero-resistant wild-type C57/Bl6 mice where these chronically inflamed, pre-atherosclerotic 'lesions' fail to develop into atheroma even under hypercholesterolemic conditions (Galkina et al., 2006;Jongstra-Bilen et al., 2006).

Taken together, the evidence so far suggests that disruptions in gut homeostasis (Wang et al., 2011), lipid metabolism, and systemic inflammation interact with d-flow at the artery wall to induce aberrant EC function (Nam et al., 2009;Ni et al., 2010;Chiu and Chien, 2011) and immune cell recruitment into the arterial wall (Galkina et al., 2006;Galkina and Ley, 2009;Drechsler et al., 2010;Alberts-Grill et al., 2012), which, in turn, establish a sustained, 'pro-atherogenic' immune response against lipid- and vascular tissue-derived autoantigens and cause atherosclerosis (Hansson and Hermansson, 2011).

1.2 Immune Cells and Atherosclerosis

Immune cells, also commonly called leukocytes, have been shown to accumulate in atherosclerotic arteries since the early 1980s (Gerrity et al., 1979). As a whole, leukocytes are the most diverse and widely distributed class of somatic cells found in vertebrate animals, and can be found in virtually every tissue of the body. Leukocytes are typically classified into adaptive and innate immune cells, and derive from lymphoid and myeloid progenitor cells, respectively in the bone marrow. Adaptive immune cells consist of T-cells and B-cells, which are responsible for immune memory. Innate

immune cells consist of monocyte/macrophages, neutrophils, mast cells, dendritic cells (DCs), and natural killer cells (NK cells). These cells are responsible for pathogen sensing, early control of infections, and the initiation of adaptive immune responses. Both innate and adaptive immune responses have been shown to play an important role in the initiation and progression of atherosclerosis (Hansson, 2005;Andersson et al., 2010;Hansson and Hermansson, 2011). The known contributions of specific leukocyte subsets to the control or pathogenesis of vascular inflammation will be discussed in brief below.

T-cells

T-cells reside in the outer, adventitial layer of large arteries under normal, steady-state conditions (Galkina and Ley, 2007a). This adventitial T-cell homing occurs largely as a consequence of constitutive CC-chemokine ligand 7 (CCL7)/L-selectin (CD62L)-dependent steady-state homing (Galkina et al., 2006;Maffia et al., 2007), suggesting that the adventitia of large arteries is a peripheral tissue-associated lymphoid tissue, containing naïve T-cells, like similar tissues found in the gut, lungs, and liver. Arterial recruitment of T-cells is accelerated under pro-atherogenic conditions such as hypercholesterolemia, and during early and advanced stages of atherosclerosis, where they accumulate in adventitia as well as in the innermost, intimal layer of the artery wall (Sato et al., 2006;Zhang et al., 2006;Galkina and Ley, 2007b;Han et al., 2008;Galkina and Ley, 2009). The majority of T-cells that accumulate in the artery wall during atherogenesis are TCR$\alpha\beta^{+}CD4^{+}$ cells (CD4 T-cells), and bear an activated Th1 effector phenotype that lack expression of CD62L and CCR7 and instead express phenotypic

markers of effector $CD4^+$ T-cells such as CCR5 and CD44 (Hansson et al., 1989;Wick et al., 1997;Hansson, 2005). Lesional $CD4^+$ T-cells contribute to vascular inflammation and atherosclerotic plaque development in the early stages of atherosclerosis, and have also been linked to thinning of the fibrous cap, the expansion of the lipid-rich necrotic core, and plaque rupture in more advanced lesions (Hansson, 2005;Hansson et al., 2006;Hansson and Hermansson, 2011). Within the lesion, $CD4^+$ T-cells have been shown to facilitate vascular inflammation via mechanisms of direct cytotoxicity and cytokine secretion (Nakajima et al., 2002;Hansson, 2005;Niessner et al., 2006;Pryshchep et al., 2006;Sato et al., 2006;Erbel et al., 2007). Perhaps most significantly, $CD4^+$ T-cells secrete large amounts of the pro-inflammatory cytokine, interferon-gamma (IFNγ) upon activation (Hansson et al., 1989;Zhou et al., 1998;Andersson et al., 2010). The pro-atherogenic role of IFNγ in atherosclerosis has been well-established. IFNγ administration exacerbates atherosclerosis development in apolipoprotein E-deficient ($ApoE^{-/-}$) and low-density lipoprotein receptor-deficient ($LDLR^{-/-}$) mice (Gupta et al., 1997;Tellides et al., 2000;Whitman et al., 2000;Buono et al., 2003;Andersson et al., 2010). Conversely, IFNγ-deficiency inhibits atherosclerosis development in $ApoE^{-/-}$ and $LDLR^{-/-}$ mice (Gupta et al., 1997;Buono et al., 2003). IFNγ has been shown to mediate numerous pro-atherogenic functions within atherosclerotic lesions including increased T-cell and macrophage recruitment into the plaque, increased foam cell formation, increased MHC-II expression among lesional cells, and enhanced activation of DCs (Harvey and Ramji, 2005;Leon and Zuckerman, 2005;Kleemann et al., 2008). The importance of $CD4^+$ T-cells in mediating vascular inflammation is highlighted by the fact that atherosclerosis development is severely inhibited in immunodeficient *scid/scid*

$ApoE^{-/-}$ mice, which lack T- and B-cells, and is restored by adoptive transfer of $CD4^+$ T-cells (Zhou et al., 2000). Alternatively, Th17 T-cells, which secrete the pro-inflammatory cytokine IL-17, have also been implicated in promoting atherosclerosis (Taleb et al., 2009;van Es et al., 2009;Gao et al., 2010), suggesting that $CD4^+$ T-cell responses are responsible for mediating complex inflammatory adaptive immune responses within the artery wall.

In contrast to the primarily cell-mediated responses induced by Th1 and Th17 T-cells, Th2 T-cell responses are characterized by secretion of anti-inflammatory cytokines IL-4, IL-5, IL-10, and IL-13, and drive largely humoral, or antibody-mediated immune responses by shaping B-cell activation (Abbas et al., 1996). In the context of atherosclerosis, severe hypercholesterolemia has been shown to induce a switch from a Th1 to Th2 T-cell response in $ApoE^{-/-}$ mice (Zhou et al., 1998). However, Th2-mediated immune responses have been shown to inhibit atherosclerosis development and progression through the secretion of anti-inflammatory cytokines and the induction of neutralizing antibody responses against lipid-derived vascular antigens in B-cells (Schulte et al., 2008).

Regulatory T-cells

T-cell mediated inflammation is tightly controlled by another specialized class of $CD4^+$ T-cells called regulatory T-cells (Tregs), which are critical in maintaining immunological tolerance throughout the body (Sakaguchi et al., 2006). The presence of pro-atherogenic T-cell responses against autoantigens such as heat-shock protein 60 (HSP-60) and low-

density lipoprotein (LDL) clearly indicate that atherosclerosis has an autoimmune component. As such, Tregs have been shown to inhibit atherosclerosis by secreting anti-inflammatory, anti-atherogenic cytokines like IL-10 (Mallat et al., 1999;Mallat et al., 2003;Binder et al., 2004;Ait-Oufella et al., 2006;Mor et al., 2007;Kleemann et al., 2008). Adoptive transfer of purified Tregs inhibits atherosclerosis development in recipient $ApoE^{-/-}$ mice and reduces the production of Th1-dependent IFNγ and IgG2a, while increasing IL-10 (Mallat et al., 2003). Furthermore, it was shown that under conditions of chronic hypercholesterolemia in $LDLR^{-/-}$ mice, the balance between pro-inflammatory T-cells and Tregs in mouse aorta shifts in favor of inflammation as Treg numbers decline, corresponding with disease progression (Maganto-Garcia et al., 2011). This suggests that reduced Treg number and function in the vascular wall contributes to the loss of tissue homeostasis that occurs during atherogenesis, which fits nicely with the role of Tregs in maintaining adaptive immune tolerance throughout the body.

B-cells

Like T-cells, B-cells have been shown to reside within the adventitia of healthy large arteries and have also been detected within atherosclerotic plaques, albeit in smaller numbers than T-cells (Galkina and Ley, 2007a). Unlike other types of immune cells which mediate various aspects of immunity through the secretion of cytokines and other chemical mediators, B-cells are the only class of cells capable of producing antibodies, which are capable of neutralizing toxins or viral pathogens by binding to and masking key epitopes, or of targeting bacteria for opsonization by macrophages, fixation and lysis by the complement system, or for antibody-dependent cellular cytotoxicity (ADCC) by

NK cells. The role of B-cells in atherosclerosis is still under debate as there is evidence to support both a pro- and anti-atherogenic role in the disease. Data from several studies indicate a protective role for B-cells in atherosclerosis via antibody-mediated clearance of pro-atherogenic antigens such as oxidized LDL (oxLDL). For instance, adoptive transfer of bone marrow from B-cell-deficient mice into lethally irradiated $LDLR^{-/-}$ mice aggravated atherosclerosis and reduced production of anti-oxLDL antibodies (Major et al., 2002). Adoptive transfer of splenic B-cells from aged $ApoE^{-/-}$ mice was also shown to reduce atherosclerosis in young $ApoE^{-/-}$ recipients (Caligiuri et al., 2002). An innate sub-class of B-cells, called B-1 B-cells, has been described which constitutively produce natural IgM antibodies without the need for T-cell help (Hardy and Hayakawa, 2005;Kearney, 2005). Supporting previous evidence showing a neutralizing, protective role for B-cell-derived antibodies during atherosclerosis, a recent study found that upwards of 30% of natural IgM antibodies react against epitopes derived from oxidized phospholipids such as oxLDL, and also bind successfully to atherosclerotic plaques (Chou et al., 2009). However, confusing matters, more recent work has shown that the antibody-mediated depletion of conventional B-cells ameliorates atherosclerosis development, while adoptive transfer of purified splenic B-cells exacerbates the disease, in contradiction to previous reports (Kyaw et al., 2010).

Macrophages

Macrophages were the first immune cells found within atherosclerotic plaques and are present during all stages of lesion development (Gerrity et al., 1979). Macrophages enter the arterial wall as circulating monocytes in response to chemotactic factors produced by

inflamed vascular cells such as MCP-1 (also known as CCL2) and CX_3-chemokine ligand 1 (CX_3CL1; also known as fractalkine), and differentiate in response to local inflammatory signals, such as extracellular lipids (Boring et al., 1998;Gu et al., 1998;Combadiere et al., 2003;Lesnik et al., 2003). Lesional macrophages uptake extracellular lipids via a family of specialized scavenger receptors like CD36, CD68, lectin-type oxidized low-density lipoprotein receptor 1 (LOX1), scavenger receptor A (SR-A) and SR-B1 (Steinberg, 1997), and differentiate into foam cells. Accumulation of macrophage foam cells within the vascular intima is a hallmark of early atherosclerosis (Libby, 2002;Hansson, 2005;Hansson et al., 2006) and mice deficient in monocyte chemoattractant proteins or their receptors develop reduced atherosclerosis (Hansson and Libby, 2006). Alternatively, macrophages are plastic inflammatory mediators that come in two basic types: M1 inflammatory macrophages which secrete a number of pro-inflammatory cytokines within plaques, including IL-1, IL-6, IL-12, IL-15, IL-18, tumor necrosis factor-alpha (TNFα), and macrophage migration inhibitory factor (MIF); and M2 'wound healing' macrophages which promote angiogenesis by secreting vascular endothelial cell growth factor (VEGF) and reduce tissue inflammation within lesions by secreting the anti-inflammatory cytokines IL-10, IL-13, transforming growth factor-beta (TGF-β) (Galkina and Ley, 2009;Woollard and Geissmann, 2010). Macrophages also further disease pathogenesis by secreting a wide number of proteases of the matrix metalloproteinase (MMP) and cathepsin families which break down elastin and collagen fibers in atherosclerotic plaques promoting leukocyte infiltration and plaque destabilization and rupture (Weber et al., 2008).

Dendritic cells

DCs were first identified in the arterial intima of atherosclerotic lesions in rabbits and humans during the 1990s (Bobryshev and Lord, 1995). While increased in atherosclerotic plaques, DCs are also present in healthy large arteries during steady state conditions. Interestingly, in both healthy and diseased arteries, intimal DCs show a distribution patterns that corresponds closely with flow-disturbed, atheroprone regions of the arterial tree, such as bifurcations and curvatures, but accumulate in robust numbers in atherosclerotic plaques (Millonig et al., 2001;Jongstra-Bilen et al., 2006;Randolph, 2008;Choi et al., 2009;Paulson et al., 2010;Choi et al., 2011). DCs, along with macrophages, represent a class of professional antigen-presenting cells (APCs), which express high levels of the major histocompatability complex class II (MHC-II) molecule and link innate and adaptive immune responses by presenting endogenous and exogenous antigens to T cells. They reside in low numbers throughout the peripheral tissues of the body and in more concentrated numbers within secondary lymphoid tissues such as the lymph nodes and spleen, as well as in specialized lymphoid tissues associated with the gut, the lungs, and the liver. The DC network within the body plays an important role in host defense against pathogens and cancer immunosurveillance, and is critical for maintaining self-tolerance and the prevention of autoimmunity (Banchereau et al., 2000;Koltsova and Ley, 2011). A growing literature suggests that DCs play a key role in the establishment of pro-atherogenic immune responses within the artery wall (Galkina and Ley, 2009;Niessner and Weyand, 2010;Koltsova and Ley, 2011), and, as a result, these enigmatic cells will be discussed at greater depth later in this Chapter.

Natural killer cells

NK cells have been identified in both early and advanced atherosclerotic lesions in humans and mice (Galkina and Ley, 2009). Of note, NK cells are capable of secreting large amounts of the pro-atherogenic cytokine IFNγ, especially following exposure to interferon-alpha (IFNα), IL-12, or TNFα, all of which are produced by multiple cell types present within atherosclerotic plaques. As their name suggests, NK cells also possess a potent cytotoxic ability and are capable of killing antibody-tagged cells (ADCC) as well as those expressing ligands for various activating NK cell receptors through the release of cytotoxic granules. The role of NK cells in atherosclerosis is poorly understood due to a lack of good NK cell deficient mouse models (Galkina and Ley, 2009). Studies in several different mouse models that lack fully functional NK cells have demonstrated mixed results, showing that defective NK cell function can increase or reduce atherosclerosis depending on the study (Schiller et al., 2002;Whitman et al., 2004).

Neutrophils

Neutrophils are short-lived phagocytic innate immune cells that belong to a family of polymoprhonuclear cells called granulocytes. Leukocytosis and especially neutrophilia are independent risk factors for coronary heart disease (Galkina and Ley, 2009). Despite this link, the functional role of neutrophils in atherosclerosis has not been studied extensively. However, several studies have shown that neutrophils accumulate in atherosclerotic lesions in $ApoE^{-/-}$ or $LDLR^{-/-}$ mice (van Leeuwen et al., 2008;Yvan-Charvet et al., 2008;Zernecke et al., 2008), as have neutrophil-derived inflammatory mediators such as myeloperoxidase (MPO), α-defensins, and azurocidin (Soehnlein and

Weber, 2009). It has recently been shown that neutrophil-derived inflammatory mediators and chemokines play an important role in the recruitment of monocytes, macrophages, and DCs, and help regulate phagocytic capacity and cytokine release in these cells (Soehnlein et al., 2008;Soehnlein et al., 2009;Soehnlein and Lindbom, 2010). It was recently shown that neutrophilia occurs in response to hypercholesterolemia in $LDLR^{-/-}$ mice and that neutrophils enter nascent atherosclerotic lesions and contribute to early lesion development (Drechsler et al., 2010).

1.3 DC Function in Atherosclerosis

A pro-atherogenic role has been described for DCs in atherosclerosis that is intimately tied to their ability to uptake subintimal lipids and drive pro-atherogenic T-cell responses in the artery wall. Modified lipoproteins such as oxLDL accumulate in the arterial wall. These lipids are taken up by resident vascular DCs (vDCs), which become the first foam cells and initiate early lesion development (Paulson et al., 2010). DCs and T-cells both accumulate in developing atheroma (Hansson et al., 1989;Ross, 1999;Galkina et al., 2006;Jongstra-Bilen et al., 2006;Alberts-Grill et al., 2012), where uptake of oxLDL induces immune activation of DCs by stimulating expression of costimulatory molecules such as CD40, CD80, and CD86 and promoting their ability to prime $CD4^+$ T-cells (Alderman et al., 2002;Packard et al., 2008). The resulting LDL-specific, $CD4^+$ T-cells are capable of enhancing atherosclerosis when adoptively transferred into naïve recipient mice (Zhou et al., 2006;Hermansson et al., 2010). In humans, clonally expanded $CD4^+$ T-cells reactive to autoantigens like oxLDL or heat-shock protein-60 (HSP60) have been found in both the plaques and circulation of patients where they correlate positively with

plaque inflammation and the incidence of clinically active disease (Stemme et al., 1995;Liuzzo et al., 2000;Paulsson et al., 2000;Hansson, 2005;Weber et al., 2008). However, save for oxLDL, specific reactive epitopes for atherosclerosis-associated autoantigens have yet to be mapped (Hansson and Hermansson, 2011). Adoptive transfer of bone marrow-derived DCs loaded with LDL oxidized by malondialdehyde treatment similarly aggravates atherosclerosis in mice (Hjerpe et al., 2010), providing further direct evidence that DCs can promote pro-atherogenic $CD4^+$ T-cell responses in the plaque. Lesional $CD4^+$ T-cells have been shown to co-localize with DCs in the shoulder regions of plaques as well as in the adventitia of arteries (Nakajima et al., 2002;Hansson, 2005;Niessner et al., 2006;Sato et al., 2006;Erbel et al., 2007), suggesting that these cells interact locally within the plaque during atherogenesis. The requirement for DCs in the immunopathology of atherosclerosis is also supported by evidence from a surgical plaque regression model of murine aortic arch, which showed that DC emigration occurs concomitantly with lesion regression (Reis et al., 2001;Llodra et al., 2004;Randolph, 2008), suggesting that lesional DC numbers correspond with disease severity.

The evidence gathered thus far points to MHC-II-dependent DC-$CD4^+$ T-cell interactions as an essential step driving T-cell pathology during atherogenesis. For instance, disruption of DC-$CD4^+$ T-cell interaction by antibody blockade of MHC-II or by genetic disruption of the MHC-II antigen processing and presentation pathway inhibits T-cell pathogenesis and leads to reduced IFNγ production and atherosclerosis development (Sukhova et al., 2003;Rodgers et al., 2006;Sato et al., 2006;Sun et al., 2010).

Furthermore, activated DCs have been shown to actively recruit T-cells into lesions via the secretion of IL-12 (Zhang et al., 2006).

DCs also strongly influence Treg responses, making them important negative regulators of inflammation as well. For instance, constitutive DC ablation produces a spontaneous systemic and fatal autoimmune disease, characterized by excessive Th1 and Th17 T-cell responses in peripheral tissues (Ohnmacht et al., 2009), confirming an essential role for DCs in maintaining tissue homeostasis and immune tolerance. Numerous studies have also demonstrated that the DC-mediated immunization against atherosclerosis-related autoantigens such as oxLDL, HSP-60, and HSP-65 inhibits atherosclerosis development via B-cell- and Treg-dependent mechanisms (George et al., 1998;Harats et al., 2002;Maron et al., 2002;van Puijvelde et al., 2007;Nilsson et al., 2009;Habets et al., 2010). Thus, it appears that DCs play a dual role in mediating both inflammatory and tolerogenic adaptive immune responses in the artery wall, making it essential to explore DC function in the vasculature in order to achieve a clear understanding of atherosclerosis and the role of the immune system in vascular biology.

1.4 Characterizing Vascular DC Subsets

DCs play an important role in controlling inflammation in the artery wall. However, understanding the mechanisms by which they exert this control has been impeded by the phenotypic and functional heterogeneity of these cells, and their similarity to other myeloid cell lineages such as monocytes and macrophages. DCs and macrophages are a heterogeneous group of cells that derive from the myeloid lineage of blood cells

(Geissmann et al., 2010) and vary in phenotype and function and also vary from tissue to tissue (Pulendran, 2004;Koltsova and Ley, 2011). Together, DCs and macrophages constitute the largest immune cell population found in the atherosclerotic plaque, and are present during all stages of the disease. However, distinguishing macrophage and DC subsets in the vascular wall has proven difficult as several vDC subsets have been described which express classic monocyte/macrophage markers such as CD11b, F4/80, and Ly-6C (Hume, 2008;Randolph, 2008;Choi et al., 2011;Koltsova and Ley, 2011;Weber et al., 2011). Additionally, monocytes and macrophages have been shown to upregulate the classical DC marker CD11c under hypercholesterolemic conditions (Wu et al., 2009;Gower et al., 2011), and MHC-II expression during inflammation (Liu et al., 2009;Koltsova and Ley, 2011). Thus, extensive phenotypic and functional characterization is required in order to distinguish vDCs from macrophages. While both $CD11c^+$ and $MHC\text{-}II^+$ macrophage subsets have been identified in atherosclerotic plaques, arterial wall leukocytes that co-express CD11c and MHC-II bear a distinct 'dendritic' morphology and are much more efficient activators of T-cells than $MHC\text{-}II^+$ macrophages, suggesting these populations are bona-fide DCs (Choi et al., 2011;Koltsova and Ley, 2011). The phenotypic and functional characterization of the various plaque resident macrophage populations has been fairly well studied and reviewed elsewhere (Woollard and Geissmann, 2010;Ley et al., 2011). However, efforts to phenotype and functionally define vDC subsets have been inconsistent. Recent advances in isolating vascular immune cells now allow the extensive phenotyping of cells using flow cytometry techniques (Galkina et al., 2006;Choi et al., 2011;Weber et al., 2011;Alberts-Grill et al., 2012). As such, there is now a pressing need to establish basic standards for

the phenotypic and functional characterization of novel vDC subsets. So far, several distinct vDC populations have been identified that localize to specific regions of aorta (Millonig et al., 2001;Choi et al., 2009;Cybulsky and Jongstra-Bilen, 2010;Niessner and Weyand, 2010;Choi et al., 2011;Weber et al., 2011) (Table 1.1). The following sections will discuss these vDC subsets in depth, and summarize the current knowledge of their phenotype, origin, and function in atherosclerosis.

Table 1.1. *Phenotype and function of vDCs*

	$CD103^+$ cDCs	**Mo-DCs**	**TiP-DCs**	**$CCL17^+$ DCs**	**Plasmacytoid DCs**
Phenotype	$CD11c^+$ $MHC\text{-}II^+$ $CD8\alpha^{+/-}$ $DEC205^-$ $CD11b^-$ $33D1^-$ $CD103^+$ $CD14^-$ $F4/80^-$ $CD115^-$ $Ly6C^-$ $PDCA\text{-}1^-$ Siglec H^- $CD86^+$ $CD40^+$ $B220^-$	$CD11c^+$ $MHC\text{-}II^+$ $CD11b^+$ $33D1^+$? $CD103^-$ $CD14^+$ $F4/80^+$ $CD115^+$ $Ly6C^{+/-}$ $PDCA\text{-}1^-$ Siglec H^- $CD86^+$ $CD40^+$ $B220^-$	$CD11c^{int}$ $MHC\text{-}II^+$ $DEC205^-$ $CD11b^{int}$ $CD103^{lo}$ $CD115^+$ $Ly6C^+$ $PDCA\text{-}1^-$ Siglec H^- $CD86^{lo}$ $CD40^+$ $B220^-$	$CD11c^+$ $MHC\text{-}II^+$ $CD8\alpha^-$ $CD11b^+$ $CD103^-$ $F4/80^-$ $CD115^-$? $PDCA\text{-}1^-$ Siglec H^- $CD86^+$ $CD40^+$ $B220^-$	$CD11c^{lo}$ $MHC\text{-}II^{lo}$ $CD8\alpha^{+/-}$ $DEC205^{+/-}$ $CD11b^-$ $33D1^-$ $CD103^-$ $CD115^-$? $PDCA\text{-}1^+$ Siglec H^+ $CD86^-$ $CD40^-$ $B220^+$
Precursor	Pre-DC	monocyte	monocyte	?	Pre-DC
GF dependency	Flt3L	M-CSF	M-CSF	?	
Resident?	Yes	Yes	?	No	Yes
Localization	Intima	Intima	?	Intima Adventitia	Intima Adventitia
<u>Function</u>					
Ag capture	+	+	+	+	+
Ag processing	+	+	+	+	?
T-cell priming	+	+	+	+	-/?
IL-12 production	?	+			
IL-10 production	?	-/?	?	?	?
CCL17 production	-	-	-	+	-
IFNα production	-	-	-	-	+
TNFα production	?	?	+	?	?
NO synthesis	-	?	+	-	-

Monocyte-derived DCs

The most abundant DC subset found to reside in mouse aorta is the monocyte-derived DC (Mo-DC), although further study is required to determine the presence of these cells in human vessels. Mo-DCs reside primarily within the intima of atheroprone vascular regions in healthy adult aorta and accumulate in substantial numbers during atherosclerosis. In addition to the classical DC markers of CD11c and MHC-II, these cells notably express the common monocyte markers CD11b, F4/80, and CD14, and selectively react to antibodies against DC-SIGN (Cheong et al., 2010a;Cheong et al., 2010b;Choi et al., 2011). Like monocytes, macrophages, and other monocyte-derived cells, Mo-DCs express CX_3-chemokine receptor 1 (CX_3CR1) and lack expression of the gut DC marker, CD103. Mo-DCs require the hematopoietic growth factor, macrophage-colony stimulating factor (M-CSF) for their differentiation, proliferation, and survival, and are absent from aorta in M-CSF-deficient *op/op* mice (Choi et al., 2011). While very similar to macrophages both developmentally and phenotypically, mixed leukocyte reaction studies demonstrated that isolated aortic Mo-DCs can activate $CD4^+$ T-cells as efficiently as splenic DCs, revealing them as true DCs (Choi et al., 2011).

Vascular Mo-DCs, expressing CD11c, MHC-II, and the M-CSF receptor, CD115, may play an important role in the phagocytosis and clearance of apoptotic cells from vascular intima during steady state conditions or lesion regression (Llodra et al., 2004;Randolph, 2008), although a more recent study clearly demonstrates that these cells lack the phagocytic capacity of monocytes or macrophages (Choi et al., 2011). However, this same study also showed that Mo-DCs are quite capable of capturing antigen and

presenting it to naïve T-cells (Choi et al., 2011). Mo-DCs have also been shown to emigrate from atherosclerotic plaques under normocholesterolemic conditions and home to draining lymph nodes via the efferent lymphatics (Llodra et al., 2004), suggesting that Mo-DC may prime pro-atherogenic $CD4^+$ T-cell responses by carrying vascular antigens back to secondary lymphoid tissues and presenting them to antigen-specific T-cells (Pugh et al., 1983;Huang et al., 2000). However, Mo-DC emigration is disrupted in hypercholesterolemic $ApoE^{-/-}$ mice, leading to rapid intimal Mo-DC accumulation and foam cell formation (Llodra et al., 2004;Paulson et al., 2010). One study showed that hypercholesterolemia severely inhibits DC migration, while stimulating DC maturation and local inflammation in peripheral tissue sites such as the skin (Angeli et al., 2004). These data, along with more recent data showing that Mo-DCs are poorly phagocytic (Choi et al., 2011), suggest that under pro-atherogenic conditions such as hyperlipidemia, Mo-DC may enter the vascular intima as phagocytic monocytes where they uptake lipid, differentiate into Mo-DC, and present antigen locally to oxLDL-specific $CD4^+$ T-cells. This concept is supported by the fact that oxLDL can induce monocyte differentiation into phenotypically mature DCs, that secrete IL-12 and effectively stimulate T-cells (Perrin-Cocon et al., 2001). However, up until now, we have lacked the appropriate animal models required to confirm whether or not this scenario is true, leading to contention within the field as to whether pro-atherogenic $CD4^+$ T-cell priming occurs within secondary lymphoid tissues or locally within the artery wall.

It is also unclear whether Mo-DCs represent a single DC subset as currently defined. Work in gut immunobiology has uncovered a specialized, inflammatory DC subset that

expresses TNFα and inducible nitric oxide synthase (iNOS) (Tip-DC), and bears many phenotypic similarities with Mo-DCs. Tip-DCs reside within the gut-associated lymphoid tissues (GALT) (Tezuka et al., 2007), where they are involved in mediating IgA production in the gut (Tezuka and Ohteki, 2010). Phenotypically, Tip-DCs have been described $iNOS^{+}CD11c^{int}CD11b^{+}MHC\text{-}II^{+}Ly6C^{+}CD103^{low}$ cells which were initially identified by their capacity to secrete TNFα and the vasodilator, nitric oxide (NO) in response to *Listeria Monocytogenes* infection (Serbina et al., 2003;Tezuka and Ohteki, 2010). While Tip-DCs have not yet been identified from vascular tissues in mice or humans, their phenotype suggests they arise from $Ly6C^{+}$ inflammatory monocytes (Tezuka and Ohteki, 2010). Increased levels TNFα and NO are both found in atherosclerotic plaques (Chiu and Chien, 2011;Alberts-Grill et al., 2012), making the Tip-DC an interesting candidate for mediating early inflammatory responses during atherogenesis.

$CD103^{+}$ classical DCs

Classical $CD11c^{+}MHC\text{-}II^{+}CD103^{+}$ DCs ($CD103^{+}$ cDCs) represent a novel resident vascular DC subset with a possible immunoregulatory role in atherosclerosis. They are phenotypically distinct from Mo-DCs in that they lack expression of the Mo-DC markers CD11b, 33D1, and DEC209, as well as CX_3CR1, a chemokine receptor common to most monocyte-derived cells (Choi et al., 2011). $CD103^{+}$ cDCs differentiate from the common dendritic precursor cell (CDP) and respond to the CDP growth factor fms-like thyrosine kinase 3 (Flt3) ligand (Naik et al., 2006;Onai et al., 2006;Liu et al., 2009). While both $CD103^{+}$ cDC and Mo-DC are potent activators of T-cells, disruption of Flt3-Flt3 ligand

signaling in $Flt3^{-/-}$ mice leads to ablation of $CD103^{+}$ cDC while leaving M-CSF-dependent Mo-DC intact within aorta, showing independent regulation of two distinct DC populations. Loss of this Flt3 ligand-dependent DC population results in the marked loss of functional Treg populations in the peripheral and secondary lymphoid tissues, suggesting a central role for $CD103^{+}$ cDCs in priming and maintaining Tregs, maintaining tissue homeostasis, and preventing autoimmunity (Choi et al., 2011). In atheroprone $ApoE^{-/-}$ mice, Flt3 deficiency aggravates atherosclerosis development, causes Treg deficiency in aorta, increases pro-inflammatory cytokine production (IFNγ, TNFα), and decreases anti-inflammatory cytokine production (IL-10) (Choi et al., 2011). While these data would suggest that $CD103^{+}$ cDCs preferentially present antigen to arterial wall Tregs, there is of yet no direct evidence showing that $CD103^{+}$ cDCs and Tregs co-localize within atherosclerotic plaques.

Plasmacytoid DCs

A third, native DC subset, the plasmacytoid DC (pDC), has been identified which resides primarily in the arterial adventitia (Niessner and Weyand, 2010), although they are also found in the shoulder regions of atherosclerotic lesions in humans (Yilmaz et al., 2004) and mice (Jongstra-Bilen et al., 2006), clustered with $CD11c^{+}MHC\text{-}II^{+}$ DCs. Unlike other $CD11c^{+}MHC\text{-}II^{+}$ DCs, pDCs express only low levels of both CD11c and MHC-II, and express the markers PDCA-1 and sialic acid-binding immunoglobulin-like lectin H (Siglec-H) in mice (Blasius et al., 2006). In humans pDC are identified by expression of IL-3 receptor-α chain (CD123) (Grouard et al., 1997) and blood DC antigen 2 and 4 (BDCA-2 and BDCA-4) (Dzionek et al., 2001). In contrast to the previously described

vDC subsets, pDCs are poor activators of T-cells (Niessner and Weyand, 2010). Instead, pDCs provide a potent defense against viral and some microbial infections through their unique ability to produce large amounts of potent pro-inflammatory cytokines termed type I interferons, especially IFNα □□□(Kadowaki et al., 2000;Kadowaki et al., 2001;Ito et al., 2006). IFNα has been shown to enhance atherosclerosis in mice (Kadowaki et al., 2000;Levy et al., 2003;Doring et al., 2012), by amplifying the inflammatory capacity of several different cell types present during atherosclerosis. In addition to inducing the maturation of $CD11c^+$ DCs (Ito et al., 2001), and skewing T-cells towards the pro-inflammatory Th1 effector phenotype (Kadowaki et al., 2000), IFNα□ stimulates IFNγ production and upregulation of the death receptor ligand, TNF-related apoptosis inducing ligand (TRAIL) in T-cells, resulting in T-cell-mediating killing of vascular smooth muscle cells, which potentially contributes to plaque instability (Niessner et al., 2006). Furthermore, exposure of $CD11c^+MHC\text{-}II^+$ DCs to IFNα induced the upregulation of toll-like receptor 4 (TLR4), sensitizing them to bacterial lipopolysaccharide (LPS) and modified self-lipid antigens (oxLDL), and increased production of the pro-inflammatory cytokines TNFα, IL-12, and IL-23 (Niessner et al., 2006).

A second, atheroprotective pathway has been identified in pDCs which relies on the synthesis and release of Indoleamine 2,3-dioxygenase (IDO) in response to interferon signaling (Puccetti and Grohmann, 2007;Johnson et al., 2009). IDO release from pDCs has been shown to facilitate the differentiation of Tregs from naïve $CD4^+$ T-cells and can control effector T-cell responses by influencing their tryptophan metabolism (Puccetti

and Grohmann, 2007;Johnson et al., 2009), which in light of the pro-atherogenic effects of pDC-produced IFNα, implies a more complex, homeostatic role for pDCs in regulating atherosclerosis. Indeed, multiple pDC depletion studies have produced similarly conflicting results. Daissermont *et al.* reported that pDC depletion aggravated atherosclerosis development and led to increased T-cell proliferation in atherosclerotic lesions (Daissormont et al., 2011). Further work by Nakajima *et al.*, suggests that this atheroprotective effect of pDCs is IDO-dependent, by showing that increasing IDO expression by oral administration of eicosapentaenoic acid, inhibited DC maturation, resulted in diminished lesional effector T-cell numbers, and substantial lesion regression (Nakajima et al., 2011). However, a second pDC depletion study found that pDC depletion significantly decreased early lesion development and that specific stimulation of pDCs with type A CpG oligonucleotides led to increased disease (Doring et al., 2012).

CCL17$^+$ DCs

In contrast to the previously described vDC subsets, which are all present in arterial intima or adventitia during steady-state conditions, recent work by Weber *et al.*, (2011) identified a distinct subset of vDCs that are characterized by the expression of the DC-derived chemokine CCL17 (Alferink et al., 2003;Weber et al., 2011). Unlike other vDCs, CCL17$^+$ DCs are absent from the arterial wall during steady-state conditions, but accumulate in the intima and adventitia of atherosclerotic arteries. These cells bear a CD11c$^+$MHC-II$^+$CD11b$^+$ phenotype, but unlike Mo-DCs, do not express CD115 or F4/80. Like other mature DC subsets, they display increased expression of costimulatory markers CD40, CD80, and CD86, suggesting they are capable of activating T-cells within

the plaque. Indeed, multiphoton microscopy studies show that $CCL17^+$ DCs co-localize with $CD4^+$ T-cells in atherosclerotic lesions and form distinct immune synapses with them (Weber et al., 2011). While it is unknown whether or not $CCL17^+$ DCs activate pro-atherogenic T-cells *in vivo*, they were shown to disrupt Treg homeostasis in a CCL17-dependent manner. Disruption of this anti-Treg function in CCL17-deficient mice led to reduced atherosclerosis and decreased accumulation of macrophages and T-cells within lesions. Additionally, Treg presence and expansion was increased within lesions of CCL17-deficient mice (Weber et al., 2011). Together, these data establish a clear role for $CCL17^+$ DCs in disrupting vascular Treg homeostasis and mediating $CD4^+$ T-cell homing into atherosclerotic lesions.

1.5 DC Function in Vascular Homeostasis

Role of d-flow in EC activation and lipid/DC accumulation

Atheroprone regions of the vasculature differ from athero-resistant regions in the physiological blood flow patterns and hemodynamic forces they are exposed to, with atherosclerosis preferentially occurring in branches and curvatures where blood flow is disturbed and exerts nonuniform and irregular shear forces on the vascular endothelium (Chiu and Chien, 2011). D-flow results in several key changes in endothelial cell biology and function that alter the normal inflammatory status of the endothelium, allowing these regions to uniquely acquire resident vDC and macrophage populations (Jongstra-Bilen et al., 2006;Choi et al., 2009;Paulson et al., 2010;Chiu and Chien, 2011). There is extensive evidence showing that exposure to d-flow induces EC inflammation, leading to the upregulation of ICAM-1 and VCAM-1 (Walpola et al., 1995;Endres et al.,

1997;Nakashima et al., 1998;Iiyama et al., 1999;Suo et al., 2007;Nam et al., 2009), which are essential for the recruitment of vDCs into the arterial intima under steady-state and disease conditions (Cybulsky et al., 2001;Jongstra-Bilen et al., 2006). *In vivo* studies of d-flow show numerous changes in EC gene and microRNA expression in response to experimentally-induced d-flow in carotid artery (Ni et al., 2010;Ni et al., 2011). In addition to upregulation of ICAM-1 and VCAM-1, d-flow also induces expression of various chemotactic molecules necessary for early leukocyte homing to the arterial wall. These include CCL2 (MCP-1), which is responsible for recruitment of monocytes and some DCs to the arterial wall (Serbina and Pamer, 2006;Tsou et al., 2007), CCL9, a chemokine involved in $CD4^+$ T-cell trafficking (Hara et al., 1995;Mohamadzadeh et al., 1996) and in attracting $CD11b^+CCR1^+$ DCs to the gut (Zhao et al., 2003), CXCL16, which has been implicated in recruiting T-cells, DCs, and macrophages into atherosclerotic lesions (Galkina et al., 2007), and CXCL12, which is expressed in human and mouse atherosclerotic lesions, but whose role in atherosclerosis remains unclear (Kraaijeveld et al., 2007). In addition to the induction of chemokine and adhesion molecule expression, d-flow also disrupts vascular homeostasis in several other ways important to the development of atherosclerosis, increasing endothelial permeability to macromolecules such as lipoproteins, increasing EC and smooth muscle cell (SMC) turnover and proliferation, promoting EC expression of pro-coagulatory molecules such as von Willebrand factor (vWF) and tissue factor (TF), which leads to enhanced platelet aggregation and fibrin deposition (Lerman et al., 1998;Gimbrone et al., 2000;Bonetti et al., 2003;Chiu and Chien, 2011). Chronic, low-level inflammation persists in flow-disturbed regions of the vasculature including endothelial ICAM-1 and VCAM-1

expression, intimal DC accumulation, and adventitial macrophage accumulation (Jongstra-Bilen et al., 2006;Choi et al., 2009;Choi et al., 2011), suggesting that d-flow "primes" the vessel wall for sustaining chronic inflammation. Furthermore, experimental induction of d-flow in the athero-protected left common carotid artery in combination with hypercholesterolemic diet induces the infiltration of a wide array of leukocytes into the intima including T-cells, DCs, NK cells, neutrophils, and macrophages in as little as 4 days, while laminar-shear exposed regions like the right common carotid artery fail to accumulate leukocytes (Alberts-Grill et al., 2012). Together, these data suggest that d-flow plays an active role in driving vascular inflammation by triggering endothelial cell inflammation and attracting leukocytes into the artery wall. However, the slow progression of atherosclerosis in spite of flow-induced inflammation suggests the presence of some homeostatic mechanisms to control inflammation.

Role of DCs in vascular homeostasis

Much of the discussion in the literature on resident vDCs and macrophages has focused on their pro- or anti-atherogenic potential. However, resident leukocyte populations play a critical role in the homeostasis of numerous tissues in the body including the gut, liver, and lungs (Tezuka and Ohteki, 2010). However, the role that resident vDCs and macrophages play in maintaining vascular homeostasis, and how these functions fail during the early stages of atherogenesis is poorly understood. The majority of resident vDCs reside within the arterial intima and present either a Mo-DC ($CD11c^{+}$MHC-$II^{+}CD14^{+}CD11b^{+}F4/80^{+}$DC-$SIGN^{+}$) or $CD103^{+}$ cDC ($CD11c^{+}$MHC-$II^{+}CD103^{+}CD11b^{-}$) phenotype (Choi et al., 2009;Choi et al., 2011). Many of these cells also take up

extracellular lipid and express the foam cell marker, CD68, an event which can precede intimal macrophage accumulation, although how commonly this occurs under steady-state conditions is not well known (Galkina and Ley, 2009;Cybulsky and Jongstra-Bilen, 2010;Paulson et al., 2010). While there is some data to suggest that resident vDCs of the $CD103^+$ cDC phenotype may serve an anti-inflammatory, homeostatic role during atherogenesis (Choi et al., 2011), their role under steady state conditions has also not been established. However, $CD103^+$ cDCs are also known to reside within the intestinal mucosa, where they induce Tregs and other immune-suppressive $CD4^+$ T-cells (Coombes et al., 2007;Sun et al., 2007). Several lines of evidence suggest that $CD103^+$ cDC-derived retinoic acid (RA) is responsible for Treg induction in the intestines (Tezuka and Ohteki, 2010), although more work is needed to determine whether $CD103^+$ cDC-derived RA plays an important role in promoting vascular Treg responses (Rhee et al., 2012).

Mechanisms by which DCs break homeostasis during atherogenesis

The mechanisms by which vDC homeostasis is disrupted during atherogenesis and how this disruption is related to disturbed flow and vascular endothelial responses are poorly understood. However, several major theories have been proposed to explain what goes wrong in the vessel wall during atherogenesis. Based on studies in mice, Cybulsky and Jongstra-Bilen (2010) proposed that DC homeostasis breaks down due to DC uptake of lipid. They showed that prior to endothelial activation and monocyte infiltration, resident intimal DCs uptake lipid, rapidly proliferate, and become the first foam cells in nascent lesions under hypercholesterolemic conditions (Cybulsky and Jongstra-Bilen, 2010;Paulson et al., 2010). In support of this theory, Randolph (2008) proposed that DC

trafficking to and from vascular tissues occurs during steady-state conditions. Based on aortic transplant studies in mice, she showed that under hypercholesterolemic conditions, DC emigration out of the vessel wall breaks down, leading to rapid vDC accumulation, which is resolved during lesion regression when large numbers of DCs migrate into draining lymph nodes (Llodra et al., 2004;Randolph, 2008). As described above, d-flow induces increased permeability to circulating lipids and other studies have shown that modified lipoproteins such as oxLDL can trigger DC activation in a TLR4-dependent manner, providing a feasible link between d-flow and atherosclerosis development. However, this lipid-centered theory does not explain how innate and adaptive immune responses against self- and modified lipid-antigens are initiated and potentiated during atherogenesis (Hansson and Hermansson, 2011).

An alternate theory posits that in aggregate, the direct and indirect effects of infection with pathogenic organisms promote vascular inflammation and contribute to the failure of vascular tissue homeostasis over time (Epstein et al., 2000;Elkind, 2010;Elkind et al., 2010). Numerous pathogenic organisms have been linked to atherosclerosis in both clinical and animal studies [reviewed in (Rosenfeld and Campbell, 2011)]. In one clinical study testing the effect of pathogen burden on the incidence of coronary artery disease (CAD), over 75% of CAD patients showed immunity against 3 of the 5 CAD-linked pathogens tested (cytomegalovirus, *C. pneumoniae*, hepatitis A virus, and herpes simplex virus type 1 or 2) and disease incidence increased with disease burden independent of traditional risk factors (Zhu et al., 2000). Furthermore, the link between infectious disease and atherosclerosis is supported by evidence from large population-

based studies, which have found molecules specific to at least 20 different pathogenic microorganisms present in the plaques of large subsets of the patient population, including live, viable organisms for at least 3 (Rosenfeld and Campbell, 2011). Numerous studies in experimental mouse models have found that infection with several different pathogens, such as *P. gingivalis*, *C. pneumoniae*, and *H. pylori*, accelerates atherosclerosis, leading to increased lipid and leukocyte accumulation in lesions and increased pro-inflammatory cytokine production (Hu et al., 1999;Moazed et al., 1999;Liu et al., 2000;Blessing et al., 2001;Burnett et al., 2001;Rothstein et al., 2001;Ezzahiri et al., 2002;Li et al., 2002;Mach et al., 2002;Erkkila et al., 2004;Ayada et al., 2007;Ford et al., 2007;Koizumi et al., 2008;Champagne et al., 2009;Gitlin and Loftin, 2009;Hayashi et al., 2010;Hayashi et al., 2011;Rosenfeld and Campbell, 2011). While the evidence supporting a major role for infectious microorganisms in atherogenesis is hard to ignore, the specific molecular mechanisms of this association have been difficult to piece together into a comprehensive theory of infectious disease, vascular inflammation, and atherosclerosis.

Niessner and Weyand (2010) posited a unified theory linking infection to the disruption of vascular homeostasis in which discontinuous infectious events expose resident vascular DCs to pathogen-derived molecules that serve as danger signals, activating resident DCs and allowing them to initiate pro-atherogenic adaptive immune responses against self- and modified self-antigens present in the arterial wall environment (Niessner and Weyand, 2010). DCs sense pathogen- and injury-related danger signals using a set of specialized transmembrane proteins called toll-like receptors that recognize structurally

conserved molecules derived from viral and microbial pathogens. TLR signaling serves as a crucial checkpoint for DC activation and the initiation of the immune response, making this a key potential regulator of vascular homeostasis (Matzinger, 2007). Stimulation of vascular DCs with TLR ligands (e.g. LPS, CpGs, etc.) induces DC maturation and activation, including the robust expression of costimulatory molecules CD40, CD80, and CD86, which are crucial for the induction of adaptive immune responses (Pryshchep et al., 2008;Niessner and Weyand, 2010). A pro-atherogenic role has been described for TLRs (Frantz et al., 2007). Knockout of MyD88, a signaling molecule downstream of most TLRs, inhibits atherosclerosis (Bjorkbacka et al., 2004). Also, knockout of TLR2, and especially TLR4 inhibits atherosclerosis development in either $ApoE^{-/-}$ or $LDLR^{-/-}$ mice and also reduces circulating levels of IL-12 and MCP-1 (Michelsen et al., 2004;Mullick et al., 2005). TLR4 recognizes bacterial LPS as well as oxLDL, making it a likely pro-inflammatory signaling receptor in atherosclerosis (Alderman et al., 2002;Shen et al., 2008). Meanwhile, TLR2 signaling has been shown to play a role in *C. pnemoniae* accelerated atherosclerosis (Naiki et al., 2008). Furthermore, TLR7, TLR8, and TLR9, which are expressed primarily by pDCs, and recognize nucleic acid motifs derived from bacterial and viral pathogens, may mediate IFNα production in response to viral infection (Niessner and Weyand, 2010). While direct evidence for such a link has yet to be found, viral DNA or RNA from several viruses that infect 80-90% of the human population (i.e., Cytomegalovirus, Hepatitis C, Epstein Barr virus, Herpes simplex viruses, as well as parvoviruses and enteroviruses) have been found in human plaques (Rosenfeld and Campbell, 2011). As described above, IFNα has a strong pro-

atherogenic effect and can sensitize neighboring DCs and T-cells, thus aiding in the disruption of immune tolerance.

Table 1.2. *Effect of genetic knockout models on atherosclerosis*

Knockout Model	Role of Gene	Effect on Atherosclerosis	Reference
IFNγ receptor	Pro-inflammatory cytokine receptor	Decrease	Gupta et al., 1997
TNFα	Pro-inflammatory cytokine	Decrease	Ohta et al., 2005
MyD88	TLR signaling protein	Decrease	Björkbacka et al., 2004
TLR2	Pathogen sensor	Decrease	Mullick et al., 2005
TLR4	LPS, oxLDL, pathogen sensor	Decrease	Björkbacka et al., 2004
CatS	Leukocyte infiltration, matrix degradation, MHC-II-dependent Ag presentation	Decrease	Sukhova et al., 2003
Invariant Chain	MHC-II-dependent Ag presentation	Decrease	Sun et al., 2010
MHC-I	Defect in $CD8^+$ T-cells	Increase	Fyfe et al., 1994
IL-12	Th1 T-cell differentiation/homing	Decrease	Davenport and Tipping, 2003
CCL17	T-cell chemotaxis, inhibits Treg function	Decrease	Weber et al., 2011
VCAM-1	Leukocyte adhesion to endothelium	Decrease	Cybulsky et al., 2001
CX_3CR1	DC/monocyte chemokine receptor	Decrease	Liu et al., 2008
CD1d	Natural killer T-cell deficiency	Decrease	Major et al., 2004
C3	Defective classical and alternative complement	Increase	Buono et al., 2002
C5	Defective terminal complement complex formation	No effect	Patel et al., 2001
Flt3	$CD103^+$ cDC development	Increase	Choi et al., 2011

1.6 Summary of Vascular DC Function

From the data accumulated thus far, it is clear that DCs play a complex and essential role in the maintenance of vascular tissue homeostasis under steady-state conditions in addition to mediating the balance between pro-atherogenic Th1 and Th17 T-cells and atheroprotective Tregs during atherogenesis. These opposing functions are mediated by phenotypically distinct subsets of vascular DCs, with $CD103^+$ resident vascular cDCs playing a protective role via their ability to promote Tregs in the artery wall, and infiltrating $CCL17^+$ DCs, which disrupt vascular Treg homeostasis in a CCL-17-dependent manner. Meanwhile, Mo-DCs represent a numerically dominant vDC subset that may be responsible for priming latent, pro-atherogenic T-cell responses under normocholesterolemic conditions by carrying vascular antigens to the secondary lymphoid tissues and presenting them to T-cells. These cells are likely to further contribute to atherogenesis by rapidly accumulating within vascular intima and differentiating into foam cells under hypercholesterolemic conditions.

However, like pDCs, Mo-DCs likely represent phenotypically and functionally diverse vDC subsets with the potential to push vascular inflammation in either direction. As such, a more mature understanding of the heterogeneity of vDC phenotype and function will require further study in order to rigorously satisfy certain phenotypic and functional criteria when describing new vDC subsets (Table 1.3). Furthermore, while some of the chemokines/chemokine receptors responsible for DC homing into vascular tissues have already been described, the finer points of how regional blood flow dynamics and vascular physiology govern vDC function in healthy and diseased arteries is still poorly

understood. In particular, the role of d-flow in controlling the trafficking and function of various vDC subsets, and immune cells as a whole, has yet to be determined in a controlled experimental model *in vivo*.

Table 1.3. *Salient features necessary for the proper identification and characterization of vDC subsets*

1. Extensive surface phenotyping of DC and monocyte/macrophage markers. CD11c, MHC-II, 33D1, CD11b, PDCA-1, Siglec H, CD8a, DEC205, DC-SIGN, CD103, F4/80, CD115, CD14, CD68, CD1d, langerin (CD207)
2. Expression of inducible markers of DC maturation. CD40, CD80, CD86, CD83
3. Chemokine receptor expression profiles. CCR2 (monocytes), CCR4 (macrophages), CCR5 (macrophages), CCR6 (immature splenic DCs), CCR7 (mature DCs), CXCR1 (monocytes), CXCR3 (pDCs), CX_3CR1 (monocytes, DCs)
5. TLR expression profiles. TLR2 (monocyte/macrophages, DCs), TLR3 (DCs), TLR4 (monocyte/macrophages, DCs), TLR9 (pDCs)
4. Cytokine/chemokine expression profiles. TNFα, IL-10, IL-23, CCL17, CCL21, CCL19, IFNg, IFNa, TGF-b, IL-6, IL-12
5. Expression of other important secreted metabolites/factors. IDO, retinoic acid (RA), iNOS, nitric oxide (NO)
6. DC-specific morphological characteristics • Exhibit classic, stellate, 'dendritic' morphology
7. DC-specific functional characteristics • Potent activation of naïve, effector, and memory T-cells • Promotion of anti-atherogenic Treg/Th2 responses vs. pro-atherogenic Th1/Th17 responses

1.7 Partial Carotid Ligation Model of Atherosclerosis

The majority of atherosclerosis research in animal models has been performed by examining the spontaneous development of atherosclerosis in animals susceptible to atheroma formation (Jokinen et al., 1985). Mouse models have proven particularly useful in the study of atherosclerosis as $ApoE^{-/-}$ or $LDLR^{-/-}$ mice develop plaque in focal, naturally flow-disturbed regions of aortic sinus or aortic arch after several months of cholesterol rich diet (Paigen et al., 1987;Zadelaar et al., 2007). Unfortunately, the relatively long disease latency in these models makes it difficult to conduct sensitive kinetic studies. Furthermore, it is technically difficult to apply extensive RNA-based genomics approaches in these models because they only develop plaques in small, focal regions of the vasculature.

To overcome this issue we used a novel partial carotid ligation model of atherosclerosis in the mouse to examine flow-dependent accumulation of vDCs and other immune cells in the artery wall during atherogenesis. In contrast to spontaneous mouse models of atherosclerosis, we recently showed that partial ligation of mouse carotid artery causes d-flow with characteristic low and oscillatory wall shear stress, leading to lipid-laden plaque development in hypercholesterolemic $ApoE^{-/-}$ mice in only 2 weeks (Nam et al., 2009). Using this model, we have shown that disturbed flow induces broad changes in the gene expression profile of ECs within hours to days, with characteristic expression of ICAM-1 and VCAM-1 occuring within 2 days (Nam et al., 2009;Ni et al., 2010;Ni et al., 2011). Impairment of the vascular relaxation response, a key aspect of endothelial dysfunction, occurs within 1 week via mechanisms involving endothelial nitric oxide

synthase (eNOS) uncoupling (Li et al., 2010;Li et al., 2011), and is closely followed by the robust and homogenous formation of atheroma along the entire length of the common carotid artery within 2 weeks (Nam et al., 2009;Li et al., 2010). The atherosclerotic plaques induced in our model exhibit characteristic morphological features of human and murine plaques including lipid-rich necrotic cores, foam cell formation, extracellular lipid crystallization (cholesterol clefts), fibrous cap formation, and intimal, medial, and adventitial hyperplasia which eventually lead to vessel occlusion (Nam et al., 2009) (Fig. 1.1). The accelerated and robust nature of atheroma development in our partial ligation model make it an ideal experimental platform for examining time sensitive mechanisms of vascular inflammation and leukocyte recruitment. Additionally, our model provides an excellent system in which to rapidly test the efficacy of therapeutic interventions in a matter of weeks as opposed to months.

Several other experimental mouse models of d-flow-dependent atherosclerosis have been developed to date. Complete ligation of common carotid artery has been previously used to study atherosclerosis (Kumar and Lindner, 1997;Khatri et al., 2004). However, this model results in non-physiological, no flow conditions within the left common carotid artery (LCA) and may promote confounding endothelial denudation and thrombosis events (Xu, 2004). Alternatively, blood flow patterns in LCA have been modified through the placement of a perivascular cuff around the artery. Cuff placement produces three distinct regions of shear stress, with low shear occurring just proximal to the cuff, high shear within the cuff, and high and oscillatory shear occurring just distal to the cuff (Cheng et al., 2006).

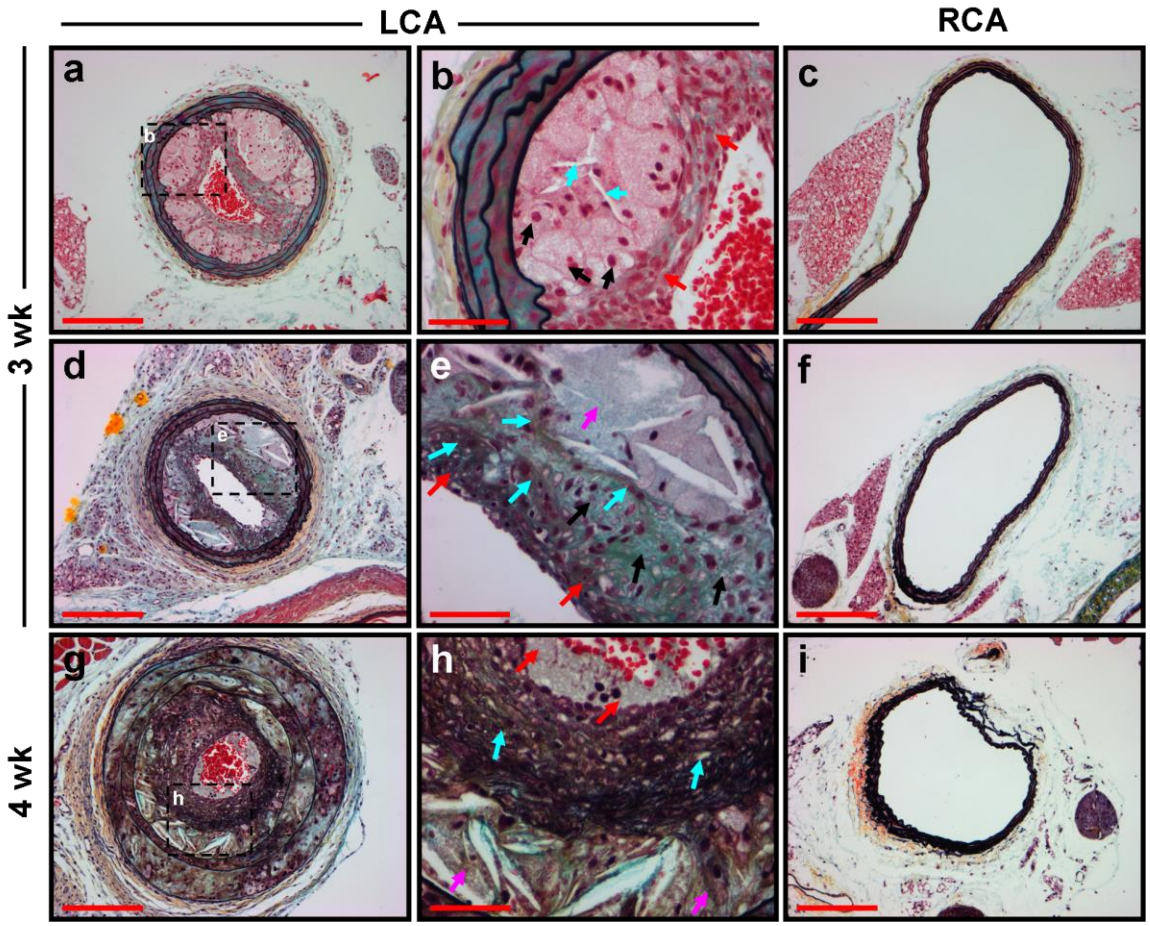

Figure 1.1. Advanced atheroma morphology in 3 and 4 week flow-disturbed atherosclerotic lesions. *Rusell-Movat Pentachrome staining was performed on paraffinized left (LCA) and right (RCA) common carotid artery obtained from ApoE$^{-/-}$ mice 3 (A-F) and 4 (G-I) weeks post-ligation. A, Shows atheroma (10x) with fibrous cap (blue-green stain) and multiple lipid-rich core regions (pink staining). Dashed region in (A) is shown at 40x magnification in (B), which shows fibrous cap (red arrows) overlying foam cells (black arrows) within the lipid-rich core, along with extracellular cholesterol accumulations (cyan arrows). D, Shows fibroatheroma (10x) with a thickened fibrous cap (dark blue-green staining region) and fibrous tissue deposition (light blue-green staining region) covering lipid-rich necrotic core (pale blue staining) with extensive extracellular cholesterol accumulations. Dashed region in (D) is shown at 40x magnification in (E), which shows fibrous cap (red arrows) with fibronectin-rich regions (black arrows) and collagen streaks (cyan arrows), overlying a nuclei-poor necrotic core region (magenta arrow). G, Shows a late, healed atheroma with extensive elastin (black staining) and collagen (brown staining) deposition. Dashed region in (G) is shown at 40x magnification in (H), which shows neointimal formation (red arrows), heavy elastin deposition (cyan arrows), and a collagen rich, healed necrotic core region (magenta arrows). Contralateral disease-free RCA is shown in panels (C), (F), and (I).*

Like partial and complete carotid ligation, perivascular cuff placement induces markedly accelerated atherosclerosis development in $ApoE^{-/-}$ or $LDLR^{-/-}$ mice fed a cholesterol rich diet (Lardenoye et al., 2000;Sasaki et al., 2007), and the model has been recently used to assess the therapeutic efficacy of non-immune polyclonal IgM treatment on atherosclerosis development (Cesena et al., 2012). However, perivascular cuff models suffer some serious drawbacks when compared with partial carotid ligation models. For instance, the cuff model uniquely dissociates the oscillatory and low shear stress components of d-flow (Cheng et al., 2006). Typically, natural d-flow conditions display colocalized low and oscillatory shear stress, making the cuff model somewhat non-physiological. Furthermore, the cuff physically contacts the carotid adventitia, leading to potential vascular injury concerns and preventing the study of flow- and disease-dependent alterations in adventitial biology. In contrast, partial carotid ligation has been established as an effective model of flow reduction in the study of vascular remodeling (Sullivan and Hoying, 2002;Korshunov and Berk, 2003) and atherosclerosis development (Nam et al., 2009;Li et al., 2011;Alberts-Grill et al., 2012).

This dissertation will focus on characterizing d-flow-mediated immune pathogenesis in the partial carotid ligation model. Chapter 2 focuses on the characterization of immune cell infiltration dynamics and inflammatory cytokine expression during the establishment of vascular inflammation and atherosclerotic lesion development in our model. Chapter 3 observes the dynamics of circulating leukocytes in the blood during d-flow-induced atherosclerosis. Chapters 4 and 5 look at the role of DC-T-cell interactions in mediating vascular inflammation and plaque growth.

1.8 References

Abbas, A.K., Murphy, K.M., and Sher, A. (1996). Functional diversity of helper T lymphocytes. *Nature* 383, 787-793.

Ait-Oufella, H., Salomon, B.L., Potteaux, S., Robertson, A.K., Gourdy, P., Zoll, J., Merval, R., Esposito, B., Cohen, J.L., Fisson, S., Flavell, R.A., Hansson, G.K., Klatzmann, D., Tedgui, A., and Mallat, Z. (2006). Natural regulatory T cells control the development of atherosclerosis in mice. *Nat Med* 12, 178-180.

Alberts-Grill, N., Rezvan, A., Son, D.J., Qiu, H., Kim, C.W., Kemp, M.L., Weyand, C.M., and Jo, H. (2012). Dynamic immune cell accumulation during flow-induced atherogenesis in mouse carotid artery: an expanded flow cytometry method. *Arterioscler Thromb Vasc Biol* 32, 623-632.

Alderman, C.J., Bunyard, P.R., Chain, B.M., Foreman, J.C., Leake, D.S., and Katz, D.R. (2002). Effects of oxidised low density lipoprotein on dendritic cells: a possible immunoregulatory component of the atherogenic micro-environment? *Cardiovasc Res* 55, 806-819.

Alferink, J., Lieberam, I., Reindl, W., Behrens, A., Weiss, S., Huser, N., Gerauer, K., Ross, R., Reske-Kunz, A.B., Ahmad-Nejad, P., Wagner, H., and Forster, I. (2003). Compartmentalized production of CCL17 in vivo: strong inducibility in peripheral dendritic cells contrasts selective absence from the spleen. *J Exp Med* 197, 585-599.

Andersson, J., Libby, P., and Hansson, G.K. (2010). Adaptive immunity and atherosclerosis. *Clin Immunol* 134, 33-46.

Angeli, V., Llodra, J., Rong, J.X., Satoh, K., Ishii, S., Shimizu, T., Fisher, E.A., and Randolph, G.J. (2004). Dyslipidemia associated with atherosclerotic disease systemically alters dendritic cell mobilization. *Immunity* 21, 561-574.

Asakura, T., and Karino, T. (1990). Flow patterns and spatial distribution of atherosclerotic lesions in human coronary arteries. *Circ Res* 66, 1045-1066.

Ayada, K., Yokota, K., Kobayashi, K., Shoenfeld, Y., Matsuura, E., and Oguma, K. (2007). Chronic infections and atherosclerosis. *Ann N Y Acad Sci* 1108, 594-602.

Banchereau, J., Briere, F., Caux, C., Davoust, J., Lebecque, S., Liu, Y.J., Pulendran, B., and Palucka, K. (2000). Immunobiology of dendritic cells. *Annu Rev Immunol* 18, 767-811.

Binder, C.J., Hartvigsen, K., Chang, M.K., Miller, M., Broide, D., Palinski, W., Curtiss, L.K., Corr, M., and Witztum, J.L. (2004). IL-5 links adaptive and natural immunity specific for epitopes of oxidized LDL and protects from atherosclerosis. *J Clin Invest* 114, 427-437.

Bjorkbacka, H., Kunjathoor, V.V., Moore, K.J., Koehn, S., Ordija, C.M., Lee, M.A., Means, T., Halmen, K., Luster, A.D., Golenbock, D.T., and Freeman, M.W. (2004). Reduced atherosclerosis in MyD88-null mice links elevated serum cholesterol levels to activation of innate immunity signaling pathways. *Nat Med* 10, 416-421.

Blasius, A.L., Cella, M., Maldonado, J., Takai, T., and Colonna, M. (2006). Siglec-H is an IPC-specific receptor that modulates type I IFN secretion through DAP12. *Blood* 107, 2474-2476.

Blessing, E., Campbell, L.A., Rosenfeld, M.E., Chough, N., and Kuo, C.C. (2001). Chlamydia pneumoniae infection accelerates hyperlipidemia induced atherosclerotic lesion development in C57BL/6J mice. *Atherosclerosis* 158, 13-17.

Bobryshev, Y.V., and Lord, R.S. (1995). Ultrastructural recognition of cells with dendritic cell morphology in human aortic intima. Contacting interactions of Vascular Dendritic Cells in athero-resistant and athero-prone areas of the normal aorta. *Arch Histol Cytol* 58, 307-322.

Bonetti, P.O., Lerman, L.O., and Lerman, A. (2003). Endothelial dysfunction: a marker of atherosclerotic risk. *Arterioscler Thromb Vasc Biol* 23, 168-175.

Boring, L., Gosling, J., Cleary, M., and Charo, I.F. (1998). Decreased lesion formation in CCR2-/- mice reveals a role for chemokines in the initiation of atherosclerosis. *Nature* 394, 894-897.

Buono, C., Come, C.E., Witztum, J.L., Maguire, G.F., Connelly, P.W., Carroll, M., and Lichtman, A.H. (2002). Influence of C3 deficiency on atherosclerosis. *Circulation* 105**,** 3025-3031.

Buono, C., Come, C.E., Stavrakis, G., Maguire, G.F., Connelly, P.W., and Lichtman, A.H. (2003). Influence of interferon-gamma on the extent and phenotype of diet-induced atherosclerosis in the LDLR-deficient mouse. *Arterioscler Thromb Vasc Biol* 23**,** 454-460.

Burnett, M.S., Gaydos, C.A., Madico, G.E., Glad, S.M., Paigen, B., Quinn, T.C., and Epstein, S.E. (2001). Atherosclerosis in apoE knockout mice infected with multiple pathogens. *J Infect Dis* 183, 226-231.

Caligiuri, G., Nicoletti, A., Poirier, B., and Hansson, G.K. (2002). Protective immunity against atherosclerosis carried by B cells of hypercholesterolemic mice. *J Clin Invest* 109, 745-753.

Cesena, F.H., Dimayuga, P.C., Yano, J., Zhao, X., Kirzner, J., Zhou, J., Chan, L.F., Lio, W.M., Cercek, B., Shah, P.K., and Chyu, K.Y. (2012). Immune-modulation by polyclonal IgM treatment reduces atherosclerosis in hypercholesterolemic apoE-/- mice. *Atherosclerosis* 220, 59-65.

Champagne, C., Yoshinari, N., Oetjen, J.A., Riche, E.L., Beck, J.D., and Offenbacher, S. (2009). Gender differences in systemic inflammation and atheroma formation following Porphyromonas gingivalis infection in heterozygous apolipoprotein E-deficient mice. *J Periodontal Res* 44, 569-577.

Cheng, C., Tempel, D., Van Haperen, R., Van Der Baan, A., Grosveld, F., Daemen, M.J., Krams, R., and De Crom, R. (2006). Atherosclerotic lesion size and vulnerability are determined by patterns of fluid shear stress. *Circulation* 113, 2744-2753.

Cheng, C.P., Parker, D., and Taylor, C.A. (2002). Quantification of wall shear stress in large blood vessels using Lagrangian interpolation functions with cine phase-contrast magnetic resonance imaging. *Ann Biomed Eng* 30, 1020-1032.

Cheong, C., Matos, I., Choi, J.H., Dandamudi, D.B., Shrestha, E., Longhi, M.P., Jeffrey, K.L., Anthony, R.M., Kluger, C., Nchinda, G., Koh, H., Rodriguez, A., Idoyaga, J., Pack, M., Velinzon, K., Park, C.G., and Steinman, R.M. (2010a). Microbial stimulation fully differentiates monocytes to DC-SIGN/CD209(+) dendritic cells for immune T cell areas. *Cell* 143, 416-429.

Cheong, C., Matos, I., Choi, J.H., Schauer, J.D., Dandamudi, D.B., Shrestha, E., Makeyeva, J.A., Li, X., Li, P., Steinman, R.M., and Park, C.G. (2010b). New monoclonal anti-mouse DC-SIGN antibodies reactive with acetone-fixed cells. *J Immunol Methods* 360, 66-75.

Chiu, J.J., and Chien, S. (2011). Effects of disturbed flow on vascular endothelium: pathophysiological basis and clinical perspectives. *Physiol Rev* 91, 327-387.

Choi, J.H., Cheong, C., Dandamudi, D.B., Park, C.G., Rodriguez, A., Mehandru, S., Velinzon, K., Jung, I.H., Yoo, J.Y., Oh, G.T., and Steinman, R.M. (2011). Flt3 signaling-dependent dendritic cells protect against atherosclerosis. *Immunity* 35, 819-831.

Choi, J.H., Do, Y., Cheong, C., Koh, H., Boscardin, S.B., Oh, Y.S., Bozzacco, L., Trumpfheller, C., Park, C.G., and Steinman, R.M. (2009). Identification of antigen-presenting dendritic cells in mouse aorta and cardiac valves. *J Exp Med* 206, 497-505.

Chou, M.Y., Fogelstrand, L., Hartvigsen, K., Hansen, L.F., Woelkers, D., Shaw, P.X., Choi, J., Perkmann, T., Backhed, F., Miller, Y.I., Horkko, S., Corr, M., Witztum, J.L., and Binder, C.J. (2009). Oxidation-specific epitopes are dominant targets of innate natural antibodies in mice and humans. *J Clin Invest* 119, 1335-1349.

Combadiere, C., Potteaux, S., Gao, J.L., Esposito, B., Casanova, S., Lee, E.J., Debre, P., Tedgui, A., Murphy, P.M., and Mallat, Z. (2003). Decreased atherosclerotic lesion formation in CX3CR1/apolipoprotein E double knockout mice. *Circulation* 107, 1009-1016.

Coombes, J.L., Siddiqui, K.R., Arancibia-Carcamo, C.V., Hall, J., Sun, C.M., Belkaid, Y., and Powrie, F. (2007). A functionally specialized population of mucosal CD103+ DCs induces Foxp3+ regulatory T cells via a TGF-beta and retinoic acid-dependent mechanism. *J Exp Med* 204, 1757-1764.

Cybulsky, M.I., Iiyama, K., Li, H., Zhu, S., Chen, M., Iiyama, M., Davis, V., Gutierrez-Ramos, J.C., Connelly, P.W., and Milstone, D.S. (2001). A major role for VCAM-1, but not ICAM-1, in early atherosclerosis. *J Clin Invest* 107, 1255-1262.

Cybulsky, M.I., and Jongstra-Bilen, J. (2010). Resident intimal dendritic cells and the initiation of atherosclerosis. *Curr Opin Lipidol* 21, 397-403.

Daissormont, I.T., Christ, A., Temmerman, L., Sampedro Millares, S., Seijkens, T., Manca, M., Rousch, M., Poggi, M., Boon, L., Van Der Loos, C., Daemen, M., Lutgens, E., Halvorsen, B., Aukrust, P., Janssen, E., and Biessen, E.A. (2011). Plasmacytoid dendritic cells protect against atherosclerosis by tuning T-cell proliferation and activity. *Circ Res* 109, 1387-1395.

Davenport, P. and Tipping, P.G. (2003). The role of interleukin-4 and interleukin-12 in the progression of atherosclerosis in apolipoprotein E-deficient mice. *Am J Pathol* 163, 1117–25.

Del Gaudio, C., Morbiducci, U., and Grigioni, M. (2006). Time dependent non-Newtonian numerical study of the flow field in a realistic model of aortic arch. *Int J Artif Organs* 29, 709-718.

Doring, Y., Manthey, H.D., Drechsler, M., Lievens, D., Megens, R.T., Soehnlein, O., Busch, M., Manca, M., Koenen, R.R., Pelisek, J., Daemen, M.J., Lutgens, E., Zenke, M., Binder, C.J., Weber, C., and Zernecke, A. (2012). Auto-antigenic

protein-DNA complexes stimulate plasmacytoid dendritic cells to promote atherosclerosis. *Circulation* 125, 1673-1683.

Drechsler, M., Megens, R.T., Van Zandvoort, M., Weber, C., and Soehnlein, O. (2010). Hyperlipidemia-triggered neutrophilia promotes early atherosclerosis. *Circulation* 122, 1837-1845.

Dzionek, A., Sohma, Y., Nagafune, J., Cella, M., Colonna, M., Facchetti, F., Gunther, G., Johnston, I., Lanzavecchia, A., Nagasaka, T., Okada, T., Vermi, W., Winkels, G., Yamamoto, T., Zysk, M., Yamaguchi, Y., and Schmitz, J. (2001). BDCA-2, a novel plasmacytoid dendritic cell-specific type II C-type lectin, mediates antigen capture and is a potent inhibitor of interferon alpha/beta induction. *J Exp Med* 194, 1823-1834.

Elkind, M.S. (2010). Infectious burden: a new risk factor and treatment target for atherosclerosis. *Infect Disord Drug Targets* 10, 84-90.

Elkind, M.S., Luna, J.M., Moon, Y.P., Boden-Albala, B., Liu, K.M., Spitalnik, S., Rundek, T., Sacco, R.L., and Paik, M.C. (2010). Infectious burden and carotid plaque thickness: the northern Manhattan study. *Stroke* 41, e117-122.

Endres, M., Laufs, U., Merz, H., and Kaps, M. (1997). Focal expression of intercellular adhesion molecule-1 in the human carotid bifurcation. *Stroke* 28, 77-82.

Epstein, S.E., Zhu, J., Burnett, M.S., Zhou, Y.F., Vercellotti, G., and Hajjar, D. (2000). Infection and atherosclerosis: potential roles of pathogen burden and molecular mimicry. *Arterioscler Thromb Vasc Biol* 20, 1417-1420.

Erbel, C., Sato, K., Meyer, F.B., Kopecky, S.L., Frye, R.L., Goronzy, J.J., and Weyand, C.M. (2007). Functional profile of activated dendritic cells in unstable atherosclerotic plaque. *Basic Res Cardiol* 102, 123-132.

Erkkila, L., Laitinen, K., Haasio, K., Tiirola, T., Jauhiainen, M., Lehr, H.A., Aalto-Setala, K., Saikku, P., and Leinonen, M. (2004). Heat shock protein 60 autoimmunity and early lipid lesions in cholesterol-fed C57BL/6JBom mice during Chlamydia pneumoniae infection. *Atherosclerosis* 177, 321-328.

Ezzahiri, R., Nelissen-Vrancken, H.J., Kurvers, H.A., Stassen, F.R., Vliegen, I., Grauls, G.E., Van Pul, M.M., Kitslaar, P.J., and Bruggeman, C.A. (2002). Chlamydophila pneumoniae (Chlamydia pneumoniae) accelerates the formation of complex atherosclerotic lesions in Apo E3-Leiden mice. *Cardiovasc Res* 56, 269-276.

Farmakis, T.M., Soulis, J.V., Giannoglou, G.D., Zioupos, G.J., and Louridas, G.E. (2004). Wall shear stress gradient topography in the normal left coronary arterial tree: possible implications for atherogenesis. *Curr Med Res Opin* 20, 587-596.

Ford, P.J., Gemmell, E., Timms, P., Chan, A., Preston, F.M., and Seymour, G.J. (2007). Anti-P. gingivalis response correlates with atherosclerosis. *J Dent Res* 86, 35-40.

Frantz, S., Ertl, G., and Bauersachs, J. (2007). Mechanisms of disease: Toll-like receptors in cardiovascular disease. *Nat Clin Pract Cardiovasc Med* 4, 444-454.

Fyfe, A.I., Qiao, J.H., and Lusis, A.J. (1994). Immune-deficient mice develop typical atherosclerotic fatty streaks when fed an atherogenic diet. *J Clin Invest* 94**,** 2516-2520.

Galkina, E., Harry, B.L., Ludwig, A., Liehn, E.A., Sanders, J.M., Bruce, A., Weber, C., and Ley, K. (2007). CXCR6 promotes atherosclerosis by supporting T-cell

homing, interferon-gamma production, and macrophage accumulation in the aortic wall. *Circulation* 116, 1801-1811.

Galkina, E., Kadl, A., Sanders, J., Varughese, D., Sarembock, I.J., and Ley, K. (2006). Lymphocyte recruitment into the aortic wall before and during development of atherosclerosis is partially L-selectin dependent. *J Exp Med* 203, 1273-1282.

Galkina, E., and Ley, K. (2007a). Leukocyte influx in atherosclerosis. *Curr Drug Targets* 8, 1239-1248.

Galkina, E., and Ley, K. (2007b). Vascular adhesion molecules in atherosclerosis. *Arterioscler Thromb Vasc Biol* 27, 2292-2301.

Galkina, E., and Ley, K. (2009). Immune and inflammatory mechanisms of atherosclerosis (*). *Annu Rev Immunol* 27, 165-197.

Gao, Q., Jiang, Y., Ma, T., Zhu, F., Gao, F., Zhang, P., Guo, C., Wang, Q., Wang, X., Ma, C., Zhang, Y., Chen, W., and Zhang, L. (2010). A critical function of Th17 proinflammatory cells in the development of atherosclerotic plaque in mice. *J Immunol* 185, 5820-5827.

Geissmann, F., Manz, M.G., Jung, S., Sieweke, M.H., Merad, M., and Ley, K. (2010). Development of monocytes, macrophages, and dendritic cells. *Science* 327, 656-661.

George, J., Afek, A., Gilburd, B., Levkovitz, H., Shaish, A., Goldberg, I., Kopolovic, Y., Wick, G., Shoenfeld, Y., and Harats, D. (1998). Hyperimmunization of apo-E-deficient mice with homologous malondialdehyde low-density lipoprotein suppresses early atherogenesis. *Atherosclerosis* 138, 147-152.

Gerrity, R.G., Naito, H.K., Richardson, M., and Schwartz, C.J. (1979). Dietary induced atherogenesis in swine. Morphology of the intima in prelesion stages. *Am J Pathol* 95, 775-792.

Gimbrone, M.A., Jr., Topper, J.N., Nagel, T., Anderson, K.R., and Garcia-Cardena, G. (2000). Endothelial dysfunction, hemodynamic forces, and atherogenesis. *Ann N Y Acad Sci* 902, 230-239; discussion 239-240.

Gitlin, J.M., and Loftin, C.D. (2009). Cyclooxygenase-2 inhibition increases lipopolysaccharide-induced atherosclerosis in mice. *Cardiovasc Res* 81, 400-407.

Gower, R.M., Wu, H., Foster, G.A., Devaraj, S., Jialal, I., Ballantyne, C.M., Knowlton, A.A., and Simon, S.I. (2011). CD11c/CD18 expression is upregulated on blood monocytes during hypertriglyceridemia and enhances adhesion to vascular cell adhesion molecule-1. *Arterioscler Thromb Vasc Biol* 31, 160-166.

Grouard, G., Rissoan, M.C., Filgueira, L., Durand, I., Banchereau, J., and Liu, Y.J. (1997). The enigmatic plasmacytoid T cells develop into dendritic cells with interleukin (IL)-3 and CD40-ligand. *J Exp Med* 185, 1101-1111.

Gu, L., Okada, Y., Clinton, S.K., Gerard, C., Sukhova, G.K., Libby, P., and Rollins, B.J. (1998). Absence of monocyte chemoattractant protein-1 reduces atherosclerosis in low density lipoprotein receptor-deficient mice. *Mol Cell* 2, 275-281.

Gupta, S., Pablo, A.M., Jiang, X., Wang, N., Tall, A.R., and Schindler, C. (1997). IFN-gamma potentiates atherosclerosis in ApoE knock-out mice. *J Clin Invest* 99**,** 2752-2761.

Habets, K.L., Van Puijvelde, G.H., Van Duivenvoorde, L.M., Van Wanrooij, E.J., De Vos, P., Tervaert, J.W., Van Berkel, T.J., Toes, R.E., and Kuiper, J. (2010).

Vaccination using oxidized low-density lipoprotein-pulsed dendritic cells reduces atherosclerosis in LDL receptor-deficient mice. *Cardiovasc Res* 85, 622-630.

Han, J.W., Shimada, K., Ma-Krupa, W., Johnson, T.L., Nerem, R.M., Goronzy, J.J., and Weyand, C.M. (2008). Vessel wall-embedded dendritic cells induce T-cell autoreactivity and initiate vascular inflammation. *Circ Res* 102, 546-553.

Hansson, G.K. (2005). Inflammation, atherosclerosis, and coronary artery disease. *N Engl J Med* 352, 1685-1695.

Hansson, G.K., and Hermansson, A. (2011). The immune system in atherosclerosis. *Nat Immunol* 12, 204-212.

Hansson, G.K., Holm, J., and Jonasson, L. (1989). Detection of activated T lymphocytes in the human atherosclerotic plaque. *Am J Pathol* 135, 169-175.

Hansson, G.K., and Libby, P. (2006). The immune response in atherosclerosis: a double-edged sword. *Nat Rev Immunol* 6, 508-519.

Hansson, G.K., Robertson, A.K., and Soderberg-Naucler, C. (2006). Inflammation and atherosclerosis. *Annu Rev Pathol* 1, 297-329.

Hara, T., Bacon, K.B., Cho, L.C., Yoshimura, A., Morikawa, Y., Copeland, N.G., Gilbert, D.J., Jenkins, N.A., Schall, T.J., and Miyajima, A. (1995). Molecular cloning and functional characterization of a novel member of the C-C chemokine family. *J Immunol* 155, 5352-5358.

Harats, D., Yacov, N., Gilburd, B., Shoenfeld, Y., and George, J. (2002). Oral tolerance with heat shock protein 65 attenuates Mycobacterium tuberculosis-induced and high-fat-diet-driven atherosclerotic lesions. *J Am Coll Cardiol* 40, 1333-1338.

Hardy, R.R., and Hayakawa, K. (2005). Development of B cells producing natural autoantibodies to thymocytes and senescent erythrocytes. *Springer Semin Immunopathol* 26, 363-375.

Harvey, E.J., and Ramji, D.P. (2005). Interferon-gamma and atherosclerosis: pro- or anti-atherogenic? *Cardiovasc Res* 67, 11-20.

Hayashi, C., Madrigal, A.G., Liu, X., Ukai, T., Goswami, S., Gudino, C.V., Gibson, F.C., 3rd, and Genco, C.A. (2010). Pathogen-mediated inflammatory atherosclerosis is mediated in part via Toll-like receptor 2-induced inflammatory responses. *J Innate Immun* 2, 334-343.

Hayashi, C., Viereck, J., Hua, N., Phinikaridou, A., Madrigal, A.G., Gibson, F.C., 3rd, Hamilton, J.A., and Genco, C.A. (2011). Porphyromonas gingivalis accelerates inflammatory atherosclerosis in the innominate artery of ApoE deficient mice. *Atherosclerosis* 215, 52-59.

Hermansson, A., Ketelhuth, D.F., Strodthoff, D., Wurm, M., Hansson, E.M., Nicoletti, A., Paulsson-Berne, G., and Hansson, G.K. (2010). Inhibition of T cell response to native low-density lipoprotein reduces atherosclerosis. *J Exp Med* 207, 1081-1093.

Hjerpe, C., Johansson, D., Hermansson, A., Hansson, G.K., and Zhou, X. (2010). Dendritic cells pulsed with malondialdehyde modified low density lipoprotein aggravate atherosclerosis in Apoe(-/-) mice. *Atherosclerosis* 209, 436-441.

Hu, H., Pierce, G.N., and Zhong, G. (1999). The atherogenic effects of chlamydia are dependent on serum cholesterol and specific to Chlamydia pneumoniae. *J Clin Invest* 103, 747-753.

Huang, F.P., Platt, N., Wykes, M., Major, J.R., Powell, T.J., Jenkins, C.D., and Macpherson, G.G. (2000). A discrete subpopulation of dendritic cells transports apoptotic intestinal epithelial cells to T cell areas of mesenteric lymph nodes. *J Exp Med* 191, 435-444.

Hume, D.A. (2008). Macrophages as APC and the dendritic cell myth. *J Immunol* 181, 5829-5835.

Iiyama, K., Hajra, L., Iiyama, M., Li, H., Dichiara, M., Medoff, B.D., and Cybulsky, M.I. (1999). Patterns of vascular cell adhesion molecule-1 and intercellular adhesion molecule-1 expression in rabbit and mouse atherosclerotic lesions and at sites predisposed to lesion formation. *Circ Res* 85, 199-207.

Ito, T., Amakawa, R., Inaba, M., Ikehara, S., Inaba, K., and Fukuhara, S. (2001). Differential regulation of human blood dendritic cell subsets by IFNs. *J Immunol* 166, 2961-2969.

Ito, T., Kanzler, H., Duramad, O., Cao, W., and Liu, Y.J. (2006). Specialization, kinetics, and repertoire of type 1 interferon responses by human plasmacytoid predendritic cells. *Blood* 107, 2423-2431.

Johnson, B.A., 3rd, Baban, B., and Mellor, A.L. (2009). Targeting the immunoregulatory indoleamine 2,3 dioxygenase pathway in immunotherapy. *Immunotherapy* 1, 645-661.

Jokinen, M.P., Clarkson, T.B., and Prichard, R.W. (1985). Animal models in atherosclerosis research. *Exp Mol Pathol* 42, 1-28.

Jongstra-Bilen, J., Haidari, M., Zhu, S.N., Chen, M., Guha, D., and Cybulsky, M.I. (2006). Low-grade chronic inflammation in regions of the normal mouse arterial intima predisposed to atherosclerosis. *J Exp Med* 203, 2073-2083.

Kadowaki, N., Antonenko, S., Lau, J.Y., and Liu, Y.J. (2000). Natural interferon alpha/beta-producing cells link innate and adaptive immunity. *J Exp Med* 192, 219-226.

Kadowaki, N., Ho, S., Antonenko, S., Malefyt, R.W., Kastelein, R.A., Bazan, F., and Liu, Y.J. (2001). Subsets of human dendritic cell precursors express different toll-like receptors and respond to different microbial antigens. *J Exp Med* 194, 863-869.

Kearney, J.F. (2005). Innate-like B cells. *Springer Semin Immunopathol* 26, 377-383.

Khatri, J.J., Johnson, C., Magid, R., Lessner, S.M., Laude, K.M., Dikalov, S.I., Harrison, D.G., Sung, H.J., Rong, Y., and Galis, Z.S. (2004). Vascular oxidant stress enhances progression and angiogenesis of experimental atheroma. *Circulation* 109, 520-525.

Kleemann, R., Zadelaar, S., and Kooistra, T. (2008). Cytokines and atherosclerosis: a comprehensive review of studies in mice. *Cardiovasc Res* 79, 360-376.

Kleinstreuer, C., Hyun, S., Buchanan, J.R., Jr., Longest, P.W., Archie, J.P., Jr., and Truskey, G.A. (2001). Hemodynamic parameters and early intimal thickening in branching blood vessels. *Crit Rev Biomed Eng* 29, 1-64.

Koizumi, Y., Kurita-Ochiai, T., Oguchi, S., and Yamamoto, M. (2008). Nasal immunization with Porphyromonas gingivalis outer membrane protein decreases P. gingivalis-induced atherosclerosis and inflammation in spontaneously hyperlipidemic mice. *Infect Immun* 76, 2958-2965.

Koltsova, E.K., and Ley, K. (2011). How dendritic cells shape atherosclerosis. *Trends Immunol* 32, 540-547.

Korshunov, V.A., and Berk, B.C. (2003). Flow-induced vascular remodeling in the mouse: a model for carotid intima-media thickening. *Arterioscler Thromb Vasc Biol* 23, 2185-2191.

Kraaijeveld, A.O., De Jager, S.C., Van Berkel, T.J., Biessen, E.A., and Jukema, J.W. (2007). Chemokines and atherosclerotic plaque progression: towards therapeutic targeting? *Curr Pharm Des* 13, 1039-1052.

Ku, D.N., Giddens, D.P., Zarins, C.K., and Glagov, S. (1985). Pulsatile flow and atherosclerosis in the human carotid bifurcation. Positive correlation between plaque location and low oscillating shear stress. *Arteriosclerosis* 5, 293-302.

Kumar, A., and Lindner, V. (1997). Remodeling with neointima formation in the mouse carotid artery after cessation of blood flow. *Arterioscler Thromb Vasc Biol* 17, 2238-2244.

Kyaw, T., Tay, C., Khan, A., Dumouchel, V., Cao, A., To, K., Kehry, M., Dunn, R., Agrotis, A., Tipping, P., Bobik, A., and Toh, B.H. (2010). Conventional B2 B cell depletion ameliorates whereas its adoptive transfer aggravates atherosclerosis. *J Immunol* 185, 4410-4419.

Lardenoye, J.H., Delsing, D.J., De Vries, M.R., Deckers, M.M., Princen, H.M., Havekes, L.M., Van Hinsbergh, V.W., Van Bockel, J.H., and Quax, P.H. (2000). Accelerated atherosclerosis by placement of a perivascular cuff and a cholesterol-rich diet in ApoE*3Leiden transgenic mice. *Circ Res* 87, 248-253.

Lei, M., Kleinstreuer, C., and Truskey, G.A. (1995). Numerical investigation and prediction of atherogenic sites in branching arteries. *J Biomech Eng* 117, 350-357.

Leon, M.L., and Zuckerman, S.H. (2005). Gamma interferon: a central mediator in atherosclerosis. *Inflamm Res* 54, 395-411.

Lerman, A., Burnett, J.C., Jr., Higano, S.T., Mckinley, L.J., and Holmes, D.R., Jr. (1998). Long-term L-arginine supplementation improves small-vessel coronary endothelial function in humans. *Circulation* 97, 2123-2128.

Lesnik, P., Haskell, C.A., and Charo, I.F. (2003). Decreased atherosclerosis in CX3CR1-/- mice reveals a role for fractalkine in atherogenesis. *J Clin Invest* 111, 333-340.

Levy, Z., Rachmani, R., Trestman, S., Dvir, A., Shaish, A., Ravid, M., and Harats, D. (2003). Low-dose interferon-alpha accelerates atherosclerosis in an LDL receptor-deficient mouse model. *Eur J Intern Med* 14, 479-483.

Ley, K., Miller, Y.I., and Hedrick, C.C. (2011). Monocyte and macrophage dynamics during atherogenesis. *Arterioscler Thromb Vasc Biol* 31, 1506-1516.

Li, L., Chen, W., Rezvan, A., Jo, H., and Harrison, D.G. (2011). Tetrahydrobiopterin deficiency and nitric oxide synthase uncoupling contribute to atherosclerosis induced by disturbed flow. *Arterioscler Thromb Vasc Biol* 31, 1547-1554.

Li, L., Messas, E., Batista, E.L., Jr., Levine, R.A., and Amar, S. (2002). Porphyromonas gingivalis infection accelerates the progression of atherosclerosis in a heterozygous apolipoprotein E-deficient murine model. *Circulation* 105, 861-867.

Li, L., Rezvan, A., Salerno, J.C., Husain, A., Kwon, K., Jo, H., Harrison, D.G., and Chen, W. (2010). GTP cyclohydrolase I phosphorylation and interaction with GTP

cyclohydrolase feedback regulatory protein provide novel regulation of endothelial tetrahydrobiopterin and nitric oxide. *Circ Res* 106, 328-336.

Libby, P. (2002). Inflammation in atherosclerosis. *Nature* 420, 868-874.

Liu, K., Victora, G.D., Schwickert, T.A., Guermonprez, P., Meredith, M.M., Yao, K., Chu, F.F., Randolph, G.J., Rudensky, A.Y., and Nussenzweig, M. (2009). In vivo analysis of dendritic cell development and homeostasis. *Science* 324, 392-397.

Liu, L., Hu, H., Ji, H., Murdin, A.D., Pierce, G.N., and Zhong, G. (2000). Chlamydia pneumoniae infection significantly exacerbates aortic atherosclerosis in an LDLR-/- mouse model within six months. *Mol Cell Biochem* 215, 123-128.

Liu, P., Yu, Y.R., Spencer, J.A., Johnson, A.E., Vallanat, C.T., Fong, A.M., Patterson, C., and Patel, D.D. (2008). CX3CR1 deficiency impairs dendritic cell accumulation in arterial intima and reduces atherosclerotic burden. *Arterioscler Thromb Vasc Biol* 28**,** 243-250.

Liuzzo, G., Goronzy, J.J., Yang, H., Kopecky, S.L., Holmes, D.R., Frye, R.L., and Weyand, C.M. (2000). Monoclonal T-cell proliferation and plaque instability in acute coronary syndromes. *Circulation* 101, 2883-2888.

Llodra, J., Angeli, V., Liu, J., Trogan, E., Fisher, E.A., and Randolph, G.J. (2004). Emigration of monocyte-derived cells from atherosclerotic lesions characterizes regressive, but not progressive, plaques. *Proc Natl Acad Sci U S A* 101, 11779-11784.

Lutz, R.J., Cannon, J.N., Bischoff, K.B., Dedrick, R.L., Stiles, R.K., and Fry, D.L. (1977). Wall shear stress distribution in a model canine artery during steady flow. *Circ Res* 41, 391-399.

Mach, F., Sukhova, G.K., Michetti, M., Libby, P., and Michetti, P. (2002). Influence of Helicobacter pylori infection during atherogenesis in vivo in mice. *Circ Res* 90, E1-4.

Maffia, P., Zinselmeyer, B.H., Ialenti, A., Kennedy, S., Baker, A.H., Mcinnes, I.B., Brewer, J.M., and Garside, P. (2007). Images in cardiovascular medicine. Multiphoton microscopy for 3-dimensional imaging of lymphocyte recruitment into apolipoprotein-E-deficient mouse carotid artery. *Circulation* 115, e326-328.

Maganto-Garcia, E., Tarrio, M.L., Grabie, N., Bu, D.X., and Lichtman, A.H. (2011). Dynamic changes in regulatory T cells are linked to levels of diet-induced hypercholesterolemia. *Circulation* 124, 185-195.

Major, A.S., Fazio, S., and Linton, M.F. (2002). B-lymphocyte deficiency increases atherosclerosis in LDL receptor-null mice. *Arterioscler Thromb Vasc Biol* 22, 1892-1898.

Major, A.S., Wilson, M.T., Mccaleb, J.L., Ru Su, Y., Stanic, A.K., Joyce, S., Van Kaer, L., Fazio, S., and Linton, M.F. (2004). Quantitative and qualitative differences in proatherogenic NKT cells in apolipoprotein E-deficient mice. *Arterioscler Thromb Vasc Biol* 24**,** 2351-2357.

Mallat, Z., Besnard, S., Duriez, M., Deleuze, V., Emmanuel, F., Bureau, M.F., Soubrier, F., Esposito, B., Duez, H., Fievet, C., Staels, B., Duverger, N., Scherman, D., and Tedgui, A. (1999). Protective role of interleukin-10 in atherosclerosis. *Circ Res* 85, e17-24.

Mallat, Z., Gojova, A., Brun, V., Esposito, B., Fournier, N., Cottrez, F., Tedgui, A., and Groux, H. (2003). Induction of a regulatory T cell type 1 response reduces the

development of atherosclerosis in apolipoprotein E-knockout mice. *Circulation* 108, 1232-1237.

Maron, R., Sukhova, G., Faria, A.M., Hoffmann, E., Mach, F., Libby, P., and Weiner, H.L. (2002). Mucosal administration of heat shock protein-65 decreases atherosclerosis and inflammation in aortic arch of low-density lipoprotein receptor-deficient mice. *Circulation* 106, 1708-1715.

Matzinger, P. (2007). Friendly and dangerous signals: is the tissue in control? *Nat Immunol* 8, 11-13.

Michelsen, K.S., Wong, M.H., Shah, P.K., Zhang, W., Yano, J., Doherty, T.M., Akira, S., Rajavashisth, T.B., and Arditi, M. (2004). Lack of Toll-like receptor 4 or myeloid differentiation factor 88 reduces atherosclerosis and alters plaque phenotype in mice deficient in apolipoprotein E. *Proc Natl Acad Sci U S A* 101, 10679-10684.

Millonig, G., Niederegger, H., Rabl, W., Hochleitner, B.W., Hoefer, D., Romani, N., and Wick, G. (2001). Network of vascular-associated dendritic cells in intima of healthy young individuals. *Arterioscler Thromb Vasc Biol* 21, 503-508.

Moazed, T.C., Campbell, L.A., Rosenfeld, M.E., Grayston, J.T., and Kuo, C.C. (1999). Chlamydia pneumoniae infection accelerates the progression of atherosclerosis in apolipoprotein E-deficient mice. *J Infect Dis* 180, 238-241.

Mohamadzadeh, M., Poltorak, A.N., Bergstressor, P.R., Beutler, B., and Takashima, A. (1996). Dendritic cells produce macrophage inflammatory protein-1 gamma, a new member of the CC chemokine family. *J Immunol* 156, 3102-3106.

Mor, A., Planer, D., Luboshits, G., Afek, A., Metzger, S., Chajek-Shaul, T., Keren, G., and George, J. (2007). Role of naturally occurring CD4+ CD25+ regulatory T cells in experimental atherosclerosis. *Arterioscler Thromb Vasc Biol* 27, 893-900.

Mullick, A.E., Tobias, P.S., and Curtiss, L.K. (2005). Modulation of atherosclerosis in mice by Toll-like receptor 2. *J Clin Invest* 115, 3149-3156.

Naik, S.H., Metcalf, D., Van Nieuwenhuijze, A., Wicks, I., Wu, L., O'keeffe, M., and Shortman, K. (2006). Intrasplenic steady-state dendritic cell precursors that are distinct from monocytes. *Nat Immunol* 7, 663-671.

Naiki, Y., Sorrentino, R., Wong, M.H., Michelsen, K.S., Shimada, K., Chen, S., Yilmaz, A., Slepenkin, A., Schroder, N.W., Crother, T.R., Bulut, Y., Doherty, T.M., Bradley, M., Shaposhnik, Z., Peterson, E.M., Tontonoz, P., Shah, P.K., and Arditi, M. (2008). TLR/MyD88 and liver X receptor alpha signaling pathways reciprocally control Chlamydia pneumoniae-induced acceleration of atherosclerosis. *J Immunol* 181, 7176-7185.

Nakajima, K., Yamashita, T., Kita, T., Takeda, M., Sasaki, N., Kasahara, K., Shinohara, M., Rikitake, Y., Ishida, T., Yokoyama, M., and Hirata, K. (2011). Orally administered eicosapentaenoic acid induces rapid regression of atherosclerosis via modulating the phenotype of dendritic cells in LDL receptor-deficient mice. *Arterioscler Thromb Vasc Biol* 31, 1963-1972.

Nakajima, T., Schulte, S., Warrington, K.J., Kopecky, S.L., Frye, R.L., Goronzy, J.J., and Weyand, C.M. (2002). T-cell-mediated lysis of endothelial cells in acute coronary syndromes. *Circulation* 105, 570-575.

Nakashima, Y., Raines, E.W., Plump, A.S., Breslow, J.L., and Ross, R. (1998). Upregulation of VCAM-1 and ICAM-1 at atherosclerosis-prone sites on the endothelium in the ApoE-deficient mouse. *Arterioscler Thromb Vasc Biol* 18, 842-851.

Nam, D., Ni, C.W., Rezvan, A., Suo, J., Budzyn, K., Llanos, A., Harrison, D., Giddens, D., and Jo, H. (2009). Partial carotid ligation is a model of acutely induced disturbed flow, leading to rapid endothelial dysfunction and atherosclerosis. *Am J Physiol Heart Circ Physiol* 297, H1535-1543.

Nerem, R.M., Alexander, R.W., Chappell, D.C., Medford, R.M., Varner, S.E., and Taylor, W.R. (1998). The study of the influence of flow on vascular endothelial biology. *Am J Med Sci* 316, 169-175.

Ni, C.W., Qiu, H., and Jo, H. (2011). MicroRNA-663 upregulated by oscillatory shear stress plays a role in inflammatory response of endothelial cells. *Am J Physiol Heart Circ Physiol* 300, H1762-1769.

Ni, C.W., Qiu, H., Rezvan, A., Kwon, K., Nam, D., Son, D.J., Visvader, J.E., and Jo, H. (2010). Discovery of novel mechanosensitive genes in vivo using mouse carotid artery endothelium exposed to disturbed flow. *Blood* 116, e66-73.

Niessner, A., Sato, K., Chaikof, E.L., Colmegna, I., Goronzy, J.J., and Weyand, C.M. (2006). Pathogen-sensing plasmacytoid dendritic cells stimulate cytotoxic T-cell function in the atherosclerotic plaque through interferon-alpha. *Circulation* 114, 2482-2489.

Niessner, A., and Weyand, C.M. (2010). Dendritic cells in atherosclerotic disease. *Clin Immunol* 134, 25-32.

Nilsson, J., Fredrikson, G.N., Bjorkbacka, H., Chyu, K.Y., and Shah, P.K. (2009). Vaccines modulating lipoprotein autoimmunity as a possible future therapy for cardiovascular disease. *J Intern Med* 266, 221-231.

Ohnmacht, C., Pullner, A., King, S.B., Drexler, I., Meier, S., Brocker, T., and Voehringer, D. (2009). Constitutive ablation of dendritic cells breaks self-tolerance of CD4 T cells and results in spontaneous fatal autoimmunity. *J Exp Med* 206, 549-559.

Onai, N., Obata-Onai, A., Tussiwand, R., Lanzavecchia, A., and Manz, M.G. (2006). Activation of the Flt3 signal transduction cascade rescues and enhances type I interferon-producing and dendritic cell development. *J Exp Med* 203, 227-238.

Packard, R.R., Maganto-Garcia, E., Gotsman, I., Tabas, I., Libby, P., and Lichtman, A.H. (2008). CD11c(+) dendritic cells maintain antigen processing, presentation capabilities, and CD4(+) T-cell priming efficacy under hypercholesterolemic conditions associated with atherosclerosis. *Circ Res* 103, 965-973.

Paigen, B., Morrow, A., Holmes, P.A., Mitchell, D., and Williams, R.A. (1987). Quantitative assessment of atherosclerotic lesions in mice. *Atherosclerosis* 68, 231-240.

Paulson, K.E., Zhu, S.N., Chen, M., Nurmohamed, S., Jongstra-Bilen, J., and Cybulsky, M.I. (2010). Resident intimal dendritic cells accumulate lipid and contribute to the initiation of atherosclerosis. *Circ Res* 106, 383-390.

Paulsson, G., Zhou, X., Tornquist, E., and Hansson, G.K. (2000). Oligoclonal T cell expansions in atherosclerotic lesions of apolipoprotein E-deficient mice. *Arterioscler Thromb Vasc Biol* 20, 10-17.

Perrin-Cocon, L., Coutant, F., Agaugue, S., Deforges, S., Andre, P., and Lotteau, V. (2001). Oxidized low-density lipoprotein promotes mature dendritic cell transition from differentiating monocyte. *J Immunol* 167, 3785-3791.

Pryshchep, O., Ma-Krupa, W., Younge, B.R., Goronzy, J.J., and Weyand, C.M. (2008). Vessel-specific Toll-like receptor profiles in human medium and large arteries. *Circulation* 118, 1276-1284.

Pryshchep, S., Sato, K., Goronzy, J.J., and Weyand, C.M. (2006). T cell recognition and killing of vascular smooth muscle cells in acute coronary syndrome. *Circ Res* 98, 1168-1176.

Puccetti, P., and Grohmann, U. (2007). IDO and regulatory T cells: a role for reverse signalling and non-canonical NF-kappaB activation. *Nat Rev Immunol* 7, 817-823.

Pugh, C.W., Macpherson, G.G., and Steer, H.W. (1983). Characterization of nonlymphoid cells derived from rat peripheral lymph. *J Exp Med* 157, 1758-1779.

Pulendran, B. (2004). Modulating TH1/TH2 responses with microbes, dendritic cells, and pathogen recognition receptors. *Immunol Res* 29, 187-196.

Randolph, G.J. (2008). Emigration of monocyte-derived cells to lymph nodes during resolution of inflammation and its failure in atherosclerosis. *Curr Opin Lipidol* 19, 462-468.

Reis, E.D., Li, J., Fayad, Z.A., Rong, J.X., Hansoty, D., Aguinaldo, J.G., Fallon, J.T., and Fisher, E.A. (2001). Dramatic remodeling of advanced atherosclerotic plaques of the apolipoprotein E-deficient mouse in a novel transplantation model. *J Vasc Surg* 34, 541-547.

Rhee, E.J., Nallamshetty, S., and Plutzky, J. (2012). Retinoid metabolism and its effects on the vasculature. *Biochim Biophys Acta* 1821, 230-240.

Rodgers, K.J., Watkins, D.J., Miller, A.L., Chan, P.Y., Karanam, S., Brissette, W.H., Long, C.J., and Jackson, C.L. (2006). Destabilizing role of cathepsin S in murine atherosclerotic plaques. *Arterioscler Thromb Vasc Biol* 26, 851-856.

Roger, V.L., Go, A.S., Lloyd-Jones, D.M., Adams, R.J., Berry, J.D., Brown, T.M., Carnethon, M.R., Dai, S., De Simone, G., Ford, E.S., Fox, C.S., Fullerton, H.J., Gillespie, C., Greenlund, K.J., Hailpern, S.M., Heit, J.A., Ho, P.M., Howard, V.J., Kissela, B.M., Kittner, S.J., Lackland, D.T., Lichtman, J.H., Lisabeth, L.D., Makuc, D.M., Marcus, G.M., Marelli, A., Matchar, D.B., Mcdermott, M.M., Meigs, J.B., Moy, C.S., Mozaffarian, D., Mussolino, M.E., Nichol, G., Paynter, N.P., Rosamond, W.D., Sorlie, P.D., Stafford, R.S., Turan, T.N., Turner, M.B., Wong, N.D., and Wylie-Rosett, J. (2010). Heart Disease and Stroke Statistics--2011 Update: A Report From the American Heart Association. *Circulation*.

Rosenfeld, M.E., and Campbell, L.A. (2011). Pathogens and atherosclerosis: update on the potential contribution of multiple infectious organisms to the pathogenesis of atherosclerosis. *Thromb Haemost* 106, 858-867.

Ross, R. (1999). Atherosclerosis--an inflammatory disease. *N Engl J Med* 340, 115-126.

Rothstein, N.M., Quinn, T.C., Madico, G., Gaydos, C.A., and Lowenstein, C.J. (2001). Effect of azithromycin on murine arteriosclerosis exacerbated by Chlamydia pneumoniae. *J Infect Dis* 183, 232-238.

Sakaguchi, S., Ono, M., Setoguchi, R., Yagi, H., Hori, S., Fehervari, Z., Shimizu, J., Takahashi, T., and Nomura, T. (2006). Foxp3+ CD25+ CD4+ natural regulatory T cells in dominant self-tolerance and autoimmune disease. *Immunol Rev* 212, 8-27.

Sasaki, T., Nakamura, K., and Kuzuya, M. (2007). Plaque rupture model in mice. *Methods Mol Med* 139, 67-75.

Sato, K., Niessner, A., Kopecky, S.L., Frye, R.L., Goronzy, J.J., and Weyand, C.M. (2006). TRAIL-expressing T cells induce apoptosis of vascular smooth muscle cells in the atherosclerotic plaque. *J Exp Med* 203, 239-250.

Schiller, N.K., Boisvert, W.A., and Curtiss, L.K. (2002). Inflammation in atherosclerosis: lesion formation in LDL receptor-deficient mice with perforin and Lyst(beige) mutations. *Arterioscler Thromb Vasc Biol* 22, 1341-1346.

Schulte, S., Sukhova, G.K., and Libby, P. (2008). Genetically programmed biases in Th1 and Th2 immune responses modulate atherogenesis. *Am J Pathol* 172, 1500-1508.

Serbina, N.V., and Pamer, E.G. (2006). Monocyte emigration from bone marrow during bacterial infection requires signals mediated by chemokine receptor CCR2. *Nat Immunol* 7, 311-317.

Serbina, N.V., Salazar-Mather, T.P., Biron, C.A., Kuziel, W.A., and Pamer, E.G. (2003). TNF/iNOS-producing dendritic cells mediate innate immune defense against bacterial infection. *Immunity* 19, 59-70.

Shen, L.H., Zhou, L., Wang, B.Y., Pu, J., Hu, L.H., Chai, D.J., Wang, L., Zeng, J.Z., and He, B. (2008). Oxidized low-density lipoprotein induces differentiation of RAW264.7 murine macrophage cell line into dendritic-like cells. *Atherosclerosis* 199, 257-264.

Soehnlein, O., and Lindbom, L. (2010). Phagocyte partnership during the onset and resolution of inflammation. *Nat Rev Immunol* 10, 427-439.

Soehnlein, O., and Weber, C. (2009). Myeloid cells in atherosclerosis: initiators and decision shapers. *Semin Immunopathol* 31, 35-47.

Soehnlein, O., Weber, C., and Lindbom, L. (2009). Neutrophil granule proteins tune monocytic cell function. *Trends Immunol* 30, 538-546.

Soehnlein, O., Zernecke, A., Eriksson, E.E., Rothfuchs, A.G., Pham, C.T., Herwald, H., Bidzhekov, K., Rottenberg, M.E., Weber, C., and Lindbom, L. (2008). Neutrophil secretion products pave the way for inflammatory monocytes. *Blood* 112, 1461-1471.

Steinberg, D. (1997). Low density lipoprotein oxidation and its pathobiological significance. *J Biol Chem* 272, 20963-20966.

Stemme, S., Faber, B., Holm, J., Wiklund, O., Witztum, J.L., and Hansson, G.K. (1995). T lymphocytes from human atherosclerotic plaques recognize oxidized low density lipoprotein. *Proc Natl Acad Sci U S A* 92, 3893-3897.

Sukhova, G.K., Zhang, Y., Pan, J.H., Wada, Y., Yamamoto, T., Naito, M., Kodama, T., Tsimikas, S., Witztum, J.L., Lu, M.L., Sakara, Y., Chin, M.T., Libby, P., and Shi, G.P. (2003). Deficiency of cathepsin S reduces atherosclerosis in LDL receptor-deficient mice. *J Clin Invest* 111, 897-906.

Sullivan, C.J., and Hoying, J.B. (2002). Flow-dependent remodeling in the carotid artery of fibroblast growth factor-2 knockout mice. *Arterioscler Thromb Vasc Biol* 22, 1100-1105.

Sun, C.M., Hall, J.A., Blank, R.B., Bouladoux, N., Oukka, M., Mora, J.R., and Belkaid, Y. (2007). Small intestine lamina propria dendritic cells promote de novo generation of Foxp3 T reg cells via retinoic acid. *J Exp Med* 204, 1775-1785.

Sun, J., Hartvigsen, K., Chou, M.Y., Zhang, Y., Sukhova, G.K., Zhang, J., Lopez-Ilasaca, M., Diehl, C.J., Yakov, N., Harats, D., George, J., Witztum, J.L., Libby, P., Ploegh, H., and Shi, G.P. (2010). Deficiency of antigen-presenting cell invariant chain reduces atherosclerosis in mice. *Circulation* 122, 808-820.

Suo, J., Ferrara, D.E., Sorescu, D., Guldberg, R.E., Taylor, W.R., and Giddens, D.P. (2007). Hemodynamic shear stresses in mouse aortas: implications for atherogenesis. *Arterioscler Thromb Vasc Biol* 27, 346-351.

Taleb, S., Romain, M., Ramkhelawon, B., Uyttenhove, C., Pasterkamp, G., Herbin, O., Esposito, B., Perez, N., Yasukawa, H., Van Snick, J., Yoshimura, A., Tedgui, A., and Mallat, Z. (2009). Loss of SOCS3 expression in T cells reveals a regulatory role for interleukin-17 in atherosclerosis. *J Exp Med* 206, 2067-2077.

Tellides, G., Tereb, D.A., Kirkiles-Smith, N.C., Kim, R.W., Wilson, J.H., Schechner, J.S., Lorber, M.I., and Pober, J.S. (2000). Interferon-gamma elicits arteriosclerosis in the absence of leukocytes. *Nature* 403, 207-211.

Tezuka, H., Abe, Y., Iwata, M., Takeuchi, H., Ishikawa, H., Matsushita, M., Shiohara, T., Akira, S., and Ohteki, T. (2007). Regulation of IgA production by naturally occurring TNF/iNOS-producing dendritic cells. *Nature* 448, 929-933.

Tezuka, H., and Ohteki, T. (2010). Regulation of intestinal homeostasis by dendritic cells. *Immunol Rev* 234, 247-258.

Tsou, C.L., Peters, W., Si, Y., Slaymaker, S., Aslanian, A.M., Weisberg, S.P., Mack, M., and Charo, I.F. (2007). Critical roles for CCR2 and MCP-3 in monocyte mobilization from bone marrow and recruitment to inflammatory sites. *J Clin Invest* 117, 902-909.

Van Es, T., Van Puijvelde, G.H., Ramos, O.H., Segers, F.M., Joosten, L.A., Van Den Berg, W.B., Michon, I.M., De Vos, P., Van Berkel, T.J., and Kuiper, J. (2009). Attenuated atherosclerosis upon IL-17R signaling disruption in LDLr deficient mice. *Biochem Biophys Res Commun* 388, 261-265.

Van Leeuwen, M., Gijbels, M.J., Duijvestijn, A., Smook, M., Van De Gaar, M.J., Heeringa, P., De Winther, M.P., and Tervaert, J.W. (2008). Accumulation of myeloperoxidase-positive neutrophils in atherosclerotic lesions in LDLR-/- mice. *Arterioscler Thromb Vasc Biol* 28, 84-89.

Van Puijvelde, G.H., Van Es, T., Van Wanrooij, E.J., Habets, K.L., De Vos, P., Van Der Zee, R., Van Eden, W., Van Berkel, T.J., and Kuiper, J. (2007). Induction of oral tolerance to HSP60 or an HSP60-peptide activates T cell regulation and reduces atherosclerosis. *Arterioscler Thromb Vasc Biol* 27, 2677-2683.

Vanderlaan, P.A., Reardon, C.A., and Getz, G.S. (2004). Site specificity of atherosclerosis: site-selective responses to atherosclerotic modulators. *Arterioscler Thromb Vasc Biol* 24, 12-22.

Walpola, P.L., Gotlieb, A.I., Cybulsky, M.I., and Langille, B.L. (1995). Expression of ICAM-1 and VCAM-1 and monocyte adherence in arteries exposed to altered shear stress. *Arterioscler Thromb Vasc Biol* 15, 2-10.

Wang, Z., Klipfell, E., Bennett, B.J., Koeth, R., Levison, B.S., Dugar, B., Feldstein, A.E., Britt, E.B., Fu, X., Chung, Y.M., Wu, Y., Schauer, P., Smith, J.D., Allayee, H., Tang, W.H., Didonato, J.A., Lusis, A.J., and Hazen, S.L. (2011). Gut flora metabolism of phosphatidylcholine promotes cardiovascular disease. *Nature* 472, 57-63.

Weber, C., Meiler, S., Doring, Y., Koch, M., Drechsler, M., Megens, R.T., Rowinska, Z., Bidzhekov, K., Fecher, C., Ribechini, E., Van Zandvoort, M.A., Binder, C.J., Jelinek, I., Hristov, M., Boon, L., Jung, S., Korn, T., Lutz, M.B., Forster, I., Zenke, M., Hieronymus, T., Junt, T., and Zernecke, A. (2011). CCL17-expressing dendritic cells drive atherosclerosis by restraining regulatory T cell homeostasis in mice. *J Clin Invest* 121, 2898-2910.

Weber, C., Zernecke, A., and Libby, P. (2008). The multifaceted contributions of leukocyte subsets to atherosclerosis: lessons from mouse models. *Nat Rev Immunol* 8, 802-815.

Whitman, S.C., Rateri, D.L., Szilvassy, S.J., Yokoyama, W., and Daugherty, A. (2004). Depletion of natural killer cell function decreases atherosclerosis in low-density lipoprotein receptor null mice. *Arterioscler Thromb Vasc Biol* 24, 1049-1054.

Whitman, S.C., Ravisankar, P., Elam, H., and Daugherty, A. (2000). Exogenous interferon-gamma enhances atherosclerosis in apolipoprotein E-/- mice. *Am J Pathol* 157, 1819-1824.

Wick, G., Romen, M., Amberger, A., Metzler, B., Mayr, M., Falkensammer, G., and Xu, Q. (1997). Atherosclerosis, autoimmunity, and vascular-associated lymphoid tissue. *FASEB J* 11, 1199-1207.

Woollard, K.J., and Geissmann, F. (2010). Monocytes in atherosclerosis: subsets and functions. *Nat Rev Cardiol* 7, 77-86.

Wu, H., Gower, R.M., Wang, H., Perrard, X.Y., Ma, R., Bullard, D.C., Burns, A.R., Paul, A., Smith, C.W., Simon, S.I., and Ballantyne, C.M. (2009). Functional role of CD11c+ monocytes in atherogenesis associated with hypercholesterolemia. *Circulation* 119, 2708-2717.

Xu, Q. (2004). Mouse models of arteriosclerosis: from arterial injuries to vascular grafts. *Am J Pathol* 165, 1-10.

Yilmaz, A., Lochno, M., Traeg, F., Cicha, I., Reiss, C., Stumpf, C., Raaz, D., Anger, T., Amann, K., Probst, T., Ludwig, J., Daniel, W.G., and Garlichs, C.D. (2004). Emergence of dendritic cells in rupture-prone regions of vulnerable carotid plaques. *Atherosclerosis* 176, 101-110.

Yvan-Charvet, L., Welch, C., Pagler, T.A., Ranalletta, M., Lamkanfi, M., Han, S., Ishibashi, M., Li, R., Wang, N., and Tall, A.R. (2008). Increased inflammatory gene expression in ABC transporter-deficient macrophages: free cholesterol accumulation, increased signaling via toll-like receptors, and neutrophil infiltration of atherosclerotic lesions. *Circulation* 118, 1837-1847.

Zadelaar, S., Kleemann, R., Verschuren, L., De Vries-Van Der Weij, J., Van Der Hoorn, J., Princen, H.M., and Kooistra, T. (2007). Mouse models for atherosclerosis and pharmaceutical modifiers. *Arterioscler Thromb Vasc Biol* 27, 1706-1721.

Zernecke, A., Bot, I., Djalali-Talab, Y., Shagdarsuren, E., Bidzhekov, K., Meiler, S., Krohn, R., Schober, A., Sperandio, M., Soehnlein, O., Bornemann, J., Tacke, F., Biessen, E.A., and Weber, C. (2008). Protective role of CXC receptor 4/CXC

ligand 12 unveils the importance of neutrophils in atherosclerosis. *Circ Res* 102, 209-217.

Zhang, X., Niessner, A., Nakajima, T., Ma-Krupa, W., Kopecky, S.L., Frye, R.L., Goronzy, J.J., and Weyand, C.M. (2006). Interleukin 12 induces T-cell recruitment into the atherosclerotic plaque. *Circ Res* 98, 524-531.

Zhao, X., Sato, A., Dela Cruz, C.S., Linehan, M., Luegering, A., Kucharzik, T., Shirakawa, A.K., Marquez, G., Farber, J.M., Williams, I., and Iwasaki, A. (2003). CCL9 is secreted by the follicle-associated epithelium and recruits dome region Peyer's patch CD11b+ dendritic cells. *J Immunol* 171, 2797-2803.

Zhou, X., Nicoletti, A., Elhage, R., and Hansson, G.K. (2000). Transfer of CD4(+) T cells aggravates atherosclerosis in immunodeficient apolipoprotein E knockout mice. *Circulation* 102, 2919-2922.

Zhou, X., Paulsson, G., Stemme, S., and Hansson, G.K. (1998). Hypercholesterolemia is associated with a T helper (Th) 1/Th2 switch of the autoimmune response in atherosclerotic apo E-knockout mice. *J Clin Invest* 101, 1717-1725.

Zhou, X., Robertson, A.K., Hjerpe, C., and Hansson, G.K. (2006). Adoptive transfer of CD4+ T cells reactive to modified low-density lipoprotein aggravates atherosclerosis. *Arterioscler Thromb Vasc Biol* 26, 864-870.

Zhu, J., Quyyumi, A.A., Norman, J.E., Csako, G., Waclawiw, M.A., Shearer, G.M., and Epstein, S.E. (2000). Effects of total pathogen burden on coronary artery disease risk and C-reactive protein levels. *Am J Cardiol* 85, 140-146.

CHAPTER 2:

DYNAMIC IMMUNE CELL ACCUMULATION DURING FLOW-INDUCED ATHEROGENESIS IN MOUSE CAROTID ARTERY: AN EXPANDED FLOW CYTOMETRY METHOD

2.1. Introduction

Atherosclerosis is an inflammatory disease driven in large part by immune cells that infiltrate into the arterial wall, leading to the development of lipid laden plaques (Libby, 2002;Hansson, 2005;Galkina and Ley, 2009). The infiltration of immune cells and proliferation of smooth muscle cells (SMCs) into the artery wall plays a central role in atherogenesis. Macrophages, dendritic cells (DCs), and T-cells have all been shown to migrate into the intimal and adventitial regions of vessels in both the early and latter stages of atherogenesis in humans and in mice (Hansson et al., 2006;Hansson and Hermansson, 2011). Once present in the artery wall, each of these cell types contributes to atherogenesis in specific ways, such as presentation of atherogenic antigens to T-cells (DCs) (Hermansson et al., 2010;Hjerpe et al., 2010;Niessner and Weyand, 2010;Hansson and Hermansson, 2011), foam cell formation by taking up lipids (macrophages, SMCs, DCs) (Paulson et al., 2010), pro-inflammatory cytokine production (macrophages, T-cells) (Eid et al., 2009;Erbel et al., 2009;Galkina and Ley, 2009;McLaren and Ramji, 2009), fibrous cap formation (SMCs), cytotoxicity (T-cells) (Nakajima et al., 2002;Nakajima et al., 2003;Pryshchep et al., 2006), and extracellular matrix degradation (macrophages) (Hansson and Hermansson, 2011).

Recently, we have shown that partial ligation of mouse carotid artery causes disturbed flow (d-flow) with characteristic low and oscillatory wall shear stress, leading to lipid-laden plaque development in apolipoprotein E-deficient ($ApoE^{-/-}$) mice fed a high-fat diet (Nam et al., 2009). Using this model, we have shown that d-flow induces broad changes in the gene expression profile of endothelial cells (hours to days), including inter-cellular

adhesion molecule 1 (ICAM-1) and vascular cell adhesion molecule 1 (VCAM-1) within 2 days (Nam et al., 2009;Ni et al., 2010). Impaired vascular relaxation response, another key aspect of endothelial dysfunction, occurs within 1 week via mechanisms involving eNOS uncoupling (Li et al., 2010;Li et al., 2011b), followed by the robust and homogenous formation of atheroma along the entire length of the common carotid artery within 2 weeks and features of advanced plaques such as intraplaque neovascular genesis by 4 weeks (Nam et al., 2009;Li et al., 2010).

While these results show a strong link between d-flow, inflammation, and atherosclerosis, the direct effect of d-flow on immune cell accumulation in the arterial wall during atherogenesis has not been established. However, in typical mouse models of diet-induced atherosclerosis, sufficient lesion growth typically takes more than two months in focal regions exposed to naturally d-flow (Paigen et al., 1987). This makes it difficult to conduct sensitive kinetic studies due to relatively small and non-homogenous lesion areas. In contrast, our flow-induced atherosclerosis model develops robust and homogenous atheroma along the entire length of the common carotid within two weeks, making it an ideal experimental platform to quantify and define relationships between immune cell accumulation and inflammation in the arterial wall.

Advances in multi-parameter flow cytometry allow for the surface phenotyping of a broad number of leukocyte cell types and their subsets using a single staining panel (Chattopadhyay et al., 2006;Frischmann and Muller, 2006;Perfetto et al., 2006). Flow cytometry has been previously used to track 1 to 4 different immune cell types in the

vascular wall using 4 to 7 phenotypic markers (Galkina et al., 2006;Swirski et al., 2007;Smith et al., 2010;Zhou et al., 2010). Here we developed a 10-fluorochrome, 13-parameter flow cytometry method to phenotype and quantify seven major leukocyte subsets implicated in the pathogenesis of atherosclerosis. The flow cytometry data were validated by immunofluorescence staining studies and cytokine and chemokine gene expression profile studies were carried out to gain further functional insights into the mechanisms of leukocyte accumulation.

Here, we show that flow-disturbance causes rapid and dynamic immune cell accumulation in the arterial wall. Following flow disturbance, monocyte/macrophages and DCs rapidly infiltrate along with smaller numbers of T-cells, NK cells, and granulocytes within 7 days. Monocyte/macrophage and DC numbers then rapidly contract during plaque growth between 7 and 14 days post-ligation. The peak leukocyte accumulation was strongly correlated with interferon gamma (IFNγ) production.

2.2. Methods

Mice. Male ApoE$^{-/-}$ mice (B6.129P2-ApoE^{tm1Unc}/J) were purchased from The Jackson Laboratory (Bar Harbor) and were fed *ad libitum* with standard chow diet until surgery at 8 to 9 weeks of age. The ApoE^{tm1Unc} mutation was from a 129P2/OlaHsd-derived E14Tg2a embryonic stem cell line and was backcrossed to the C57BL/6J for 10 generations.

Partial carotid ligation surgery. Partial carotid ligation surgeries were performed as previously described (Nam et al., 2009;Nam et al., 2010). Mice were anesthetized by intra-peritoneal injection of a mixture of xylazine (10 mg/kg) and ketamine (80 mg/kg). The surgical site was epilated, disinfected with Betadine, and a ventral mid-line incision (4 to 5 mm in length) was made in the neck using micro-scissors. The LCA bifurcation was exposed by blunt dissection and three of four caudal LCA branches (left external carotid, internal carotid, and occipital arteries) were carefully dissected free of surrounding connective tissue and ligated with 6-0 silk sutures, leaving the superior thyroid artery intact (Fig. 2.1A). The surgical incision was then closed with Tissue-Mend (Veterinary Product Laboratories), and mice were monitored until recovery in a chamber under a heating lamp. Following partial carotid ligation, $ApoE^{-/-}$ mice were maintained for 4 to 28 days on the Paigen's high-fat diet (HFD; Science Diets) containing 1.25% cholesterol, 15% fat, and 0.5% cholic acid (Paigen et al., 1987). In some studies, sham-ligated animals were operated on as described above except the ligating sutures were not tightened to impede blood flow.

Cells. For flow cytometry analyses of vascular wall leukocytes, partially-ligated male $ApoE^{-/-}$ mice maintained on HFD were sacrificed by CO_2 inhalation and perfused by cardiac puncture with saline containing 10 U/ml of heparin at 4 days (n=12), 7 days (n=12), 14 days (n=12), 21 days (n=12) and 28 days (n=15) post-ligation. Additionally, sham-ligated $ApoE^{-/-}$ mice (n=9) were fed HFD and sacrificed at 7 days post-surgery. Following sacrifice, LCA and RCA were dissected free of surrounding connective tissue and perivascular fat with care taken not to disrupt associated adventitial tissues and

excised by using micro-scissors to cut ~1mm below the carotid bifurcation and ~1 mm above the aortic arch (Fig. 2.1B). Leukocytes were isolated as previously described (Galkina et al., 2006). Excised arteries were placed in ~2 ml of chilled Hanks balanced salt solution, and then pooled (n=3) in 1.5 ml microcentrifuge tubes in 1 ml of chilled digestion buffer consisting of 450 U/ml collagenase I-S, 125 U/ml collagenase XI, 60 U/ml hyaluronidase (Sigma-Aldritch), and 60 U/ml DNAse I (Applichem) in phosphate buffered saline (PBS) supplemented with calcium and magnesium. Pooled arteries were minced finely for 5-10 min using sharp dissection scissors, transferred to a 12-well flat-bottom tissue culture dish, and digested at 37°C for 1 hour at 5% CO_2, with gentle shaking every 15 min. Single cell suspensions were obtained by shearing the digested arteries with a 21½ gauge needle 8-10 times. Cells were transferred to 5 ml FACS tubes (BD Biosciences), washed once in PBS without calcium and magnesium (10 min, 500 *g*, 4°C) and resuspended in 1 ml PBS for staining (Fig. 2.1C).

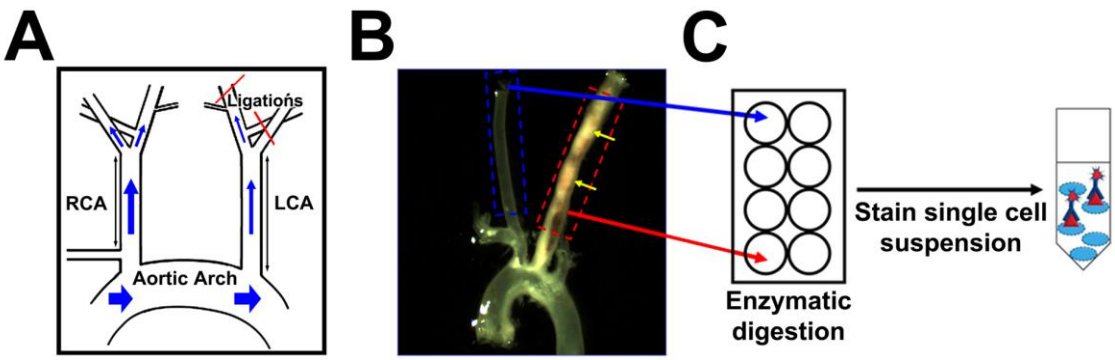

Figure 2.1. Partial carotid ligation procedure and arterial leukocyte preparation. *A, D-flow was induced in the LCA of ApoE$^{-/-}$ mice by partial ligation surgery, while the contralateral RCA was used as an internal control. B, Ligated mice were fed a HFD for 4 to 28 days. Shown is a representative micrograph displaying diffuse atherosclerosis (yellow arrows) in LCA, but not in RCA, two weeks post-ligation. C, LCAs (dashed red box) and RCAs (dashed blue box in (B) obtained from 3 mice at a given time point were pooled (regarded as n=1) and vascular leukocytes extracted.*

Flow cytometry. Single cell suspensions from pooled carotid artery samples or peripheral blood were incubated for 30 min on ice with Fixable Live/Dead Yellow stain (Invitrogen) to discriminate dead cells, washed once (10 min, 500 *g*, 4°C) in chilled FACS buffer (PBS supplemented with 0.5% bovine serum albumin), and incubated for 10 min on ice with FC Block (2.4G2, BD Biosciences) to prevent nonspecific binding of FC receptors in tissue. Blocked samples were then incubated (30 min, on ice, in dark) with a cocktail containing CD45-biotin (30-F11), CD8a-V450 (53-6.7), CD11c-V450 (HL3), CD4-FITC (RM4-4), Gr-1-FITC (RB6-8C5), CD49b-PE (DX5), NK1.1-PE (PK136), CD3e-PerCP-Cy5.5 (145-2C11), and CD11b-APC-Cy7 (M1/70) monoclonal antibodies (mAb) from BD Biosciences; CD19-PE-Texas Red (6D5) from Invitrogen; and F4/80-PE-Cy7 (BM8) and MHCII-APC (M5/114.15.2) mAb from eBioscience. After staining, cells were washed in chilled FACS buffer, stained with streptavidin-conjugated Qdot 655 (Invitrogen) for 30 min on ice, washed in chilled FACS buffer, and resuspended in BD Stabilizing Fixative (BD Biosciences). Immunofluorescence was detected using a LSR II flow cytometer (BD Immunocytometry Systems) equipped with a 488 nm blue laser, 633 nm red laser, and 405 nm violet laser and set using custom filter settings as follows. Live/Dead Yellow stain was excited using the 405 nm violet laser and detected using a 560/40 dichroic filter with a 550 nm long-pass filter. Qdot 655 fluorescence was excited using the 405 nm violet laser and detected using a 660/20 dichroic filter with a 640 nm long-pass filter. Lastly, to reduce Qdot 655 spillover, a 712/20 dichroic filter with a 685 nm long-pass filter was used to detect PerCP-Cy5.5 fluorescence. In order to determine absolute cell numbers per sample, 50 µl of AccuCount Ultra Rainbow Fluorescent

Particles (Spherotech, Inc.) were added to each sample immediately prior to flow cytometry.

Compensation for flow cytometry analyses. Compensation was performed to account for fluorescence spillover of each fluorochrome into multiple detection channels. Anti-rat/hamster IgG-kappa compensation beads (BD Biosciences) were incubated with individual stains of CD8a-V450, CD4-FITC, CD49b-PE, CD19-PE Texas Red, CD3e-PerCP-Cy5.5, F4/80-PE-Cy7, MHCII-APC, and CD11b-APC-Cy7. Single color controls for CD45-Qdot 655 were performed by incubating compensation beads with anti-CD45-biotinylated Ab, followed by streptavidin-conjugated Qdot 655 (Invitrogen). For Live/Dead Yellow compensation, $5x10^5$ splenocytes were heat-killed by incubation at 50°C for 30 min and pooled with $5x10^5$ fresh splenocytes in 1 ml chilled PBS and stained with 1 μl of Live/Dead Yellow (30 min, on ice). In addition to bead-based compensation, populations of fresh and digested splenocytes were single-stained with each individual marker in the panel in order to properly set fluorochrome channel voltages to accommodate adequate signal-to-noise ratios for all cell markers/cell types typed in the panel, and to validate each antibody/fluorochrome pairing for use with digestion (Galkina et al., 2006) (Fig. 2.2A). FlowJo analysis software (ver5.0; Tree Star, Inc.) was used to automatically generate an initial compensation matrix using bead-compensated samples. The initial compensation matrix was then manually readjusted using freshly prepared single-stained splenocytes in order to accommodate optimal discrimination of diverse leukocyte populations bearing different auto-fluorescent properties and avoid unnecessary over-compensation artifacts. Lastly, gating strategies were determined using

fluorescence minus one (FMO) techniques in which populations of fresh and digested splenocytes were stained with 13 different FMO panels, each lacking one out of the 13 different panel markers (Fig. 2.2B). This strategy properly accounts for out-of-channel fluorescence as well as any unavoidable compensation artifacts that may remain when determining positive and negative lineage gates (Roederer, 2002b;a;Perfetto et al., 2006).

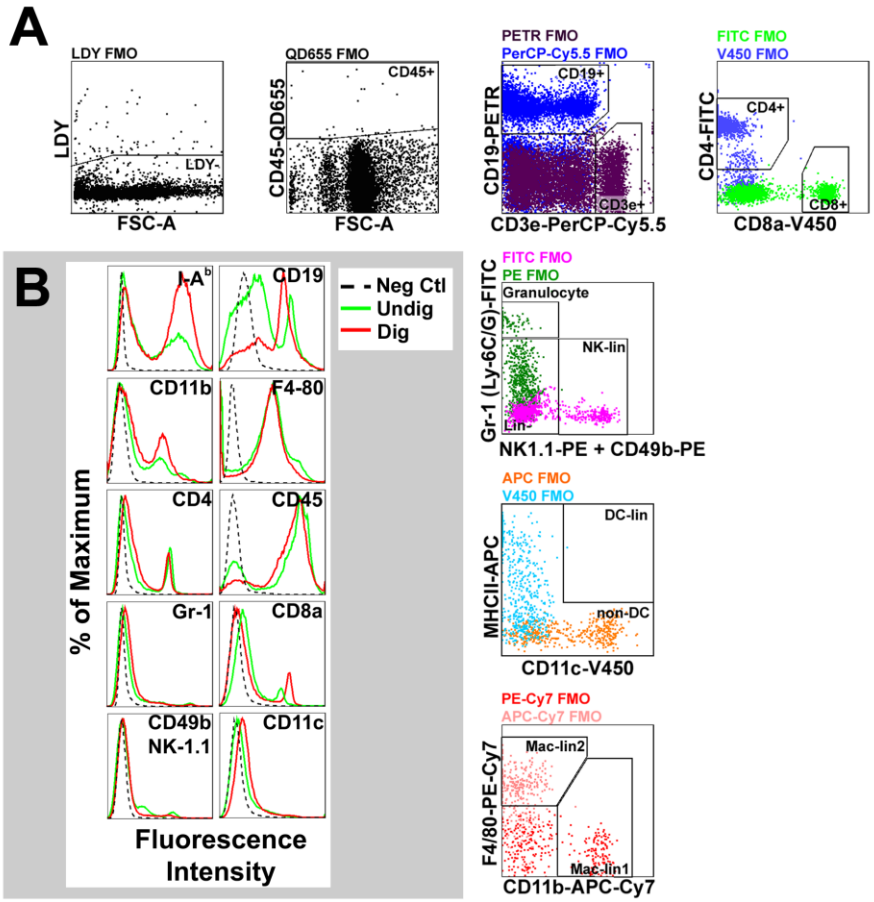

Figure 2.2. Fluorescence minus one gating controls and single-color stain controls for 13-parameter flow cytometry method. *A, Fluorescence minus one (FMO) control staining was performed on digested C57/Bl6 splenocytes in order to determine appropriate gate assignments for the 13-parameter flow cytometry method. Dot plots above show FMO samples and gate assignments for each step of the gating strategy. The displayed antibody/fluorochrome conjugates are identified at the left and bottom of each plot. Excluded fluorochromes are listed at the top of each plot. For bivariate plots of multiple fluorochromes, excluded fluorochromes labels are color-coded to match their corresponding dot plots. B, Single-color stain controls were performed on enzymatically digested (red histograms) and undigested (green histograms) splenocytes. Dotted black histograms denote unstained negative controls. In (A), FSC-A, forward scatter area; LDY, Live/Dead Yellow stain; QD655, Quantum Dot 655; PETR, PE-Texas Red.*

Gating strategy for flow cytometry analyses. Splenocytes, peripheral blood leukocytes, or digested arterial wall cells obtained from $ApoE^{-/-}$ mice were incubated with a cell viability marker, followed by 12 different antibodies against cell surface lineage markers and analyzed by flow cytometry (Fig. 2.3). Initially, single cell populations were gated based on forward scatter characteristics using FlowJo analysis software (1). AccuCount beads were added immediately prior to flow analysis to allow quantification of cell numbers per sample and separated from cells based on ultra-bright fluorescence (2). Live cells were distinguished from dead or damaged cells using a fixable cell viability stain (Live/Dead Yellow) to substantially reduce background signal (3). Pan-leukocyte anti-CD45 was used to identify leukocytes and filter out non-leukocytic vascular cells such as endothelial cells and vascular smooth muscle cells (4). $CD45^+$ leukocytes were gated into three fractions using anti-CD3 and anti-CD19 coupled to non-overlapping fluorochromes (PerCP-Cy5.5 and PE-Texas Red) to identify T- and B-lymphocytes, and non-lymphocytes ($CD3e^-CD19^-$), respectively (6). Gated cells of the T-lymphocyte ($CD3e^+$) and non-lymphocyte fractions were both labeled with antibodies coupled to FITC and V450. The $CD3e^+$ fraction was divided into $CD4^+$ or $CD8^+$ T-cells using CD4-FITC and CD8a-V450 (6a). Non-lymphocytes ($CD3e^-CD19^-$) were designated as granulocytes using Gr-1 (anti-Ly-6G/Ly-6C)-FITC and NK cells identified using NK1.1 and anti-CD49b coupled to PE (7). Among the remaining myeloid cells, dendritic cells (DCs) were defined as $MHCII^+CD11c^+$ events using MHCII-APC and CD11c-V450 (8). Monocyte/macrophages were identified using antibodies to the pan-monocyte markers F4/80 coupled to PE-Cy7 and CD11b coupled to APC-Cy7 ($F4/80^{+/-}CD11b^+$) (9). The coupling of multiple antibodies to a single fluorochrome was used only when "stacked"

markers could be discriminated by a third, independent marker on a different channel (such as CD3e-PerCP-Cy5.5). Cell counts for each cell type and for AccuCount beads were calculated by FlowJo software and absolute cell count per carotid artery was determined using the following equation: ((A/B) x (C/D)) x 40, where A = number of cells recorded for the test sample, B = number of AccuCount beads recorded, C = number of AccuCount beads per 50µl (50,000), and D = volume of test sample in µl.

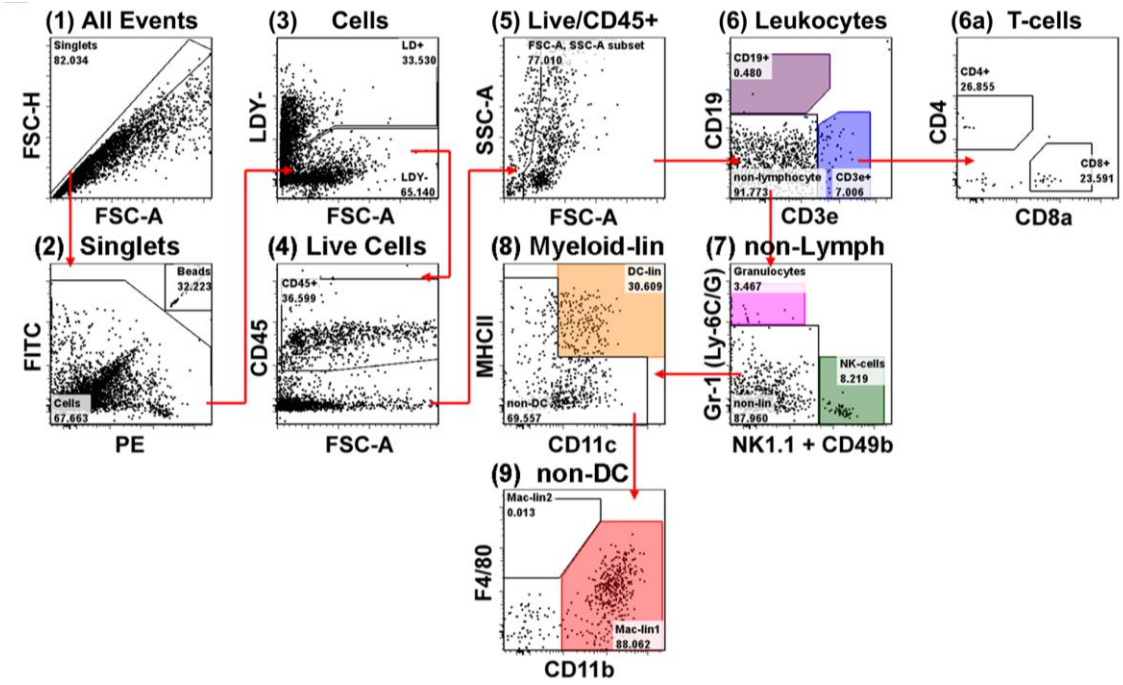

Figure 2.3. Development of a thirteen-parameter immunophenotyping study of leukocytes in the murine carotid artery. *Shows the gating strategy used for flow cytometry analyses for a representative arterial leukocyte sample harvested from LCA 7 days post-ligation. Ultra-bright counting beads (2) were used to calculate absolute cell counts. Gate numbers indicate percent of parent. FSC-H, forward scatter height; FSC-A, forward scatter area; SSC-A, side scatter area.*

Immunostaining and TUNEL assays. Mice were euthanized and perfused with saline containing heparin as described above. LCA and RCA were collected *en bloc* along with the heart, aortic arch, trachea, esophagus, and surrounding fat tissue as previously

described (Nam et al., 2009). Tissue was embedded in optimal cutting temperature (OCT) compound (Tissue-Tek), frozen on liquid nitrogen and stored at –80°C until used. Frozen sections were made starting from the level of the right subclavian artery bifurcation, 300 μm was trimmed away and three sets of ten consecutive 7 μm thick sections were taken at 300 μm intervals constituting the 'proximal' and 'middle' portions of the artery.

Sections were fixed in chilled 4% paraformaldehyde in PBS or a 1:1 mixture of methanol/acetone for 10 min and then blocked (1 hr, at RT) using 0.1% (w/v) BSA or 10% (v/v) goat or donkey serum in PBS. Staining for vascular wall leukocytes was performed overnight at 4°C in a humidified chamber using the following primary antibodies: biotinylated anti-CD45.2 mAb for total leukocytes (104; eBioscience); biotinylated anti-CD11c for DCs (HL3; BD Biosciences); rat anti-mouse CD3 antibody for total T-cells (KT3; ABD Serotec); rat anti-mouse CD68 for macrophages/foam cells (FA-11; ABD Serotec); rat anti-mouse CD11b for myeloid cells/macrophages (M1/70; Abcam); and polyclonal rabbit anti-mouse αSMA for smooth muscle cells (Thermo Scientific). Isotype controls were performed using biotinylated Armenian Hamster IgG (eBio299Arm; eBioscience), biotinylated rat IgG2a, and purified rat IgG2a and IgG2b isotype control Ab (AbD Serotec). Secondary staining was performed using streptavidin-conjugated rhodamine red X (RRX; Invitrogen), DyLight 549-conjugated donkey anti-rat, DyLight 549-conjugated donkey anti-rabbit, streptavidin-conjugated Dylight 549, or RRX-conjugated goat anti-rat secondary antibodies (Jackson Immunoresearch).

In situ apoptosis was measured in cryosections of LCA and RCA using the TUNEL-TMR *In Situ* Cell Death Detection Kit (Roche Applied Science) according to the manufacturer's protocol. In short, freshly thawed cryosections were fixed in 4% paraformaldehyde in PBS for 20 min at RT and then washed in PBS for 30 min at RT. After 2 more 5 min washes in PBS, 50 μl of TUNEL reaction mixture (TdT enzyme solution with tetramethylrhodamine-dUTP (TMR) labeling solution) was added to the tissue sections and sections were incubated in the dark in a humidified chamber at 37°C for 60 min. Positive control assays were performed by incubating sections in recombinant DNase I for 10 min at RT prior to incubation with the TUNEL reaction mixture. For negative control assays, only TMR labeling solution (without TdT enzyme) was added during incubation with the TUNEL reaction mixture.

Antibody- and TUNEL-stained sections were mounted with Prolong Gold antifade mounting medium with DAPI (Invitrogen). Immunofluorescence stains were imaged using a Zeiss Axioskop 2 Plus fluorescence microscope (Carl Zeiss, Inc.) mounted with a Zeiss Axiocam camera (Carl Zeiss, Inc.). All images were captured with a 40x objective lens using the AxioVision 4 software (Carl Zeiss, Inc.) and modified post-capture to balance brightness and contrast independently for each channel using the AxioVision 4 software, followed by uniform leveling of signal brightness in each color channel using Adobe Photoshop (Adobe Systems, Inc.).

Quantitative analysis of immunofluorescence staining. Frozen cross-sections of LCA and RCA immunostained for CD45 (leukocytes), αSMA (SMCs), and by TUNEL assay

(apoptosis) were counterstained with DAPI to identify nuclei as described above. Total $DAPI^+$ nuclei and $CD45^+$, αSMA^+, or $TUNEL^+$ nuclei per artery were quantified for samples obtained 7 days (n=7, from 28 images per stain), 14 days (n=6, from 24 images per stain), and 21 days (n=7, from 28 images per stain) post-ligation using Image J software (NIH). Stains were quantified for additional sham-ligated animals (n=3, from 12 images). For αSMA-stained samples, only intimal nuclei were counted, while intimal, medial, and adventitial nuclei were counted for CD45 and TUNEL stains. The ratio of positive staining nuclei to total $DAPI^+$ nuclei was calculated for all images.

PCR array assay and analysis. LCA and RCA from partially ligated $ApoE^{-/-}$ mice at 4 (n=4), 7 (n=4) or 14 (n=3) days post-ligation were excised as described above and snap frozen in liquid nitrogen. Frozen carotids were then ground by mortar and pestle in 700 µl of Qiazol Lysis Reagent (Qiagen) and total RNA was extracted using the miRNeasy Mini Kit (Qiagen) according to the manufacturer's protocol. cDNA was synthesized using SuperScript III First-Strand Synthesis SuperMix (Invitrogen) according to the manufacturer's protocol. Expression levels of inflammatory cytokine and chemokine genes and their receptors were measured in cDNAs using RT^2 Profiler PCR arrays (SA Biosciences) for inflammatory cytokines & receptors as per manufacturer's protocols and run on a Step-One Plus real time PCR system (Applied Biosystems). Additional qPCR was performed on the same RNA samples as the PCR arrays for *Ifng, Tbx21, Gata3, Rorc*, and *Foxp3* genes using the following primer pairs: *Ifng* (forward 5'-AAC-AAC-CCA-CAG-GTC-CAG-CGC-3'; reverse 5'-CCA-CCC-CGA-ATC-AGC-AGC-GA-3'), *Tbx21* (forward 5'-ATA-CGA-GTG-TCC-CCT-CGC-CAC-C-3'; reverse 5'-CCG-AGG-TGT-

CCC-CAG-CCA-GTA-A-3'), *Gata3* (forward 5'-GTG-CCC-GAG-TAC-AGC-TCT-GGA-CT-3'; reverse 5'-AGA-GTC-CGC-AGG-CAT-TGC-AAA-GG-3'), *Rorc* (forward 5'-CCT-TGG-GTG-GCA-GCT-TGG-CTA-GG-3'; reverse 5'-CTT-TTC-CCA-CTT-CCT-CAG-CGC-CC-3'), and *Foxp3* (forward 5'-CAG-CTG-CCT-ACA-GTG-CCC-CTA-GT-3'; reverse 5'-AGG-TGG-TGG-GAG-GCT-GAT-CAT-GG-3'). PCR array data were processed using Microsoft Excel-based RT^2 Profiler PCR Array Data Analysis templates provided by the manufacturer (SA Biosciences). Because housekeeping gene expression increased with lesion development, total copy number per artery was calculated in LCA and RCA for each target gene and centered to the geometric mean Ct of RCA for all time points using the following equation: 100 / 2^(sample Ct – mean RCA Ct).

Cytokine bead array (CBA) ELISA assay. LCA and RCA from partially ligated $ApoE^{-/-}$ mice were excised as described above and cultured overnight in 60 μl of DMEM supplemented with 10% fetal calf serum, 100 U/mL penicillin, and 100 μg/mL streptomycin at 37°C in 5% CO_2 as previously described (Li et al., 2011a). During this time, vascular cytokine production was stimulated by adding 12-O-tetradecanoylphorbol-13-acetate (TPA, 10 μmol/L) and ionomycin (2 μmol/L; Cell Signaling Technology) to the tissue culture medium. Following incubation, levels of cytokines TNFα, IFNγ, IL-2, IL-4, and IL-5 were measured using the cytokine bead array ELISA kit (BD Biosciences) according to manufacturer's protocol. Cytokine levels were detected using a LSR II flow cytometer (BD Immunocytometry Systems). CBA array data were processed using FCAP Array software (Soft Flow, Inc.). The theoretical limit of detection for the

cytokines measured was 5.0 pg/ml (IL-2), 5.0 pg/ml (IL-4), 5.0 pg/ml (IL-5), 2.5 pg/ml (IFN-γ), and 6.3 pg/ml (TNFα).

Partial least squares regression (PLSR) modeling analysis. To extract relationships between changes in gene expression and cell infiltration dynamics over the time course of flow-disturbed atherosclerosis, a multivariate analysis method, partial least squares regression (PLSR), was applied to the quantitative flow cytometry and PCR array data collected at days 4, 7, and 14 post-ligation. This technique is useful for extracting relationships across multiple types of quantitative data and multiple treatment conditions and has been successfully used to derive information for signal transduction network features (Kemp et al., 2007), viral infection (Miller-Jensen et al., 2007), and cell fate decisions (Janes et al., 2004;Gaudet et al., 2005;Janes et al., 2005). The algorithm finds an optimal set of "latent variables", or principal components, that best captures the variance in the data through a linear combination of the X-variables (qPCR raw Ct values), as well as optimizing the regression to a dependent Y-variable set (number of immune cells counted by flow cytometry).

The multivariate analysis was performed as previously described (Rivet et al., 2011). Briefly, an $m \times n$ data matrix was created where m =97 represents the concatenated columns of each mRNA evaluated by qPCR (X-variables) along with flow cytometry values (Y-variables), and n =28 rows represent the "observations", individual samples collected at each day in LCA or RCA. The matrix was pre-processed by log transformation to achieve normal distributions of observations, then mean-centered and

unit-variance scaled to prevent biasing of the variables in the model. Models were generated using SIMCA-P software (Umetrics) and evaluated based upon the variance captured (Q^2 value) and goodness of fit (R^2Y). Genes that were statistically insignificant in a given component were trimmed from the model, which further enhanced the regression fit.

Statistical analysis. Values are expressed as mean ± SEM unless otherwise indicated. Pairwise comparisons were performed using one-way or two-way t-tests. Multiple comparisons of means were performed using 1-way ANOVA followed by Tukey's Multiple Comparison tests. Differences between groups were considered significant at P values below 0.05. All statistical analyses were performed using Prism software (GraphPad Software).

2.3. Results

Development of a 10-fluorochrome, 13-parameter immunophenotyping study of leukocytes in the murine carotid artery.

We developed a comprehensive, one-step flow cytometry method to accurately identify and quantify the composition of leukocyte sub-populations in nascent and established atherosclerotic lesions in the murine common carotid artery. Using a staining mixture containing 12 specific monoclonal antibodies conjugated to 10 different fluorochromes and a special gating strategy, we differentiated whole leukocyte populations into CD4 and CD8 T-cells, B-cells, monocyte/macrophages, DCs, granulocytes, and NK cells using mouse carotid artery (Fig. 2.3). Flow cytometry antibodies were validated on enzyme-

digested splenocytes and population gates were set according to fluorescence-minus-one controls (Fig. 2.2). The immunophenotyping method showed expected results in blood leukocytes and splenocytes (Fig. 2.4), and stains of digested aorta preparations yielded similar results to previous studies (Fig. 2.5) (Frischmann and Muller, 2006;Galkina et al., 2006).

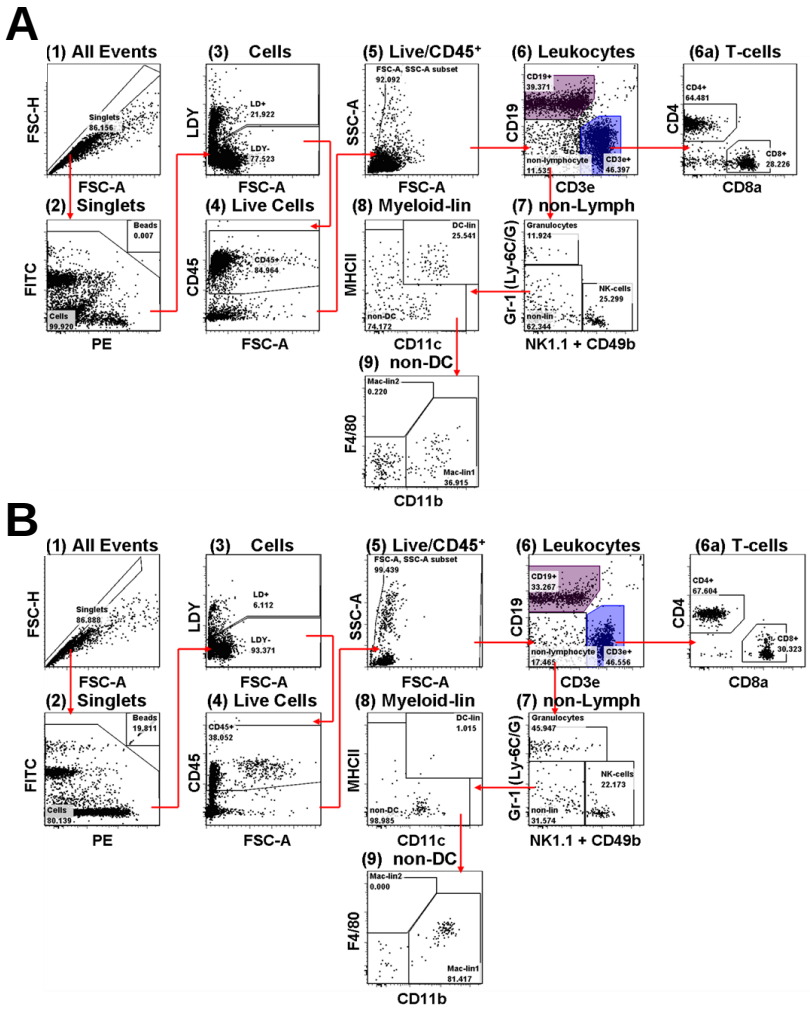

Figure 2.4. Thirteen-parameter, 10-channel flow cytometry staining in splenocytes and peripheral blood leukocytes. *Splenocytes and peripheral blood leukocytes (PBL) were harvested from untreated ApoE$^{-/-}$ mice and phenotyped using the 13-parameter flow cytometry method. A, Splenocytes were harvested by forcing spleen tissue through a 100 µm filter. Shown is a representative staining of undigested splenocytes. B, PBL were drawn by puncture of the descending aorta. Shown is a representative staining. Numbers indicate percent of parent.*

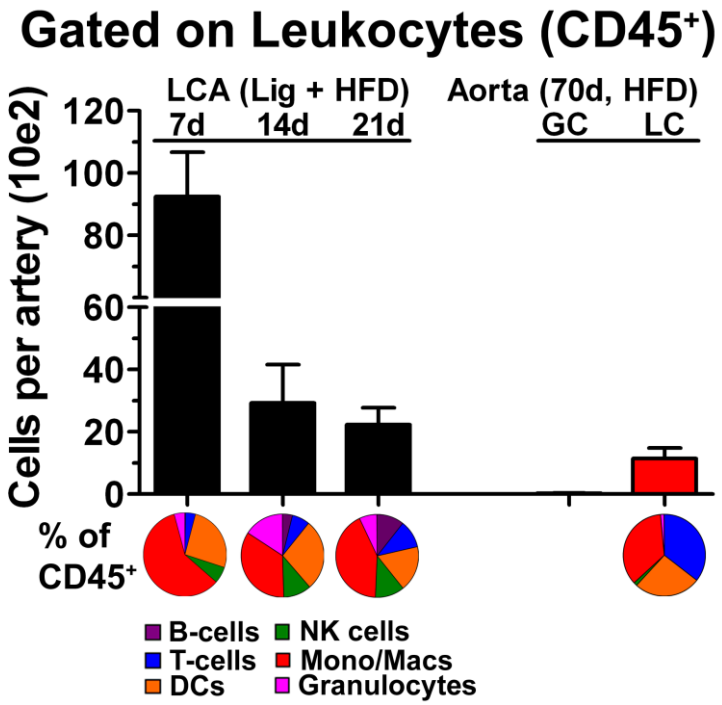

Figure 2.5. Comparison of carotid and aortic lesions using the 13-parameter flow cytometry method. *Leukocyte preparations from LCA taken 7, 14, 21, and 28 days post-ligation were compared with aortic leukocyte preparations from ApoE$^{-/-}$ mice fed a high-fat diet (HFD) for 70 days (10 weeks), in which athero-resistant aortic greater curvature (GC) and atheroprone lesser curvature (LC) were excised, pooled (n=3), and digested independently. Graph depicts absolute leukocyte numbers per artery. Pie charts below graph depict compositional analyses of total leukocyte data. n=4 for LCA samples; n=2 for aortic samples. Data are mean values ± SEM.*

Flow disturbance causes rapid and dynamic accumulation of leukocytes into the arterial wall in a time-dependent manner.

Using the 13-parameter immunotyping method, we then examined leukocyte number and composition in arterial wall during the development of atherosclerosis. Following partial ligation surgery and HFD, flow-disturbed left common carotid artery (LCA) and control right carotid arteries (RCA) obtained at 4, 7, 14, 21, and 28 days post-ligation were enzymatically digested and analyzed by flow cytometry.

As shown in Figure 2.6A, flow-disturbance caused a dynamic increase in leukocyte numbers in LCA in a time-dependent manner. Approximately 500 leukocytes were found per LCA as early as 4 days post-ligation. Leukocyte numbers peaked in LCA at ~9,200 cells at 7 days, and surprisingly, contracted to ~2,900 cells by 14 day, maintaining similar numbers in the vessel wall through 28 days post-ligation (Table 2.1). In contrast, leukocytes did not significantly infiltrate into unligated RCA or sham-operated LCA (Fig. 2.6B-C). To determine whether the decline in leukocyte numbers from day 7 to day 14 was due to cell recovery artifacts during extraction, we quantified the number of dead (LDY^+) and non-singlet, or "clumped", $CD45^+$ cells over the time course (Fig. 2.7). Leukocyte viability did not change over the time course, although significantly increased numbers of clumped $CD45^+$ cells were seen at 7 and 21 days post-ligation (Fig. 2.7). These results indicate that the decline in arterial leukocytes is not likely due to an extraction artifact.

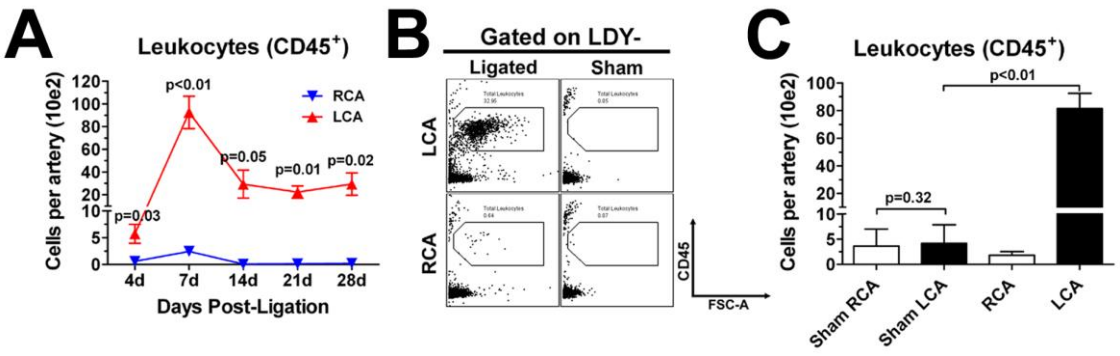

Figure 2.6. Dynamic infiltration of leukocytes into LCA in response to d-flow. *A, Leukocyte ($CD45^+$) accumulation in mouse carotids was examined by the thirteen-parameter immunophenotyping analysis using LCA or RCA over a 4 week time course following ligation and HFD. Graph depicts number of cells (in hundreds) per carotid artery (n=4 to 5 pools of 3 arteries each). B-C, Leukocyte counts in LCA and RCA were compared by our flow cytometry method, using ligated and sham-operated mice (n=3 pools of 3 arteries each) at 7 days post-ligation. Shown are representative dot plots (B) and leukocyte numbers (C). Data are mean values ± SEM. p values in (A) denote comparisons of LCA versus RCA.*

Table 2.1. *Time course analyses of dynamic leukocyte accumulation in flow-disturbed LCA*

Comparison	Mean Diff.	q	Significant? P<0.05?	Summary	ANOVA P value
Leukocytes					0.0002
4v7	86.78	8.56	Yes	***	
7v14	-63.19	6.23	Yes	**	
7v21	-70.19	6.92	Yes	**	
7v28	-63.11	6.56	Yes	**	
B-cells					0.0249
4v7	0.32	1.01	No	ns	
7v14	0.49	1.54	No	ns	
7v21	1.31	4.11	No	ns	
7v28	0.33	1.09	No	ns	
T-cells					0.0350
4v7	2.90	5.11	Yes	*	
7v14	-1.29	2.28	No	ns	
7v21	-1.12	1.98	No	ns	
7v28	-1.60	2.98	No	ns	
Dendritic Cells					0.0012
4v7	20.38	7.30	Yes	***	
7v14	-12.87	4.61	Yes	*	
7v21	-16.13	5.77	Yes	**	
7v28	-14.92	5.63	Yes	**	
NK Cells					0.0040
4v7	5.24	6.13	Yes	**	
7v14	-3.08	3.61	No	ns	
7v21	-3.29	3.86	No	ns	
7v28	-4.75	5.86	Yes	**	
Monocyte/Macrophages					<0.0001
4v7	48.76	9.24	Yes	***	
7v14	-41.82	7.93	Yes	***	
7v21	-44.54	8.44	Yes	***	
7v28	-37.48	7.49	Yes	***	
Granulocytes					0.0298
4v7	2.54	4.11	No	ns	
7v14	-0.58	0.93	No	ns	
7v21	-2.18	3.54	No	ns	
7v28	-0.37	0.63	No	ns	

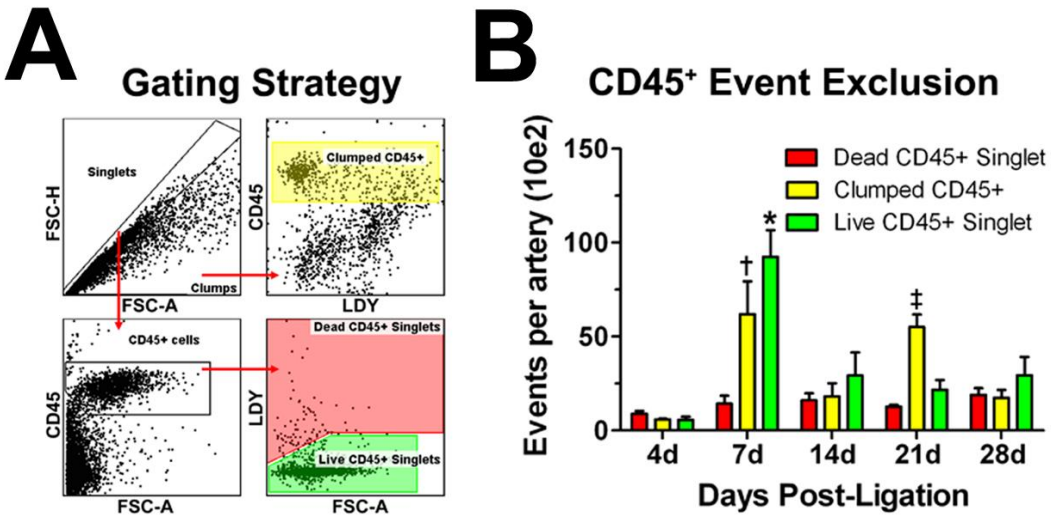

Figure 2.7. Sample quality and leukocyte viability remain fairly consistent between cell preparations from early and developed plaques. *A, The flow cytometry data from Figure 2A was further analyzed as shown in a representative gating scheme. B, The number of non-viable ($CD45^+LDY^+$; red bars) and non-singlet, or "clumped" (yellow bars) vascular leukocytes from LCA were quantified and compared against live $CD45^+$ singlets (green bars). Data are mean values ± SEM. In (B), *, $p<0.05$, 7d versus 4d, 14d, 21d, and 28d; †, $p<0.05$ versus 4d, 14d, and 28d; ‡, $p<0.05$ versus 4d.*

To further validate the flow cytometry data for dynamic leukocyte infiltration into LCA, LCA and RCA were stained with CD45 antibody. As additional controls, we used markers of SMC (αSMA) and apoptosis (TUNEL). Intense CD45 staining in LCA was observed in the intimal lesion at 7, 14, or 21 days post-ligation, as well as in the media and adventitia (especially at 7 days) (Fig. 2.8A). In contrast, CD45 staining was not observed in RCA sections in either 7 or 21 day samples as well as in sham-operated LCA and RCA. Interestingly, intimal αSMA staining was not apparent at day 7, but intense staining was found throughout the intima at day 14, which then regressed to a more localized peri-luminal pattern by day 21 (Fig. 2.8B). Further, a small number of apoptotic cells appear at day 7, which significantly and transiently increased at day 14, followed by a decrease by day 21 (Fig. 2.8C). Semi-quantitative analysis of the staining

data supports the qualitative observations. Taken together, these results suggest that the lesion growth from day 7 to day 14 is largely accounted for by SMC accumulation along with decreased but sustained presence of leukocytes (Fig. 2.8A-C).

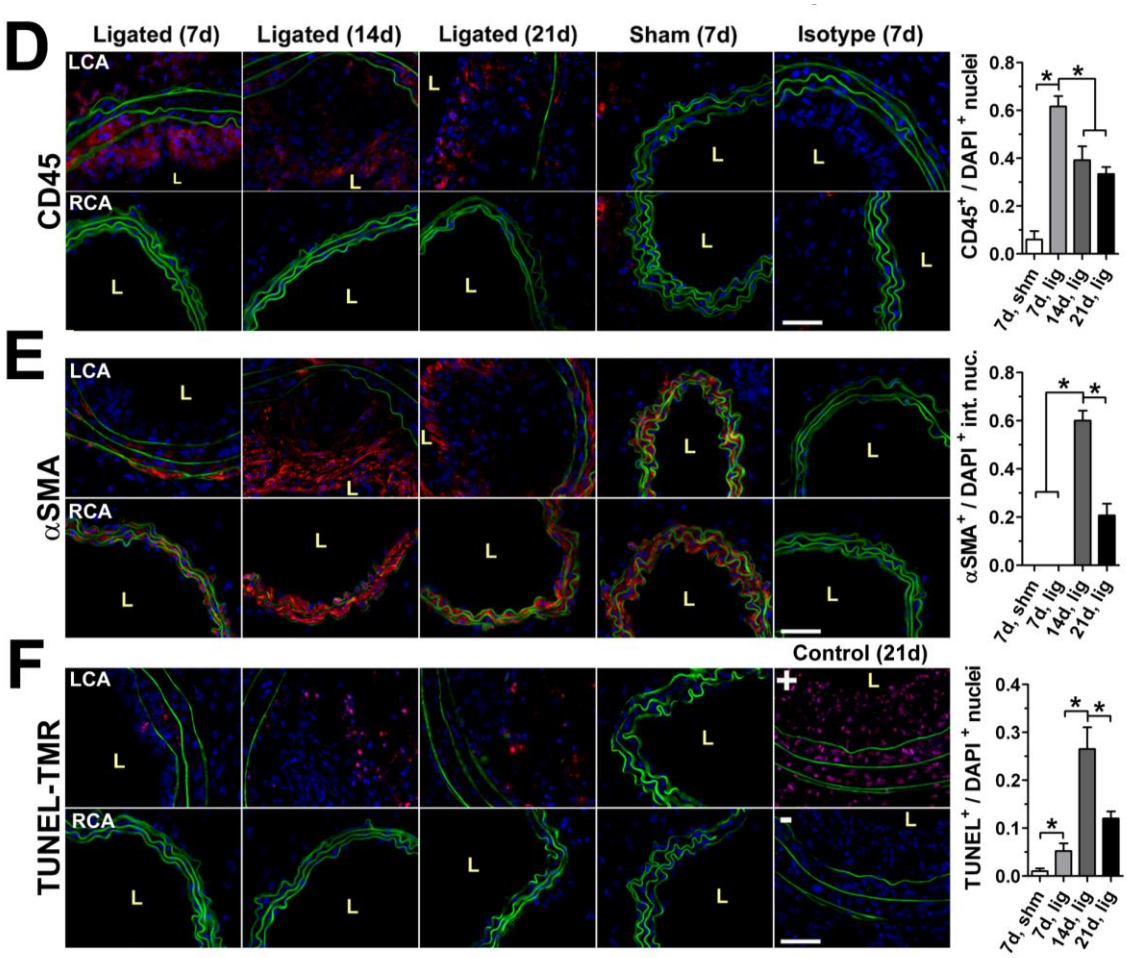

Figure 2.8. Dynamic infiltration of leukocytes into LCA in response to d-flow. *A-C, Flow cytometry data in Figure 2.6 were confirmed by immunofluorescence staining for CD45 (A), αSMA (B), or TUNEL stain (C) (red) in LCA and RCA frozen cross-sections obtained 7 (n=7), 14 (n=6), or 21 (n=7) days post-ligation along with 7 day sham-ligated controls (n=3), and isotype control stains. Elastic laminae autofluorescence (green) and nuclear staining by DAPI (blue) are shown. Quantitations of CD45$^+$, intimal αSMA$^+$, and TUNEL$^+$ staining nuclei residing in the arterial wall are shown to the right of their respective micrographs (A-C). Data are mean values ± SEM. (A-C) Magnification x40; scale bars, 50 μm; L, lumen; *, p<0.05.*

D-flow induces dynamic accumulation of innate cells, T- and B-cells in LCA.

The flow cytometry data shown in Figure 2A was further analyzed to quantify dynamic changes in specific innate and adaptive immune cell populations. Total $CD45^+$ leukocytes were gated into B-cells, T-cells, DCs, monocyte/macrophages, NK cells, and granulocytes (Fig. 2.3). The time course data showed that flow disturbance induced rapid infiltration of all four innate cell types tested (DC, monocyte/macrophage, NK cells, granulocytes) within 4 days and transiently peaking at 7 days (Fig. 2.9A; Table 2.1). The number of DCs and monocyte/macrophages in LCA significantly contracted between 7 and 14 days post-ligation, but remained steady afterwards. NK cell numbers steadily declined from day 7 to day 28 post-ligation, while granulocytes showed a non-significant, bi-phasic pattern over the time course with peaks at 7 and 28 days. In contrast, B-cells did not significantly enter the arterial wall until day 14 post-ligation, and peaked by day 21 (Fig. 2.9A). D-flow induced the infiltration of a surprisingly small, but statistically significant number of T-cells as early as day 4, which significantly increased by day 7 and remained at ~180 cells between day 14 and 28 post-ligation (Fig. 2.9A). Total infiltrating T-cells were further divided into CD4 and CD8 T-cells (Fig. 2.9B). CD4 cells were found to infiltrate into LCA as early as 4 days, peaking at 7 days and remaining high without a significant contraction for the duration of the time course. In contrast, CD8 cells were also found to infiltrate into LCA only by day 7 and remained unchanged over the time course, while maintaining ~ 2:1 ratio (CD4/CD8) (Fig. 2.9B).

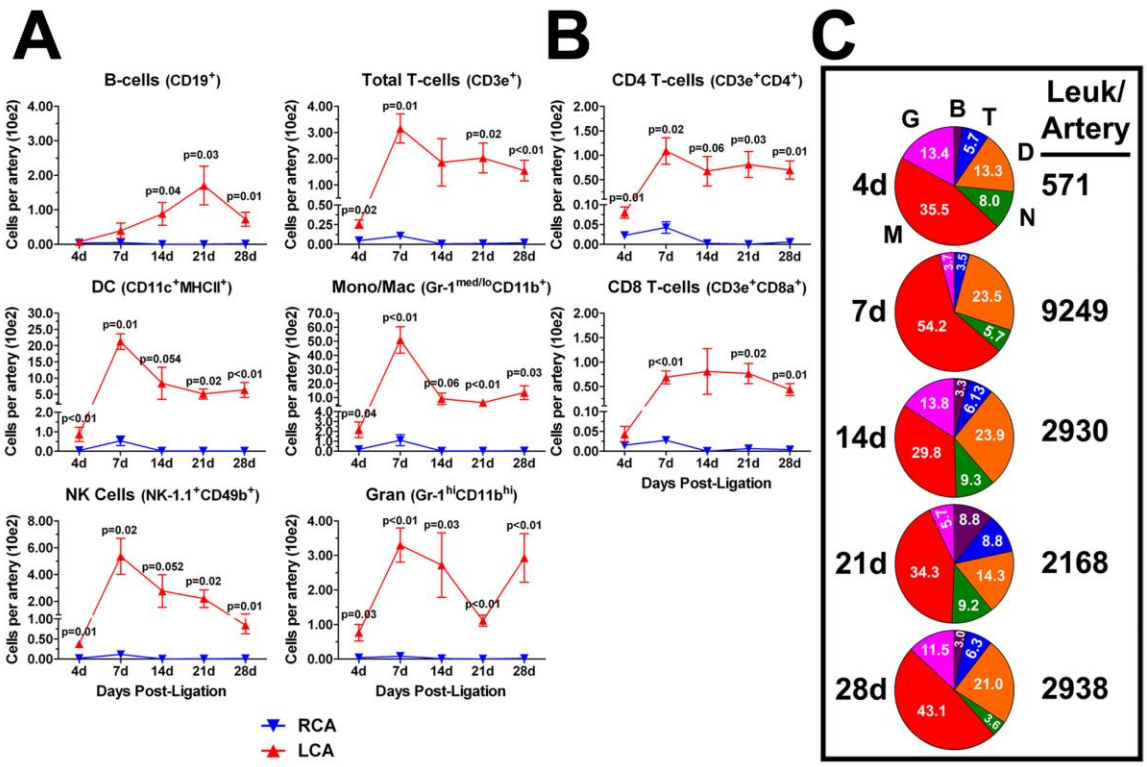

Figure 2.9. D-flow induces a transient peak accumulation of innate cells, sustained T-cell accumulation, and delayed B-cell entry into LCA. *The flow cytometry data shown in Figure 2.6 were further analyzed to quantitate dynamic changes in specific immune cell lineages. A, Leukocytes (CD45$^+$) were subdivided into six major immune cell types (B- and T-cells, DCs, monocyte/macrophage, NK cells and granulocytes) over a four week time course in LCA and RCA. B, T-cells were further subdivided into CD4 and CD8 T-cells. Shown (A-B) are absolute cell numbers (in hundreds) per carotid artery (n=4 to 5 pools of 3 arteries each). C, Pie charts show compositional analyses of vascular leukocytes in the flow-disturbed LCA, presented in (A). Each pie slice denotes mean percentage of total leukocytes (white numbers). Numbers to the right of the pie charts denote mean leukocyte numbers per carotid artery. Data are mean values ± SEM. B, B-cells; T, T-cells; D, DCs; N, NK-cells; M, macrophages; G, granulocytes.*

We next performed combined compositional analyses of leukocytes in the carotid wall by calculating the percentage of each immune cell subtype out of total leukocyte numbers over the time course (Fig. 2.9C). As expected, monocyte/macrophages were the dominant immune cell in the flow-disturbed LCA, followed by DCs. Interestingly, T-cell and B-cell percentages appear to increase as the atherosclerotic lesion develops (14 to 28 days) compared to early lesions (4 to 7 days post-ligation), as did NK cells.

D-flow induces intimal accumulations of macrophages, DCs, and CD4 T-cells in LCA. To validate the quantitative flow cytometry data, we performed immunofluorescence staining studies with antibodies specific to macrophage/foam cells, DCs, and T-cells using frozen LCA and RCA cross-sections from ligated ApoE$^{-/-}$ mice. Both 7 and 21 day post-ligation lesions stained intensely for the macrophage/foam cell marker CD68 and myeloid cell marker CD11b both in the intima and adventitia (Fig. 2.10A-B). Within the intima, CD68 and CD11b staining was localized to nuclei-dense regions of the lesion, especially at 3 weeks (Fig. 2.10B). The extensive intimal and adventitial CD68 staining in both 7 and 21 day lesions suggests that rapid foam cell differentiation occurs in leukocytes accumulating in the flow-disturbed LCA. In contrast to CD68 and CD11b staining, CD11c (DC) staining occurred mostly in intimal lesions but not in adventitia (Fig. 2.10). Similar to CD11c staining, T-cell infiltration (CD3) was also restricted to the intima in 21 day lesion, although it was also found in the media and adventitia at day 7. Since the animals were fed HFD, occasional CD11b^{+} and CD68^{+} cells were found in the adventitia of RCAs (Fig. 2.10A-B). Isotype control stains for all antibodies used showed negative staining in carotid intima, media, and adventitia (Fig. 2.10C). Collectively, these results support the flow cytometry results.

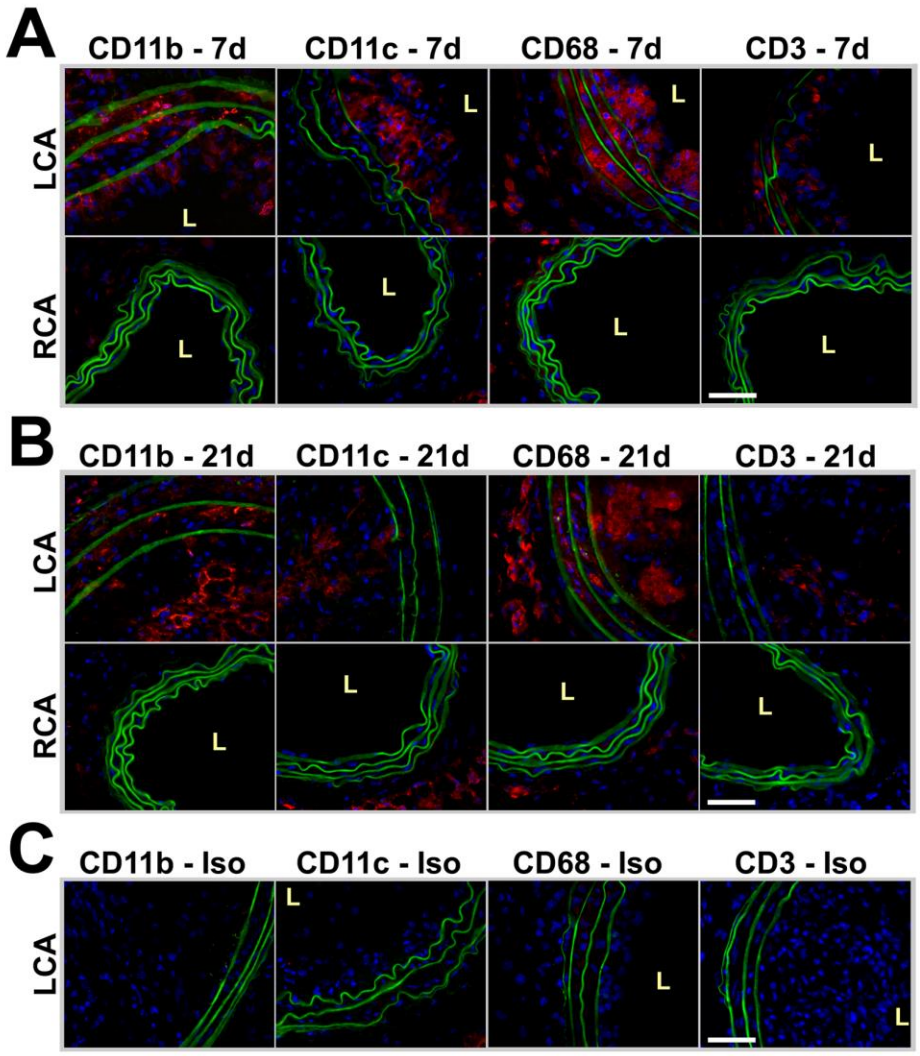

Figure 2.10. D-flow induces accumulation of macrophages, dendritic cells (DC) and T-cells in LCA. *A-B, Frozen sections from LCA and RCA obtained 7 (A) or 21 days (B) post-ligation were stained red with CD68, CD11b, CD11c, CD3, or isotype controls (C). Shown are representative images of n=7 (7d images) or n=5-7 (21d images). Elastic laminae autofluorescence (green) and nuclear staining by DAPI (blue) are shown. Magnification x40 (E); scale bars, 50 μm; L, lumen.*

D-flow induces dynamic changes in cytokine and chemokine gene expression in LCA, and show Th1 T-cell mediated inflammatory pathology.

To determine the effect of d-flow on cytokine and chemokine production in mouse carotid wall, we carried out RT^2 Profiler PCR arrays (SA Biosciences) on RNA from LCA and RCA taken at 4, 7, or 14 days post-ligation in $ApoE^{-/-}$ mice. In total, the

expression levels of 89 genes, including 5 house-keeping genes were analyzed per sample. As shown in the heat map (Fig. 2.12A) and volcano plots (Fig. 2.11), we found no significantly altered gene expression (≥3-fold) in LCA at 4 days, but 53 genes were significantly upregulated at 7 and 14 days (Table 2.2). Interestingly, however, the PCR array failed to detect interferon gamma *(Ifng)*, a well-known, critical atherogenic cytokine (Fig. 2.12A), which may have been due to a poor primer set. Therefore, we retested the same RNA samples using a different primer sequence set, and found that *Ifng* expression was significantly increased in LCA at 7 days, but not at 4 or 14 days post-ligation (Fig. 2.12B).

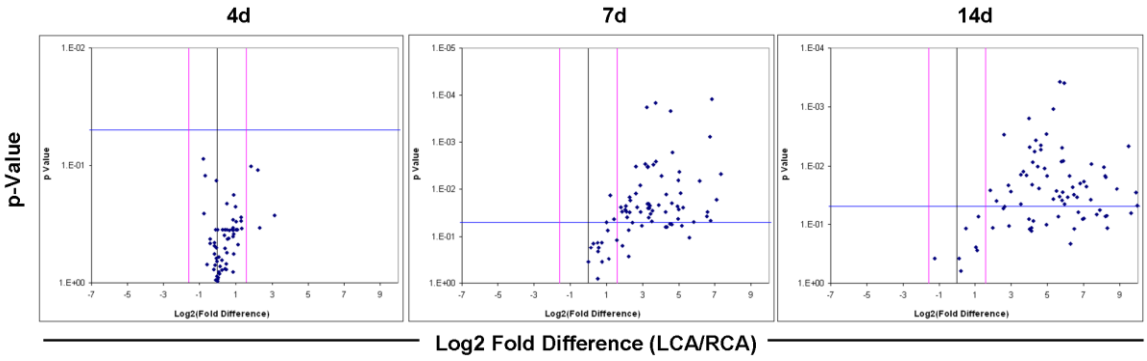

Figure 2.11. Cytokine and chemokine gene expression is upregulated by d-flow in partially-ligated LCA. *Total RNAs obtained from LCA and RCA at 4 (n=4), 7 (n=4), or 14 (n=3) days post-ligation in ApoE$^{-/-}$ mice fed the HFD were analyzed by PCR cytokine arrays (shown in Fig. 2.11A). Shown are volcano plots depicting significant increases in cytokine and chemokine gene expression in flow-disturbed LCA compared to contralateral RCA. Red lines denote significant thresholds for magnitude of fold changes (-3 ≥ x ≥ 3); blue lines denote significance threshold (p < 0.05) for Student t-tests; each blue dot represents mean fold change in the expression of one gene.*

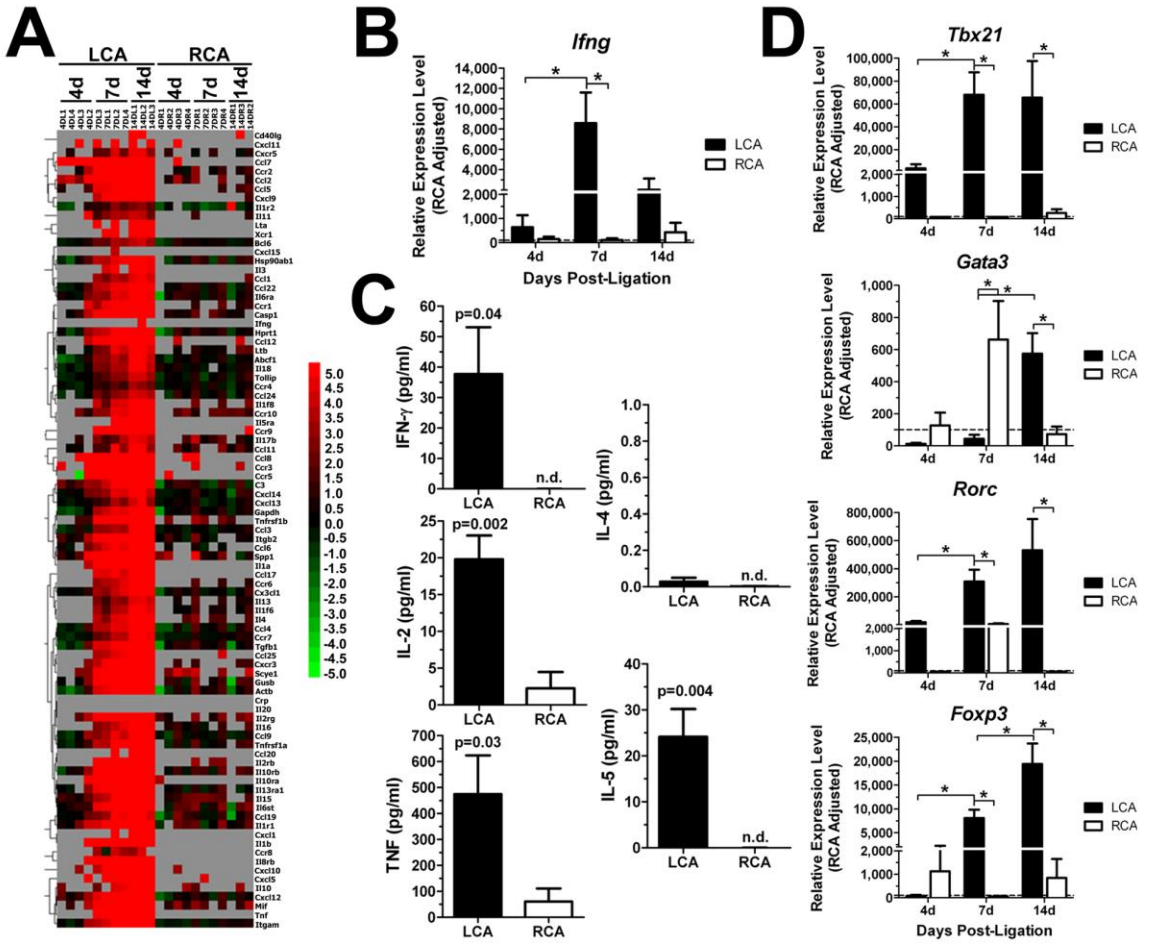

Figure 2.12. Dynamic changes in expression of cytokines and chemokines in LCA by d-flow. *A-B, D, Total RNAs obtained from LCA and RCA were analyzed by PCR cytokine arrays (A) or by qPCR (B and D). The heat map shown in (A) displays relative expression levels of cytokines and cytokine receptors in LCA compared to RCA. Green indicates downregulation, black indicates no change, and red indicates upregulation. Grey boxes indicate undetectable copy number (>35 cycles). Additional qPCR was carried out using the total RNAs to determine expression of Ifng (B) and Tbx21, Gata3, Rorc, Foxp3 (D). Shown are data for n=4 (4 and 7 day) and n=3 (14 day). C, Production of IFNγ, IL-2, TNFα□ □, IL-4, and IL-5 proteins was determined by ELISA using 7 day post-ligation LCA and RCA stimulated ex vivo with TPA and ionomycin for 16 hr (n=5). Data are mean ± SEM. *, p<0.05. n.d., not detected.*

Table 2.2. *PCR array of cytokines and chemokines expressed in LCA and RCA, and their known functions.*

A. 7 day post-ligation

Gene Symbol	Gene Name	Fold Change (LCA/RCA)	p value	Function
Chemokine Genes				
Ccl2	chemokine (C-C motif) ligand 2	138.19	0.0169	**Attracts:** monocytes, memory T-cells, DCs
Ccl7	chemokine (C-C motif) ligand 7	107.47	0.0476	**Attracts:** monocytes **Activates:** macs
Ccl5	chemokine (C-C motif) ligand 5	38.06	0.0250	**Attracts:** T-cells **Activates:** NK cells
Cxcl12	chemokine (C-X-C motif) ligand 12	34.26	0.0123	**Attracts**: lymphocytes
Ccl12	chemokine (C-C motif) ligand 12	32.06	0.0275	**Attracts:** monocytes, lymphocytes
Ccl6	chemokine (C-C motif) ligand 6	31.55	0.0427	**Expressed by:** neutrophils, macs
Cxcl9	chemokine (C-X-C motif) ligand 9	19.51	0.0310	**Attracts:** T-cells
Ccl22	chemokine (C-C motif) ligand 22	12.07	0.0030	**Expressed by:** macrophages, DCs
Ccl19	chemokine (C-C motif) ligand 19	11.55	0.0481	**Attracts:** B-cells, $CCR7^+$ T-cells, DCs
Ccl9	chemokine (C-C motif) ligand 9	10.71	0.0230	**Attracts:** $CD11b^+$ DCs
Cx3cl1	chemokine (C-X3-C motif) ligand 1	10.26	0.0210	**Attracts:** T-cells, monocytes, DCs
Cxcl10	chemokine (C-X-C motif) ligand 10	10.25	0.0405	**Attracts:** monocytes, T-cells, NK cells, DCs
Ccl4	chemokine (C-C motif) ligand 4	9.78	0.0034	**Attracts:** monocytes, NK cells
Ccl3	chemokine (C-C motif) ligand 3	9.43	0.0002	**Attracts:** neutrophils
Ccl24	chemokine (C-C motif) ligand 24	3.50	0.0242	**Attracts:** eosinophils, resting T-cells, neutrophils
Ccl1	chemokine (C-C motif) ligand 1	2.33	0.0137	**Attracts:** monocytes, NK cells, immature B-cells
Chemokine Receptor Genes				
Ccr5	chemokine (C-C motif) receptor 5	95.85	0.0305	**Binds:** CCL5, CCL3, CCL4
Ccr3	chemokine (C-C motif) receptor 3	93.04	0.0377	**Binds:** CCL11, CCL26, CCL7, CCL13, CCL5
Ccr2	chemokine (C-C motif) receptor 2	57.08	0.0497	**Binds:** CCL2
Cxcr3	chemokine (C-X-C motif) receptor 3	13.35	0.0026	**Binds:** CXCL9, CXCL10, CXCL11, CXCL4
Cxcr2	chemokine (C-X-C motif) receptor 2	11.64	0.0286	**Binds:** IL8, CXCL1, CXCL2, CXCL3, CXCL5
Cxcr4	chemokine (C-X-C motif) receptor 4	10.39	0.0258	**Binds:** CXCL12
Ccr9	chemokine (C-C motif) receptor 9	7.27	0.0082	**Binds:** CCL25
Ccr7	chemokine (C-C motif) receptor 7	6.51	0.0243	**Binds:** CCL19
Ccr6	chemokine (C-C motif) receptor 6	6.13	0.0122	**Binds:** CCL20

Gene Symbol	Gene Name	Fold Change (LCA/RCA)	p value	Function
Cytokine Genes				
Mif	macrophage migration inhibitory factor	30.23	0.0236	Macrophage fx
Tgfb1	transforming growth factor, beta 1	16.39	0.0052	Anti-inflammatory
Il1a	interleukin 1 alpha	13.32	0.0001	Pro-inflammatory
Aimp1	aminoacyl tRNA synthetase complex-interacting multifunctional protein 1	10.91	0.0336	Pro-inflammatory
Il16	interleukin 16	10.03	0.0258	T-cell activation **Attracts:** activated $CD4^+$ T-cells, $CD4^+$ DCs
Il18	interleukin 18	8.81	0.0030	Pro-inflammatory
Il1f6	interleukin 1 family, member 6	4.95	0.0170	?
Il15	interleukin 15	4.86	0.0312	NK cell activation / proliferation; homeostatic T-cell proliferation
Tnf	tumor necrosis factor	4.35	0.0390	Pro-inflammatory
Il4	interleukin 4	4.26	0.0298	Th2 T-cell differentiation
Il1f8	interleukin 1 family, member 8	4.08	0.0271	?
Il11	interleukin 11	3.65	0.0299	Platelet production; lymphopoeisis
Il13	interleukin 13	2.68	0.0425	Allergic inflammation
Cytokine Receptor Genes				
Il2rg	interleukin 2 receptor, gamma chain	104.87	0.0008	Common γ-chain subunit for IL2, IL4, IL7, IL9, IL15, IL21 receptors
Il10ra	interleukin 10 receptor, alpha	72.15	0.0067	Subunit of IL10 receptor
Il13ra1	interleukin 13 receptor, alpha 1	31.21	0.0064	Common subunit for IL13 and IL4 receptors
Il10rb	interleukin 10 receptor, beta	25.30	0.0016	Subunit of IL10 receptor
Il6st	interleukin 6 signal transducer	19.63	0.0131	
Tnfrsf1a	tumor necrosis factor receptor superfamily, member 1a	14.78	0.0221	TNF receptor
Il2rb	interleukin 2 receptor, beta chain	9.77	0.0033	IL2 receptor subunit
Il6ra	interleukin 6 receptor, alpha	9.72	0.0206	IL6 receptor subunit
Il1r2	interleukin 1 receptor, type II	7.37	0.0312	IL1A / IL1B antagonist
Other Inflammatory Genes				
Spp1	secreted phosphoprotein 1	162.32	0.0048	Th1 differentiation; anti-apoptosis; neutrophil / mast cell migration
Itgb2	integrin beta 2	113.49	0.0001	Leukocyte adhesion / extravasation
Itgam	integrin alpha M	24.34	0.0203	CD11b antigen
Casp1	caspase 1	23.31	0.0002	Cell necrosis; IL-1β and IL-18 synthesis
Abcf1	ATP-binding cassette, sub-family F (GCN20), member 1	6.11	0.0033	?
Bcl6	B-cell leukemia/lymphoma 6	4.85	0.0149	IL-4 synthesis (B-cells)

B. 14 day post-ligation

Gene Symbol	Gene Name	Fold Change (LCA/RCA)	p value	Function
Chemokine Genes				
Ccl6	chemokine (C-C motif) ligand 6	994.86	0.0480	**Expressed by:** neutrophils, macs
Ccl2	chemokine (C-C motif) ligand 2	716.07	0.0047	**Attracts:** monocytes, memory T-cells, DCs
Ccl9	chemokine (C-C motif) ligand 9	83.36	0.0231	**Attracts:** $CD11b^+$ DCs
Ccl12	chemokine (C-C motif) ligand 12	69.38	0.0346	**Attracts:** monocytes, lymphocytes
Ccl22	chemokine (C-C motif) ligand 22	61.52	0.0004	**Expressed by:** macrophages, DCs
Ccl19	chemokine (C-C motif) ligand 19	60.53	0.0452	**Attracts:** B-cells, $CCR7^+$ T-cells, DCs
Ccl4	chemokine (C-C motif) ligand 4	57.61	0.0084	**Attracts:** monocytes, NK cells
Ccl3	chemokine (C-C motif) ligand 3	56.19	0.0281	**Attracts:** neutrophils
Ccl5	chemokine (C-C motif) ligand 5	53.51	0.0086	**Attracts:** T-cells **Activates:** NK cells
Cx3cl1	chemokine (C-X3-C motif) ligand 1	51.79	0.0004	**Attracts:** T-cells, monocytes, DCs
Cxcl9	chemokine (C-X-C motif) ligand 9	31.22	0.0148	**Attracts:** T-cells
Ccl17	chemokine (C-C motif) ligand 17	19.42	0.0057	**Attracts:** T-cells
Ccl24	chemokine (C-C motif) ligand 24	15.87	0.0049	**Attracts:** eosinophils, resting T-cells, neutrophils
Ccl25	chemokine (C-C motif) ligand 25	7.90	0.0273	**Attracts:** T-cells, macrophages, DCs
Ccl1	chemokine (C-C motif) ligand 1	5.99	0.0030	**Attracts:** NK cells, monocytes, immature B-cells
Ccl20	chemokine (C-C motif) ligand 20	3.55	0.0259	**Attracts:** lymphocytes, neutrohpils, DCs
Chemokine Receptor Genes				
Ccr2	chemokine (C-C motif) receptor 2	165.90	0.0382	**Binds:** CCL2
Ccr1	chemokine (C-C motif) receptor 1	141.64	0.0224	**Binds:** CCL3, CCL5, CCL7, CCL23
Cxcr3	chemokine (C-X-C motif) receptor 3	39.99	0.0371	**Binds:** CXCL9, CXCL10, CXCL11, CXCL4
Ccr6	chemokine (C-C motif) receptor 6	30.28	0.0029	**Binds:** CCL20
Ccr7	chemokine (C-C motif) receptor 7	24.69	0.0053	**Binds:** CCL19
Ccr10	chemokine (C-C motif) receptor 10	12.72	0.0126	**Binds:** CCL27
Cxcr5	chemokine (C-X-C motif) receptor 5	11.48	0.0453	**Binds:** CXCL13
Ccr4	chemokine (C-C motif) receptor 4	7.10	0.0217	**Binds:** CCL2, CCL4, CCL5, CCL17, CCL22

Gene Symbol	Gene Name	Fold Change (LCA/RCA)	p value	Function
Cytokine Genes				
Tgfb1	transforming growth factor, beta 1	276.70	0.0106	Anti-inflammatory
Il15	interleukin 15	73.47	0.0151	NK cell activation / proliferation; homeostatic
Il1b	interleukin 1 beta	56.06	0.0384	Pro-inflammatory
Il16	interleukin 16	50.28	0.0334	T-cell activation **Attracts:** activated $CD4^+$ T-cells, $CD4^+$ DCs
Aimp1	aminoacyl tRNA synthetase complex-interacting multifunctional protein 1	44.77	0.0267	Pro-inflammatory
Il1f6	interleukin 1 family, member 6	24.51	0.0046	?
Il18	interleukin 18	22.96	0.0247	Pro-inflammatory
Il4	interleukin 4	21.73	0.0103	Th2 T-cell differentiation
Il1f8	interleukin 1 family, member 8	20.08	0.0037	?
Il17b	interleukin 17B	17.83	0.0087	Pro-inflammatory
Ltb	lymphotoxin B	17.58	0.0210	Pro-inflammatory
Il13	interleukin 13	15.74	0.0016	Allergic inflammation
Il11	interleukin 11	6.09	0.0498	Platelet production; lymphopoeisis
Il3	interleukin 3	4.50	0.0401	Myeloid progenitor cell differentiation
Cytokine Receptor Genes				
Il2rg	interleukin 2 receptor, gamma chain	456.61	0.0252	Common γ-chain subunit for IL2, IL4, IL7, IL9, IL15, IL21 receptors
Il13ra1	interleukin 13 receptor, alpha 1	292.70	0.0157	Common subunit for IL13 and IL4 receptors
Il10ra	interleukin 10 receptor, alpha	290.38	0.0150	Subunit of IL10 receptor
Il10rb	interleukin 10 receptor, beta	172.21	0.0093	Subunit of IL10 receptor
Il6st	interleukin 6 signal transducer	111.75	0.0202	
Il1r1	interleukin 1 receptor, type I	98.54	0.0346	
Tnfrsf1a	tumor necrosis factor receptor superfamily, member 1a	87.87	0.0309	TNF receptor
Il2rb	interleukin 2 receptor, beta chain	55.44	0.0049	IL2 receptor subunit
Il6ra	interleukin 6 receptor, alpha	39.71	0.0011	IL6 receptor subunit
Other Inflammatory Genes				
Spp1	secreted phosphoprotein 1	15057.95	0.0258	Th1 differentiation; anti-apoptosis; neutrophil / mast cell migration
Itgb2	integrin beta 2	958.06	0.0288	Leukocyte adhesion / extravasation
Casp1	caspase 1	128.06	0.0185	Cell necrosis; IL-1β and IL-18 synthesis
Abcf1	ATP-binding cassette, sub-family F (GCN20), member 1	28.73	0.0113	?
Bcl6	B-cell leukemia/lymphoma 6	14.13	0.0146	IL-4 synthesis (B-cells)
Tollip	toll interacting protein	11.45	0.0141	Inhibits TLR signaling

To further determine IFNγ production by cells in flow-disturbed lesions, cytokine expression was induced *ex vivo* by culturing LCA and RCA overnight in the presence of 12-O-tetradecanoylphorbol-13-acetate (TPA) and ionomycin. Production of IFNγ, tumor necrosis factor alpha (TNFα□), interleukin 2 (IL-2), interleukin 4 (IL-4), and interleukin 5 (IL-5) protein expression was assessed in culture supernatants by cytokine bead array ELISA. IFNγ, IL-2 and TNFα production was robustly increased in LCA, but not in RCA, obtained from 7 day post-ligated mice (Fig. 2.11C). IL-5 was increased as well in LCA, while IL-4 levels were not detected in LCA or RCA by the ELISA (Fig. 2.12C). These results suggest that d-flow induces Th1-skewed inflammation.

To further examine the Th1-skewed response, we performed additional qPCR for Th-lineage specific transcription factors, *Tbx21* (for Th1), *Gata3* (for Th2), *Rorc* (for Th17) and *Foxp3* (for Treg) using the same samples used in Figure 5A. We found that *Tbx21* was upregulated by 7 and 14 days, while *Gata3* did not change in LCA until 14 days post-ligation (Fig. 2.12D). These results are consistent with the *Ifng* qPCR result and the ELISA data (Fig. 2.12B-C), confirming the presence of a Th1-skewed immune response in the flow-disturbed LCA. In addition, *Rorc* and *Foxp3* transcription factors were upregulated at 7 and 14 days, indicating the presence of Th17 and Treg cells in LCA as well.

Vascular inflammation kinetics correspond with immune cell infiltration kinetics in vivo – a modeling study.

PLSR analysis was used to model the relationship between changes in cytokine/cytokine receptor gene expression and leukocyte accumulation dynamics in the arterial wall following exposure to d-flow. The optimized model consisted of 4 statistically significant components with a R^2Y =0.943 and Q^2 =0.757, suggesting a strong fit between observed changes in gene expression and immune cell numbers. Days 7 and 14 form distinct clusters on the scores plot indicating a separation of gene expression trends between the two days of collection (Fig. 2.13). From the scores plot, the positive PC2 direction roughly relates with information contained in day 7 samples, and the positive PC1 direction with information contained in day 14 samples.

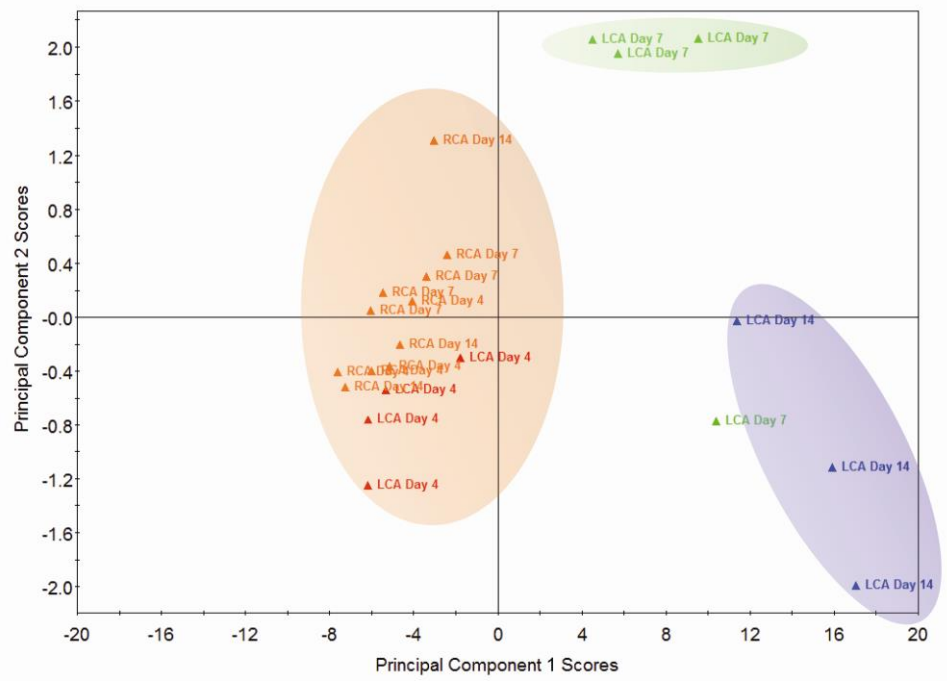

Figure 2.13. PLSR modeling distinguishes time sensitive changes in cytokine and chemokine gene expression following partial carotid ligation. *The scores plot of the contributions of individual LCA and RCA samples to the trained model separates time and flow conditions that induce expression of inflammatory cytokines from those that do not. Plot shows relatively uninflamed samples, LCA samples at 4 days post-ligation (red symbols) and RCA samples at any time point (orange symbols), versus samples showing a progressive increase in inflammation; LCA at 7 days post-ligation (green symbols) and LCA at 14 days post-ligation (blue symbols). Samples grouped by similar gene expression profiles are depicted by colored ovals.*

Similarly, a loadings scatter plot maps the relative importance, or weight contribution, of X or Y-block variables to a principal component. There is a separation between most X- and Y-variables, save for IFNγ, which shows a strong correlation with the number of immune cells recruited into LCA by day 7 post-ligation (Fig. 2.14). In contrast, the strong relation of the remaining genes to day 14 LCA samples suggests that the inflammatory cytokine response increases after immune cell recruitment, corresponding with SMC migration into the carotid intima and plaque growth (Fig. 2.8B).

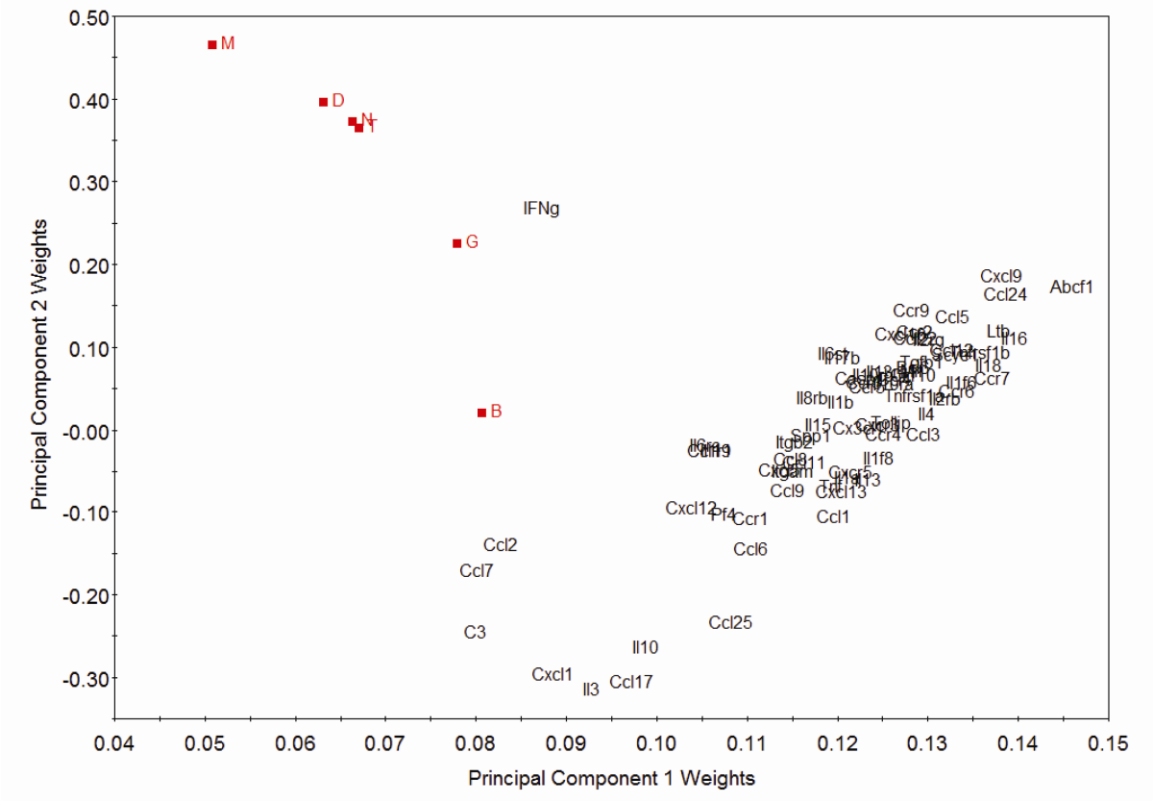

Figure 2.14. PLSR modeling links IFNγ expression with increased leukocyte accumulation in flow-disturbed arterial wall at 7 days, preceding increased inflammation and plaque growth at 14 days post-ligation. *The loading scatterplot of weights projects arterial wall leukocyte numbers from the flow cytometry experiments (red squares) on the same plot as changes in cytokine and chemokine expression from the qPCR array data set (black). Data from our PCR primer set for IFNγ has been substituted for the original array data. B, B-cells; T, T-cells, D, DCs, N, NK cells, M, monocyte/macrophages; G, granulocytes.*

2.4 Discussion

The involvement of immune cells in atherogenesis has been well-established (Galkina and Ley, 2009). While multi-parameter or multiplex flow cytometry methods that are capable of analyzing up to 15 different markers have been used (Wood, 2005;Chattopadhyay et al., 2006;Frischmann and Muller, 2006;Hotson et al., 2009;Song et al., 2010;Yamamoto et al., 2011), they have not been applied to study immune cell kinetics in atherosclerosis to our knowledge. Multi-parameter flow cytometry studies in the atherosclerosis field have typically used up to 4-7 surface phenotype markers despite the discovery of increasingly more complex subsets of macrophages and DCs important to atherogenesis (Galkina et al., 2006;Gotsman et al., 2006;Galkina et al., 2007;Guzik et al., 2007;Tacke et al., 2007;Combadiere et al., 2008;Hjerpe et al., 2010;Bu et al., 2011). To overcome this issue, we developed a robust 13-parameter, 10-fluorochrome flow cytometry method to analyze the kinetics of 7 distinct leukocyte types in atherosclerotic lesions.

We applied this flow cytometry method to lesion samples from our d-flow model of atherosclerosis. The major advantage of this murine model is that it induces atherogenesis rapidly and reproducibly along the entire length of LCA, beginning with a healthy disease-free artery and leading to a fully-developed atheroma in only a few weeks. This allowed us to track week-to-week and even day-to-day changes in immune cell populations within the developing atherosclerotic lesion. The flow cytometry findings in LCA and RCA were validated by immunostaining with CD45, CD11b, CD11c, CD3, and CD68 (Fig. 2.6, 2.8 and 2.10). CD45, CD11b, and CD68 stains show that some vascular

wall leukocytes detected by the flow cytometry method likely reside within the adventitia or media and do not necessarily represent intimal plaque leukocytes. In contrast to flow-disturbed LCA, athero-resistant RCA and sham-operated LCA contained only a few resident leukocytes and did not show sustained immune cell accumulations throughout the study.

The most dominant feature of our immune cell kinetic results was a surge of leukocyte numbers at 7 days post-ligation, followed by substantial contraction of innate leukocytes at day 14, primarily comprised of monocyte/macrophages and DCs (Fig. 2.9, Table 2.1). This appears to be in conflict with previous studies that reported progressive leukocyte accumulation, especially of monocyte-derived macrophages and DCs, in the arterial wall during atherogenesis (Galkina et al., 2006;Randolph, 2008;Galkina and Ley, 2009;Potteaux et al., 2011). Immunostaining for SMCs (αSMA) and *in situ* apoptosis show heavy SMC migration and increased cell death in intimal plaques, corresponding with decreased CD45 staining at 14 and 21 days post-ligation (Fig. 2.8). Together, the data suggest that leukocyte death, along with fibrous cap formation, account for some of the observed leukocyte regression. However, cell egress early during lesion initiation cannot be ruled out as a potential mechanism for macrophage/DC loss in our model, which is interesting since efflux of monocyte-derived cells has been shown to be primarily associated with lesion regression (Randolph, 2008;Potteaux et al., 2011). Another limitation in comparing these findings to previous work is that in our model, flow disturbance induces an accelerated atherogenesis with proportionately low numbers of T-cells and increased numbers of monocyte/macrophages, DCs, NK cells, and

granulocytes compared to previous findings in aorta (Fig. 2.5) (Galkina et al., 2006). Whether this is due to the d-flow-model used or the arteries examined in this study requires further research, although neutrophil margination and transmigration has been previously reported in atherosclerosis of the carotid bifurcation (Drechsler et al., 2010).

The surge in leukocyte accumulation correlates with the initiation of inflammatory cytokine and chemokine expression in our PCR Array studies (Fig. 2.12, Table 2.2), especially pro-atherogenic cytokines TNFα and IFNγ, which have been shown to play central, necessary roles in atherogenesis (Tedgui and Mallat, 2006;Galkina and Ley, 2009;McLaren and Ramji, 2009). These findings suggest that the early surge in immune cells contributes directly to the increased inflammation and rapid plaque growth seen in our model, a conjecture supported by the PLSR modeling analysis, which shows that the immune cell kinetics measured in our study correlate well with changes in inflammatory gene expression (Fig. 2.13 and 2.14). In particular, the analysis indicated a predominant role for IFNγ in immune cell-mediated inflammatory pathology within the flow-disturbed region, leading to a cascade of subsequent pro-inflammatory gene upregulation and atheromatous plaque development by day 14.

Additionally, atherosclerosis-associated chemokines for monocytes (*Ccl2*, *Cxcl2*, *Ccl7*), DCs (*Cx3cl1*, *Ccl19*, *Ccl9*), T-cells (*Ccl5*, *Cxcl9*), neutrophils (*Ccl3*, *Ccl24*), NK cells (*Cxcl10*, *Ccl4*), and B-cells (*Cxcl12*, *Ccl19*) were detected in flow-disturbed LCA (Table 2.2), further linking d-flow to established mechanisms of leukocyte trafficking in atherosclerosis (Galkina and Ley, 2009). These results correspond with recent whole

genome profiles of human coronary and carotid artery plaques (Cagnin et al., 2009). We also found significantly increased levels of the Th1 T-cell-specific transcription factor T-bet (*Tbx21*) at day 7 post-ligation, which were sustained through day 14 (Fig. 2.12), which correlate with the sustained, albeit low, numbers of CD4 and CD8 T-cells seen in LCA at 14 days post-ligation and beyond (Fig. 2.9B). The presence of T-bet expression in LCA suggests that flow-disturbance induces the Th1-skewed adaptive immune response typical of atherosclerosis (Schulte et al., 2008). This was confirmed by ELISA array assays, which showed a distinct Th1 cytokine signature in flow-disturbed LCA stimulated *ex vivo*. Our model also showed the presence of Th17 T-cells (*Rorc*) and Tregs (*Foxp3*) in the plaque along with slight increases in *Il17a* and *Il10* gene expression (Fig. 2.12) as previously reported in humans and mice (Gotsman et al., 2006;Gotsman et al., 2007;Eid et al., 2009;Erbel et al., 2009).

Flow cytometry provides a more accurate and unbiased method to quantify arterial immune cells than previously used histological approaches. However, the use of enzymatic tissue digestion and homogenization to extract vascular leukocytes may induce cell death (Fig. 2.7) or other enzymatic extraction-dependent artifacts that may affect the flow cytometry results systematically or in a sub-population-dependent manner. Furthermore, low leukocyte counts in some of our samples (i.e., greater (GC) and lesser (LC) curvature of the aortic arch and LCA at 4 days post-ligation) could undermine the statistical accuracy of our quantitative and phenotypic percentage data (Fig. 2.6A, 2.5, 2.9). As such, our flow cytometry results need to be interpreted with appropriate caution.

Our studies establish partial carotid ligation as an effective animal model to study the inflammatory pathogenesis of atherosclerosis. We provide a comprehensive quantitative description of infiltrating leukocyte number and composition over the entire life span of an atherosclerotic lesion. We show that rather than being progressive, leukocyte accumulation in the flow-disturbed vascular lesion is dynamic, and that peak leukocyte accumulation immediately precedes major plaque development.

2.5 References

Bu, D.X., Tarrio, M., Maganto-Garcia, E., Stavrakis, G., Tajima, G., Lederer, J., Jarolim, P., Freeman, G.J., Sharpe, A.H., and Lichtman, A.H. (2011). Impairment of the programmed cell death-1 pathway increases atherosclerotic lesion development and inflammation. *Arterioscler Thromb Vasc Biol* 31**,** 1100-1107.

Cagnin, S., Biscuola, M., Patuzzo, C., Trabetti, E., Pasquali, A., Laveder, P., Faggian, G., Iafrancesco, M., Mazzucco, A., Pignatti, P.F., and Lanfranchi, G. (2009). Reconstruction and functional analysis of altered molecular pathways in human atherosclerotic arteries. *BMC Genomics* 10**,** 13.

Chattopadhyay, P.K., Price, D.A., Harper, T.F., Betts, M.R., Yu, J., Gostick, E., Perfetto, S.P., Goepfert, P., Koup, R.A., De Rosa, S.C., Bruchez, M.P., and Roederer, M. (2006). Quantum dot semiconductor nanocrystals for immunophenotyping by polychromatic flow cytometry. *Nat Med* 12**,** 972-977.

Combadiere, C., Potteaux, S., Rodero, M., Simon, T., Pezard, A., Esposito, B., Merval, R., Proudfoot, A., Tedgui, A., and Mallat, Z. (2008). Combined inhibition of CCL2, CX3CR1, and CCR5 abrogates Ly6C(hi) and Ly6C(lo) monocytosis and almost abolishes atherosclerosis in hypercholesterolemic mice. *Circulation* 117**,** 1649-1657.

Drechsler, M., Megens, R.T., Van Zandvoort, M., Weber, C., and Soehnlein, O. (2010). Hyperlipidemia-triggered neutrophilia promotes early atherosclerosis. *Circulation* 122**,** 1837-1845.

Eid, R.E., Rao, D.A., Zhou, J., Lo, S.F., Ranjbaran, H., Gallo, A., Sokol, S.I., Pfau, S., Pober, J.S., and Tellides, G. (2009). Interleukin-17 and interferon-gamma are

produced concomitantly by human coronary artery-infiltrating T cells and act synergistically on vascular smooth muscle cells. *Circulation* 119**,** 1424-1432.

Erbel, C., Chen, L., Bea, F., Wangler, S., Celik, S., Lasitschka, F., Wang, Y., Bockler, D., Katus, H.A., and Dengler, T.J. (2009). Inhibition of IL-17A attenuates atherosclerotic lesion development in apoE-deficient mice. *J Immunol* 183**,** 8167-8175.

Frischmann, U., and Muller, W. (2006). Nine fluorescence parameter analysis on a four-color fluorescence activated flow cytometer. *Cytometry A* 69**,** 124-126.

Galkina, E., Harry, B.L., Ludwig, A., Liehn, E.A., Sanders, J.M., Bruce, A., Weber, C., and Ley, K. (2007). CXCR6 promotes atherosclerosis by supporting T-cell homing, interferon-gamma production, and macrophage accumulation in the aortic wall. *Circulation* 116**,** 1801-1811.

Galkina, E., Kadl, A., Sanders, J., Varughese, D., Sarembock, I.J., and Ley, K. (2006). Lymphocyte recruitment into the aortic wall before and during development of atherosclerosis is partially L-selectin dependent. *J Exp Med* 203**,** 1273-1282.

Galkina, E., and Ley, K. (2009). Immune and inflammatory mechanisms of atherosclerosis (*). *Annu Rev Immunol* 27**,** 165-197.

Gaudet, S., Janes, K.A., Albeck, J.G., Pace, E.A., Lauffenburger, D.A., and Sorger, P.K. (2005). A compendium of signals and responses triggered by prodeath and prosurvival cytokines. *Mol Cell Proteomics* 4**,** 1569-1590.

Gotsman, I., Grabie, N., Gupta, R., Dacosta, R., Macconmara, M., Lederer, J., Sukhova, G., Witztum, J.L., Sharpe, A.H., and Lichtman, A.H. (2006). Impaired regulatory

T-cell response and enhanced atherosclerosis in the absence of inducible costimulatory molecule. *Circulation* 114**,** 2047-2055.

Gotsman, I., Gupta, R., and Lichtman, A.H. (2007). The influence of the regulatory T lymphocytes on atherosclerosis. *Arterioscler Thromb Vasc Biol* 27**,** 2493-2495.

Guzik, T.J., Hoch, N.E., Brown, K.A., Mccann, L.A., Rahman, A., Dikalov, S., Goronzy, J., Weyand, C., and Harrison, D.G. (2007). Role of the T cell in the genesis of angiotensin II induced hypertension and vascular dysfunction. *J Exp Med* 204**,** 2449-2460.

Hansson, G.K. (2005). Inflammation, atherosclerosis, and coronary artery disease. *N Engl J Med* 352**,** 1685-1695.

Hansson, G.K., and Hermansson, A. (2011). The immune system in atherosclerosis. *Nat Immunol* 12**,** 204-212.

Hansson, G.K., Robertson, A.K., and Soderberg-Naucler, C. (2006). Inflammation and atherosclerosis. *Annu Rev Pathol* 1**,** 297-329.

Hermansson, A., Ketelhuth, D.F., Strodthoff, D., Wurm, M., Hansson, E.M., Nicoletti, A., Paulsson-Berne, G., and Hansson, G.K. (2010). Inhibition of T cell response to native low-density lipoprotein reduces atherosclerosis. *J Exp Med* 207**,** 1081-1093.

Hjerpe, C., Johansson, D., Hermansson, A., Hansson, G.K., and Zhou, X. (2010). Dendritic cells pulsed with malondialdehyde modified low density lipoprotein aggravate atherosclerosis in Apoe(-/-) mice. *Atherosclerosis* 209**,** 436-441.

Hotson, A.N., Hardy, J.W., Hale, M.B., Contag, C.H., and Nolan, G.P. (2009). The T cell STAT signaling network is reprogrammed within hours of bacteremia via secondary signals. *J Immunol* 182**,** 7558-7568.

Janes, K.A., Albeck, J.G., Gaudet, S., Sorger, P.K., Lauffenburger, D.A., and Yaffe, M.B. (2005). A systems model of signaling identifies a molecular basis set for cytokine-induced apoptosis. *Science* 310**,** 1646-1653.

Janes, K.A., Kelly, J.R., Gaudet, S., Albeck, J.G., Sorger, P.K., and Lauffenburger, D.A. (2004). Cue-signal-response analysis of TNF-induced apoptosis by partial least squares regression of dynamic multivariate data. *J Comput Biol* 11**,** 544-561.

Kemp, M.L., Wille, L., Lewis, C.L., Nicholson, L.B., and Lauffenburger, D.A. (2007). Quantitative network signal combinations downstream of TCR activation can predict IL-2 production response. *J Immunol* 178**,** 4984-4992.

Li, L., Chen, W., Rezvan, A., Jo, H., and Harrison, D.G. (2011a). Tetrahydrobiopterin deficiency and nitric oxide synthase uncoupling contribute to atherosclerosis induced by disturbed flow. *Arterioscler Thromb Vasc Biol* 31**,** 1547-1554.

Li, L., Chen, W., Rezvan, A., Jo, H., and Harrison, D.G. (2011b). Tetrahydrobiopterin Deficiency and Nitric Oxide Synthase Uncoupling Contribute to Atherosclerosis Induced by Disturbed Flow. *Arterioscler Thromb Vasc Biol*.

Li, L., Rezvan, A., Salerno, J.C., Husain, A., Kwon, K., Jo, H., Harrison, D.G., and Chen, W. (2010). GTP cyclohydrolase I phosphorylation and interaction with GTP cyclohydrolase feedback regulatory protein provide novel regulation of endothelial tetrahydrobiopterin and nitric oxide. *Circ Res* 106**,** 328-336.

Libby, P. (2002). Inflammation in atherosclerosis. *Nature* 420**,** 868-874.

Mclaren, J.E., and Ramji, D.P. (2009). Interferon gamma: a master regulator of atherosclerosis. *Cytokine Growth Factor Rev* 20**,** 125-135.

Miller-Jensen, K., Janes, K.A., Brugge, J.S., and Lauffenburger, D.A. (2007). Common effector processing mediates cell-specific responses to stimuli. *Nature* 448**,** 604-608.

Nakajima, T., Goek, O., Zhang, X., Kopecky, S.L., Frye, R.L., Goronzy, J.J., and Weyand, C.M. (2003). De novo expression of killer immunoglobulin-like receptors and signaling proteins regulates the cytotoxic function of CD4 T cells in acute coronary syndromes. *Circ Res* 93**,** 106-113.

Nakajima, T., Schulte, S., Warrington, K.J., Kopecky, S.L., Frye, R.L., Goronzy, J.J., and Weyand, C.M. (2002). T-cell-mediated lysis of endothelial cells in acute coronary syndromes. *Circulation* 105**,** 570-575.

Nam, D., Ni, C.W., Rezvan, A., Suo, J., Budzyn, K., Llanos, A., Harrison, D., Giddens, D., and Jo, H. (2009). Partial carotid ligation is a model of acutely induced disturbed flow, leading to rapid endothelial dysfunction and atherosclerosis. *Am J Physiol Heart Circ Physiol* 297**,** H1535-1543.

Nam, D., Ni, C.W., Rezvan, A., Suo, J., Budzyn, K., Llanos, A., Harrison, D.G., Giddens, D.P., and Jo, H. (2010). A model of disturbed flow-induced atherosclerosis in mouse carotid artery by partial ligation and a simple method of RNA isolation from carotid endothelium. *J Vis Exp*.

Ni, C.W., Qiu, H., Rezvan, A., Kwon, K., Nam, D., Son, D.J., Visvader, J.E., and Jo, H. (2010). Discovery of novel mechanosensitive genes in vivo using mouse carotid artery endothelium exposed to disturbed flow. *Blood* 116**,** e66-73.

Niessner, A., and Weyand, C.M. (2010). Dendritic cells in atherosclerotic disease. *Clin Immunol* 134**,** 25-32.

Paigen, B., Morrow, A., Holmes, P.A., Mitchell, D., and Williams, R.A. (1987). Quantitative assessment of atherosclerotic lesions in mice. *Atherosclerosis* 68**,** 231-240.

Paulson, K.E., Zhu, S.N., Chen, M., Nurmohamed, S., Jongstra-Bilen, J., and Cybulsky, M.I. (2010). Resident intimal dendritic cells accumulate lipid and contribute to the initiation of atherosclerosis. *Circ Res* 106**,** 383-390.

Perfetto, S.P., Ambrozak, D., Nguyen, R., Chattopadhyay, P., and Roederer, M. (2006). Quality assurance for polychromatic flow cytometry. *Nat Protoc* 1**,** 1522-1530.

Potteaux, S., Gautier, E.L., Hutchison, S.B., Van Rooijen, N., Rader, D.J., Thomas, M.J., Sorci-Thomas, M.G., and Randolph, G.J. (2011). Suppressed monocyte recruitment drives macrophage removal from atherosclerotic plaques of Apoe-/- mice during disease regression. *J Clin Invest* 121**,** 2025-2036.

Pryshchep, S., Sato, K., Goronzy, J.J., and Weyand, C.M. (2006). T cell recognition and killing of vascular smooth muscle cells in acute coronary syndrome. *Circ Res* 98**,** 1168-1176.

Randolph, G.J. (2008). Emigration of monocyte-derived cells to lymph nodes during resolution of inflammation and its failure in atherosclerosis. *Curr Opin Lipidol* 19**,** 462-468.

Rivet, C.A., Hill, A.S., Lu, H., and Kemp, M.L. (2011). Predicting cytotoxic T-cell age from multivariate analysis of static and dynamic biomarkers. *Mol Cell Proteomics* 10**,** M110 003921.

Roederer, M. (2002a). Compensation in flow cytometry. *Curr Protoc Cytom* Chapter 1**,** Unit 1 14.

Roederer, M. (2002b). Multiparameter FACS analysis. *Curr Protoc Immunol* Chapter 5**,** Unit 5 8.

Schulte, S., Sukhova, G.K., and Libby, P. (2008). Genetically programmed biases in Th1 and Th2 immune responses modulate atherogenesis. *Am J Pathol* 172**,** 1500-1508.

Smith, E., Prasad, K.M., Butcher, M., Dobrian, A., Kolls, J.K., Ley, K., and Galkina, E. (2010). Blockade of interleukin-17A results in reduced atherosclerosis in apolipoprotein E-deficient mice. *Circulation* 121**,** 1746-1755.

Song, K., Bolton, D.L., Wei, C.J., Wilson, R.L., Camp, J.V., Bao, S., Mattapallil, J.J., Herzenberg, L.A., Andrews, C.A., Sadoff, J.C., Goudsmit, J., Pau, M.G., Seder, R.A., Kozlowski, P.A., Nabel, G.J., Roederer, M., and Rao, S.S. (2010). Genetic immunization in the lung induces potent local and systemic immune responses. *Proc Natl Acad Sci U S A* 107**,** 22213-22218.

Sukhova, G.K., Zhang, Y., Pan, J.H., Wada, Y., Yamamoto, T., Naito, M., Kodama, T., Tsimikas, S., Witztum, J.L., Lu, M.L., Sakara, Y., Chin, M.T., Libby, P., and Shi, G.P. (2003). Deficiency of cathepsin S reduces atherosclerosis in LDL receptor-deficient mice. *J Clin Invest* 111**,** 897-906.

Swirski, F.K., Libby, P., Aikawa, E., Alcaide, P., Luscinskas, F.W., Weissleder, R., and Pittet, M.J. (2007). Ly-6Chi monocytes dominate hypercholesterolemia-associated monocytosis and give rise to macrophages in atheromata. *J Clin Invest* 117**,** 195-205.

Tacke, F., Alvarez, D., Kaplan, T.J., Jakubzick, C., Spanbroek, R., Llodra, J., Garin, A., Liu, J., Mack, M., Van Rooijen, N., Lira, S.A., Habenicht, A.J., and Randolph,

G.J. (2007). Monocyte subsets differentially employ CCR2, CCR5, and CX3CR1 to accumulate within atherosclerotic plaques. *J Clin Invest* 117**,** 185-194.

Tedgui, A., and Mallat, Z. (2006). Cytokines in atherosclerosis: pathogenic and regulatory pathways. *Physiol Rev* 86**,** 515-581.

Wood, B.L. (2005). Ten-color immunophenotyping of hematopoietic cells. *Curr Protoc Cytom* Chapter 6**,** Unit6 21.

Yamamoto, T., Price, D.A., Casazza, J.P., Ferrari, G., Nason, M., Chattopadhyay, P.K., Roederer, M., Gostick, E., Katsikis, P.D., Douek, D.C., Haubrich, R., Petrovas, C., and Koup, R.A. (2011). Surface expression patterns of negative regulatory molecules identify determinants of virus-specific CD8+ T-cell exhaustion in HIV infection. *Blood* 117**,** 4805-4815.

Zhou, J., Tang, P.C., Qin, L., Gayed, P.M., Li, W., Skokos, E.A., Kyriakides, T.R., Pober, J.S., and Tellides, G. (2010). CXCR3-dependent accumulation and activation of perivascular macrophages is necessary for homeostatic arterial remodeling to hemodynamic stresses. *J Exp Med* 207**,** 1951-1966.

CHAPTER 3:

DISTURBED FLOW INDUCES SUSTAINED LEUCOPENIA DURING ATHEROGENESIS IN HYPERLIPIDEMIC APOE$^{-/-}$ MICE

3.1 Introduction

Atherosclerotic lesions are characterized by abnormal lipid accumulation, cell death, fibrosis, and chronic vascular inflammation (Libby, 2002;Hansson, 2005). Leukocyte recruitment into the vascular wall at specific, atheroprone regions of large arteries has been identified as a key pathogenic step in the development of the disease (Hansson and Libby, 2006;Galkina and Ley, 2009;Hansson and Hermansson, 2011). In human patients, the vulnerable atherosclerotic plaques responsible for symptomatic cardiovascular disease are characterized by a thin fibrous cap, large extracellullar lipid pool, an expanded leukocytic infiltrate, and are actively inflamed (Virmani et al., 2006). Unfortunately, identifying patients at risk for acute cardiovascular events such as myocardial infarction or stroke is difficult because current methods of identifying pathogenically active lesions are exceedingly invasive.

Because of this, great effort has been put into the discovery of novel biomarkers that can accurately predict the presence of actively inflamed, vulnerable plaques and are also present in the blood and thus easily accessible by a simple blood test (Weber and Noels, 2011;Dadu et al., 2012). Unfortunately, no biomarkers have been found that can discriminate pathogenic atherosclerosis-associated inflammation from other common sources of inflammation such as infection or autoimmune disease. However, highlighting the importance of leukocyte trafficking and recruitment during active atherogenesis, studies looking at the composition of peripheral blood leukocytes (PBLs) have identified several immune cell populations whose increased presence in the blood positively correlates with clinically active disease in humans (Liuzzo et al., 2000), or have been

shown to promote atherosclerosis in mouse models of the disease (Swirski et al., 2007;Drechsler et al., 2010). While these findings suggest that the identification of 'biomarker' PBL populations holds promise as a potential clinical diagnostic tool, atherosclerosis takes years to develop in humans and months in mouse models. Furthermore the inflammatory pathogenesis of atherosclerosis is intricately confounded by co-morbid pro-inflammatory conditions such as hyperlipidemia, which has been shown to increase the number of circulating monocytes, neutrophils, lymphocytes, and progenitor cells, making it difficult to isolate hyperlipidemia-dependent changes in the PBL compartment from those that may be caused by vascular inflammation associated with the vulnerable plaque (Swirski et al., 2007;Soehnlein et al., 2009;Drechsler et al., 2010;Gomes et al., 2010).

Recently, we developed an accelerated model of atherosclerosis using partial ligation surgery of the distal branches of the mouse left common carotid artery (LCA), which causes d-flow with characteristic low and oscillatory wall shear stress, and leads to lipid-laden plaque development within 2 weeks along the entire length of the common carotid artery in apolipoprotein E-deficient ($ApoE^{-/-}$) mice fed a high-fat diet (HFD) (Nam et al., 2009). Using this model, we have shown that d-flow induces broad changes in the gene expression profile of endothelial cells (hours to days), including inter-cellular adhesion molecule 1 (ICAM-1) and vascular cell adhesion molecule 1 (VCAM-1) within 2 days (Nam et al., 2009;Ni et al., 2010), a requisite step for leukocyte recruitment (Cybulsky et al., 2001). Extensive leukocyte infiltration into the flow-disturbed artery wall, including monocytes, dendritic cells (DCs), T-cells, granulocytes, and NK cells, occurred within 4

to 7 days, and preceded atherosclerotic lesion development at 14 days post-ligation (Alberts-Grill et al., 2012). Furthermore, immune cell infiltration was shown to correspond with progressive pro-atherogenic, pro-inflammatory cytokine expression (i.e., interferon-gamma, RANTES, and monocyte chemoattractant peptide 1 (MCP-1)), highlighting the link between d-flow, leukocyte recruitment, vascular inflammation, and atherosclerosis (Alberts-Grill et al., 2012).

In order to better understand how atherogenesis acutely influences PBL trafficking patterns, we quantified seven major leukocyte subsets in blood samples taken from ligated (atherosclerotic) and sham-operated (non-atherosclerotic) ApoE$^{-/-}$ mice over a 4 week time course. Here, we hypothesized that the rapid leukocyte recruitment, pro-inflammatory cytokine expression, and atherosclerosis development in flow-disturbed LCA should disrupt PBL trafficking patterns in the blood in ligated versus sham-operated mice.

3.2 Methods

Mice. Male ApoE$^{-/-}$ mice (B6.129P2-ApoEtm1Unc/J) were purchased from The Jackson Laboratory (Bar Harbor) and were fed *ad libitum* with standard chow diet until surgery at 8 to 9 weeks of age. The ApoEtm1Unc mutation was from a 129P2/OlaHsd-derived E14Tg2a embryonic stem cell line and was backcrossed to the C57BL/6J for 10 generations.

Partial carotid ligation surgery. Partial carotid ligation surgeries were performed as previously described (Nam et al., 2009;Nam et al., 2010). Mice were anesthetized by intra-peritoneal injection of a mixture of xylazine (10 mg/kg) and ketamine (80 mg/kg). The surgical site was epilated, disinfected with Betadine, and a ventral mid-line incision (4 to 5 mm in length) was made in the neck using micro-scissors. The LCA bifurcation was exposed by blunt dissection and three of four caudal LCA branches (left external carotid, internal carotid, and occipital arteries) were carefully dissected free of surrounding connective tissue and ligated with 6-0 silk sutures, leaving the superior thyroid artery intact. The surgical incision was then closed with Tissue-Mend (Veterinary Product Laboratories), and mice were monitored until recovery in a chamber under a heating lamp. Following partial carotid ligation, $ApoE^{-/-}$ mice were maintained for 4 to 28 days on the Paigen's high-fat diet (HFD; Science Diets) containing 1.25% cholesterol, 15% fat, and 0.5% cholic acid (Paigen et al., 1987). In some studies, sham-ligated animals were operated on as described above except the ligating sutures were not tightened to impede blood flow.

Cells. Peripheral blood leukocytes were collected from partially ligated or sham-ligated mice fed HFD for 7 to 28 days. Peripheral blood was drawn by tail-vein bleed with heparin as anticoagulant and 50 μl of blood was used for flow cytometry experiments. Red blood cells were removed using chilled RBC lysis buffer (eBioscience) and washed in PBS according to manufacturer's protocol.

Flow cytometry. Single cell suspensions from peripheral blood samples were stained as previously described (Alberts-Grill et al., 2012). In short, samples were stained with Fixable Live/Dead Yellow stain (Invitrogen) to discriminate dead cells, and then stained with a cocktail containing CD45-biotin (30-F11), CD8a-V450 (53-6.7), CD11c-V450 (HL3), CD4-FITC (RM4-4), Gr-1-FITC (RB6-8C5), CD49b-PE (DX5), NK1.1-PE (PK136), CD3e-PerCP-Cy5.5 (145-2C11), and CD11b-APC-Cy7 (M1/70) monoclonal antibodies (mAb) from BD Biosciences; CD19-PE-Texas Red (6D5) from Invitrogen; and F4/80-PE-Cy7 (BM8) and MHCII-APC (M5/114.15.2) mAb from eBioscience. CD45-biotin staining was visualized using streptavidin-conjugated Qdot 655 (Invitrogen). Immunofluorescence was detected using a LSR II flow cytometer (BD Immunocytometry Systems) as previously described (Alberts-Grill et al., 2012). In order to determine absolute cell numbers per sample, 50 µl of AccuCount Ultra Rainbow Fluorescent Particles (Spherotech, Inc.) were added to each sample immediately prior to flow cytometry.

Gating of flow cytometry data was performed as previously described (Fig. 3.1) (Alberts-Grill et al., 2012) using FlowJo analysis software. Absolute cell counts per µl of blood were determined using the following equation: ((A/B) x (C/D)), where A = number of cells recorded for the test sample, B = number of AccuCount beads recorded, C = number of AccuCount beads per 50µl (50,000), and D = volume of test sample in µl.

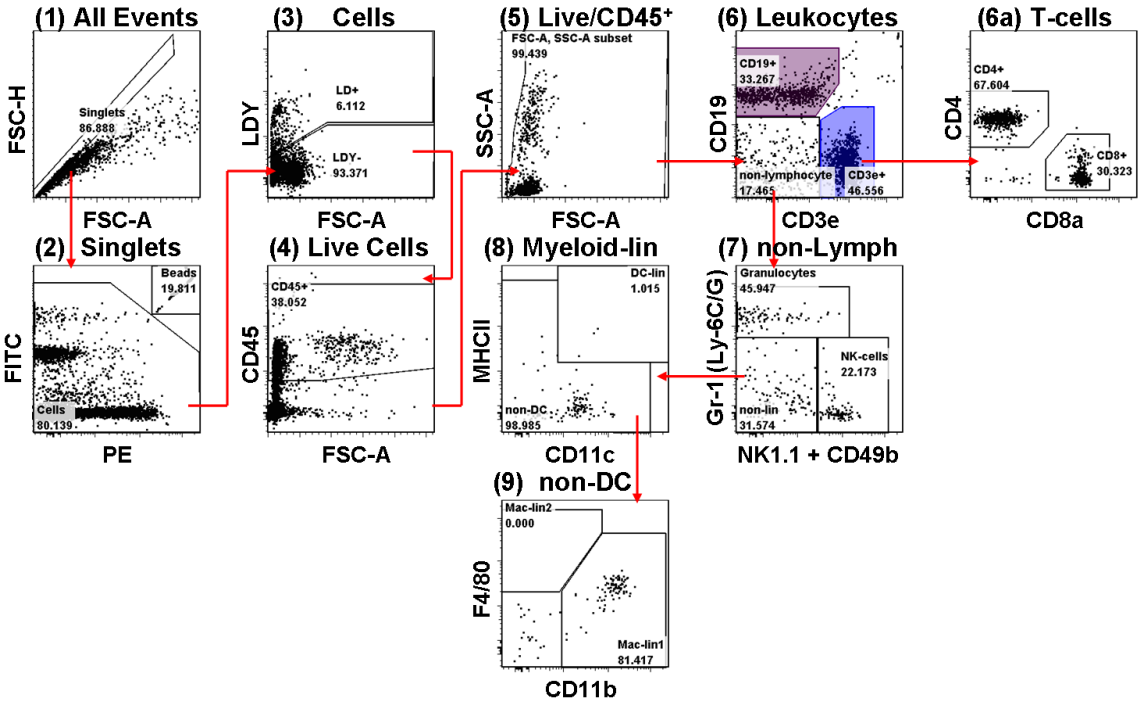

Figure 3.1. Gating strategy for leukocyte phenotyping panel. *A 10-color, 13-parameter leukocyte phenotyping panel was used to measure numbers of circulating B-cells (6), T-cells (6), NK cells (7), granulocytes (7), DCs (8), and monocytes (9) in the peripheral blood of ligated and sham-operated ApoE$^{-/-}$ mice. Figure shows the step-by-step gating strategy used for flow cytometry analyses for a representative baseline peripheral blood sample taken from an 8wk-old ApoE$^{-/-}$ mouse. Ultra-bright counting beads (2) were used to calculate absolute cell counts. Gate numbers indicate percent of parent. FSC-H, forward scatter height; FSC-A, forward scatter area; SSC-A, side scatter area.*

Statistical analysis. Values are expressed as mean ± SEM. Pairwise comparisons were performed using one-tailed t-tests. Differences between groups were considered significant at P values below 0.05. All statistical analyses were performed using Prism software (GraphPad Software).

3.3 Results

Flow disturbance abrogates hyperlipidemia-induced leukocytosis.

Flow cytometry was used to analyze leukocyte trafficking patterns in ligated and sham-operated ApoE$^{-/-}$ mice fed a high-fat diet (HFD) using a recently developed, 13-parameter

immunophenotyping flow cytometry method (Alberts-Grill et al., 2012). Overall circulating $CD45^+$ leukocyte numbers increased ~3.5-fold (from ~2000 – 7000 cells/μl) by 7 days post-surgery in sham-operated hyperlipidemic mice, and remained significantly elevated over baseline levels for the duration of the time course (Fig. 3.2). The addition of focal d-flow and atherosclerosis development in partially ligated mice, completely abrogated the hyperlipidemia-induced leukocytosis, and even led to a significant reduction in circulating leukocytes at 14 days post-ligation, corresponding with atherosclerotic plaque development in our model.

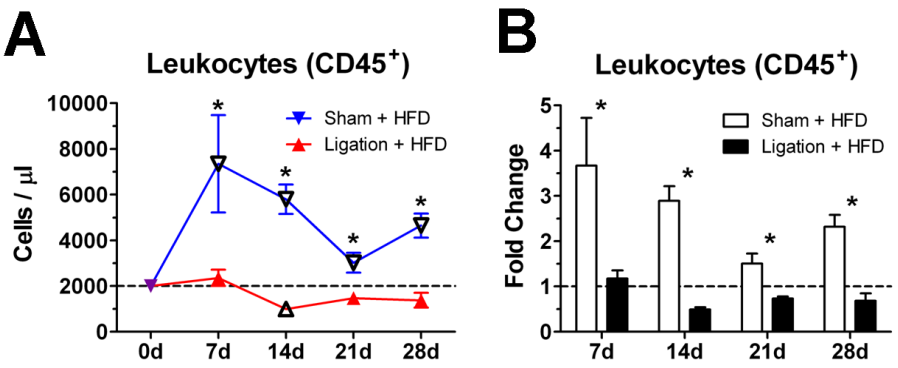

Figure 3.2. Flow disturbance abrogates hyperlipidemia-induced leukocytosis. *A, Circulating leukocyte ($CD45^+$) numbers were measured by flow cytometry in peripheral blood samples taken from ligated (red triangles) and sham-operated (blue triangles) $ApoE^{-/-}$ mice fed HFD over a 4 week time course. Graphs depict number of cells per microliter of blood (n=4-6). Open triangles indicate significant fold change from baseline (purple triangles and dashed lines). Stars denote significant differences between ligated and sham-operated controls. B, Graphs indicate fold change from baseline for the data shown in (A) for ligated (black bars) and sham-operated (white bars) animals. *, $p<0.05$.*

D-flow induces prolonged lymphopenia.

The flow cytometry data from Figure 3.2 was further analyzed to track T- and B-lymphocyte trafficking patterns in response to d-flow and hyperlipidemia. The induction of HFD increased circulating T-cell numbers by ~2-fold (from ~800 – 1600 cells/μl) in sham-ligated animals at days 7 and 14 post-surgery, which dropped to ~0.5-fold (~500

cells/μl) below baseline by 21 days post-surgery, and returned to baseline by 28 days post-surgery (~700 cells/μl) (Fig. 3.3). In contrast, induction of d-flow in LCA in ligated ApoE$^{-/-}$ mice produced a marked T-lymphopenia, showing a significant decrease (from ~800 - 200 cells/μl) in circulating T-cell numbers from 14 days post-ligation through to the end of the time course. Analyses of CD4^{+} and CD8^{+} T-cell subsets showed that high fat diet and d-flow effected CD4 and CD8 T-cells equivalently, with CD4 T-cells maintaining a characteristic 2:1 ratio compared to CD8 T-cells (Fig. 3.3).

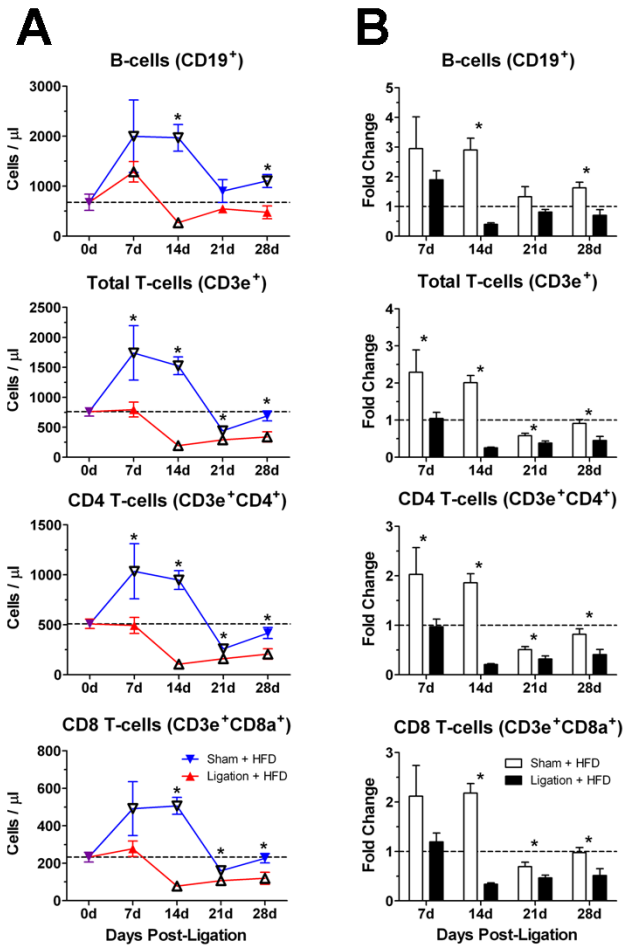

Figure 3.3. Flow disturbance induces prolonged lymphopenia. *The effect of experimentally induced d-flow on lymphocyte circulation was tested using the flow cytometry data from Figure 2 to quantify total circulating B-cells and T-cells. Total CD3^{+} T-cells were further subdivided into CD4^{+} and CD8^{+} T-cells. A, Graphs show absolute cell number per microliter of blood for ligated ApoE$^{-/-}$ mice fed HFD (red triangles) or sham-ligated animals fed HFD (blue triangles) over a 4 week time course (n=4-6). Open triangles indicate significant fold change from baseline (purple triangles and dashed lines). Stars denote significant differences between ligated and sham-operated controls. B, Graphs indicate fold change from baseline for the data shown in (A) for ligated (black bars) and sham-operated (white bars) animals. *, p<0.05.*

Overall, sham-operated animals showed higher circulating T-cell levels than ligated mice at every time point tested. A similar trend was seen in B-cells, which showed a transient ~3-fold increase (from ~840 – 2000 cells/μl) above baseline by 7 days post-surgery, and returned to baseline by 21 days post-surgery (Fig. 3.3). D-flow produced a roughly inverse effect in ligated mice, with a focal decrease (from ~840 – 180 cells/μl) in circulating B-cell numbers at 14 days post-ligation. As with overall T-cell levels, circulating B-cell numbers were generally higher in sham-operated animals from day 14 post-ligation through day 28 post-ligation in comparison with ligated mice.

D-flow inhibits high-fat diet-induced monocytosis.

Next, trafficking patterns of circulating monocytes and DCs were analyzed (Fig. 3.4). Like with the adaptive immune cells, both monocyte and DC numbers increased within 7 days following induction of HFD, increasing by up to 6 fold (from ~120 – 660 monocytes/μl; from ~1 – 6 DCs/μl) and maintaining an increased presence in the circulation for the duration of the time course. D-flow in LCA prevented hypercholesterolemia-induced increases in circulating monocytes and DCs, and even led to a transitory decrease in monocyte circulating at 14 days post-ligation. Overall, circulating monocyte and DC numbers were significantly reduced in ligated versus sham-operated mice.

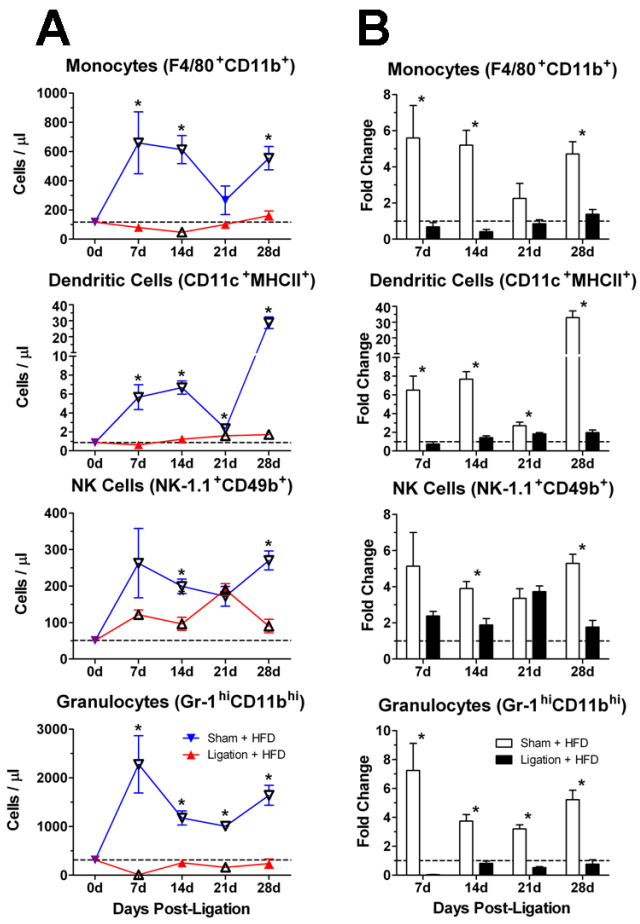

Figure 3.4. D-flow-induced atheroma development reduces circulating numbers of innate immune cells. *The effect of experimentally induced d-flow on innate immune cell circulation was tested using the flow cytometry data from Figure 3.2 to quantify circulating monocytes, DCs, granulocytes, and NK cells. A, Graphs show absolute cell number per microliter of blood for ligated ApoE$^{-/-}$ mice fed HFD (red triangles) or sham-ligated animals fed HFD (blue triangles) over a 4 week time course (n=4-6). Open triangles indicate significant fold change from baseline (purple triangles and dashed lines). Stars denote significant differences between ligated and sham-operated controls. B, Graphs indicate fold change from baseline for the data shown in (A) for ligated (black bars) and sham-operated (white bars) animals. *, p<0.05.*

D-flow induces transient waves of neutropenia and delays and decreases HFD-induced NK cell trafficking.

Similar to the trend seen in monocyte and DC trafficking, initiation of HFD in sham-operated mice induced a strong neutrophilia with circulating granulocyte numbers increasing by ~4-8-fold over baseline (from ~350 – 2300 cells/µl) (Fig. 3.4). In contrast, d-flow produced two distinct episodes of neutropenia in ligated mice with decreased granulocyte numbers at both 7 days (from ~350 – 20 cells/µl) and 21 days post-ligation (from ~300 – 180 cells/µl). Unlike the other cell types measured, circulating NK cell numbers increased in both ligated and sham-operated animals. However, the increase

seen in ligated mice was delayed and diminished from that observed in sham-operated mice.

3.4 Discussion

It has been well established that the trafficking patterns of circulating blood leukocytes change during atherogenesis, suggesting a potential non-invasive method of identifying at-risk patients with aggressive atherosclerotic disease (Liuzzo et al., 2000;Swirski et al., 2007;Drechsler et al., 2010). However, previous studies in both mice and humans have looked at PBL trafficking in the context of gradual lesion development over a time period of months or years, making it difficult to isolate perturbations in PBL trafficking caused by atherosclerosis from those caused the myriad pro-inflammatory risk factors that occur alongside the disease, such as hypercholesterolemia and hypertension. To overcome this issue, we utilized a d-flow model of atherosclerosis that allowed us to observe PBL trafficking dynamics in the context of rapid atherosclerotic plaque development over a period of weeks, while also isolating d-flow/atherosclerosis-mediated effects from those caused by hypercholesterolemia.

The major advantage of this murine model is that it induces atherogenesis rapidly and reliably along the entire length of a previously healthy LCA in only a few weeks, complete with rapid and dynamic leukocyte recruitment into the vascular wall, and the sustained and progressive expression of pro-inflammatory atherosclerosis-associated cytokines (Nam et al., 2009;Nam et al., 2010;Ni et al., 2010;Alberts-Grill et al., 2012). This intense and focal vascular inflammation has been shown to influence circulating

levels of pro-inflammatory cytokines, including the colony stimulating factors (GM-CSF, G-CSF, and M-CSF) which promote monocyte and neutrophil proliferation in the bone marrow, and CCL2, which in concert with its receptor CCR2, mediates monocyte release from the bone marrow and recruitment into the vascular wall (Serbina and Pamer, 2006;Tsou et al., 2007;Kleemann et al., 2008;Galkina and Ley, 2009). In contrast, sham ligation, in which the ligating sutures are placed around the appropriate LCA branches, but not tightened, does not induce the characteristic d-flow, local immune cell infiltration and vascular inflammation, and rapid plaque development seen in ligated LCA (Nam et al., 2009;Alberts-Grill et al., 2012), making it an ideal control condition for HFD-induced hypercholesterolemia.

Both hypercholesterolemia (in sham-operated mice) and lesion development (in ligated mice) produced significant changes in circulating leukocyte levels that correspond with d-flow-induced lesion development (Fig. 3.2). In agreement with previous reports in mice, hypercholesterolemic sham-operated mice showed significant increases in circulating T- and B-cells (Fig. 3.3) and even larger, sustained increases in circulating monocytes, DCs, granulocytes, and NK cells over baseline levels (Fig. 3.4), most of which have been shown to increase in the circulation of $ApoE^{-/-}$ or low-density lipoprotein receptor-deficient ($LDLR^{-/-}$) mice under pro-atherogenic diet conditions (Swirski et al., 2007;Drechsler et al., 2010), although circulating DCs levels have been reported to drop in patients with established atherosclerosis (Van Vre et al., 2011). Since hypercholesterolemia is so strongly interrelated with atherosclerosis, it was surprising then, to find that PBL trafficking patterns differed so greatly in ligated mice, despite

being fed the same pro-atherogenic HFD diet as sham-operated controls (Fig. 3.3 and 3.4). The overall levels of every PBL subset measured were significantly lower in ligated animals than in sham-operated mice, and, especially for T-cells, significantly lower than baseline levels as well. Substantial numbers of monocytes and DCs were seen to accumulate in the LCA in response to d-flow and HFD (Alberts-Grill et al., 2012), suggesting that heavy recruitment into the developing atherosclerotic lesion may account for the reduced numbers of both these cell subsets seen in the circulation. Furthermore, levels of apoptosis were significantly increased in lesions at 14 and 21 days post-ligation, suggesting that continual recruitment from the blood is required to maintain leukocyte populations within the plaque. Granulocytes showed a similarly bi-phasic dynamic in the blood that was relatively inverted when compared to granulocyte recruitment dynamic in LCA lesions (Alberts-Grill et al., 2012). Furthermore, neutrophils are known to be a very short-lived population within atherosclerotic lesions, surviving only a matter of hours, which may explain the large difference in granulocyte numbers leaving the blood and those found within LCA lesions in ligated mice.

However, leukocyte recruitment dynamics into LCA fail to explain the profound lymphopenic effect of d-flow and atherogenesis on PBL composition, as relatively low numbers of T-cells were recruited into LCA lesions, despite increased expression of several T-cell chemotactic factors in flow-disturbed LCA (Alberts-Grill et al., 2012). Furthermore, compared to innate immune cells like granulocytes and monocytes, T-cells are very long-lived cells, making apoptosis an unlikely explanation for their numerical scarcity within LCA lesions. It is possible, then, that large numbers of T-cells are

sequestered within the secondary lymphoid tissues (i.e., lymph nodes and spleen) in response to d-flow and lesion development, perhaps as a consequence of antigen presentation by DCs and macrophages. Indeed, circulating T-cells are known to regularly pass through the secondary lymphoid tissues as part of their normal trafficking patterns (Gowans and Knight, 1964). Furthermore, pro-atherogenic conditions such as hypercholesterolemia are known to activate vascular DCs and possibly macrophages, causing DC maturation, after which they leave the vessel wall and home to draining lymphoid tissues where they present modified lipid and molecular stress antigens like oxLDL and HSP-60 to T-cells (Buono et al., 2005;Zhou et al., 2006;Hansson and Hermansson, 2011).

One key shortcoming of this study is that it did not look at leukocyte numbers in disease-relevant lymphoid tissues such as draining lymph nodes (for LCA) or spleen, or in other tissues known to undergo important immune changes during hypercholesterolemia and atherosclerosis like the fatty tissues of the liver and other adipose tissues (Tilg and Moschen, 2006;Katagiri et al., 2007;Galkina and Ley, 2009). Such an expanded analysis would have answered the question of where all these PBLs go during atherogenesis in ligated mice, and perhaps provided some mechanistic insight into why their trafficking dynamics differ so differently from hypercholesterolemic sham-operated mice. Also, this study, as well as our previous study of leukocyte dynamics within developing flow-disturbed LCA lesions (Alberts-Grill et al., 2012), fails to adequately track individual leukocyte populations in order to accurately define their trafficking patterns. Previous studies have employed clever techniques to monitor immune cell trafficking such as the

adoptive transfer of purified immune cell populations (i.e., T-cells or monocytes) that express a unique fluorescent marker protein or are labeled with a fluorescent marker dye such as carboxyfluorescein succinimidyl ester (CFSE) or 5- (and 6)-([(4-chloromethyl) benzoyl]amino) tetramethylrhodamine (CMTMR) into marker-negative recipient mice (Galkina et al., 2006;Galkina et al., 2007). Other studies have used undigestible fluorescent latex beads or quantum dots to track the entry of labeled monocytes into atherosclerotic plaques and determine whether lesional macrophage/DC trafficking dynamics were due to cell egress from the vascular tissues or cell death (Randolph, 2008;Jayagopal et al., 2009;Potteaux et al., 2011). Unfortunately, the use of these cell tracking techniques was incompatible with the flow cytometry techniques used in this study, making the PBL dynamics reported here poor indicators of actual leukocyte trafficking at best.

Taken together, the aggregate data suggest that d-flow and active atherogenesis uniquely alters the trafficking dynamics of both innate and adaptive classes of circulating PBLs independently of hypercholesterolemia-mediated effects. As such, previous reports that identified hypercholesterolemia-induced neutrophilia and inflammatory monocytosis as key pathogenic factors in atherogenesis may have reported phenomena that are more closely related to chronic hypercholesterolemia than atherosclerotic lesion development (Swirski et al., 2007;Drechsler et al., 2010). Further studies of PBL trafficking during d-flow-induced atherosclerosis using a less inflammatory pro-atherogenic diet than the Paigen high-fat diet are required to confirm these results. Also, it is unfortunately difficult to dissect hypercholesterolemia from atherosclerosis in the mouse as both ApoE^{-}

$^{/-}$ and LDLR$^{-/-}$ mouse models rely heavily on dyslipidemia- and hypercholesterolemia-mediated inflammatory pathogenesis to drive atherosclerosis development. It is perhaps more valid, then, to test the effect of d-flow-induced atherosclerosis on PBL trafficking in animals that spontaneously develop atherosclerosis without requiring genetic disruption of key lipid metabolism pathways such as rabbits, pigs, or dogs.

3.5 References

Alberts-Grill, N., Rezvan, A., Son, D.J., Qiu, H., Kim, C.W., Kemp, M.L., Weyand, C.M., and Jo, H. (2012). Dynamic immune cell accumulation during flow-induced atherogenesis in mouse carotid artery: an expanded flow cytometry method. *Arterioscler Thromb Vasc Biol* 32**,** 623-632.

Buono, C., Binder, C.J., Stavrakis, G., Witztum, J.L., Glimcher, L.H., and Lichtman, A.H. (2005). T-bet deficiency reduces atherosclerosis and alters plaque antigen-specific immune responses. *Proc Natl Acad Sci U S A* 102**,** 1596-1601.

Cybulsky, M.I., Iiyama, K., Li, H., Zhu, S., Chen, M., Iiyama, M., Davis, V., Gutierrez-Ramos, J.C., Connelly, P.W., and Milstone, D.S. (2001). A major role for VCAM-1, but not ICAM-1, in early atherosclerosis. *J Clin Invest* 107**,** 1255-1262.

Dadu, R.T., Nambi, V., and Ballantyne, C.M. (2012). Developing and assessing cardiovascular biomarkers. *Transl Res* 159**,** 265-276.

Drechsler, M., Megens, R.T., Van Zandvoort, M., Weber, C., and Soehnlein, O. (2010). Hyperlipidemia-triggered neutrophilia promotes early atherosclerosis. *Circulation* 122**,** 1837-1845.

Galkina, E., Harry, B.L., Ludwig, A., Liehn, E.A., Sanders, J.M., Bruce, A., Weber, C., and Ley, K. (2007). CXCR6 promotes atherosclerosis by supporting T-cell homing, interferon-gamma production, and macrophage accumulation in the aortic wall. *Circulation* 116**,** 1801-1811.

Galkina, E., Kadl, A., Sanders, J., Varughese, D., Sarembock, I.J., and Ley, K. (2006). Lymphocyte recruitment into the aortic wall before and during development of atherosclerosis is partially L-selectin dependent. *J Exp Med* 203**,** 1273-1282.

Galkina, E., and Ley, K. (2009). Immune and inflammatory mechanisms of atherosclerosis (*). *Annu Rev Immunol* 27**,** 165-197.

Gomes, A.L., Carvalho, T., Serpa, J., Torre, C., and Dias, S. (2010). Hypercholesterolemia promotes bone marrow cell mobilization by perturbing the SDF-1:CXCR4 axis. *Blood* 115**,** 3886-3894.

Gowans, J.L., and Knight, E.J. (1964). The Route of Re-Circulation of Lymphocytes in the Rat. *Proc R Soc Lond B Biol Sci* 159**,** 257-282.

Hansson, G.K. (2005). Inflammation, atherosclerosis, and coronary artery disease. *N Engl J Med* 352**,** 1685-1695.

Hansson, G.K., and Hermansson, A. (2011). The immune system in atherosclerosis. *Nat Immunol* 12**,** 204-212.

Hansson, G.K., and Libby, P. (2006). The immune response in atherosclerosis: a double-edged sword. *Nat Rev Immunol* 6**,** 508-519.

Jayagopal, A., Su, Y.R., Blakemore, J.L., Linton, M.F., Fazio, S., and Haselton, F.R. (2009). Quantum dot mediated imaging of atherosclerosis. *Nanotechnology* 20**,** 165102.

Katagiri, H., Yamada, T., and Oka, Y. (2007). Adiposity and cardiovascular disorders: disturbance of the regulatory system consisting of humoral and neuronal signals. *Circ Res* 101**,** 27-39.

Kleemann, R., Zadelaar, S., and Kooistra, T. (2008). Cytokines and atherosclerosis: a comprehensive review of studies in mice. *Cardiovasc Res* 79**,** 360-376.

Libby, P. (2002). Inflammation in atherosclerosis. *Nature* 420**,** 868-874.

Liuzzo, G., Goronzy, J.J., Yang, H., Kopecky, S.L., Holmes, D.R., Frye, R.L., and Weyand, C.M. (2000). Monoclonal T-cell proliferation and plaque instability in acute coronary syndromes. *Circulation* 101**,** 2883-2888.

Nam, D., Ni, C.W., Rezvan, A., Suo, J., Budzyn, K., Llanos, A., Harrison, D., Giddens, D., and Jo, H. (2009). Partial carotid ligation is a model of acutely induced disturbed flow, leading to rapid endothelial dysfunction and atherosclerosis. *Am J Physiol Heart Circ Physiol* 297**,** H1535-1543.

Nam, D., Ni, C.W., Rezvan, A., Suo, J., Budzyn, K., Llanos, A., Harrison, D.G., Giddens, D.P., and Jo, H. (2010). A model of disturbed flow-induced atherosclerosis in mouse carotid artery by partial ligation and a simple method of RNA isolation from carotid endothelium. *J Vis Exp*.

Ni, C.W., Qiu, H., Rezvan, A., Kwon, K., Nam, D., Son, D.J., Visvader, J.E., and Jo, H. (2010). Discovery of novel mechanosensitive genes in vivo using mouse carotid artery endothelium exposed to disturbed flow. *Blood* 116**,** e66-73.

Paigen, B., Morrow, A., Holmes, P.A., Mitchell, D., and Williams, R.A. (1987). Quantitative assessment of atherosclerotic lesions in mice. *Atherosclerosis* 68**,** 231-240.

Potteaux, S., Gautier, E.L., Hutchison, S.B., Van Rooijen, N., Rader, D.J., Thomas, M.J., Sorci-Thomas, M.G., and Randolph, G.J. (2011). Suppressed monocyte recruitment drives macrophage removal from atherosclerotic plaques of Apoe-/- mice during disease regression. *J Clin Invest* 121**,** 2025-2036.

Randolph, G.J. (2008). Emigration of monocyte-derived cells to lymph nodes during resolution of inflammation and its failure in atherosclerosis. *Curr Opin Lipidol* 19**,** 462-468.

Serbina, N.V., and Pamer, E.G. (2006). Monocyte emigration from bone marrow during bacterial infection requires signals mediated by chemokine receptor CCR2. *Nat Immunol* 7**,** 311-317.

Soehnlein, O., Drechsler, M., Hristov, M., and Weber, C. (2009). Functional alterations of myeloid cell subsets in hyperlipidaemia: relevance for atherosclerosis. *J Cell Mol Med* 13**,** 4293-4303.

Swirski, F.K., Libby, P., Aikawa, E., Alcaide, P., Luscinskas, F.W., Weissleder, R., and Pittet, M.J. (2007). Ly-6Chi monocytes dominate hypercholesterolemia-associated monocytosis and give rise to macrophages in atheromata. *J Clin Invest* 117**,** 195-205.

Tilg, H., and Moschen, A.R. (2006). Adipocytokines: mediators linking adipose tissue, inflammation and immunity. *Nat Rev Immunol* 6**,** 772-783.

Tsou, C.L., Peters, W., Si, Y., Slaymaker, S., Aslanian, A.M., Weisberg, S.P., Mack, M., and Charo, I.F. (2007). Critical roles for CCR2 and MCP-3 in monocyte mobilization from bone marrow and recruitment to inflammatory sites. *J Clin Invest* 117**,** 902-909.

Van Vre, E.A., Van Brussel, I., Bosmans, J.M., Vrints, C.J., and Bult, H. (2011). Dendritic cells in human atherosclerosis: from circulation to atherosclerotic plaques. *Mediators Inflamm* 2011**,** 941396.

Virmani, R., Burke, A.P., Farb, A., and Kolodgie, F.D. (2006). Pathology of the vulnerable plaque. *J Am Coll Cardiol* 47**,** C13-18.

Weber, C., and Noels, H. (2011). Atherosclerosis: current pathogenesis and therapeutic options. *Nat Med* 17**,** 1410-1422.

Zhou, X., Robertson, A.K., Hjerpe, C., and Hansson, G.K. (2006). Adoptive transfer of CD4+ T cells reactive to modified low-density lipoprotein aggravates atherosclerosis. *Arterioscler Thromb Vasc Biol* 26**,** 864-870.

CHAPTER 4:

THE EFFECT OF CATHEPSIN S DEFICIENCY ON LEUKOCYTE RECRUITMENT AND ATHEROSCLEROSIS IN THE FLOW-DISTURBED CAROTID ARTERY

4.1 Introduction

The pathogenesis of atherosclerosis depends intimately on the infiltration of pro-inflammatory leukocytes and the establishment of chronic Th1-skewed inflammation within the vessel wall, leading to development of lipid laden plaques (Galkina and Ley, 2009;Hansson and Hermansson, 2011). Leukocyte infiltration has been shown to depend heavily on inflammatory signaling in endothelial cells (ECs) in response to disturbed patterns of blood flow, leading to the upregulation of the adhesion molecule, vascular cell adhesion molecule 1 (VCAM-1) and secretion of pro-atherogenic cytokines like monocyte chemoattractant protein 1 (MCP-1) and CXCL8, which attract immune cells such as monocytes and mediate binding to ECs and migration into the vascular intima (Walpola et al., 1995;Endres et al., 1997;Nakashima et al., 1998;Iiyama et al., 1999;Suo et al., 2007;Galkina and Ley, 2009;Nam et al., 2009). In addition to monocytes, dendritic cells (DCs), neutrophils, and T-cells all migrate into the vascular intima where they contribute to atherogenesis in various ways, such as the induction and support of pro-atherogenic T-cell responses (DCs) (Hermansson et al., 2010;Hjerpe et al., 2010;Niessner and Weyand, 2010;Hansson and Hermansson, 2011), proinflammatory cytokine production (macrophages, neutrophils, DCs, T-cells) (Eid et al., 2009;Erbel et al., 2009;Galkina and Ley, 2009;McLaren and Ramji, 2009;Drechsler et al., 2010), cytotoxicity (T-cells) (Nakajima et al., 2002;Nakajima et al., 2003;Pryshchep et al., 2006), and extracellular matrix degradation (macrophages) (Hansson and Hermansson, 2011).

Since the range of leukocyte-mediated pro-atherogenic mechanisms is so diverse and involve so many different cell types, it is important to identify key molecular

'bottlenecks' which mediate multiple pathogenic behaviors without being integral to normal physiological vascular and immune function. Recently we developed a d-flow-induced model of atherosclerosis in which partial ligation of mouse carotid artery causes d-flow with characteristic low and oscillatory wall shear stress, leading to lipid-laden plaque development in apolipoprotein E-deficient ($ApoE^{-/-}$) mice fed a high-fat diet within 2 weeks (Nam et al., 2009). Using this model, we demonstrated that d-flow induces broad changes in the gene expression profile of ECs, including the upregulation of VCAM-1 and ICAM-1 (Nam et al., 2009;Ni et al., 2010), followed by rapid vascular leukocyte accumulation, progressive pro-inflammatory cytokine production (Alberts-Grill et al., 2012), and impaired vascular relaxation responses (Li et al., 2010;Li et al., 2011b).

The rapid leukocyte recruitment and development of sustained vascular inflammation shown by this model make it ideal to screen and define key molecular mechanisms in this process and assess their therapeutic potential. Genome-wide microarray studies in our model identified several proteases of the cathepsin family, including cathepsin S (CatS), cathepsin K (CatK), and cathepsin L (CatL) which are upregulated in response to d-flow in carotid artery (Ni et al., 2010). These cysteine proteases have potent elastinolytic (Shi et al., 1992;Xin et al., 1992) and collagenolytic (Maciewicz and Etherington, 1988) activities. CatS and CatK are over-expressed, and their endogenous inhibitor, cystatin C, reciprocally under-expressed in human plaques (Sukhova et al., 1998;Shi et al., 1999a). Cathepsin family proteins are expressed by a number of cell types including endothelial cells, vascular smooth muscle cells (SMCs), monocytes, macrophages, DCs, and B-cells

(Sukhova et al., 2003). Deficiency of CatS, but not CatK, inhibits the development of atherosclerosis in ApoE$^{-/-}$and low density lipoprotein receptor-deficient (LDLR$^{-/-}$) mice (Sukhova et al., 2003;Rodgers et al., 2006). Studies examining the pathogenic mechanism of CatS during atherogenesis showed that the enzyme plays a key role in regulating leukocyte migration into vascular intima by degrading the elastin-rich endothelial basement membrane (Sukhova et al., 2003). Furthermore, CatS was shown to promote destabilization in established plaques by degrading SMC-derived elastin and collagen (Sukhova et al., 2003;Rodgers et al., 2006;de Nooijer et al., 2009).

Furthermore, CatS is an essential protease required for invariant chain processing, and thus plays a critical role in the presentation of exogenous antigen to CD4^{+} T-cells via major histocompatibility complex class II (MHC-II) molecules (Nakagawa et al., 1999;Shi et al., 1999b;Beers et al., 2005). As such, CatS deficiency leads to impaired immune responses and decreased T-cell numbers in atherosclerotic plaques (Nakagawa et al., 1999;Shi et al., 1999b;Sukhova et al., 2003). The contributions of pro-atherogenic CD4^{+} T-cell responses against vascular antigens such as oxidized LDL (oxLDL) and heat-shock protein 60 (HSP-60) to atherosclerosis have been well established (Buono et al., 2005;Hermansson et al., 2010;Hansson and Hermansson, 2011). However, the effect of CatS deficiency on the initiation and potentiation of these pro-atherogenic T-cell responses has not been examined.

Thus, it is clear that CatS plays an integral role in several pathogenic processes critical to atherogenesis. However, the relationship between d-flow, CatS function, and vascular

inflammation is not well understood. To explore this, we performed a set of preliminary studies to assess the effect of CatS deficiency on leukocyte recruitment, T-cell activation, and vascular inflammation in flow-disturbed atherosclerosis using our partial carotid ligation model. We hypothesized that CatS deficiency would disrupt d-flow-dependent leukocyte recruitment to the vascular wall and retard $CD4^+$ T-cell activation, leading to delayed development of atherosclerosis. CatS-deficiency delayed total leukocyte recruitment into the flow-disturbed LCA, and especially reduced lesional DC and T-cell numbers. Furthermore, hyperlipidemia induced splenic $CD4^+$ T-cell activation within 7 days which was inhibited in $CatS^{-/-}$ mice. However, reduced leukocyte recruitment and $CD4^+$ T-cell activation did not reduce the capacity of LCA to produce pro-inflammatory cytokines like IFNγ and TNFα, or to develop atherosclerosis.

4.2 Methods

Mice. Male $ApoE^{-/-}$ mice (B6.129P2-$ApoE^{tm1Unc}$/J) were purchased from The Jackson Laboratory (Bar Harbor) and were fed *ad libitum* with standard chow diet until surgery at 8 to 9 weeks of age. The $ApoE^{tm1Unc}$ mutation was from a 129P2/OlaHsd-derived E14Tg2a embryonic stem cell line and was backcrossed to the C57BL/6J for 10 generations. $CatS^{-/-}$ mice (NOD.D1-$Ctss^{tm1Eae}$/RclJ) backcrossed onto the C57BL/6J background were a generous gift from Guo-Ping Shi (Sukhova et al., 2003). These mice were crossbred with $ApoE^{-/-}$ mice (described above) to generate $CatS^{-/-}ApoE^{-/-}$ mice, and genotypes were confirmed by PCR using mouse tail genomic DNA.

Partial carotid ligation surgery. Partial carotid ligation surgeries were performed as previously described (Nam et al., 2009;Nam et al., 2010;Alberts-Grill et al., 2012). Mice were anesthetized by intra-peritoneal injection of a mixture of xylazine (10 mg/kg) and ketamine (80 mg/kg). The surgical site was epilated, disinfected with Betadine, and a ventral mid-line incision (4 to 5 mm in length) was made in the neck using micro-scissors. The LCA bifurcation was exposed by blunt dissection and three of four caudal LCA branches (left external carotid, internal carotid, and occipital arteries) were carefully dissected free of surrounding connective tissue and ligated with 6-0 silk sutures, leaving the superior thyroid artery intact. The surgical incision was then closed with Tissue-Mend (Veterinary Product Laboratories), and mice were monitored until recovery in a chamber under a heating lamp. Following partial carotid ligation, animals were maintained for 7 to 21 days on the Paigen's high-fat diet (HFD; Science Diets) containing 1.25% cholesterol, 15% fat, and 0.5% cholic acid (Paigen et al., 1987). In some studies, sham-ligated animals were operated on as described above except the ligating sutures were not tightened to impede blood flow as previously reported (Alberts-Grill et al., 2012).

Cells. For flow cytometry analyses of vascular wall leukocytes, partially-ligated male $ApoE^{-/-}$ and $CatS^{-/-}ApoE^{-/-}$ mice maintained on HFD were sacrificed by CO_2 inhalation and perfused by cardiac puncture with saline containing 10 U/ml of heparin at 7 and 14 days post-ligation. Following sacrifice, arterial leukocyte preparations were isolated as previously described (Alberts-Grill et al., 2012). In short, LCA and RCA were excised, placed in chilled Hanks balanced salt solution, and then pooled (n=3) in chilled digestion

buffer (450 U/ml collagenase I-S, 125 U/ml collagenase XI, 60 U/ml hyaluronidase (Sigma-Aldritch), and 60 U/ml DNAse I (Applichem) in phosphate buffered saline (PBS) supplemented with calcium and magnesium). Pooled arteries were minced finely and digested at 37°C for 1 hour at 5% CO_2, and single cell suspensions obtained by shearing the digested arteries with a 21½ gauge needle. Cells were then washed in PBS without calcium and magnesium (10 min, 500 *g*, 4°C) and resuspended in 1 ml PBS for staining.

Peripheral blood leukocytes (PBLs) and splenocytes were also collected from partially ligated $ApoE^{-/-}$ and $CatS^{-/-}ApoE^{-/-}$ mice fed HFD for 7 to 14 days. Splenocytes were harvested by grinding spleens against a 75 micron, nylon mesh filter (BD Biosciences) and collecting cells in chilled Hanks balanced salt solution. Peripheral blood was drawn by tail-vein bleed with heparin as anticoagulant and 50 µl of blood was used for flow cytometry experiments. Red blood cells were removed using chilled RBC lysis buffer (eBioscience) and washed in PBS according to manufacturer's protocol.

Flow cytometry. For flow cytometry analyses of arterial leukocyte composition, single cell suspensions of arterial leukocytes were stained as previously described (Alberts-Grill et al., 2012). In short, samples were stained with Fixable Live/Dead Yellow stain (Invitrogen) to discriminate dead cells, and then stained with a cocktail containing CD45-biotin (30-F11), CD8a-V450 (53-6.7), CD11c-V450 (HL3), CD4-FITC (RM4-4), Gr-1-FITC (RB6-8C5), CD49b-PE (DX5), NK1.1-PE (PK136), CD3e-PerCP-Cy5.5 (145-2C11), and CD11b-APC-Cy7 (M1/70) monoclonal antibodies (mAb) from BD Biosciences; CD19-PE-Texas Red (6D5) from Invitrogen; and F4/80-PE-Cy7 (BM8) and

MHCII-APC (M5/114.15.2) mAb from eBioscience. CD45-biotin staining was visualized using streptavidin-conjugated Qdot 655 (Invitrogen). Immunofluorescence was detected using a LSR II flow cytometer (BD Immunocytometry Systems) as previously described (Alberts-Grill et al., 2012). In order to determine absolute cell numbers per sample, 50 µl of AccuCount Ultra Rainbow Fluorescent Particles (Spherotech, Inc.) were added to each sample immediately prior to flow cytometry. Gating of flow cytometry data were performed as previously described (Fig. 4.1) (Alberts-Grill et al., 2012) using FlowJo

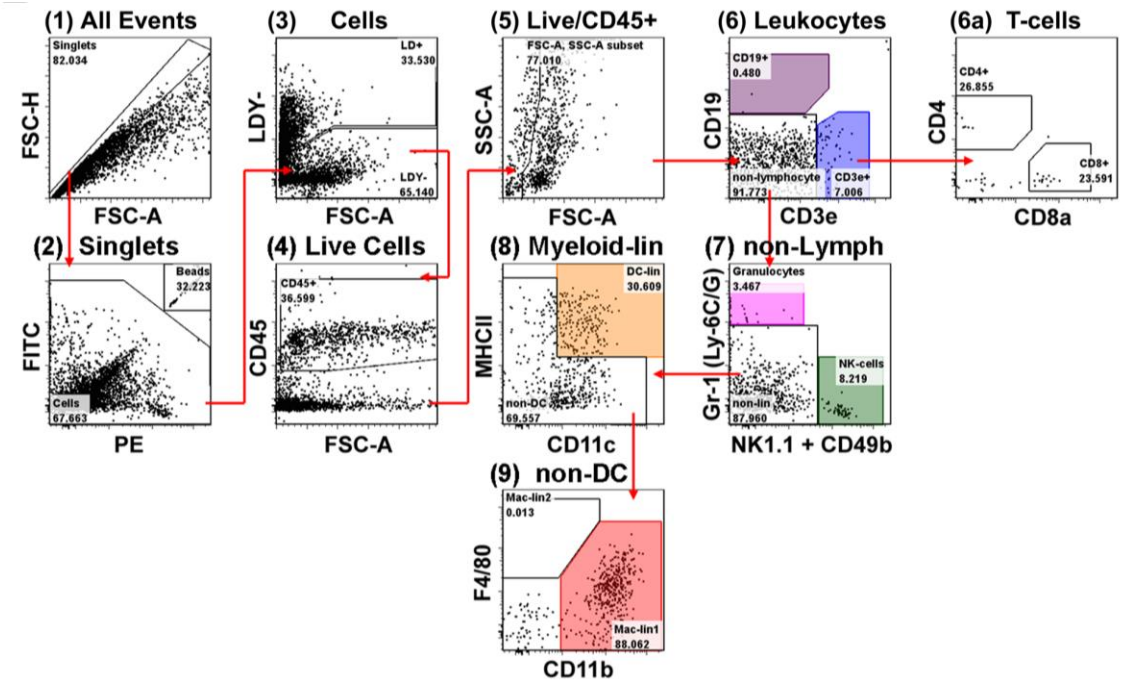

Figure 4.1. Gating strategy for leukocyte phenotyping panel. *A 10-color, 13-parameter leukocyte phenotyping panel was used to identify B-cells (6), T-cells (6), NK cells (7), granulocytes (7), DCs (8), and monocytes (9). Figure shows the gating strategy used for flow cytometry analyses for a representative arterial leukocyte sample harvested from ApoE$^{-/-}$ LCA 7 days post-ligation. Ultra-bright counting beads (2) were used to determine absolute cell counts. Gate numbers indicate percent of parent. FSC-H, forward scatter height; FSC-A, forward scatter area; SSC-A, side scatter area.*

analysis software. Absolute cell counts per µl of blood were determined using the following equation: ((A/B) x (C/D)), where A = number of cells recorded for the test

sample, B = number of AccuCount beads recorded, C = number of AccuCount beads per 50µl (50,000), and D = volume of test sample in µl.

Alternatively, splenocytes or PBLs were stained with Fixable Live/Dead Yellow stain (Invitrogen) to discriminate dead cells, and then stained with a cocktail containing CD8a-V450 (53-6.7), CD4-FITC (RM4-4), CD25-PE (3C7), CD3e-PerCP-Cy5.5 (145-2C11), B220-PE-Cy7 (RA3-6B2), CD44-APC (IM7), and CD62L-APC-Cy7 (MEL-14) monoclonal antibodies (mAb) from BD Biosciences; and CD45-PE-Texas Red (30-F11) from Invitrogen. Immunofluorescence was detected using a LSR II flow cytometer (BD Immunocytometry Systems) using standard channel and filter settings. Gating of flow cytometry data were performed as shown in Figure 4.2 using FlowJo analysis software.

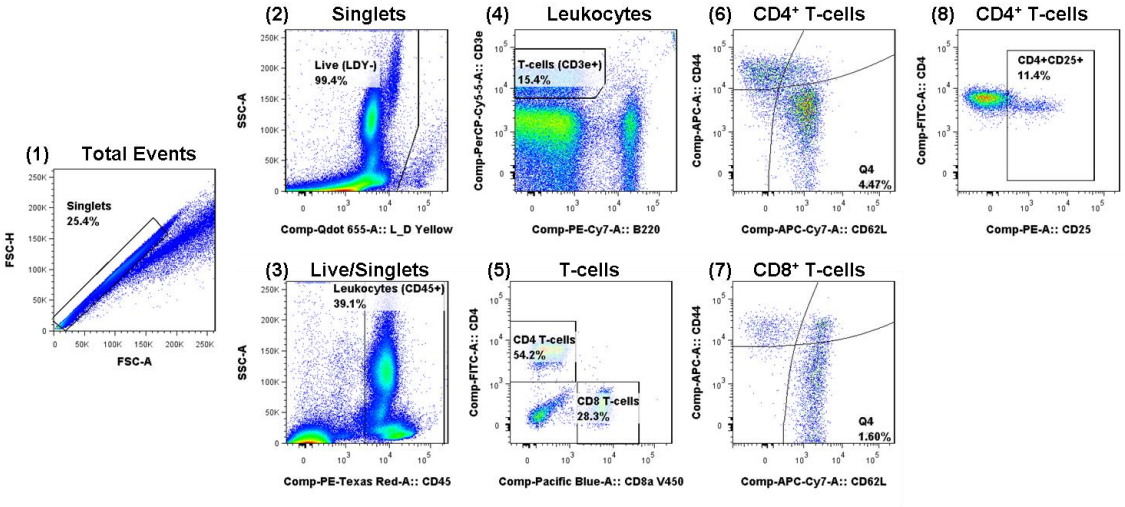

Figure 4.2. Gating strategy for T-cell phenotyping panel. *Splenocytes and PBLs were stained with anti-CD45, -CD3e, -B220, -CD4, -CD8a, -CD44, -CD62L, and -CD25 mAbs. Figure shows the gating strategy for a representative peripheral blood sample taken at baseline (0 days) from an ApoE$^{-/-}$ mouse maintained on chow diet. FACS plots identify CD45^{+} leukocytes (3), total CD3^{+} T-cells (4), and CD4^{+} and CD8^{+} T-cells (5). CD44 and CD62L staining is shown for both CD4^{+} (6), and CD8^{+} T-cells (7). Gating for CD4^{+}CD25^{+} Tregs is also shown (8). Numbers in FACS plots denote percent of parent.*

Cytokine bead array (CBA) ELISA assay. LCA and RCA from partially ligated $ApoE^{-/-}$ and $CatS^{-/-}ApoE^{-/-}$ mice were excised as described above and cultured overnight in 60 µl of DMEM supplemented with 10% fetal calf serum, 100 U/mL penicillin, and 100 µg/mL streptomycin at 37°C in 5% CO_2 as previously described (Li et al., 2011a). During this time, vascular cytokine production was stimulated by adding 12-O-tetradecanoylphorbol-13-acetate (TPA, 10 µmol/L) and ionomycin (2 µmol/L; Cell Signaling Technology) to the tissue culture medium. Following incubation, levels of cytokines TNFα, IFNγ, IL-2, IL-4, and IL-5 were measured using the cytokine bead array ELISA kit (BD Biosciences) according to manufacturer's protocol. Cytokine levels were detected using a LSR II flow cytometer (BD Immunocytometry Systems). CBA array data were processed using FCAP Array software (Soft Flow, Inc.). The theoretical limit of detection for the cytokines measured was 5.0 pg/ml (IL-2), 5.0 pg/ml (IL-4), 5.0 pg/ml (IL-5), 2.5 pg/ml (IFN-γ), and 6.3 pg/ml (TNFα).

Oil-Red-O staining of carotid lesions. Mice were euthanized and perfused with saline containing heparin as described above. LCA and RCA were collected *en bloc* along with the heart, aortic arch, trachea, esophagus, and surrounding fat tissue as previously described (Nam et al., 2009). Tissue was embedded in optimal cutting temperature (OCT) compound (Tissue-Tek), frozen on liquid nitrogen and stored at –80°C until used. Frozen sections were made starting from the level of the right subclavian artery bifurcation, 300 µm was trimmed away and five sets of ten consecutive 7 µm thick sections were taken at 300 µm intervals constituting the 'proximal,' 'middle,' and 'distal' portions of the artery. Oil-Red-O staining of LCA and RCA was performed using frozen

sections as previously described (Nam et al., 2009). Micrographs were taken with an Olympus IX71 inverted microscope. Images were analyzed with Image J software (NIH) to quantify lesion size in each animal as previously described (Lessner et al., 2002).

Statistical analysis. Values are expressed as mean ± SEM. Pairwise comparisons were performed using two-tailed t-tests. Differences between groups were considered significant at P values below 0.05. All statistical analyses were performed using Prism software (GraphPad Software).

4.3 Results

CatS deficiency disrupts leukocyte recruitment into flow-disturbed LCA prior to lesion development.

Using the 13-parameter flow cytometry immunotyping method, we examined leukocyte recruitment into the artery wall during the development of atherosclerosis in $ApoE^{-/-}$ and $CatS^{-/-}ApoE^{-/-}$ mice. Following partial carotid ligation surgery and HFD, flow-disturbed LCA and control RCA obtained at 7 and 14 days post-ligation were enzymatically digested and the number and composition of arterial wall leukocytes were analyzed by flow cytometry. As shown in Figure 4.3A and B, leukocyte recruitment was significantly reduced in the flow-disturbed LCA of $CatS^{-/-}ApoE^{-/-}$ mice (~4500 leukocytes/artery) at 7 days post-ligation as compared with $ApoE^{-/-}$ animals (~9000 leukocytes/artery) (Table 4.1). However, by 14 days post-ligation no significant differences were seen in LCA taken from $CatS^{-/-}ApoE^{-/-}$ and $ApoE^{-/-}$ mice (Fig. 4.3C and D, Table 4.2).

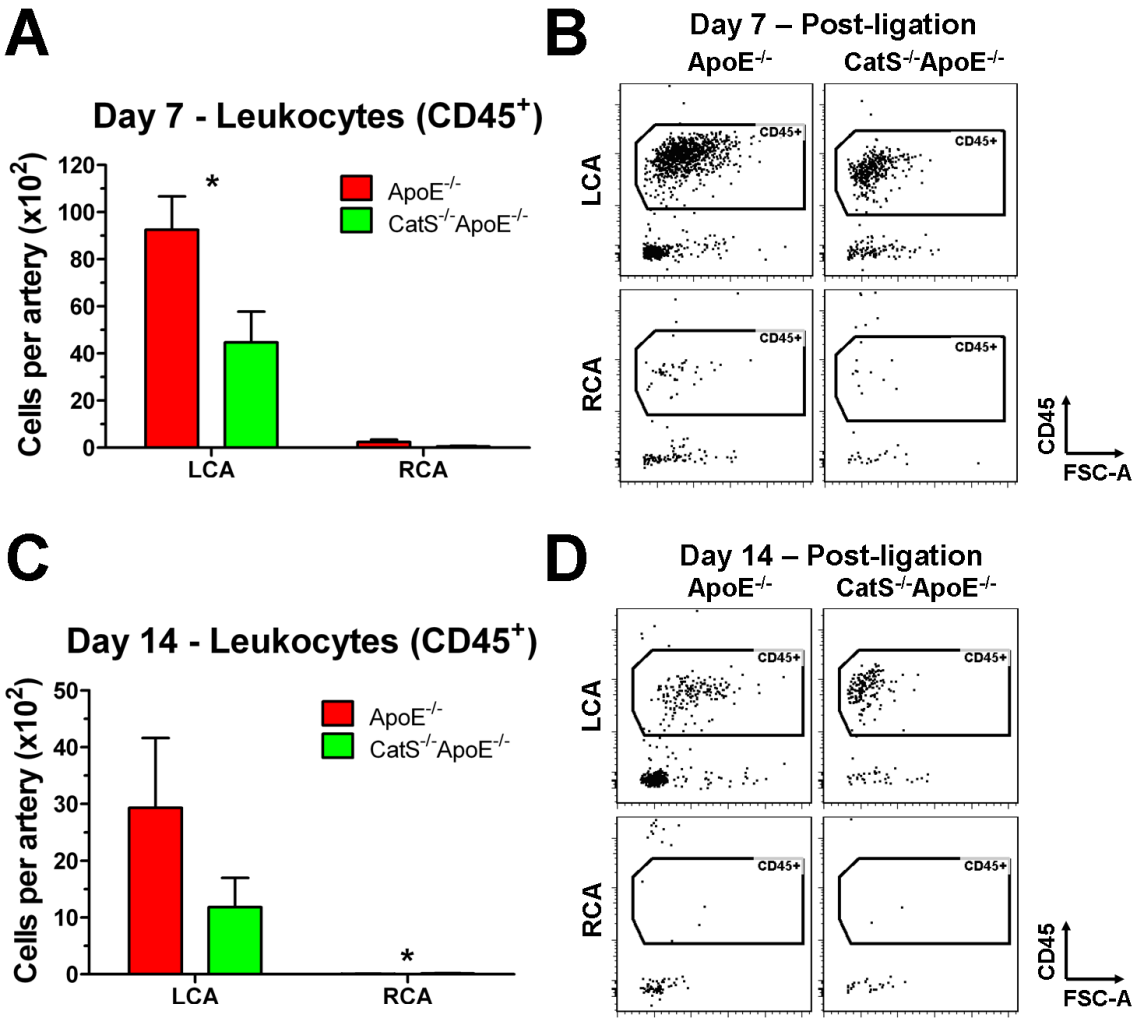

Figure 4.3. CatS deficiency disrupts leukocyte recruitment into flow-disturbed LCA. *Leukocyte (CD45$^+$) accumulation in LCA and RCA from ApoE$^{-/-}$ (red bars) and CatS$^{-/-}$ApoE$^{-/-}$ (green bars) was examined by the thirteen-parameter immunophenotyping analysis at 7 or 14 days following ligation and HFD. A-B, Graph (A) depicts number of cells (in hundreds) per carotid artery (n=4 pools of 3 arteries each) at 7 days post-ligation and representative dot plots (B). C-D, Graph (C) depicts number of cells (in hundreds) per carotid artery (n=3 to 4 pools of 3 arteries each) at 14 days post-ligation and representative dot plots (D). Data are mean values ± SEM. *, $p < 0.05$.*

Table 4.1. *Summary of two-tailed t-test analyses of leukocyte accumulation in LCA and RCA of ligated $ApoE^{-/-}$ and $CatS^{-/-}ApoE^{-/-}$ mice at 7 days post-ligation.*

Comparison	Mean Diff. ($x10^2$)	t	t test P value
Leukocytes			
ApoE, LCA v RCA	90.04	6.321	0.0007
CatS, LCA v RCA	44.14	2.708	0.0267
LCA, ApoE v CatS	47.76	2.413	0.0423
RCA, ApoE v CatS	1.86	1.858	0.1125
B-cells			
ApoE, LCA v RCA	0.35	1.590	0.1630
CatS, LCA v RCA	0.04	0.967	0.3618
LCA, ApoE v CatS	0.34	1.929	0.0898
RCA, ApoE v CatS	0.03	1.997	0.0928
T-cells			
ApoE, LCA v RCA	3.04	5.472	0.0016
CatS, LCA v RCA	0.77	5.876	0.0004
LCA, ApoE v CatS	2.32	5.077	0.0010
RCA, ApoE v CatS	0.05	1.165	0.2883
Dendritic Cells			
ApoE, LCA v RCA	20.71	8.585	0.0001
CatS, LCA v RCA	0.20	4.907	0.0012
LCA, ApoE v CatS	12.73	3.705	0.0060
RCA, ApoE v CatS	0.46	1.846	0.1144
NK Cells			
ApoE, LCA v RCA	5.24	3.902	0.0080
CatS, LCA v RCA	2.49	3.797	0.0053
LCA, ApoE v CatS	2.82	2.262	0.0536
RCA, ApoE v CatS	0.07	1.790	0.1236
Monocyte/Macrophages			
ApoE, LCA v RCA	49.82	5.299	0.0018
CatS, LCA v RCA	24.10	2.451	0.0399
LCA, ApoE v CatS	26.69	2.167	**0.0621**
RCA, ApoE v CatS	0.96	1.721	0.1360
Granulocytes			
ApoE, LCA v RCA	3.22	6.464	0.0007
CatS, LCA v RCA	0.34	2.028	0.0771
LCA, ApoE v CatS	1.09	0.964	0.3633
RCA, ApoE v CatS	0.01	0.317	0.7621

Table 4.2. *Summary of two-tailed t-test analyses of leukocyte accumulation in LCA and RCA of ligated ApoE$^{-/-}$ and CatS$^{-/-}$ApoE$^{-/-}$ mice at 14 days post-ligation.*

Comparison	Mean Diff. (x10^2)	t	t test P value
Leukocytes			
ApoE, LCA v RCA	29.22	2.372	**0.0554**
CatS, LCA v RCA	11.65	2.255	**0.0871**
LCA, ApoE v CatS	17.48	1.150	0.3022
RCA, ApoE v CatS	-0.08	2.751	0.0403
B-cells			
ApoE, LCA v RCA	0.88	2.687	0.0362
CatS, LCA v RCA	-	-	-
LCA, ApoE v CatS	0.76	1.922	0.1126
RCA, ApoE v CatS	-	-	-
T-cells			
ApoE, LCA v RCA	1.86	2.054	**0.0858**
CatS, LCA v RCA	1.11	2.091	0.1047
LCA, ApoE v CatS	0.75	0.647	0.5463
RCA, ApoE v CatS	-0.002	0.378	0.721
Dendritic Cells			
ApoE, LCA v RCA	8.37	1.691	0.1418
CatS, LCA v RCA	3.367	2.116	0.1018
LCA, ApoE v CatS	5.00	0.833	0.4430
RCA, ApoE v CatS	-0.003	0.332	0.7537
NK Cells			
ApoE, LCA v RCA	2.76	2.269	**0.0637**
CatS, LCA v RCA	1.00	2.389	**0.0753**
LCA, ApoE v CatS	1.76	1.190	0.2874
RCA, ApoE v CatS	0.002	0.378	0.7210
Monocyte/Macrophages			
ApoE, LCA v RCA	9.10	2.178	**0.0723**
CatS, LCA v RCA	3.76	2.224	**0.0903**
LCA, ApoE v CatS	5.28	1.027	0.3515
RCA, ApoE v CatS	-0.05	2.036	**0.0973**
Granulocytes			
ApoE, LCA v RCA	2.71	2.900	0.0273
CatS, LCA v RCA	0.67	2.241	**0.0885**
LCA, ApoE v CatS	2.05	1.805	0.1307
RCA, ApoE v CatS	0.005	0.655	0.5416

The flow cytometry data shown in Figure 4.3 was further analyzed to determine whether CatS plays a role in the recruitment of specific innate and adaptive immune cell populations into flow-disturbed LCA. Total $CD45^{+}$ leukocytes were gated into B-cells, T-cells, DCs, monocyte/macrophages, NK cells, and granulocytes, and T-cells were further divided into CD4 and CD8 T-cells (Fig. 4.1). At 7 days post-ligation, recruitment T-cells (including both CD4 and CD8 T-cells), but not B-cells, was significantly reduced in CatS-deficient animals (Fig. 4.4A).

Among innate immune cells, recruitment of DCs was significantly reduced in $CatS^{-/-}$ $ApoE^{-/-}$ mice at 7 days post-ligation, while monocyte/macrophages showed a non-significant trend towards reduced infiltration into the LCA of $CatS^{-/-}ApoE^{-/-}$ mice. However, the majority of plaque DCs also expressed monocyte/macrophage markers such as CD11b and F4/80, suggesting a monocytic origin (data not shown). CatS deficiency did not effect the recruitment of granulocytes or NK cells (Fig. 4.4B). There were no significant differences in the accrual of any innate or adaptive immune cell subsets by 14 days post-ligation (Fig. 4.4C-D).

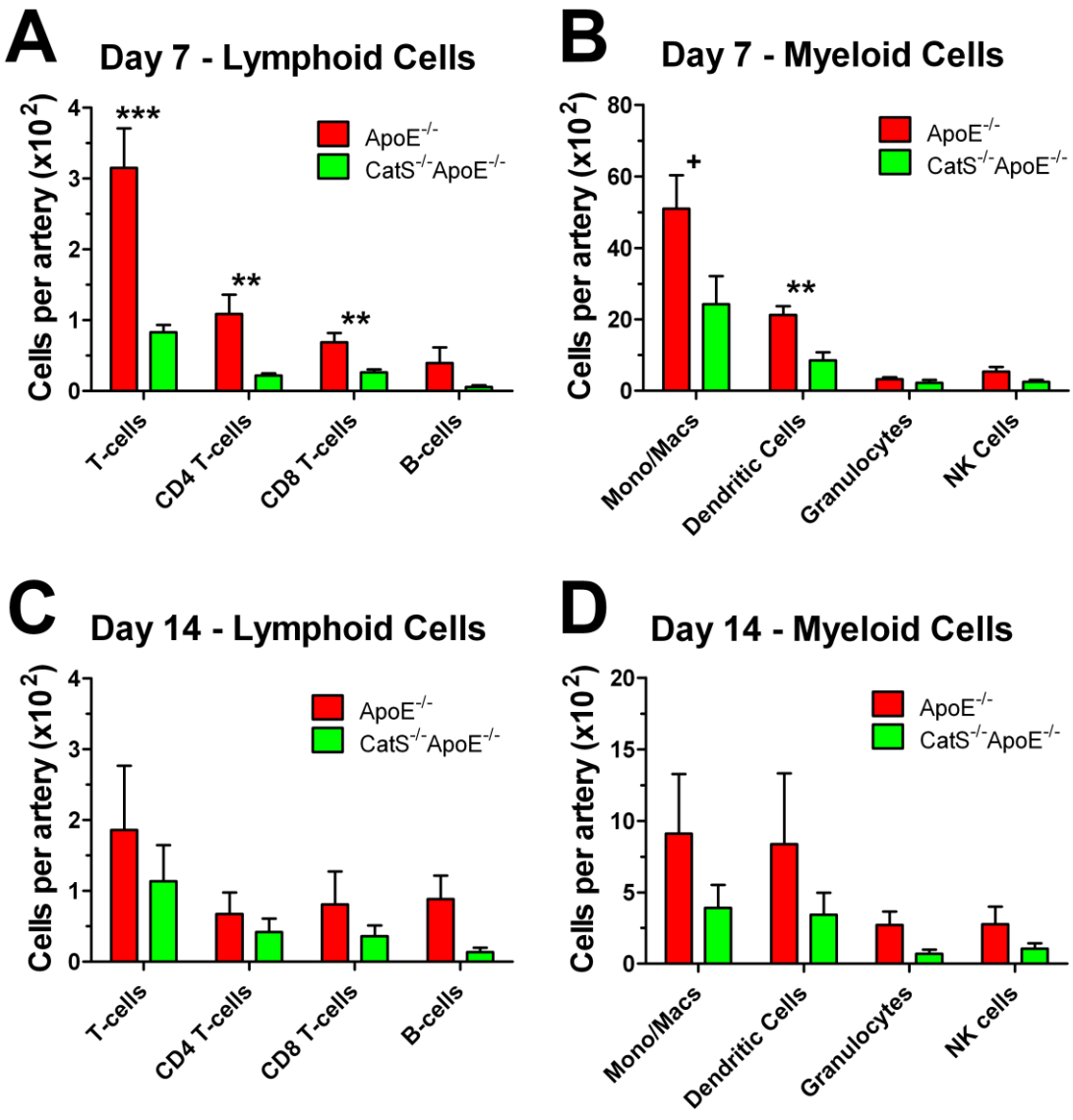

Figure 4.4. CatS deficiency disrupts innate and adaptive immune cell recruitment into flow-disturbed LCA. *The flow cytometry data shown in Figure 4.2 were further analyzed to quantify dynamic changes in specific innate and adaptive immune cell lineages. A-D, Leukocytes ($CD45^+$) found in flow-disturbed LCA were subdivided into four innate (monocyte/macrophages, DCs, granulocytes, and NK cells) and two adaptive (T- and B-cells) immune cell types. T-cells were further subdivided into CD4 and CD8 T-cells. Shown are absolute cell numbers (in hundreds) per carotid artery (n=3 to 6 pools of 3 arteries each) for $ApoE^{-/-}$ (red bars) and $CatS^{-/-}ApoE^{-/-}$ (green bars) mice taken at 7 (A-B) and 14 days post-ligation (C-D). *, $p<0.05$; **, $p<0.01$; ***, $p<0.001$.*

Hypercholesterolemia induces rapid activation of CD4$^+$ T-cells.

Systemic T-cell responses have been shown to develop against autoantigens like oxLDL and HSP60 during atherogenesis in both humans and mouse models (Liuzzo et al., 2000;Buono et al., 2005). However, immunodominant epitopes for these antigens have yet to be finely mapped. In order to follow T-cell responses in our d-flow model of atherosclerosis in a more general fashion, peripheral blood leukocytes (PBLs) and splenocytes were stained for T-cell lineage markers (CD3, CD4, CD8a, and CD25) as well as markers of T-cell activation and lymphoid tissue homing (CD44 and CD62L) and analyzed by flow cytometry (Fig. 4.2). To determine whether HFD or partial carotid ligation surgery promote CD4 or CD8 T-cell responses, flow cytometry was performed on PBLs and splenocytes taken from HFD-fed ligated or sham-operated ApoE$^{-/-}$ mice at 7 days post-ligation. Cells from untreated ApoE$^{-/-}$ mice fed a chow diet were used to establish baseline circulating and splenic T-cell levels.

Levels of CD4 effector/memory (CD44$^+$CD62L$^-$) and central memory (CD44$^+$CD62L$^+$) T-cells were significantly increased in the spleens of both sham-operated and ligated mice at 7 days post-surgery, but were only elevated in the blood of ligated mice (Fig. 4.5A-B). This suggests that HFD very rapidly induces CD4 T-cell responses independent of d-flow, while d-flow promotes CD4 effector/memory T-cell trafficking. In contrast, levels of effector/memory CD8 T-cells remained unchanged in the blood and spleen of both sham-operated and ligated mice (Fig. 4.5C), suggesting that T-cell responses induced by pro-atherogenic conditions are dominated by CD4$^+$ T-cells.

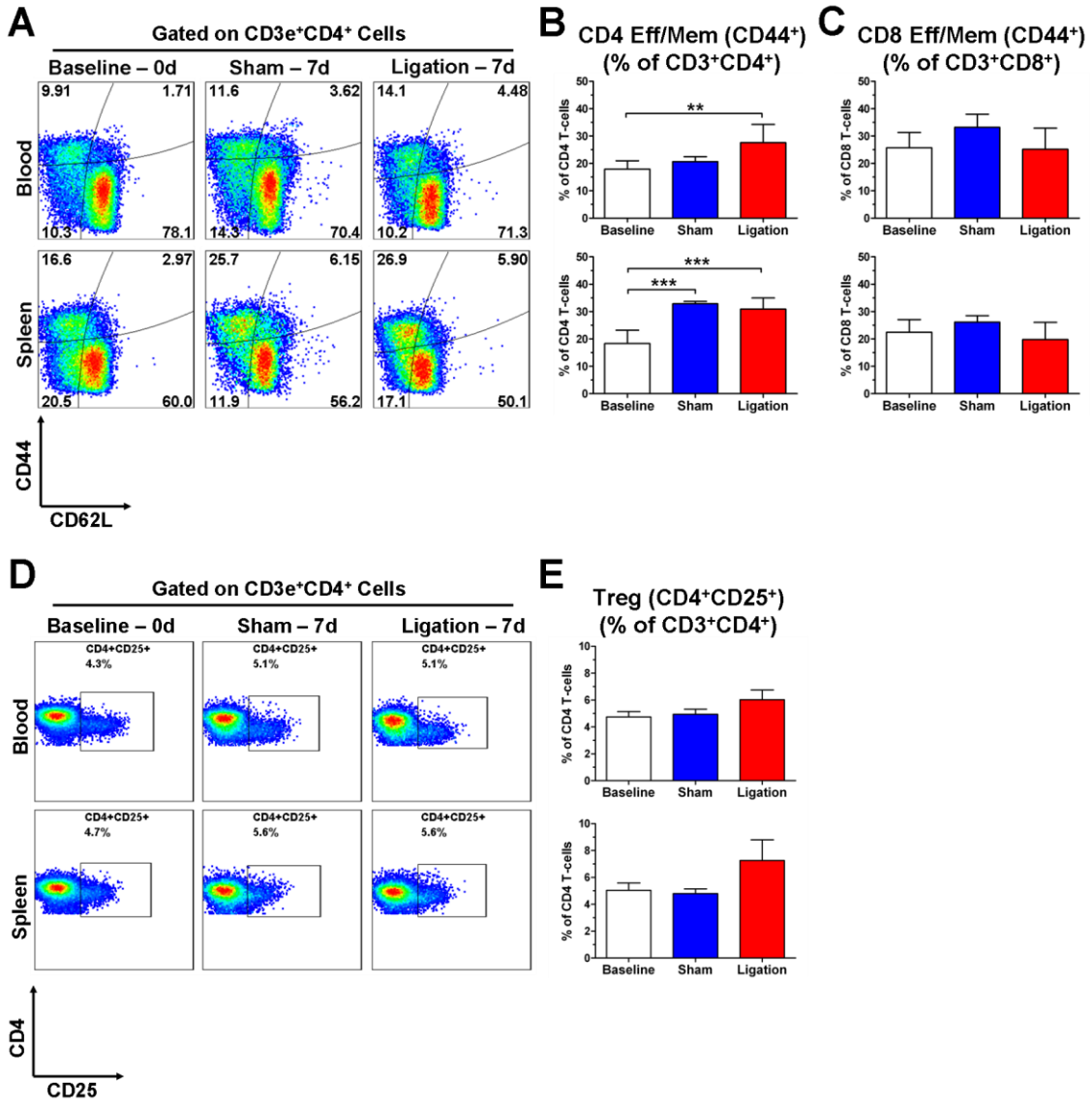

Figure 4.5. Hypercholesterolemia rapidly activates CD4$^+$ T-cells. *PBLs and splenocytes were collected from ligated (red bars) and sham-operated (blue bars) ApoE$^{-/-}$ mice fed HFD for 7 days, stained for T-cell lineage markers (CD3, CD4, CD8a, CD25, CD44, and CD62L), and analyzed by flow cytometry. Untreated ApoE$^{-/-}$ mice fed chow diet were used as baseline controls (white bars). A, Shows representative FACS plots of CD44 and CD62L staining in CD4 T-cells. Quadrant numbers denote percentage of total CD4 T-cells. B-C, Graphs show mean percentage of effector/memory (CD44$^+$) T-cells in the CD4 (B) and CD8 (C) compartments. D-E, Show representative FACS plots of CD4 and CD25 staining (D), and mean percentage of CD25$^+$ CD4 T-cells (E). *, $p<0.05$; **, $p<0.01$; ***, $p<0.001$.*

As a preliminary study to test whether HFD also induced regulatory (Treg) T-cell responses, peripheral blood and splenic $CD4^+$ T-cells were also stained for CD25. Treg ($CD4^+CD25^+$) levels were unchanged from baseline in both blood and spleen at 7 days post-surgery in ligated and sham-operated mice (Fig. 4.5D-E), suggesting that pro-atherogenic conditions favor the induction of effector T-cell responses over Treg responses.

CatS is required for $CD4^+$ and $CD8^+$ T-cell activation under hypercholesterolemic conditions.

CatS is known to play an essential role in the presentation of exogenous antigens to CD4 T-cells (Nakagawa et al., 1999;Shi et al., 1999b). Therefore, peripheral blood and splenic T-cells were taken from HFD-fed $ApoE^{-/-}$ and $CatS^{-/-}ApoE^{-/-}$ mice at 7 days post-ligation, and stained and analyzed by flow cytometry as described above. Untreated $ApoE^{-/-}$ and $CatS^{-/-}ApoE^{-/-}$ animals maintained on chow diet were used to establish baseline cell levels.

CatS-deficient mice had significantly lower levels of circulating, but not splenic, CD4 effector/memory ($CD44^+CD62L^-$) and central memory ($CD44^+CD62L^+$) T-cells at baseline, while CD8 effector/memory T-cell levels did not initially differ between $ApoE^{-/-}$ and $CatS^{-/-}ApoE^{-/-}$ mice (Fig. 4.6).

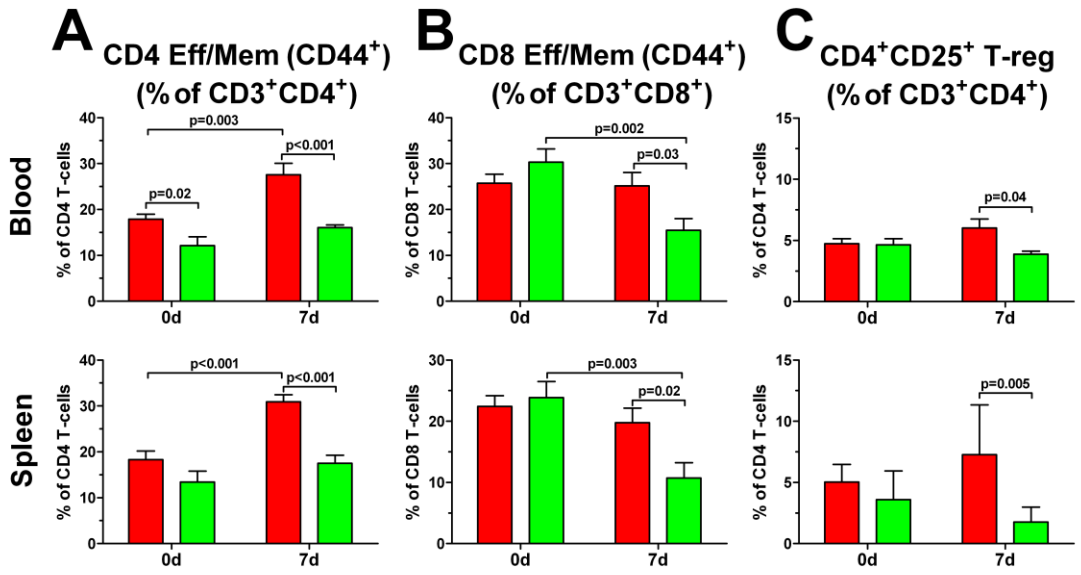

Figure 4.6. CatS is required for CD4$^+$ and CD8$^+$ T-cell activation under hypercholesterolemic conditions. *PBLs and splenocytes were collected from ligated ApoE$^{-/-}$ (red bars) and CatS$^{-/-}$ApoE$^{-/-}$ (green bars) fed HFD for at 7 days, stained for T-cell lineage markers (CD3, CD4, CD8a, CD25, CD44, and CD62L), and analyzed by flow cytometry. Untreated mice fed chow diet were used as baseline controls. A-B, Graphs show mean percentage of effector/memory (CD44$^+$) T-cells in the CD4 (A) and CD8 (B) compartments. C, Shows mean percentage of CD4$^+$CD25$^+$ Treg present amongst total CD4 T-cells.*

CatS deficiency suppressed the expansion of effector/memory CD4 T-cells in both the blood and spleen at 7 days post-ligation, and also significantly decreased the level of circulating and splenic CD8 effector/memory T-cells. Circulating and splenic CD4$^+$CD25$^+$ Treg levels also declined in a similar fashion in CatS$^{-/-}$ApoE$^{-/-}$ mice.

To determine whether the suppression of T-cell responses in CatS-deficient mice also led to a similarly reduced capacity to produce pro-inflammatory cytokines in flow-disturbed LCA, whole LCA and control RCA were taken at 7 days post-ligation and incubated overnight with TPA and ionomycin to stimulate cytokine production. Interferon gamma (IFNγ), tumor necrosis factor alpha (TNFα□), interleukin 2 (IL-2), interleukin 4 (IL-4),

and interleukin 5 (IL-5) protein expression was assessed in culture supernatants by cytokine bead array ELISA. As shown in Figure 4.7, CatS deficiency did not influence the production of pro-inflammatory Th1-associated IFNγ or TNFα, suggesting that CatS-deficient animals fail to control pro-atherogenic inflammation in flow-disturbed LCA, despite suppressing leukocyte recruitment and T-cell responses. However, LCA from $CatS^{-/-}ApoE^{-/-}$ mice produced significantly less IL-2 and IL-5, suggesting that local T-cell and mast cell activity were suppressed compared to $ApoE^{-/-}$ mice (Fig. 4.7). The Th2-associated cytokine, IL-4 was not present in appreciable levels in either $CatS^{-/-}ApoE^{-/-}$ or $ApoE^{-/-}$ mice.

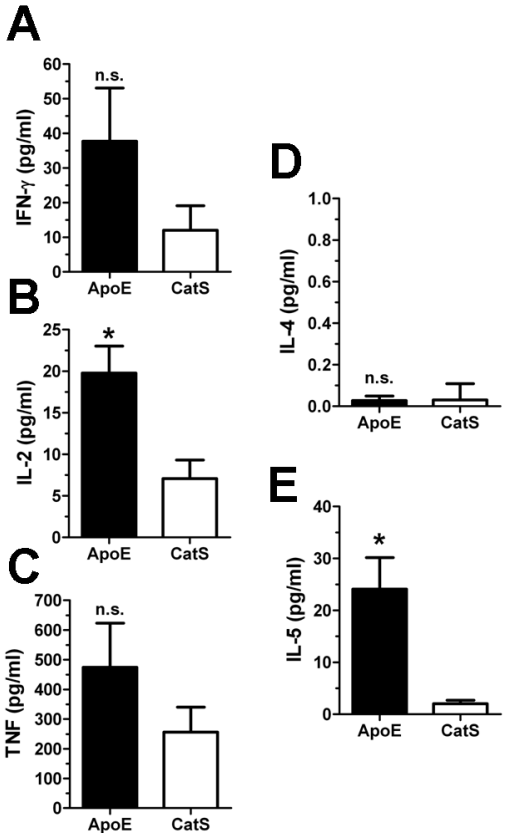

Figure 4.7. CatS deficiency fails to suppress IFNg and TNFa production capacity in flow-disturbed LCA. *A-E, Production of IFNγ (A), IL-2 (B), TNFα (C), IL-4 (D), and IL-5 (E) proteins was determined by ELISA using 7 day post-ligation LCA taken from $ApoE^{-/-}$ (black bars) or $CatS^{-/-}ApoE^{-/-}$ (white bars) mice and stimulated ex vivo with TPA and ionomycin for 16 hr (n=5). *, $p<0.05$. n.s., not significant.*

CatS deficiency fails to inhibit atherosclerosis induced by d-flow.

Finally, we tested whether CatS is required for the development of atherosclerosis in flow-disturbed LCA. Atherosclerotic lesion development was measured by oil red O staining in arterial cross-sections taken from HFD-fed $CatS^{-/-}ApoE^{-/-}$ and $ApoE^{-/-}$ 3 weeks after partial carotid ligation. Surprisingly, CatS-deficient mice did not develop less atherosclerosis in flow-disturbed LCA compared to $ApoE^{-/-}$ mice as we previously hypothesized (Figure 4.8). This result is unexpected as overall leukocyte recruitment into LCA was markedly reduced in $CatS^{-/-}ApoE^{-/-}$ mice (Fig. 4.3A), but may be explained by the retained capacity of arterial wall cells to secrete sufficient amounts of pro-atherogenic cytokines like IFNγ and TNFα (Fig. 4.7). These findings require us to reassess our initial hypothesis that CatS-deficiency reduces d-flow-induced plaque burden in $ApoE^{-/-}$ mice fed a HFD.

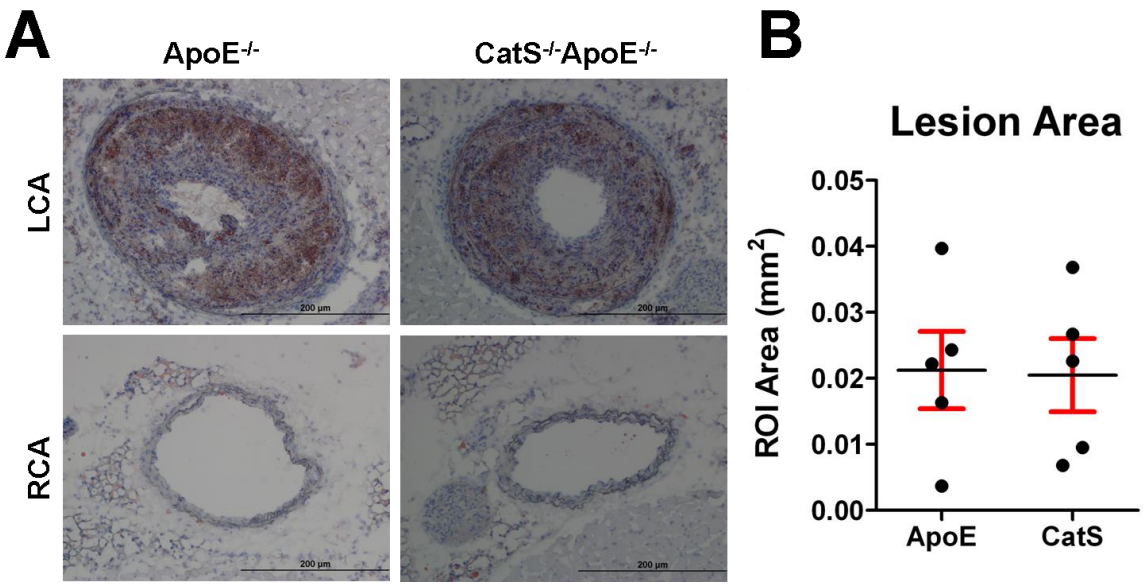

Figure 4.8. CatS deficiency fails to inhibit atherosclerosis induced by d-flow. *Atherosclerotic lesion area in ligated $ApoE^{-/-}$ (n=5) and $CatS^{-/-}ApoE^{-/-}$ (n=5) mice was determined by Oil-Red-O staining in LCA and RCA frozen cross-sections obtained 3 weeks post-ligation. A-B, Shown are images of representative Oil-Red-O stains (A), and graph of lesion area quantification (B). Magnification x10; scale bars, 200 µm.*

4.4 Discussion

CatS has been shown to play a pro-inflammatory and destabilizing role in atherosclerosis, by promoting leukocyte infiltration into the arterial wall and degrading structural elastin and collagen in established plaques (Sukhova et al., 2003;Rodgers et al., 2006;de Nooijer et al., 2009). Similarly, pro-atherogenic d-flow has been shown to promote EC inflammation and the upregulation of adhesion molecules required for leukocyte binding and infiltration (Nam et al., 2009;Chiu and Chien, 2011). However, while d-flow was recently shown to upregulate CatS in vascular endothelium (Ni et al., 2010), the relationship between CatS and d-flow is still poorly understood. Furthermore, CatS has been implicated as a requisite molecule for the potentiation of pro-atherogenic T-cell responses, but this has yet to be proven.

To answer these questions we examined leukocyte recruitment, T-cell activation, vascular inflammation, and atherosclerotic lesion development in CatS-deficient $ApoE^{-/-}$ mice using our d-flow model of atherosclerosis in the mouse. We found that CatS deficiency significantly impaired early leukocyte recruitment into flow-disturbed LCA (Fig. 4.3A) in agreement with previous reports (Sukhova et al., 2003). Further analysis of vascular leukocyte subsets using flow cytometry showed that CatS was particularly important for the recruitment of DCs and T-cells (both CD4 and CD8) (Fig. 4.4A-B). Monocyte/macrophages showed a trend toward a reduction in $CatS^{-/-}ApoE^{-/-}$ mice, which disagrees with previous reports that CatS expression in monocytes is required for monocyte migration across the subendothelial basement membrane (Sukhova et al., 2003). One possible explanation is that the majority of plaque DCs also expressed

monocyte/macrophage markers such as CD11b and F4/80 in addition to the classic DC markers CD11c and MHC-II (data not shown), suggesting a monocytic origin (Choi et al., 2011). Recruitment of other non-T-cell/non-monocyte-derived cells such as B-cells, NK cells, and granulocytes was not effected by CatS deficiency (Fig. 4.4A-B). Surprisingly, we found that deficient leukocyte recruitment was not sustained in $CatS^{-/-}ApoE^{-/-}$ LCAs taken 14 days post-ligation, following lesion development (Fig. 4.3B-C, Fig. 4.4B-C). This finding differs from previous reports that show CatS also mediates leukocyte recruitment in later and established atherosclerotic lesions (Sukhova et al., 2003;de Nooijer et al., 2009), perhaps due to differences in the models used.

T-cell staining studies in ligated and sham-operated $ApoE^{-/-}$ mice clearly show that HFD induces expansion of $CD44^{hi}$-expressing memory and effector $CD4^+$ T-cells, but not $CD8^+$ T-cells (Fig. 4.5A-C), in accordance with reports showing that pro-atherogenic conditions such as hypercholesterolemia are capable of priming pro-atherogenic $CD4^+$ T-cell responses both systemically and at sites of vascular inflammation (Buono et al., 2005;Zhou et al., 2006;Hermansson et al., 2010;Hjerpe et al., 2010). D-flow also increased activated $CD4^+$ T-cell levels in the blood (Fig. 4.5A-C), suggesting that d-flow-induced vascular inflammation may promote T-cell trafficking. However, the current studies are far from conclusive, requiring further tracking studies (Galkina et al., 2006;Galkina et al., 2007). In contrast to effector $CD4^+$ T-cells, Treg ($CD4^+CD25^+$) levels did not increase in either the spleen or blood under pro-atherogenic conditions (Fig. 4.5D-E). However, a recent report found that chronic hypercholesterolemia increased the presence of Tregs in the circulation, but not the spleen (Maganto-Garcia et al., 2011),

suggesting that the time points observed in the current study were too early to see changes in Treg behavior.

One of the key novel findings of this preliminary study was that CatS-deficiency disrupts $CD4^+$ T-cell activation during atherogenesis (Fig. 4.6A), suggesting that CatS is required for presentation of pro-atherogenic antigens to $CD4^+$ T-cells. Previous reports showed that EC- or monocyte-derived CatS mediates leukocyte recruitment (including $CD4^+$ T-cells) by digesting of subendothelial basement, and that CatS activity in established lesions promotes plaque instability, but did not demonstrate a direct role for CatS in mediating or maintaining T-cell responses in hypercholesterolemic mice (Sukhova et al., 2003;Rodgers et al., 2006;de Nooijer et al., 2009). However, it has not been determined whether or not the priming of pro-atherogenic T-cell responses preferentially occur in the vascular wall or in secondary lymphoid tissues (Galkina and Ley, 2009;Hansson and Hermansson, 2011). While $CD8^+$ T-cell responses have not been implicated in the pathogenesis of atherosclerosis (Zhou et al., 2006), we also found that ligated CatS-deficient mice failed to maintain baseline levels of $CD44^{hi}$-expressing $CD8^+$ T-cells (Fig. 4.6B), implicating CatS in the maintenance of $CD8^+$ T-cell responses via insufficient $CD4^+$ T-cell help.

Since CatS deficiency effectively inhibited $CD4^+$ T-cell activation in our model, it was surprising then, that loss of CatS failed to limit the potential of flow-disturbed LCA to produce the major pro-inflammatory cytokine, IFNγ (Fig. 4.7A), as T-cells have been established as the major source of this cytokine in human and murine lesions (Schulte et

al., 2008). CatS-deficient LCA also exhibited a reduced capacity to produce the T-cell growth factor, IL-2 (Fig. 4.7B), suggesting that vascular T-cell responses were indeed disrupted by the loss of CatS. However, TNFα levels were also unchanged in the LCA of $CatS^{-/-}ApoE^{-/-}$ mice (Fig. 4.7C), which suggests that macrophages or mast cells may have compensated for the loss of T-cell derived IFNγ and TNFα in CatS-deficient lesions. Further qPCR and immunohistochemistry studies of *in situ* IFNγ and TNFα production are required to determine if this is the case.

Several reports have demonstrated that CatS plays an important, pathogenic role in both early and late stage atherosclerosis in mice (Sukhova et al., 2003;Rodgers et al., 2006;de Nooijer et al., 2009). Therefore, it was surprising to find that CatS deficiency failed to inhibit the development of atherosclerosis after 3 weeks of ligation and HFD (Fig. 4.8). A recent study found that disruption of the MHC-II antigen presentation pathway via invariant chain knockout inhibited atherosclerosis, greatly reduced numbers of activated lesional $CD4^+$ T-cells, and inhibited IFNγ production in $LDLR^{-/-}$ mice (Sun et al., 2010), suggesting that disruption of MHC-II-mediated antigen presentation is sufficient to block vascular inflammation. One possible explanation for our surprising results is that CatS deficiency leads to a greater reduction of atherosclerosis in $LDLR^{-/-}$ mice as opposed to $ApoE^{-/-}$ mice (Sukhova et al., 2003;Rodgers et al., 2006), which may partly explain the differences seen in our preliminary study. It is also possible that the use of the highly inflammatory, cholate-containing Paigen diet led to more aggressive lesion development in our model, even in the absence of strong $CD4^+$ T-cell-driven pathology. Furthermore, although elastin and collagen content was not measured in our LCA lesions, lesions from

$CatS^{-/-}ApoE^{-/-}$ mice appeared more stable, showed less lipid deposition, and maintained larger lumens than $ApoE^{-/-}$ lesions (data not shown).

In summation, it becomes clear that further study is required to show that hypercholesterolemia and d-flow promote functional systemic and vascular T-cell responses that are inhibited by loss of CatS. In particular, these studies would be greatly benefited by the addition of conditional $CatS^{-/-}$ mice in which CatS deficiency is limited to a specific cell type such as endothelial cells, macrophages, or DCs. Such studies would allow us to isolate the dual functions of CatS as an extracellular protease and an integral part of the MHC-II-mediated antigen presentation machinery. It is also possible that CatS deficiency disrupts vascular $FoxP3^{+}$ Treg or protective humoral antibody responses in addition to blocking Th1 T-cell-mediated inflammatory pathology, which may explain why atherosclerosis was not significantly reduced in our preliminary studies. Further exploration of these mechanisms, as well as additional studies looking at the effect of $CD4^{+}$ T-cell depletion on lesion development in our model would help answer such questions. More in depth studies of lesional extracellular matrix composition, SMC content, and cytokine expression would also help shed more light on the effect of CatS deficiency on lesion development in our model.

4.5 References

Alberts-Grill, N., Rezvan, A., Son, D.J., Qiu, H., Kim, C.W., Kemp, M.L., Weyand, C.M., and Jo, H. (2012). Dynamic immune cell accumulation during flow-induced atherogenesis in mouse carotid artery: an expanded flow cytometry method. *Arterioscler Thromb Vasc Biol* 32**,** 623-632.

Beers, C., Burich, A., Kleijmeer, M.J., Griffith, J.M., Wong, P., and Rudensky, A.Y. (2005). Cathepsin S controls MHC class II-mediated antigen presentation by epithelial cells in vivo. *J Immunol* 174**,** 1205-1212.

Buono, C., Binder, C.J., Stavrakis, G., Witztum, J.L., Glimcher, L.H., and Lichtman, A.H. (2005). T-bet deficiency reduces atherosclerosis and alters plaque antigen-specific immune responses. *Proc Natl Acad Sci U S A* 102**,** 1596-1601.

Chiu, J.J., and Chien, S. (2011). Effects of disturbed flow on vascular endothelium: pathophysiological basis and clinical perspectives. *Physiol Rev* 91**,** 327-387.

Choi, J.H., Cheong, C., Dandamudi, D.B., Park, C.G., Rodriguez, A., Mehandru, S., Velinzon, K., Jung, I.H., Yoo, J.Y., Oh, G.T., and Steinman, R.M. (2011). Flt3 signaling-dependent dendritic cells protect against atherosclerosis. *Immunity* 35**,** 819-831.

De Nooijer, R., Bot, I., Von Der Thusen, J.H., Leeuwenburgh, M.A., Overkleeft, H.S., Kraaijeveld, A.O., Dorland, R., Van Santbrink, P.J., Van Heiningen, S.H., Westra, M.M., Kovanen, P.T., Jukema, J.W., Van Der Wall, E.E., Van Berkel, T.J., Shi, G.P., and Biessen, E.A. (2009). Leukocyte cathepsin S is a potent regulator of both cell and matrix turnover in advanced atherosclerosis. *Arterioscler Thromb Vasc Biol* 29**,** 188-194.

Drechsler, M., Megens, R.T., Van Zandvoort, M., Weber, C., and Soehnlein, O. (2010). Hyperlipidemia-triggered neutrophilia promotes early atherosclerosis. *Circulation* 122**,** 1837-1845.

Eid, R.E., Rao, D.A., Zhou, J., Lo, S.F., Ranjbaran, H., Gallo, A., Sokol, S.I., Pfau, S., Pober, J.S., and Tellides, G. (2009). Interleukin-17 and interferon-gamma are produced concomitantly by human coronary artery-infiltrating T cells and act synergistically on vascular smooth muscle cells. *Circulation* 119**,** 1424-1432.

Erbel, C., Chen, L., Bea, F., Wangler, S., Celik, S., Lasitschka, F., Wang, Y., Bockler, D., Katus, H.A., and Dengler, T.J. (2009). Inhibition of IL-17A attenuates atherosclerotic lesion development in apoE-deficient mice. *J Immunol* 183**,** 8167-8175.

Galkina, E., Harry, B.L., Ludwig, A., Liehn, E.A., Sanders, J.M., Bruce, A., Weber, C., and Ley, K. (2007). CXCR6 promotes atherosclerosis by supporting T-cell homing, interferon-gamma production, and macrophage accumulation in the aortic wall. *Circulation* 116**,** 1801-1811.

Galkina, E., Kadl, A., Sanders, J., Varughese, D., Sarembock, I.J., and Ley, K. (2006). Lymphocyte recruitment into the aortic wall before and during development of atherosclerosis is partially L-selectin dependent. *J Exp Med* 203**,** 1273-1282.

Galkina, E., and Ley, K. (2009). Immune and inflammatory mechanisms of atherosclerosis (*). *Annu Rev Immunol* 27**,** 165-197.

Hansson, G.K., and Hermansson, A. (2011). The immune system in atherosclerosis. *Nat Immunol* 12**,** 204-212.

Hermansson, A., Ketelhuth, D.F., Strodthoff, D., Wurm, M., Hansson, E.M., Nicoletti, A., Paulsson-Berne, G., and Hansson, G.K. (2010). Inhibition of T cell response to native low-density lipoprotein reduces atherosclerosis. *J Exp Med* 207**,** 1081-1093.

Hjerpe, C., Johansson, D., Hermansson, A., Hansson, G.K., and Zhou, X. (2010). Dendritic cells pulsed with malondialdehyde modified low density lipoprotein aggravate atherosclerosis in Apoe(-/-) mice. *Atherosclerosis* 209**,** 436-441.

Lessner, S.M., Prado, H.L., Waller, E.K., and Galis, Z.S. (2002). Atherosclerotic lesions grow through recruitment and proliferation of circulating monocytes in a murine model. *Am J Pathol* 160**,** 2145-2155.

Li, L., Chen, W., Rezvan, A., Jo, H., and Harrison, D.G. (2011a). Tetrahydrobiopterin deficiency and nitric oxide synthase uncoupling contribute to atherosclerosis induced by disturbed flow. *Arterioscler Thromb Vasc Biol* 31**,** 1547-1554.

Li, L., Chen, W., Rezvan, A., Jo, H., and Harrison, D.G. (2011b). Tetrahydrobiopterin Deficiency and Nitric Oxide Synthase Uncoupling Contribute to Atherosclerosis Induced by Disturbed Flow. *Arterioscler Thromb Vasc Biol*.

Li, L., Rezvan, A., Salerno, J.C., Husain, A., Kwon, K., Jo, H., Harrison, D.G., and Chen, W. (2010). GTP cyclohydrolase I phosphorylation and interaction with GTP cyclohydrolase feedback regulatory protein provide novel regulation of endothelial tetrahydrobiopterin and nitric oxide. *Circ Res* 106**,** 328-336.

Liuzzo, G., Goronzy, J.J., Yang, H., Kopecky, S.L., Holmes, D.R., Frye, R.L., and Weyand, C.M. (2000). Monoclonal T-cell proliferation and plaque instability in acute coronary syndromes. *Circulation* 101**,** 2883-2888.

Maciewicz, R.A., and Etherington, D.J. (1988). A comparison of four cathepsins (B, L, N and S) with collagenolytic activity from rabbit spleen. *Biochem J* 256**,** 433-440.

Maganto-Garcia, E., Tarrio, M.L., Grabie, N., Bu, D.X., and Lichtman, A.H. (2011). Dynamic changes in regulatory T cells are linked to levels of diet-induced hypercholesterolemia. *Circulation* 124**,** 185-195.

Mclaren, J.E., and Ramji, D.P. (2009). Interferon gamma: a master regulator of atherosclerosis. *Cytokine Growth Factor Rev* 20**,** 125-135.

Nakagawa, T.Y., Brissette, W.H., Lira, P.D., Griffiths, R.J., Petrushova, N., Stock, J., Mcneish, J.D., Eastman, S.E., Howard, E.D., Clarke, S.R., Rosloniec, E.F., Elliott, E.A., and Rudensky, A.Y. (1999). Impaired invariant chain degradation and antigen presentation and diminished collagen-induced arthritis in cathepsin S null mice. *Immunity* 10**,** 207-217.

Nakajima, T., Goek, O., Zhang, X., Kopecky, S.L., Frye, R.L., Goronzy, J.J., and Weyand, C.M. (2003). De novo expression of killer immunoglobulin-like receptors and signaling proteins regulates the cytotoxic function of CD4 T cells in acute coronary syndromes. *Circ Res* 93**,** 106-113.

Nakajima, T., Schulte, S., Warrington, K.J., Kopecky, S.L., Frye, R.L., Goronzy, J.J., and Weyand, C.M. (2002). T-cell-mediated lysis of endothelial cells in acute coronary syndromes. *Circulation* 105**,** 570-575.

Nam, D., Ni, C.W., Rezvan, A., Suo, J., Budzyn, K., Llanos, A., Harrison, D., Giddens, D., and Jo, H. (2009). Partial carotid ligation is a model of acutely induced disturbed flow, leading to rapid endothelial dysfunction and atherosclerosis. *Am J Physiol Heart Circ Physiol* 297**,** H1535-1543.

Nam, D., Ni, C.W., Rezvan, A., Suo, J., Budzyn, K., Llanos, A., Harrison, D.G., Giddens, D.P., and Jo, H. (2010). A model of disturbed flow-induced atherosclerosis in mouse carotid artery by partial ligation and a simple method of RNA isolation from carotid endothelium. *J Vis Exp*.

Ni, C.W., Qiu, H., Rezvan, A., Kwon, K., Nam, D., Son, D.J., Visvader, J.E., and Jo, H. (2010). Discovery of novel mechanosensitive genes in vivo using mouse carotid artery endothelium exposed to disturbed flow. *Blood* 116**,** e66-73.

Niessner, A., and Weyand, C.M. (2010). Dendritic cells in atherosclerotic disease. *Clin Immunol* 134**,** 25-32.

Paigen, B., Morrow, A., Holmes, P.A., Mitchell, D., and Williams, R.A. (1987). Quantitative assessment of atherosclerotic lesions in mice. *Atherosclerosis* 68**,** 231-240.

Pryshchep, S., Sato, K., Goronzy, J.J., and Weyand, C.M. (2006). T cell recognition and killing of vascular smooth muscle cells in acute coronary syndrome. *Circ Res* 98**,** 1168-1176.

Rodgers, K.J., Watkins, D.J., Miller, A.L., Chan, P.Y., Karanam, S., Brissette, W.H., Long, C.J., and Jackson, C.L. (2006). Destabilizing role of cathepsin S in murine atherosclerotic plaques. *Arterioscler Thromb Vasc Biol* 26**,** 851-856.

Schulte, S., Sukhova, G.K., and Libby, P. (2008). Genetically programmed biases in Th1 and Th2 immune responses modulate atherogenesis. *Am J Pathol* 172**,** 1500-1508.

Shi, G.P., Munger, J.S., Meara, J.P., Rich, D.H., and Chapman, H.A. (1992). Molecular cloning and expression of human alveolar macrophage cathepsin S, an elastinolytic cysteine protease. *J Biol Chem* 267**,** 7258-7262.

Shi, G.P., Sukhova, G.K., Grubb, A., Ducharme, A., Rhode, L.H., Lee, R.T., Ridker, P.M., Libby, P., and Chapman, H.A. (1999a). Cystatin C deficiency in human atherosclerosis and aortic aneurysms. *J Clin Invest* 104**,** 1191-1197.

Shi, G.P., Villadangos, J.A., Dranoff, G., Small, C., Gu, L., Haley, K.J., Riese, R., Ploegh, H.L., and Chapman, H.A. (1999b). Cathepsin S required for normal MHC class II peptide loading and germinal center development. *Immunity* 10**,** 197-206.

Sukhova, G.K., Shi, G.P., Simon, D.I., Chapman, H.A., and Libby, P. (1998). Expression of the elastolytic cathepsins S and K in human atheroma and regulation of their production in smooth muscle cells. *J Clin Invest* 102**,** 576-583.

Sukhova, G.K., Zhang, Y., Pan, J.H., Wada, Y., Yamamoto, T., Naito, M., Kodama, T., Tsimikas, S., Witztum, J.L., Lu, M.L., Sakara, Y., Chin, M.T., Libby, P., and Shi, G.P. (2003). Deficiency of cathepsin S reduces atherosclerosis in LDL receptor-deficient mice. *J Clin Invest* 111**,** 897-906.

Sun, J., Hartvigsen, K., Chou, M.Y., Zhang, Y., Sukhova, G.K., Zhang, J., Lopez-Ilasaca, M., Diehl, C.J., Yakov, N., Harats, D., George, J., Witztum, J.L., Libby, P., Ploegh, H., and Shi, G.P. (2010). Deficiency of antigen-presenting cell invariant chain reduces atherosclerosis in mice. *Circulation* 122**,** 808-820.

Xin, X.Q., Gunesekera, B., and Mason, R.W. (1992). The specificity and elastinolytic activities of bovine cathepsins S and H. *Arch Biochem Biophys* 299**,** 334-339.

Zhou, X., Robertson, A.K., Hjerpe, C., and Hansson, G.K. (2006). Adoptive transfer of CD4+ T cells reactive to modified low-density lipoprotein aggravates atherosclerosis. *Arterioscler Thromb Vasc Biol* 26**,** 864-870.

CHAPTER 5:

FMS-LIKE TYROSINE KINASE 3 LIGAND TREATMENT FAILS TO CONTROL DISTURBED FLOW-INDUCED ATHEROSCLEROSIS IN APOE$^{-/-}$ MICE

5.1 Introduction

The establishment of chronic, pro-inflammatory adaptive immune responses within the artery wall is a critical step in the development of atherosclerosis (Hansson and Hermansson, 2011). Both B-cell and T-cell responses develop against vascular antigens like oxLDL and HSP-60, which have been shown to contribute to atherosclerosis by mechanisms of cytokine release, antibody-antigen complex formation, and direct cellular cytotoxicity (Zhou et al., 2000;Nakajima et al., 2002;Buono et al., 2005;Niessner et al., 2006;Pryshchep et al., 2006;Sato et al., 2006;Zhou et al., 2006;Hermansson et al., 2010;Kyaw et al., 2010). Interestingly, the majority of pro-atherogenic vascular antigens established so far are autoantigens, suggesting that atherosclerosis may have an autoimmune component dependent on the breakdown of immune tolerance within the artery wall (Galkina and Ley, 2009;Hansson and Hermansson, 2011). However, the mechanisms by which tolerance against these antigens is broken in the artery wall are not entirely understood.

The evidence to date suggests that Tregs play a vital role in maintaining tolerance and inhibiting atherosclerosis development in the artery wall (Mallat et al., 1999;Mallat et al., 2003;Binder et al., 2004;Ait-Oufella et al., 2006;Mor et al., 2007;Kleemann et al., 2008). One report found that long term hypercholesterolemia results in the gradual loss of Tregs from murine aorta, which corresponded with lesion development in $LDLR^{-/-}$ mice (Maganto-Garcia et al., 2011), suggesting that the loss of vascular Treg function is a key step in the loss of tolerance in the artery wall. DCs and other APCs like macrophages are required for the initiation and maintenance of T-cell responses, through repeated MHC-

II/TCR (signal 1), costimulatory receptor (signal 2), and cytokine (signal 3) interactions. As such, an integral role for DCs in atherogenesis is emerging. Data from several papers demonstrate that DCs shape inflammatory tone in vascular tissues. For instance, Weber *et al.*, (2011) found that a CCL17-producing subset of vascular DCs that only enters the artery during atherogenesis disrupts Treg homeostasis in mouse aorta and promotes atherosclerosis (Weber et al., 2011). Adoptive transfer of oxLDL-loaded DCs was also shown to promote atherosclerosis in mice (Hjerpe et al., 2010). Conversely, substantial evidence has been gathered demonstrating the atheroprotective effect of DC-mediated immunization against pro-atherogenic autoantigens, which induce protective autoantigen clearing B-cell responses and inflammation-suppressing Treg responses (George et al., 1998;Harats et al., 2002;Maron et al., 2002;van Puijvelde et al., 2007;Nilsson et al., 2009;Habets et al., 2010). It is important, then, to understand the mechanisms by which DCs support pro-inflammatory and tolerogenic adaptive immune responses in the context of atherogenesis.

Recent evidence suggests that support of Treg and pro-atherogenic $CD4^+$ T-cell responses may be accomplished by distinct vDC subsets. Choi *et al.*, (2011) described a distinct vDC subset which express CD103 and depend on Flt3L and its receptor Flt3 for their growth and differentiation (Choi et al., 2011). These Flt3-Flt3L-dependent vDCs bear a marked phenotypic similarity to classical $CD103^+$ classical DCs (cDCs) found in other tissues like the skin, the lungs, and the gut (Ginhoux et al., 2009). Flt3-deficiency in $ApoE^{-/-}$ mice leads to ablation of $CD103^+$ cDCs from aorta, marked reduction of Tregs from aorta, spleen, and lymph nodes, and enhanced atherosclerosis, suggesting that these

DCs play an important role in maintaining Treg responses during atherogenesis (Choi et al., 2011). Additionally, Mo-DCs constitute the other major resident vDC population, although their exact role in atherosclerosis has not yet been determined.

While $CD103^+$ cDCs are known to reside within the aorta under steady-state conditions as well as during atherogenesis, their kinetics during pro-atherogenic hypercholesterolemia and d-flow are not known. Therefore, we sought to characterize the kinetics of $CD103^+$ cDC, Mo-DC, and monocyte/macrophage recruitment into the artery wall in response to d-flow and hypercholesterolemia using our model flow-disturbed atherosclerosis in murine carotid artery (Nam et al., 2009;Nam et al., 2010). Additionally, we sought to test whether $CD103^+$ cDC expansion by exogenous Flt3L treatment could change the inflammatory tone within flow-disturbed LCA and inhibit atherosclerosis. Therefore, a preliminary study was conducted looking at atherosclerosis development in LCA in $ApoE^{-/-}$ mice treated with Flt3L or saline using our partial carotid ligation model. We found that the combination of d-flow and hypercholesterolemia preferentially selects for the recruitment of monocyte-derived cells like Mo-DCs and macrophages, which rapidly outpace $CD103^+$ cDC numbers in flow-disturbed LCA. However, expansion of vascular $CD103^+$ cDCs with exogenous Flt3L treatment also non-specifically increased vascular leukocyte numbers, including Mo-DCs and macrophages, and failed to control atherosclerosis development. These findings call into question the utility of Flt3L therapy for the control of vascular inflammation and atherosclerosis.

5.2 Methods

Mice. Male ApoE$^{-/-}$ mice (B6.129P2-ApoE^{tm1Unc}/J) were purchased from The Jackson Laboratory (Bar Harbor) and were fed *ad libitum* with standard chow diet until surgery at 8 to 9 weeks of age. The ApoE^{tm1Unc} mutation was from a 129P2/OlaHsd-derived E14Tg2a embryonic stem cell line and was backcrossed to the C57BL/6J for 10 generations.

Partial carotid ligation surgery. Partial carotid ligation surgeries were performed as previously described (Nam et al., 2009;Nam et al., 2010;Alberts-Grill et al., 2012). Mice were anesthetized by intra-peritoneal injection of a mixture of xylazine (10 mg/kg) and ketamine (80 mg/kg). The surgical site was epilated, disinfected with Betadine, and a ventral mid-line incision (4 to 5 mm in length) was made in the neck using micro-scissors. The LCA bifurcation was exposed by blunt dissection and three of four caudal LCA branches (left external carotid, internal carotid, and occipital arteries) were carefully dissected free of surrounding connective tissue and ligated with 6-0 silk sutures, leaving the superior thyroid artery intact. The surgical incision was then closed with Tissue-Mend (Veterinary Product Laboratories), and mice were monitored until recovery in a chamber under a heating lamp. Following partial carotid ligation, animals were maintained for 7 to 21 days on the Paigen's high-fat diet (HFD; Science Diets) containing 1.25% cholesterol, 15% fat, and 0.5% cholic acid (Paigen et al., 1987).

Flt3L injection. Recombinant human Flt3L was obtained from Celldex. For Flt3L studies, ApoE-/- mice were injected subcutaneously with 10μg of Flt3L dissolved in

100µl of sterile, physiological saline or saline vehicle control once per day, for either 7 (for flow cytometry studies) or 14 (for Oil-Red-O plaque measurement studies) days.

Cells. For flow cytometry analyses of vascular wall leukocytes, partially-ligated male ApoE$^{-/-}$ mice maintained on HFD were sacrificed by CO_2 inhalation and perfused by cardiac puncture with saline containing 10 U/ml of heparin at 7 and 14 days post-ligation. Following sacrifice, arterial leukocyte preparations were isolated as previously described (Alberts-Grill et al., 2012). In short, LCA and RCA were excised, placed in chilled Hanks balanced salt solution, and then pooled (n=5) in chilled digestion buffer (450 U/ml collagenase I-S, 125 U/ml collagenase XI, 60 U/ml hyaluronidase (Sigma-Aldritch), and 60 U/ml DNAse I (Applichem) in phosphate buffered saline (PBS) supplemented with calcium and magnesium). Pooled arteries were minced finely and digested at 37°C for 1 hour at 5% CO_2, and single cell suspensions obtained by shearing the digested arteries with a 21½ gauge needle. Cells were then washed in PBS without calcium and magnesium (10 min, 500 *g*, 4°C) and resuspended in 1 ml PBS for staining.

Flow cytometry. Single cell suspensions of arterial leukocytes were stained with Fixable Live/Dead Yellow stain (Invitrogen) to discriminate dead cells, and then stained with a cocktail containing Ly-6C-Alexa 488 (HK1.4), F4/80-PE (BM8), NK1.1-PerCP-Cy5.5 (PK136), CD49b-PerCP-Cy5.5 (DX5), Ly-6G-PerCP-Cy5.5 (1A8), CD19-PerCP-Cy5.5 (6D5), CD11c-PE-Cy7 (N418), and CD103-Alexa 647 (2E7) monoclonal (mAb) antibodies from Biolegend; CD3e-PerCP-Cy5.5 (145-2C11) and CD11b-APC-Cy7 (M1/70) mAbs from BD Biosciences; CD45-PE-Texas Red (30-F11) mAb from

Invitrogen Life Sciences; and MHC-II (M5/114.15.2) mAb from eBioscience. Immunofluorescence was detected using a LSR II flow cytometer (BD Immunocytometry Systems). In order to determine absolute cell numbers per sample, 50 µl of AccuCount Ultra Rainbow Fluorescent Particles (Spherotech, Inc.) were added to each sample immediately prior to flow cytometry. Gating of flow cytometry data were performed as shown in Figure 5.1 using analysis software. Absolute cell counts per µl of blood were determined using the following equation: ((A/B) x (C/D)), where A = number of cells recorded for the test sample, B = number of AccuCount beads recorded, C = number of AccuCount beads per 50µl (50,000), and D = volume of test sample in µl.

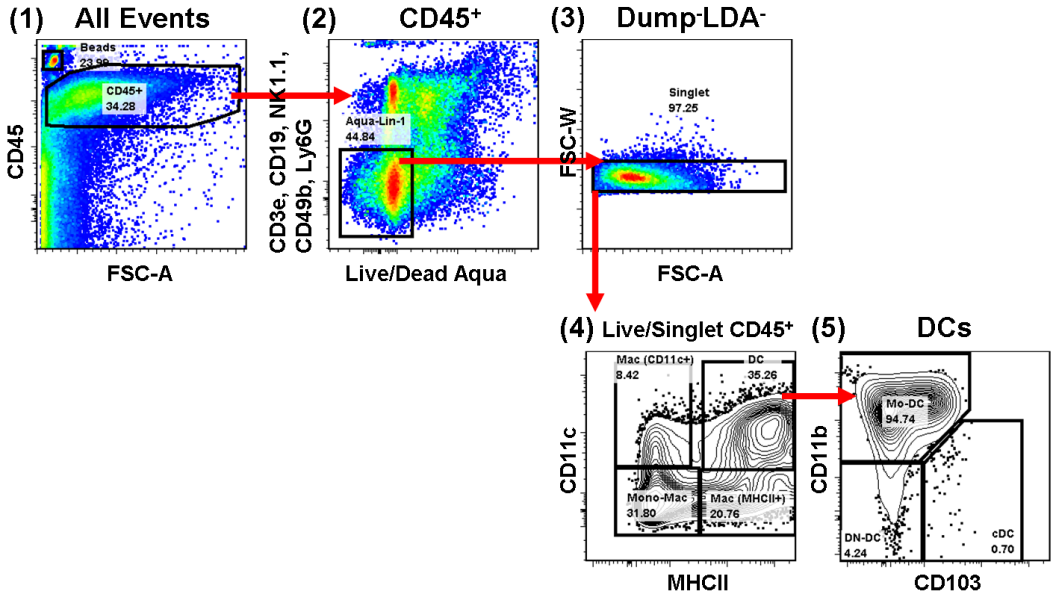

Figure 5.1. Gating strategy for DC flow cytometry panel. *Arterial leukocytes were stained with anti-CD45, -CD3e, -CD19, -NK1.1, -CD49b, -Ly-6G, -Ly-6C, -CD11b, -CD11c, -MHC-II, -F4/80, and -CD103 mAbs. $CD45^+$ leukocytes were gated (1) and dead cells and non-myeloid cells ($CD3e^+CD19^+NK1.1^+CD49b^+Ly6G^+LDA^+$) removed (2). Myeloid cells were described into monocytes ($CD11b^+F4/80^{+/-}CD11c^-MHC\text{-}II^-$), $CD11c^+$ macrophages ($CD11b^+F4/80^+CD11c^+MHC\text{-}II^-$), $MHC\text{-}II^+$ macrophages ($CD11b^+F4/80^+CD11c^-MHC\text{-}II^+$), and DCs ($CD11c^+MHC\text{-}II^+$) (4). DCs were then subdivided into monocyte-derived DCs ($CD11c^+MHC\text{-}II^+CD11b^+F4/80^+CD103^-$) and $CD103^+$ cDCs ($CD11c^+MCH\text{-}II^+CD11b^-F4/80^-CD103^+$) (5). Figure shows the gating strategy used for flow cytometry analyses for a representative arterial leukocyte sample harvested from $ApoE^{-/-}$ LCA 7 days post-ligation. Ultra-bright counting beads (1) were used to determine absolute cell counts. Gate numbers indicate percent of parent. FSC-W, forward scatter width; FSC-A, forward scatter area; SSC-A, side scatter area.*

Oil-Red-O staining of carotid lesions. Mice were euthanized and perfused with saline containing heparin as described above. LCA and RCA were collected *en bloc* along with the heart, aortic arch, trachea, esophagus, and surrounding fat tissue as previously described (Nam et al., 2009). Tissue was embedded in optimal cutting temperature (OCT) compound (Tissue-Tek), frozen on liquid nitrogen and stored at –80°C until used. Frozen sections were made starting from the level of the right subclavian artery bifurcation, 300 μm was trimmed away and five sets of ten consecutive 7 μm thick sections were taken at 300 μm intervals constituting the 'proximal,' 'middle,' and 'distal' portions of the artery. Oil-Red-O staining of LCA and RCA was performed using frozen sections as previously described (Nam et al., 2009). Micrographs were taken with an Olympus IX71 inverted microscope. Images were analyzed with Image J software (NIH) to quantify lesion size in each animal as previously described (Lessner et al., 2002).

Plasma lipid analyses. Blood was drawn from descending aorta of saline- or Flt3L-injected mice using a 27½ gauge needle coated with heparin. Blood samples were centrifuged (3000 rpm for 20 min. at 4°C), and plasma separated by carefully pipetting plasma from pelleted blood cells into a fresh 1.5 ml microcentrifuge tube. Residual blood cells were removed by a second centrifugation step (3000 rpm for 20 min. at 4°C), and samples were frozen at -20°C prior to blood lipid analysis.

Statistical analysis. Values are expressed as mean ± SEM. Pairwise comparisons were performed using two-tailed t-tests. Differences between groups were considered

significant at P values below 0.05. All statistical analyses were performed using Prism software (GraphPad Software).

5.3 Results

D-flow preferentially recruits CD11b$^+$ Mo-DCs, but not CD103$^+$ cDCs into LCA.

In order to understand the dynamics of monocyte, macrophage, and DC recruitment into 'virgin' artery wall in response to d-flow, we conducted a natural time course in ligated ApoE$^{-/-}$ mice fed a HFD. LCA and RCA were taken at 4, 7, and 14 days post-ligation and arterial leukocytes were harvested and stained with anti-CD45, -CD3e, -CD19, -NK1.1, -CD49b, -Ly-6G, -Ly-6C, -CD11b, -CD11c, -MHC-II, -F4/80, and -CD103 mAbs to identify arterial myeloid cell populations. As shown in Figure 5.2 (CD11b$^+$CD11c$^-$MHC-II$^-$) monocytes dominated the artery wall at 4 days post-ligation, along with small numbers of CD11c$^+$ and MHC-II$^+$ macrophage subsets and Mo-DCs. It is interesting to note that no CD103$^+$ cDC were detected at this time, suggesting that these cells are: 1) not native to atheroprotected laminar shear regions of the vasculature, and 2) that unlike monocytes, which can differentiate into Mo-DCs, CD103$^+$ cDC precursors may not migrate into the vessel wall in response to d-flow-mediated inflammatory mediators. This contention is supported by the fact that only sparse numbers of CD103$^+$ cDCs show up at 7, or 14 days post-ligation, despite robust accumulation of monocyte-derived DCs and macrophages at both these time points, although CD103$^+$ cDC numbers did gradually increase over time, suggesting some sort of slow, steady-state trafficking of these cells into flow-disturbed artery wall (Fig. 5.2). Together these data show that d-flow strongly

attracts monocytes into the artery wall, which then differentiate into Mo-DC and various macrophage subsets.

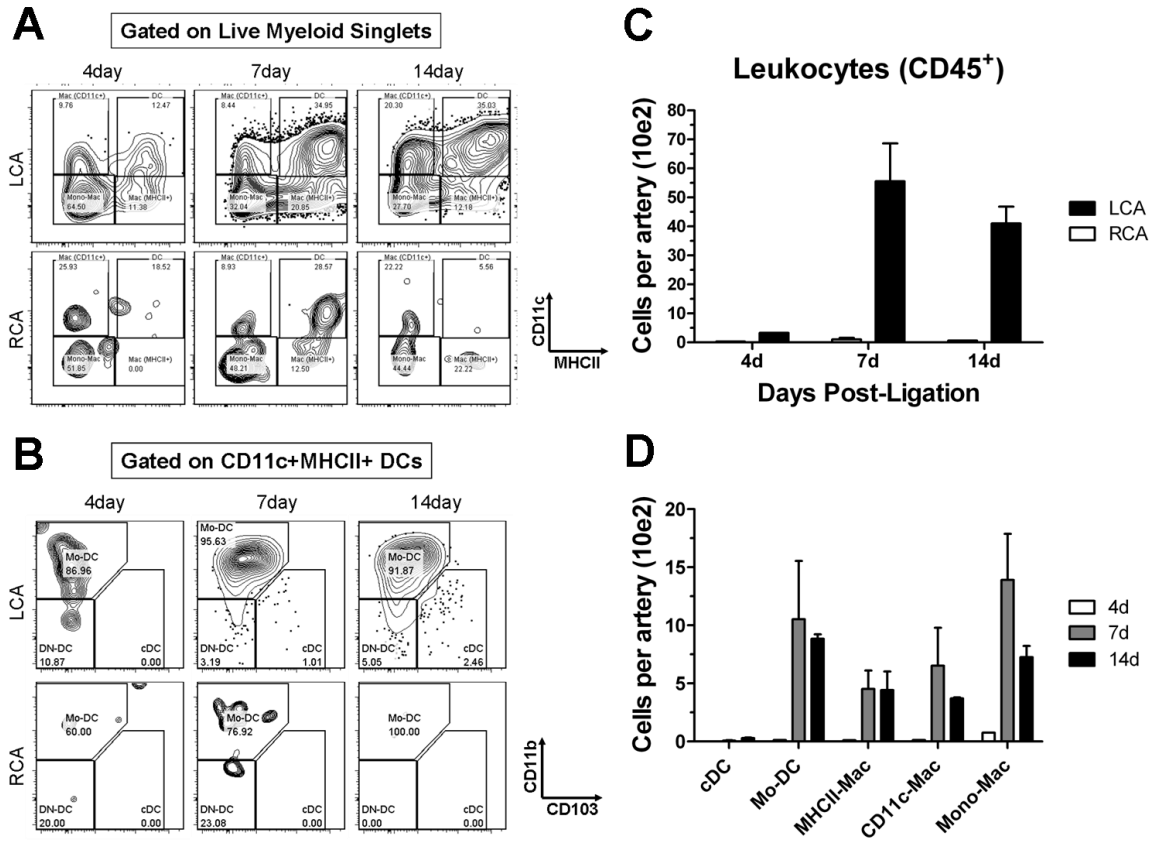

Figure 5.2. D-flow preferentially recruits CD11b^{+} Mo-DCs, but not CD103^{+} cDCs into LCA. *In order to observe the recruitment dynamics of monocyte, macrophage, and DC subsets into the artery wall, arterial leukocytes from ligated ApoE$^{-/-}$ mice fed a HFD were taken from LCA and RCA at 4 (n=1 pool of 5), 7 (n=3 pools of 5), and 14 (n=3 pools of 5) days post-ligation, and stained and gated as shown in Figure 5.1. A-B, Representative FACS plots show CD11c and MHC-II staining in gated myeloid cells (A), and CD11b and CD103 staining in gated DCs (B) in LCA and RCA samples taken over the experimental time course. Gate numbers indicate percent of parent. C-D, Graphs depict number of cells (in hundreds) per carotid artery for total CD45^{+} leukocytes (C), and for monocyte, macrophage, and DC subsets (D).*

Flt3L treatment expands vascular CD103^{+} cDC, and overall leukocyte numbers.

Next we sought to prevent the establishment of sustained vascular inflammation by selectively increasing vascular CD103^{+} cDC numbers during d-flow induced atherogenesis in LCA by injecting Flt3L. To determine whether or not Flt3L selectively expands this vDC subset, arterial leukocytes were harvested from LCA and RCA of Flt3L-treated or saline-treated ApoE$^{-/-}$ mice at 7 days post-ligation and vascular monocytes, macrophages, and DCs were analyzed by flow cytometry as described above. As shown in Figure 5.3, Flt3L treatment greatly increased the number of CD103^{+} cDCs present in flow-disturbed LCA compared to saline-treated controls. However, contrary to our initial hypothesis that Flt3L treatment would selectively increase CD103^{+} cDC numbers, Flt3L-treated animals showed large increases in total CD45^{+} leukocytes, as well as in Mo-DC, MHC-II^{+} macrophages, and monocytes. However, Flt3L treatment did not independently influence vascular leukocyte recruitment, as cell numbers did not significantly increase in the RCA of Flt3L-treated animals (Fig. 5.3A-B). These surprising data suggest that Flt3L may increase vascular inflammation by greatly enhancing d-flow dependent leukocyte recruitment.

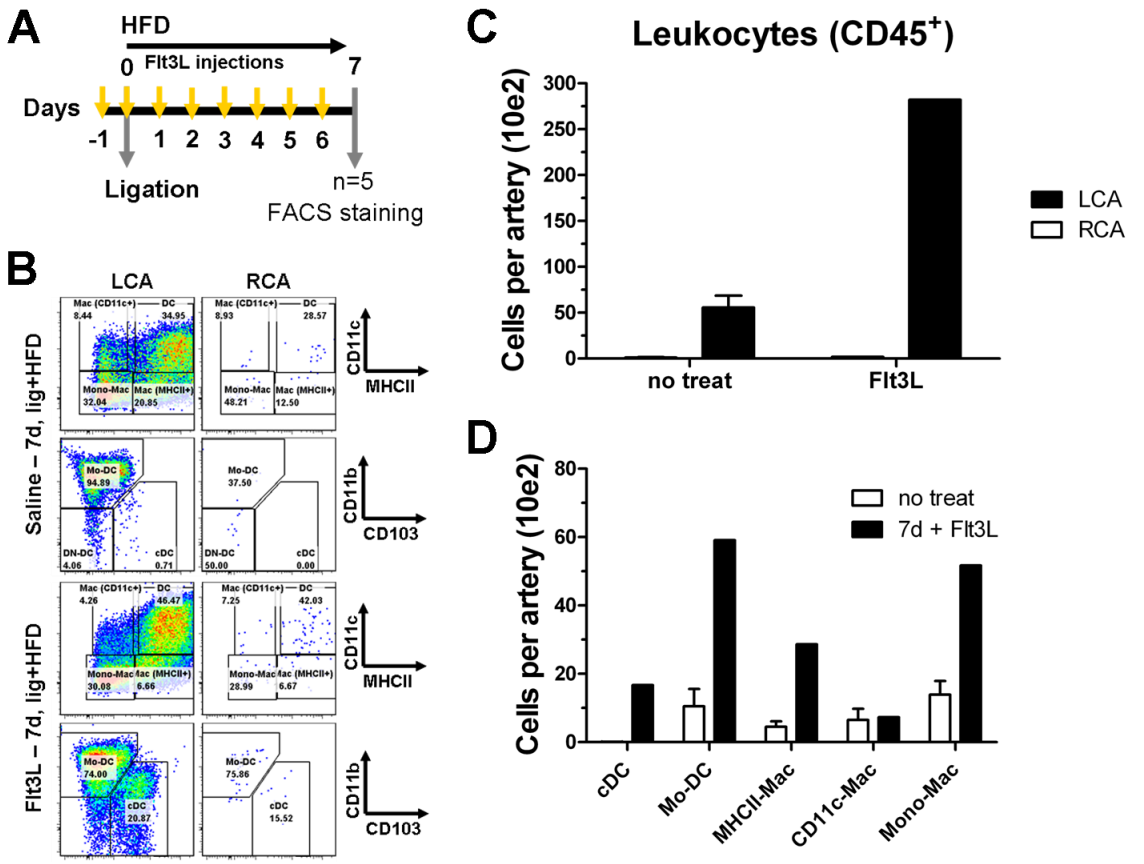

Figure 5.3. Flt3L treatment increases CD103^{+} cDC, and overall leukocyte numbers in LCA at 7 days post-ligation. *Arterial leukocytes were harvested from LCA and RCA of ligated ApoE$^{-/-}$ mice fed a HFD and injected with either 10 μg/day of Flt3L or saline vehicle control for 7 days, and stained and gated as shown in Figure 5.1. A, Diagram shows experimental time course for ligation, HFD, and injections. B, Representative FACS plots show CD11c and MHC-II staining in gated myeloid cells, and CD11b and CD103 staining in gated DCs in LCA and RCA from saline, or Flt3L-treated animals taken 7 days post-ligation. C-D, Graphs depict number of cells (in hundreds) per carotid artery for total CD45^{+} leukocytes (C), and for monocyte, macrophage, and DC subsets (D).*

The effect of Flt3L treatment on atherosclerosis development in our model was also tested. Ftl3L- or saline-treated ApoE$^{-/-}$ controls were ligated and fed a HFD, and atherosclerotic lesion area was determined by Oil-Red-O staining in frozen tissue cross-sections of LCA and RCA taken 14 days post-ligation. Flt3L treatment did not reduce lesion size in LCA compared to saline controls (Fig. 5.4), although treatment did significantly increase plasma high-density lipoprotein (HDL) levels (Fig. 5.5). Together

with the increased leukocyte recruitment into LCA of Flt3L-treated mice, these data suggest that vascular inflammation is unaffected by increased numbers of lesional $CD103^{+}$ cDCs.

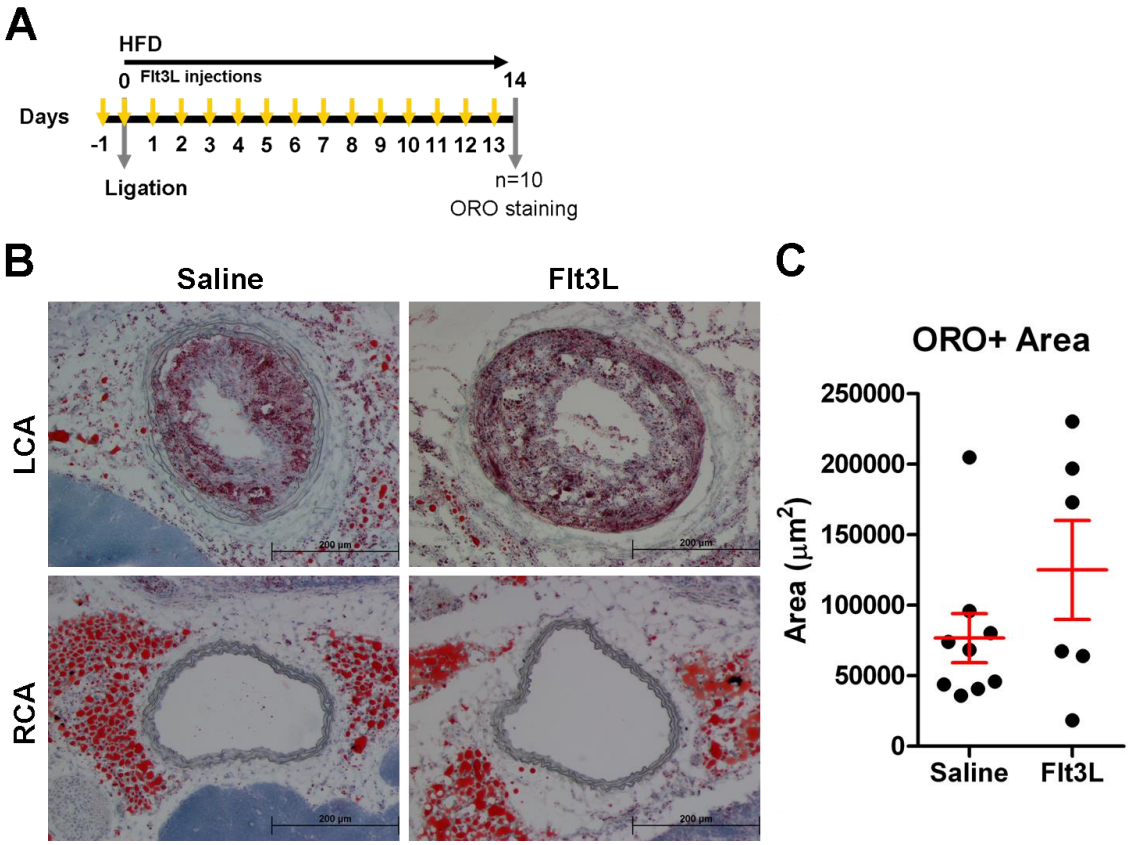

Figure 5.4. Flt3L treatment fails to inhibit d-flow-induced atherosclerosis. *Atherosclerotic lesion area in ligated ApoE$^{-/-}$ mice fed a HFD and injected with either 10 µg/day of Flt3L (n=6) or saline vehicle control (n=9) was determined by Oil-Red-O staining in LCA and RCA frozen cross-sections obtained 14 days post-ligation. A, Diagram shows experimental time course for ligation, HFD, and injections. B-C, Shown are images of representative Oil-Red-O stains (B), and graph of lesion area quantification (C). Magnification x10; scale bars, 200 µm.*

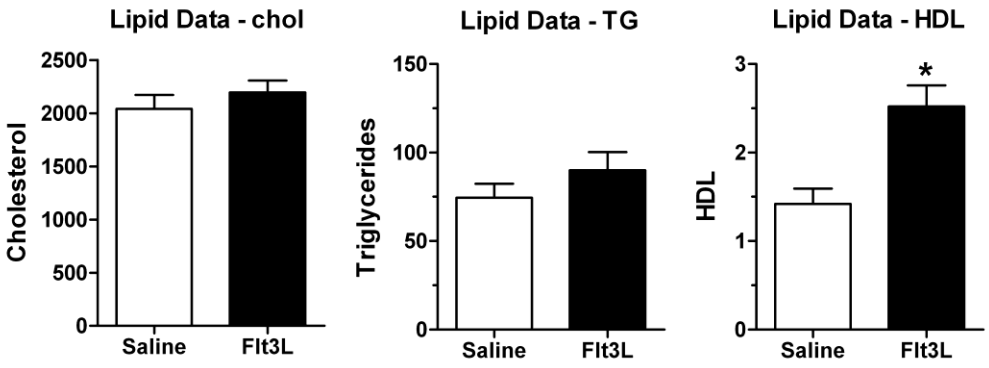

Figure 5.5. Flt3L treatment increases serum HDL levels in hypercholesterolemic ApoE$^{-/-}$ mice. *Blood was drawn from saline- (white bars) and Ftl3L-treated (black bars) ApoE$^{-/-}$ mice at 14 days post-ligation, and plasma separated by centrifugation. Total cholesterol, triglycerides (TG), and HDL levels were then measured. *, $p < 0.05$.*

5.4 Discussion

Vascular DCs have been shown to play both pro- and anti-atherogenic roles in vascular biology. Several reports show that vDCs rapidly accumulate in atheroprone vascular regions exposed to d-flow conditions in response to hypercholesterolemia (Paulson et al., 2010;Alberts-Grill et al., 2012). These vDCs uptake intimal LDL and differentiate into foam cells (Paulson et al., 2010;Alberts-Grill et al., 2012). However, recent reports have identified two major resident vDC subsets in steady-state aorta: 1) Mo-DCs, which most likely differentiate from monocytes in response to oxLDL and depend on M-CSF for proliferation and survival (Perrin-Cocon et al., 2001), and Flt3L-Flt3-dependent CD103^{+} cDCs, which support vascular Treg responses and likely serve a homeostatic role in the artery wall (Choi et al., 2009;Choi et al., 2011). Understanding the kinetics of these two distinct vDC populations in response to d-flow and hypercholesterolemia is important to our overall understanding of how vascular homeostasis becomes disrupted during the early stages of atherosclerosis. As such, we examined CD103^{+} cDC and Mo-DC kinetics

in flow-disturbed LCA and control RCA of ApoE$^{-/-}$ mice over a 2 week time course in our partial carotid ligation model of atherosclerosis. Furthermore, we asked whether modulating the balance of these two vDC subsets by injecting exogenous Flt3L effects the establishment of vascular inflammation and the development of atherosclerosis.

We found that the combination of d-flow and hypercholesterolemia induces rapid accumulation of monocytes (CD11b^{+}CD11c^{-}MHC-II^{-}), but not CD103^{+} cDCs in flow-disturbed LCA as early as 4 days post-ligation (Fig. 5.2). These monocytes quickly differentiated into Mo-DCs and CD11c^{+} and MHC-II^{+} macrophages, which peaked at 7 days post-ligation showing a kinetic similar to that reported in our previous study (Alberts-Grill et al., 2012). Siglec-H^{+} plasmacytoid DCs (pDCs), which differentiate from the same precursor cells as CD103^{+} cDCs (Ginhoux et al., 2009), were also notably absent from LCA (data not shown), suggesting that their common progenitor cell does not migrate into intima in response to d-flow-induced EC inflammation, but instead responds to some other unknown signal. These findings indicate that d-flow primarily increases monocyte recruitment, in concordance with our previous finding of increased expression of monocyte-attracting chemokines CCL2 and CCL7 in LCA at 4 days post-ligation (Alberts-Grill et al., 2012). Hypercholesterolemia has been implicated as a causal factor in the differentiation monocytes into DCs (Perrin-Cocon et al., 2001;Wu et al., 2009), CD11c^{+} macrophages (Wu et al., 2009;Gower et al., 2011), and inflammatory, MHC-II^{+} macrophages (Woollard and Geissmann, 2010;Ley et al., 2011), which may explain their steady presence within flow-disturbed LCA. The lack of CD103^{+} cDCs,

along with the rapid monocyte recruitment and development of atherosclerosis may indicate a pro-inflammatory role for Mo-DCs in the artery wall.

The second major goal of this study was to determine whether the inflammatory tone within flow-disturbed LCA could be influenced by increasing the number of $CD103^+$ cDCs. Several reports have shown that $CD103^+$ cDCs can be selectively expanded by subcutaneous injection of Flt3L (Darrasse-Jeze et al., 2009;Choi et al., 2011). Therefore we injected HFD fed, ligated $ApoE^{-/-}$ mice with either Flt3L or saline control for 7 days and checked monocyte, macrophage, and DC content of LCA and RCA at 7 days post-ligation. While Flt3L greatly increased the numbers of $CD103^+$ cDCs in flow-disturbed LCA, surprisingly, the treatment also greatly expanded total $CD45^+$ leukocyte, Mo-DC, $MHC\text{-}II^+$ macrophage, and monocyte numbers within the artery wall (Fig. 5.3). This suggests that $CD103^+$ cDCs may have multiple, context-dependent functions and can contribute to vascular inflammation under certain conditions. Unfortunately, the effect of Flt3L therapy on vascular leukocyte recruitment during atherogenesis has not been previously reported, so there is no basis for comparison to other studies.

Lastly, we examined the effect of Flt3L treatment on the development of atherosclerosis. We found that although Flt3L treatment substantially expanded $CD103^+$ cDCs in LCA, treatment did not effect the development of d-flow-induced atherosclerosis in LCA (Fig. 5.4). However, it is difficult to form any clear conclusions from these experiments as other classes of leukocytes were also non-specifically increased by Flt3L treatment, making it difficult to determine the contributions of individual immune cell subtypes to

plaque development. Previous studies looking at the effect DC expansion or deletion on atherosclerosis have shown mixed results. As previously discussed, selective deletion of $CD103^{+}$ cDCs in Flt3-deficient $ApoE^{-/-}$ mice enhanced atherosclerosis (Choi et al., 2011), in contrast to the results of this preliminary study. That finding suggests that specific DC subsets may serve a regulatory role in the artery wall. This hypothesis is supported by studies showing that vaccination with oxLDL-loaded DCs can ameliorate atherosclerosis and boost Treg function (Habets et al., 2010), demonstrating that DCs can regulate inflammation in some circumstances. However, general deletion of DCs in the CD11c-DTR mouse resulted in reduced intimal lipid accumulation and foam cell formation, suggesting that vDCs contribute to these pathologies during atherogenesis (Paulson et al., 2010). Furthermore, expansion of Mo-DC with M-CSF treatment has also been shown to aggravate atherosclerosis (Rajavashisth et al., 1998;Chitu and Stanley, 2006), although this effect may be due to expansion of vascular monocyte and macrophage numbers.

The data presented in this preliminary study are far from complete. For instance, the effect of Flt3L treatment on the production of pro-inflammatory cytokines such as IFNγ, TNFα, or CCL2 in flow-disturbed LCA was never checked. Even more importantly, indicators of Treg function, such as IL-10 production, or Foxp3 mRNA levels were also not examined. However, it is clear from the Oil-Red-O staining data (Fig. 5.4B) that Flt3L treatment led to the formation of disorganized plaques, lacking discrete fibrous cap and lipid-rich, necrotic core regions. Taken along with the flow cytometry data showing generalized vascular leukocyte expansion in LCA from Flt3L-treated animals, it is

difficult to rule out non-specific effects of Flt3L treatment as a confounding factor in these studies.

While there is strong evidence that $CD103^+$ cDCs reside in aortic intima and contribute to Treg responses in the aortic wall (Choi et al., 2011), the data from our natural time course of DC migration into inflamed, flow-disturbed LCA suggest that cDC progenitor cells do not readily migrate into inflamed endothelium as monocytes clearly do, but instead follow some other possibly indirect homing signal as they are only present within flow-disturbed regions of the vasculature that host chronic low-grade inflammation (Jongstra-Bilen et al., 2006;Choi et al., 2011). It is of interest, therefore, to understand how cDC progenitors traffic into the flow-disturbed intima, as this may uncover potential therapeutic targets to bring increased $CD103^+$ cDCs into atherosclerotic plaques without the non-specific, and likely inflammatory, side-effects of Flt3L treatment.

5.5 References

Ait-Oufella, H., Salomon, B.L., Potteaux, S., Robertson, A.K., Gourdy, P., Zoll, J., Merval, R., Esposito, B., Cohen, J.L., Fisson, S., Flavell, R.A., Hansson, G.K., Klatzmann, D., Tedgui, A., and Mallat, Z. (2006). Natural regulatory T cells control the development of atherosclerosis in mice. *Nat Med* 12, 178-180.

Alberts-Grill, N., Rezvan, A., Son, D.J., Qiu, H., Kim, C.W., Kemp, M.L., Weyand, C.M., and Jo, H. (2012). Dynamic immune cell accumulation during flow-induced atherogenesis in mouse carotid artery: an expanded flow cytometry method. *Arterioscler Thromb Vasc Biol* 32, 623-632.

Binder, C.J., Hartvigsen, K., Chang, M.K., Miller, M., Broide, D., Palinski, W., Curtiss, L.K., Corr, M., and Witztum, J.L. (2004). IL-5 links adaptive and natural immunity specific for epitopes of oxidized LDL and protects from atherosclerosis. *J Clin Invest* 114, 427-437.

Buono, C., Binder, C.J., Stavrakis, G., Witztum, J.L., Glimcher, L.H., and Lichtman, A.H. (2005). T-bet deficiency reduces atherosclerosis and alters plaque antigen-specific immune responses. *Proc Natl Acad Sci U S A* 102, 1596-1601.

Chitu, V., and Stanley, E.R. (2006). Colony-stimulating factor-1 in immunity and inflammation. *Curr Opin Immunol* 18, 39-48.

Choi, J.H., Cheong, C., Dandamudi, D.B., Park, C.G., Rodriguez, A., Mehandru, S., Velinzon, K., Jung, I.H., Yoo, J.Y., Oh, G.T., and Steinman, R.M. (2011). Flt3 signaling-dependent dendritic cells protect against atherosclerosis. *Immunity* 35, 819-831.

Choi, J.H., Do, Y., Cheong, C., Koh, H., Boscardin, S.B., Oh, Y.S., Bozzacco, L., Trumpfheller, C., Park, C.G., and Steinman, R.M. (2009). Identification of antigen-presenting dendritic cells in mouse aorta and cardiac valves. *J Exp Med* 206, 497-505.

Darrasse-Jeze, G., Deroubaix, S., Mouquet, H., Victora, G.D., Eisenreich, T., Yao, K.H., Masilamani, R.F., Dustin, M.L., Rudensky, A., Liu, K., and Nussenzweig, M.C. (2009). Feedback control of regulatory T cell homeostasis by dendritic cells in vivo. *J Exp Med* 206, 1853-1862.

Galkina, E., and Ley, K. (2009). Immune and inflammatory mechanisms of atherosclerosis (*). *Annu Rev Immunol* 27, 165-197.

George, J., Afek, A., Gilburd, B., Levkovitz, H., Shaish, A., Goldberg, I., Kopolovic, Y., Wick, G., Shoenfeld, Y., and Harats, D. (1998). Hyperimmunization of apo-E-deficient mice with homologous malondialdehyde low-density lipoprotein suppresses early atherogenesis. *Atherosclerosis* 138, 147-152.

Ginhoux, F., Liu, K., Helft, J., Bogunovic, M., Greter, M., Hashimoto, D., Price, J., Yin, N., Bromberg, J., Lira, S.A., Stanley, E.R., Nussenzweig, M., and Merad, M. (2009). The origin and development of nonlymphoid tissue CD103+ DCs. *J Exp Med* 206, 3115-3130.

Gower, R.M., Wu, H., Foster, G.A., Devaraj, S., Jialal, I., Ballantyne, C.M., Knowlton, A.A., and Simon, S.I. (2011). CD11c/CD18 expression is upregulated on blood monocytes during hypertriglyceridemia and enhances adhesion to vascular cell adhesion molecule-1. *Arterioscler Thromb Vasc Biol* 31, 160-166.

Habets, K.L., Van Puijvelde, G.H., Van Duivenvoorde, L.M., Van Wanrooij, E.J., De Vos, P., Tervaert, J.W., Van Berkel, T.J., Toes, R.E., and Kuiper, J. (2010). Vaccination using oxidized low-density lipoprotein-pulsed dendritic cells reduces atherosclerosis in LDL receptor-deficient mice. *Cardiovasc Res* 85, 622-630.

Hansson, G.K., and Hermansson, A. (2011). The immune system in atherosclerosis. *Nat Immunol* 12, 204-212.

Harats, D., Yacov, N., Gilburd, B., Shoenfeld, Y., and George, J. (2002). Oral tolerance with heat shock protein 65 attenuates Mycobacterium tuberculosis-induced and high-fat-diet-driven atherosclerotic lesions. *J Am Coll Cardiol* 40, 1333-1338.

Hermansson, A., Ketelhuth, D.F., Strodthoff, D., Wurm, M., Hansson, E.M., Nicoletti, A., Paulsson-Berne, G., and Hansson, G.K. (2010). Inhibition of T cell response to native low-density lipoprotein reduces atherosclerosis. *J Exp Med* 207, 1081-1093.

Hjerpe, C., Johansson, D., Hermansson, A., Hansson, G.K., and Zhou, X. (2010). Dendritic cells pulsed with malondialdehyde modified low density lipoprotein aggravate atherosclerosis in Apoe(-/-) mice. *Atherosclerosis* 209, 436-441.

Jongstra-Bilen, J., Haidari, M., Zhu, S.N., Chen, M., Guha, D., and Cybulsky, M.I. (2006). Low-grade chronic inflammation in regions of the normal mouse arterial intima predisposed to atherosclerosis. *J Exp Med* 203, 2073-2083.

Kleemann, R., Zadelaar, S., and Kooistra, T. (2008). Cytokines and atherosclerosis: a comprehensive review of studies in mice. *Cardiovasc Res* 79, 360-376.

Kyaw, T., Tay, C., Khan, A., Dumouchel, V., Cao, A., To, K., Kehry, M., Dunn, R., Agrotis, A., Tipping, P., Bobik, A., and Toh, B.H. (2010). Conventional B2 B cell

depletion ameliorates whereas its adoptive transfer aggravates atherosclerosis. *J Immunol* 185, 4410-4419.

Lessner, S.M., Prado, H.L., Waller, E.K., and Galis, Z.S. (2002). Atherosclerotic lesions grow through recruitment and proliferation of circulating monocytes in a murine model. *Am J Pathol* 160, 2145-2155.

Ley, K., Miller, Y.I., and Hedrick, C.C. (2011). Monocyte and macrophage dynamics during atherogenesis. *Arterioscler Thromb Vasc Biol* 31, 1506-1516.

Maganto-Garcia, E., Tarrio, M.L., Grabie, N., Bu, D.X., and Lichtman, A.H. (2011). Dynamic changes in regulatory T cells are linked to levels of diet-induced hypercholesterolemia. *Circulation* 124, 185-195.

Mallat, Z., Besnard, S., Duriez, M., Deleuze, V., Emmanuel, F., Bureau, M.F., Soubrier, F., Esposito, B., Duez, H., Fievet, C., Staels, B., Duverger, N., Scherman, D., and Tedgui, A. (1999). Protective role of interleukin-10 in atherosclerosis. *Circ Res* 85, e17-24.

Mallat, Z., Gojova, A., Brun, V., Esposito, B., Fournier, N., Cottrez, F., Tedgui, A., and Groux, H. (2003). Induction of a regulatory T cell type 1 response reduces the development of atherosclerosis in apolipoprotein E-knockout mice. *Circulation* 108, 1232-1237.

Maron, R., Sukhova, G., Faria, A.M., Hoffmann, E., Mach, F., Libby, P., and Weiner, H.L. (2002). Mucosal administration of heat shock protein-65 decreases atherosclerosis and inflammation in aortic arch of low-density lipoprotein receptor-deficient mice. *Circulation* 106, 1708-1715.

Mor, A., Planer, D., Luboshits, G., Afek, A., Metzger, S., Chajek-Shaul, T., Keren, G., and George, J. (2007). Role of naturally occurring CD4+ CD25+ regulatory T cells in experimental atherosclerosis. *Arterioscler Thromb Vasc Biol* 27, 893-900.

Nakajima, T., Schulte, S., Warrington, K.J., Kopecky, S.L., Frye, R.L., Goronzy, J.J., and Weyand, C.M. (2002). T-cell-mediated lysis of endothelial cells in acute coronary syndromes. *Circulation* 105, 570-575.

Nam, D., Ni, C.W., Rezvan, A., Suo, J., Budzyn, K., Llanos, A., Harrison, D., Giddens, D., and Jo, H. (2009). Partial carotid ligation is a model of acutely induced disturbed flow, leading to rapid endothelial dysfunction and atherosclerosis. *Am J Physiol Heart Circ Physiol* 297, H1535-1543.

Nam, D., Ni, C.W., Rezvan, A., Suo, J., Budzyn, K., Llanos, A., Harrison, D.G., Giddens, D.P., and Jo, H. (2010). A model of disturbed flow-induced atherosclerosis in mouse carotid artery by partial ligation and a simple method of RNA isolation from carotid endothelium. *J Vis Exp*.

Niessner, A., Sato, K., Chaikof, E.L., Colmegna, I., Goronzy, J.J., and Weyand, C.M. (2006). Pathogen-sensing plasmacytoid dendritic cells stimulate cytotoxic T-cell function in the atherosclerotic plaque through interferon-alpha. *Circulation* 114, 2482-2489.

Nilsson, J., Fredrikson, G.N., Bjorkbacka, H., Chyu, K.Y., and Shah, P.K. (2009). Vaccines modulating lipoprotein autoimmunity as a possible future therapy for cardiovascular disease. *J Intern Med* 266, 221-231.

Paigen, B., Morrow, A., Holmes, P.A., Mitchell, D., and Williams, R.A. (1987). Quantitative assessment of atherosclerotic lesions in mice. *Atherosclerosis* 68, 231-240.

Paulson, K.E., Zhu, S.N., Chen, M., Nurmohamed, S., Jongstra-Bilen, J., and Cybulsky, M.I. (2010). Resident intimal dendritic cells accumulate lipid and contribute to the initiation of atherosclerosis. *Circ Res* 106, 383-390.

Perrin-Cocon, L., Coutant, F., Agaugue, S., Deforges, S., Andre, P., and Lotteau, V. (2001). Oxidized low-density lipoprotein promotes mature dendritic cell transition from differentiating monocyte. *J Immunol* 167, 3785-3791.

Pryshchep, S., Sato, K., Goronzy, J.J., and Weyand, C.M. (2006). T cell recognition and killing of vascular smooth muscle cells in acute coronary syndrome. *Circ Res* 98, 1168-1176.

Rajavashisth, T., Qiao, J.H., Tripathi, S., Tripathi, J., Mishra, N., Hua, M., Wang, X.P., Loussararian, A., Clinton, S., Libby, P., and Lusis, A. (1998). Heterozygous osteopetrotic (op) mutation reduces atherosclerosis in LDL receptor- deficient mice. *J Clin Invest* 101, 2702-2710.

Sato, K., Niessner, A., Kopecky, S.L., Frye, R.L., Goronzy, J.J., and Weyand, C.M. (2006). TRAIL-expressing T cells induce apoptosis of vascular smooth muscle cells in the atherosclerotic plaque. *J Exp Med* 203, 239-250.

Van Puijvelde, G.H., Van Es, T., Van Wanrooij, E.J., Habets, K.L., De Vos, P., Van Der Zee, R., Van Eden, W., Van Berkel, T.J., and Kuiper, J. (2007). Induction of oral tolerance to HSP60 or an HSP60-peptide activates T cell regulation and reduces atherosclerosis. *Arterioscler Thromb Vasc Biol* 27, 2677-2683.

Weber, C., Meiler, S., Doring, Y., Koch, M., Drechsler, M., Megens, R.T., Rowinska, Z., Bidzhekov, K., Fecher, C., Ribechini, E., Van Zandvoort, M.A., Binder, C.J., Jelinek, I., Hristov, M., Boon, L., Jung, S., Korn, T., Lutz, M.B., Forster, I., Zenke, M., Hieronymus, T., Junt, T., and Zernecke, A. (2011). CCL17-expressing dendritic cells drive atherosclerosis by restraining regulatory T cell homeostasis in mice. *J Clin Invest* 121, 2898-2910.

Woollard, K.J., and Geissmann, F. (2010). Monocytes in atherosclerosis: subsets and functions. *Nat Rev Cardiol* 7, 77-86.

Wu, H., Gower, R.M., Wang, H., Perrard, X.Y., Ma, R., Bullard, D.C., Burns, A.R., Paul, A., Smith, C.W., Simon, S.I., and Ballantyne, C.M. (2009). Functional role of CD11c+ monocytes in atherogenesis associated with hypercholesterolemia. *Circulation* 119, 2708-2717.

Zhou, X., Nicoletti, A., Elhage, R., and Hansson, G.K. (2000). Transfer of CD4(+) T cells aggravates atherosclerosis in immunodeficient apolipoprotein E knockout mice. *Circulation* 102, 2919-2922.

Zhou, X., Robertson, A.K., Hjerpe, C., and Hansson, G.K. (2006). Adoptive transfer of CD4+ T cells reactive to modified low-density lipoprotein aggravates atherosclerosis. *Arterioscler Thromb Vasc Biol* 26, 864-870.

CHAPTER 6:

DISCUSSION

6.1 A Brief Overview of the Role of Immune Responses in Atherosclerosis

Immune responses play an important role in atherosclerosis. Therefore, it is important to identify and define the various immune cell populations that enter the vascular wall and either contribute to the sustained vascular inflammation that drives atherosclerosis, or help maintain vascular homeostasis and immune tolerance. The evidence gathered so far testifies to the enormous heterogeneity and diversity of vascular immune cells. Rather than the simple, lipid-laden macrophage-filled plaque envisioned in the early 1980's (Gerrity et al., 1979), we now know that atherosclerotic plaques are complex immune tissues that contain all the major immune cell types, including B-cells, T-cells, macrophages, DCs, neutrophils, mast cells, NK cells, and NKT cells. Complicating matters further, non-leukocytic resident vascular cells such as ECs and SMCs also play important and interactive roles with invading immune cells in the regulation of inflammation and vascular biology.

Immune cells enter the vessel wall and interact with ECs and SMCs via a wide variety of chemical mediators and direct, cell-to-cell interactions to establish distinct, integrated tissue architecture. Under inflammatory vascular conditions, primarily driven by pro-inflammatory cytokine IFNγ, SMCs proliferate within the medial layers and then migrate into intima where they secrete a collagen- and elastin-rich fibrous cap to sequester the myriad inflammatory and pro-coagulatory factors that accumulate in developing atheroma from the clotting factors in the blood (Libby, 2002). Plaques grow by establishing discrete regions of active inflammation within the so-called 'shoulder regions' of plaques, which contain a mix of SMCs, macrophages, T-cells, DCs, NK and

NKT cells (Whitman and Ramsamy, 2006), and mast cells (Lindstedt et al., 2007). While contributory roles have been established for each of these cell types in the establishment and progression of atherosclerotic disease (Galkina and Ley, 2009), it is now clear that vDCs and T-cell responses they mediate play a key, required role in the pathogenesis of this disease. However, it has become clear over the past half-decade or so that the DC/T-cell story is quite complex and involves distinct regulatory and pro-inflammatory arms. The opposing roles of Treg and pro-atherogenic Th1 T-cell responses in atherogenesis have been fairly well described, with the important players phenotypically defined, and many key molecular mediators (i.e. IFNγ and IL-10) established. In contrast, the role of the DC in this disease has remained murky, probably due to the extensive phenotypic and functional heterogeneity of this enigmatic class of immune cells. While it is quite clear that DCs can be good or bad for the cardiovascular disease patient, we are only just beginning to discover which particular DCs do what, and how they do it.

Recent developments in the field have provided us with the proper tools to define what DCs are doing in atherosclerosis. First, the development of an effective technique for extracting vascular leukocytes, even from established atherosclerotic plaques (Galkina et al., 2006), allows us to examine single cell suspensions of these hard-to-get cells with the powerful tool of flow cytometry. The second big advance has been the development of new reagents, equipment, and techniques in flow cytometry that allow dead cell exclusion and the simultaneous measurement of upwards of 26 phenotypic markers in a single sample. Together, these techniques allow sufficiently stringent phenotyping of vDCs and other vascular leukocytes in order to identify new DC subsets. A third important tool was

the development of a rapid model of murine atherosclerosis, which used partial carotid ligation to generate d-flow in the left common carotid artery (Nam et al., 2009). In combination with a pro-atherogenic HFD, ligated mice develop robust atherosclerosis along the entire length of the LCA within two weeks. In comparison, in typical mouse models of diet-induced atherosclerosis, lesion growth typically takes over two months, and extensive atherosclerosis requires at least 4-6 months. The shorter timescale of disease development in our model makes it an ideal platform to quantify and define relationships between immune cell accumulation and inflammation in the arterial wall.

6.2 Summary of Experiments and Findings

Chapter 2:

We sought to combine arterial leukocyte isolation with state-of-the-art flow cytometry techniques using our partial carotid ligation model in order to examine the relationship between d-flow, leukocyte recruitment, and vascular inflammation over the entire lifespan of an atherosclerotic lesion. To accomplish this, we developed a 13-parameter, 10-fluorochrome flow cytometry method to analyze the kinetics of 7 distinct leukocyte types (total leukocytes, B-cells, T-cells, monocyte/macrophages, DCs, NK cells, and granulocytes) in atherosclerotic lesions, and used it to analyze lesion samples from our d-flow model of atherosclerosis. This allowed us to track week-to-week and even day-to-day changes in immune cell populations within the developing atherosclerotic lesion. By extracting whole artery RNA from LCA and RCA, we were able to also track inflammatory cytokine expression over a similar time course using qPCR techniques, and correlate inflammatory gene expression with leukocyte infiltration.

We found that d-flow induces rapid immune cell recruitment into the arterial wall. These infiltrating cells were comprised primarily of monocytes, leading to the rapid accumulation of monocyte-derived macrophages and DCs, which reached peak levels prior to the development of atherosclerotic plaque. Much smaller numbers of T-cells, NK cells, and granulocytes also infiltrated into the flow-disturbed artery wall, and despite the surprisingly low T-cell numbers, established a characteristic, Th1-skewed T-cell response that was measurable by qPCR. Peak leukocyte accumulation was strongly correlated with *in situ* IFNγ production, confirming the importance of vascular immune cells to the establishment of sustained vascular inflammation during atherogenesis. In contrast to flow-disturbed LCA, athero-resistant RCA and sham-operated LCA contained only a few resident leukocytes and did not show sustained immune cell accumulations throughout the study, which demonstrates the importance of d-flow in the establishment of atherosclerosis, and the protective nature of stable laminar flow, even under hypercholesterolemic conditions.

Our immunohistochemistry studies showed that flow-disturbed lesions developed discreet $TUNEL^+$ necrotic core regions and α-SMA-rich fibrous cap regions, in addition to accumulating large foam cells that stained positive for CD11b within two weeks post-ligation. Thinning of the fibrous cap and a reorientation of α-SMA fibers was often seen by 3 weeks post-ligation. Combined with our flow cytometry and qPCR data, we demonstrate that our partial carotid ligation model reproduces key morphological aspects of established mouse models of atherosclerosis including necrotic core formation, fibrous

cap formation, fibrous cap thinning, and inflammatory cytokine expression. Flow-disturbed plaques were dominated by macrophages and DCs, which has been well-established in murine aortic plaques and in human lesions as well. The primary differences seen between our flow-disturbed carotid artery lesions and murine aortic lesions were the markedly reduced presence of lesional T-cells, and the potential of our model to develop fully occlusive plaques. Together these findings establish partial carotid ligation as an effective animal model to study the inflammatory pathogenesis of atherosclerosis, and provide a comprehensive quantitative description of infiltrating leukocyte number and composition over the entire life span of an atherosclerotic lesion.

Chapter 3:

Next we sought to use our partial carotid ligation model to discriminate d-flow- and hypercholesterolemia-induced patterns in PBL trafficking. While many studies have shown that levels of circulating blood leukocytes change during atherogenesis in both mice and humans, these studies all looked at PBL trafficking in the context of gradual lesion development over a time period of months or years, making it difficult to isolate atherosclerosis-induced perturbations in PBL trafficking from those caused by hypercholesterolemia. To overcome this issue, we used our 10-color, 13-parameter flow cytometry method to observe PBL trafficking dynamics over a 4 week period in ligated $ApoE^{-/-}$ mice (rapid atherosclerosis + hypercholesterolemia) and compared these with sham-operated $ApoE^{-/-}$ mice (hypercholesterolemia alone), allowing us to isolate d-flow/atherosclerosis-mediated effects from those caused by hypercholesterolemia.

We found that both hypercholesterolemia (in sham-operated mice) and lesion development (in ligated mice) produced significant changes in circulating leukocyte levels. Hypercholesterolemia increased the number of circulating T-cells, B-cells, monocytes, DCs, granulocytes, and NK cells, while d-flow and lesion development reduced the circulating numbers of all these cell types, despite hypercholesterolemic conditions. These data suggest that active atherogenesis uniquely alters the trafficking dynamics of both innate and adaptive classes of circulating PBLs independently of hypercholesterolemia-mediated effects, raising the possibility that active vascular inflammation produces a unique compositional 'fingerprint' in the PBL compartment.

Chapter 4:

As discussed previously, the presentation of vascular autoantigens such as oxLDL and HSP60 to T-cells via the MHC-II pathway requires functional DCs and leads to the initiation of pro-atherogenic CD4 T-cell responses that constitute an essential pro-inflammatory component during atherogenesis. Disruption of the MHC-II antigen presentation pathway reduces atherosclerosis in mice (Sun et al., 2010), suggesting that pharmacological blockade of key enzymes in this pathway may be a viable therapeutic option in humans. CatS expression in DCs is required for proper antigen presentation to CD4 T-cells, but its role in the initiation and potentiation of pro-atherogenic T-cell responses has yet to be proven. Furthermore, CatS has been shown to play a pro-inflammatory and destabilizing role in atherosclerosis, by promoting leukocyte infiltration into the arterial wall and degrading structural elastin and collagen in established plaques (Sukhova et al., 2003;Rodgers et al., 2006;de Nooijer et al., 2009).

We sought to address the role of CatS in leukocyte recruitment, pro-atherogenic T-cell activation, and vascular inflammation using methods developed in our previous studies.

We found in preliminary studies that while CatS deficiency significantly impaired vascular leukocyte recruitment, and ablated hypercholesterolemia-induced $CD4^+$ T-cell activation, flow-disturbed LCA in $CatS^{-/-}ApoE^{-/-}$ mice did not lose the capacity to produce pro-inflammatory cytokines, or develop atherosclerotic lesions. These preliminary findings contrast with our initial hypothesis as well as previously established atherosclerosis studies in CatS-deficient mice, making further studies necessary. For instance, it would be interesting to see whether oxLDL-specific $CD4^+$ T-cells, which have been previously shown to aggravate atherosclerosis (Zhou et al., 2006), have a similar effect upon adoptive transfer into CatS-deficient animals. Further work is also needed to better characterize the contribution of CatS expression in different cell types to the pathogenesis of atherosclerosis. For these studies, conditional CatS knockout mice with CatS deficient macrophages or DCs would be ideal as preliminary bone marrow transplant studies yielded uninterpretable results (data not shown). Lastly, we were unable to test whether or not CatS plays an integral role in the initiation of pro-atherogenic $CD4^+$ T-cell responses against vascular autoantigens due to the lack of appropriate reagents such as tetramers, cloned antigen-specific T-cell receptors, and finely mapped cognate antigen peptide sequences to test them. As such reagents hopefully become available in the future, they will provide an indispensible toolset for studying the role of CatS in atherosclerosis.

Chapter 5:

Vascular DCs have been shown to play both pro- and anti-atherogenic roles in vascular biology. We wanted to understand the role of DCs in maintaining vascular homeostasis. Therefore, we conducted a preliminary trial using our partial carotid ligation model to study the natural kinetics of two recently described vDC subsets during d-flow-induced atherogenesis in LCA: 1) Flt3L-dependent regulatory $CD103^+$ cDCs, and 2) M-CSF-dependent monocyte-derived DCs (Mo-DCs). We found that d-flow rapidly and overwhelmingly favored the recruitment of monocytes, which then differentiated into Mo-DCs and $CD11c^+$ and $MHC\text{-}II^+$ macrophages. On the other hand, $CD103^+$ cDCs, which differentiate from a common pre-DC precursor as pDCs, entered the LCA very gradually, and only then in small numbers. These data implicate that pre-DCs and monocytes follow different homing signals into the vessel wall. Based on the enormous differences in Mo-DC and $CD103^+$ cDC numbers in flow-disturbed LCA, it is likely that monocytes respond to chemokines induced by d-flow and intimal lipid sequestration, while pre-DCs respond to chemokines expressed under steady-state conditions. A better understanding of these differential trafficking mechanisms would provide an important piece in the puzzle of how vascular homeostasis is disrupted in the early stages of atherosclerosis.

The second major goal of this study was to determine whether the inflammatory tone within flow-disturbed LCA could be influenced by expanding the vascular $CD103^+$ cDC population. To answer this question, we expanded $CD103^+$ cDCs in LCA by subcutaneous injection of Flt3L, and confirmed the expansion of our target DC

population using flow cytometry. However, Flt3L treatment unexpectedly increased overall leukocyte accumulation in LCA, including monocytes, Mo-DCs, and macrophages. As such, Flt3L treatment did not reduce atherosclerotic plaque development in our partial carotid ligation model. The results of these preliminary experiments are hard to interpret because Flt3L therapy non-specifically enhanced vascular leukocyte accumulation so strongly. While this may imply an inflammatory role for $CD103^+$ cDCs under certain contexts, it is impossible to make conclusions with any certainty without conducting further studies.

6.3 Future Directions

We characterized immune cell infiltration and function in our partial carotid ligation model and showed its utility as an experimental platform for studying atherosclerosis. However, our attempts to use our system to explore the therapeutic potential of molecular targets shown to govern key aspects of the vascular immune response, such as CatS (Chapter 4) and Flt3L (Chapter 5) yielded inconclusive results, suggesting that our knowledge of DC function in atherosclerosis is incomplete. Indeed, many of the adoptive transfer studies done with DCs so far have used bone marrow-derived DCs, which are matured *in vitro*, in place of vDCs (Hjerpe et al., 2010). DC depletion studies using the CD11c-DTR mouse model have been shown to delete only certain DC subsets, but not others, and may deplete CD11c-expressing monocytes and macrophages as well (Okuyama et al., 2010;Paulson et al., 2010;Choi et al., 2011), further blurring our interpretation of DC function during atherosclerosis. Additionally, we only have a rudimentary understanding of how vDCs function during steady-state conditions to

maintain vascular homeostasis. As such, new experimental approaches are required to identify important subset-specific genes in vDCs that differ between homeostatic and atherogenic conditions.

Recently, our group has used the partial carotid ligation model to examine how d-flow alters EC gene expression during the initiation of vascular inflammation (Ni et al., 2010;Ni et al., 2011). We conducted genome wide microarray studies looking at purified endothelial RNA from ligated LCA (d-flow) and control RCA (laminar flow) in order to determine genes that are differentially expressed under pro- and anti-atherogenic shear conditions *in vivo*. Using a systems biology approach we were able to identify putative anti-inflammatory genes that are expressed under laminar flow, but not d-flow conditions, and pro-inflammatory genes that are upregulated in endothelium by d-flow. Differentially regulated genes were then confirmed by qPCR and immunofluorescence studies to establish flow-sensitivity. Confirmed genes were analyzed using a bioinformatics approach to identify genes that sit atop key regulatory networks and the role of these choice genes in EC function and atherosclerosis was tested *in vitro* and *in vivo* with siRNA knockdown or overexpression studies.

Since DCs are such a heterogeneous population of cells, a similar broad, genomics-based approach would be very useful in identifying key DC-specific genes that mediate homeostatic and pro-inflammatory processes in the artery wall. The partial carotid ligation model is of particular utility in this endeavor as rapid atherosclerosis in LCA only develops in the context of hypercholesterolemia in $ApoE^{-/-}$ mice. Ligated wild-type

(WT) C57/Bl6 mice undergo characteristic vascular remodeling responses, including mild medial, intimal, and adventitial thickening, coupled with $CD45^{+}$ leukocyte infiltration, but do not develop atherosclerosis, even when maintained on HFD, or adoptively transferred with splenocytes from ligated $ApoE^{-/-}$ mice fed HFD for 7 days (Fig. 6.1). This suggests that WT mice maintain vascular homeostasis, even in the face of multiple, strong pro-atherogenic stimuli. Similarly, ligated $ApoE^{-/-}$ fail to rapidly develop atherosclerosis when maintained on standard chow diet, suggesting that these mice may be useful model to study how vascular homeostasis is disrupted during the earliest stages of atherogenesis.

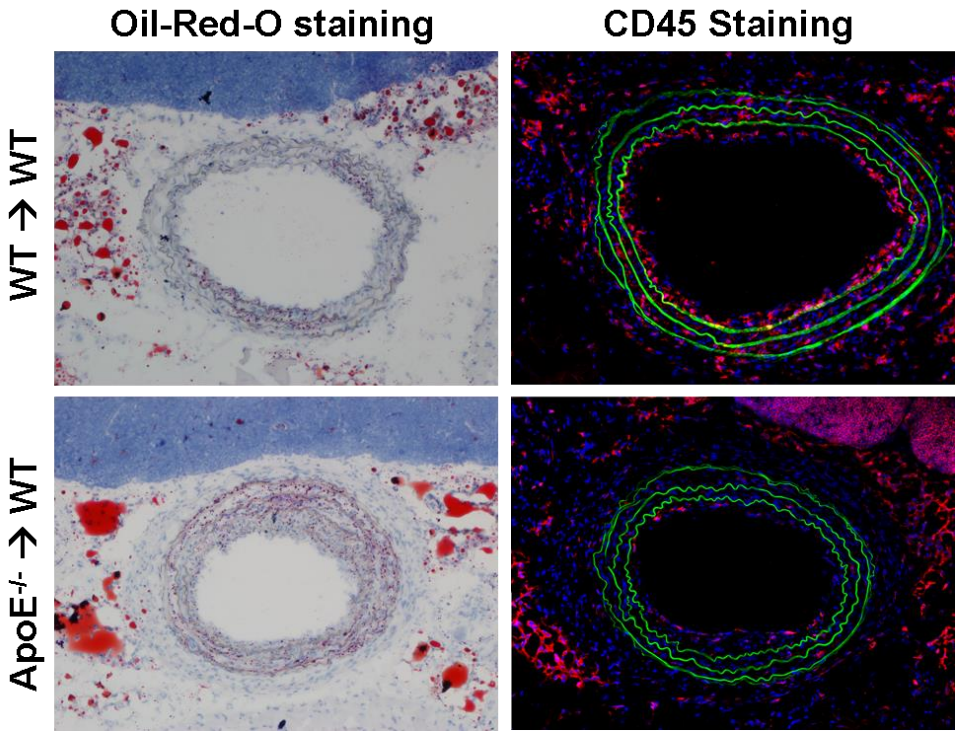

Figure 6.1. Ligation induces vascular remodeling and leukocyte infiltration in wild-type C57/Bl6 mice, but fails to cause atherosclerosis. *Wild-type (WT) C57/Bl6 mice were adoptively transferred with splenocytes harvested from either ligated WT or $ApoE^{-/-}$ mice fed a HFD for 7 days and then ligated and maintained on HFD for 14 days. Oil-Red-O and CD45 immunofluorescence staining was performed on frozen cross-sections of LCA to assess lesion development and leukocyte infiltration. Shown are representative stains.*

The initial goal of these future studies is to develop a model that meets the following conditions (Fig. 6.2):

1. Flow-disturbed LCA recruits and establishes a stable resident vDC population, but does not go on to develop atherosclerosis. (d-flow only)
2. LCA develops atherosclerosis after switching to HFD, which coincides with a measureable shift in the vDC profile. (d-flow + hyperlipidemia)
3. Lesion regression occurs after replacing HFD with chow diet.
4. vDC populations correspond with aortic DC populations in steady-state and atherosclerotic aorta in WT C57/Bl6 and ApoE$^{-/-}$ mice respectively.

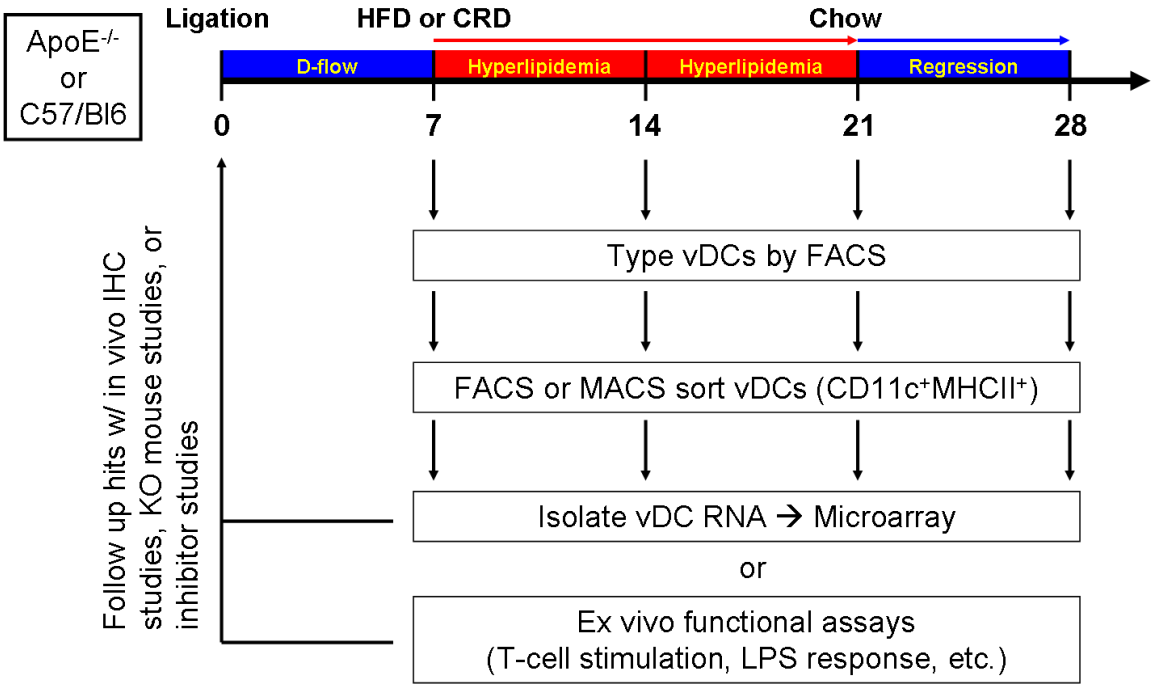

Figure 6.2. Proposed experimental model for future studies.

Development of this model promises to be a challenging undertaking and will likely require careful optimization of mouse strain and diet conditions. However once established, this model will allow us to isolate vDCs (and other immune cells) from homeostatic, early atherosclerotic, and regressive atherosclerotic arteries and use broad genomics approaches to establish characteristic gene expression profiles for each physiological condition.

6.4 Contributions to the Field

The more we learn, the more we come to understand that the immune system is intimately involved in the regulation of vascular physiology both in health and in disease. Together, the expanded flow cytometry techniques discussed in Chapter 2 and our accelerated, d-flow-induced atherosclerosis model add an important tool for the cardiologist/vascular biologist. As discussed previously (Chapter 2), our model produces the rapid development of atherosclerosis over a compressed, two week period, which allowed us to conduct time course studies with exquisite sensitivity. This provides an excellent platform for examining leukocyte recruitment kinetics into inflamed vascular tissues as demonstrated in Chapters 2 and 5, allowing the tracking of many basic, or of several well-defined immune cell subsets. Flow cytometry results are readily confirmable by immunohistochemistry studies, which also provide key morphological data. As demonstrated in Chapter 2, partial carotid ligation induces leukocyte migration into the intimal, medial, and adventitial regions of the artery. As such, these techniques can be used in conjunction with the adoptive transfer of congenic, or immunofluorescently labeled populations of purified immunocytes in order to track

various aspects of leukocyte trafficking and localization within the vascular wall. Furthermore, various methods for viewing carotid artery using intravital microscopy techniques have been recently developed. Since our model induces such rapid leukocyte infiltration into easily defined regions of the artery wall, it makes an ideal platform for observing live leukocyte trafficking into nascent or established atheroma.

A second important use for our experimental system is for rapid testing of putative atherosclerosis-related genes or pharmacological treatments. As shown in Chapters 4 and 5, we can rapidly interrogate genetic knockout mouse models such as the $CatS^{-/-}ApoE^{-/-}$ mouse, or drug therapies like with the Flt3L study to determine efficacy in reducing or exacerbating atherosclerosis. The ability to acquire pure endothelial RNA at early time points, or whole carotid artery RNA at all time points allows us to use broad genomics and systems biology approaches to uncover new pro-atherogenic or homeostatic mechanisms through comparison of flow-disturbed LCA and control RCA. In the case of genetic knockout models or new drug therapies, these genomics approaches can be useful in determining mechanism as well. Furthermore, partial carotid ligation in the absence of HFD, or in wild-type C57/BL6 mice induces comparatively mild intimal and medial thickening, as well as leukocyte infiltration without causing atherosclerosis. This likely makes an excellent model for examining immune cell function in the flow-disturbed artery under steady-state conditions.

In conclusion, the partial carotid ligation model provides a unique platform for studying temporally sensitive events during atherosclerosis, including the initial vascular and immunological responses to d-flow, which cannot be studied in standard atherosclerosis models because native atheroprone regions experience chronic d-flow. Our model system is readily usable with cutting edge flow cytometry, genomics, and microscopy techniques as it provides a large, homogenous arterial region which is inducibly subjected to d-flow, and reproducibly develops progressive vascular inflammation and atherosclerosis. Our model has the potential to become a critical tool to further our understanding of the pathophysiology of atherosclerosis, and to test new therapies.

6.5 References

Choi, J.H., Cheong, C., Dandamudi, D.B., Park, C.G., Rodriguez, A., Mehandru, S., Velinzon, K., Jung, I.H., Yoo, J.Y., Oh, G.T., and Steinman, R.M. (2011). Flt3 signaling-dependent dendritic cells protect against atherosclerosis. *Immunity* 35**,** 819-831.

De Nooijer, R., Bot, I., Von Der Thusen, J.H., Leeuwenburgh, M.A., Overkleeft, H.S., Kraaijeveld, A.O., Dorland, R., Van Santbrink, P.J., Van Heiningen, S.H., Westra, M.M., Kovanen, P.T., Jukema, J.W., Van Der Wall, E.E., Van Berkel, T.J., Shi, G.P., and Biessen, E.A. (2009). Leukocyte cathepsin S is a potent regulator of both cell and matrix turnover in advanced atherosclerosis. *Arterioscler Thromb Vasc Biol* 29**,** 188-194.

Galkina, E., Kadl, A., Sanders, J., Varughese, D., Sarembock, I.J., and Ley, K. (2006). Lymphocyte recruitment into the aortic wall before and during development of atherosclerosis is partially L-selectin dependent. *J Exp Med* 203**,** 1273-1282.

Galkina, E., and Ley, K. (2009). Immune and inflammatory mechanisms of atherosclerosis (*). *Annu Rev Immunol* 27**,** 165-197.

Gerrity, R.G., Naito, H.K., Richardson, M., and Schwartz, C.J. (1979). Dietary induced atherogenesis in swine. Morphology of the intima in prelesion stages. *Am J Pathol* 95**,** 775-792.

Hjerpe, C., Johansson, D., Hermansson, A., Hansson, G.K., and Zhou, X. (2010). Dendritic cells pulsed with malondialdehyde modified low density lipoprotein aggravate atherosclerosis in Apoe(-/-) mice. *Atherosclerosis* 209**,** 436-441.

Libby, P. (2002). Inflammation in atherosclerosis. *Nature* 420**,** 868-874.

Lindstedt, K.A., Mayranpaa, M.I., and Kovanen, P.T. (2007). Mast cells in vulnerable atherosclerotic plaques--a view to a kill. *J Cell Mol Med* 11**,** 739-758.

Nam, D., Ni, C.W., Rezvan, A., Suo, J., Budzyn, K., Llanos, A., Harrison, D., Giddens, D., and Jo, H. (2009). Partial carotid ligation is a model of acutely induced disturbed flow, leading to rapid endothelial dysfunction and atherosclerosis. *Am J Physiol Heart Circ Physiol* 297**,** H1535-1543.

Ni, C.W., Qiu, H., and Jo, H. (2011). MicroRNA-663 upregulated by oscillatory shear stress plays a role in inflammatory response of endothelial cells. *Am J Physiol Heart Circ Physiol* 300**,** H1762-1769.

Ni, C.W., Qiu, H., Rezvan, A., Kwon, K., Nam, D., Son, D.J., Visvader, J.E., and Jo, H. (2010). Discovery of novel mechanosensitive genes in vivo using mouse carotid artery endothelium exposed to disturbed flow. *Blood* 116**,** e66-73.

Okuyama, M., Kayama, H., Atarashi, K., Saiga, H., Kimura, T., Waisman, A., Yamamoto, M., and Takeda, K. (2010). A novel in vivo inducible dendritic cell ablation model in mice. *Biochem Biophys Res Commun*.

Paulson, K.E., Zhu, S.N., Chen, M., Nurmohamed, S., Jongstra-Bilen, J., and Cybulsky, M.I. (2010). Resident intimal dendritic cells accumulate lipid and contribute to the initiation of atherosclerosis. *Circ Res* 106**,** 383-390.

Rodgers, K.J., Watkins, D.J., Miller, A.L., Chan, P.Y., Karanam, S., Brissette, W.H., Long, C.J., and Jackson, C.L. (2006). Destabilizing role of cathepsin S in murine atherosclerotic plaques. *Arterioscler Thromb Vasc Biol* 26**,** 851-856.

Sukhova, G.K., Zhang, Y., Pan, J.H., Wada, Y., Yamamoto, T., Naito, M., Kodama, T., Tsimikas, S., Witztum, J.L., Lu, M.L., Sakara, Y., Chin, M.T., Libby, P., and Shi,

G.P. (2003). Deficiency of cathepsin S reduces atherosclerosis in LDL receptor-deficient mice. *J Clin Invest* 111**,** 897-906.

Sun, J., Hartvigsen, K., Chou, M.Y., Zhang, Y., Sukhova, G.K., Zhang, J., Lopez-Ilasaca, M., Diehl, C.J., Yakov, N., Harats, D., George, J., Witztum, J.L., Libby, P., Ploegh, H., and Shi, G.P. (2010). Deficiency of antigen-presenting cell invariant chain reduces atherosclerosis in mice. *Circulation* 122**,** 808-820.

Whitman, S.C., and Ramsamy, T.A. (2006). Participatory role of natural killer and natural killer T cells in atherosclerosis: lessons learned from in vivo mouse studies. *Can J Physiol Pharmacol* 84**,** 67-75.

Zhou, X., Robertson, A.K., Hjerpe, C., and Hansson, G.K. (2006). Adoptive transfer of CD4+ T cells reactive to modified low-density lipoprotein aggravates atherosclerosis. *Arterioscler Thromb Vasc Biol* 26**,** 864-870.